

Exact results in the Interacting Resonant Level Model

A thesis submitted for the degree of
Doctor of Philosophy
by

Gonzalo Camacho

University of
Kent

University of Kent
School of Physical Sciences
Canterbury, United Kingdom
December 2017

Declaration

I declare that the content of this thesis constitutes my original work, and has not been copied or edited from any others. I also declare that the numerical code used to obtain numerical data was developed entirely by myself, and was not copied or edited from any others. All data presented that has not been worked out by these simulations is referenced accordingly.

Signed: Gonzalo Camacho

*To the memory of
Gonzalo Camacho Aguado*

Introduction

Impurity models have been a fascinating field of research inside the condensed matter physics community for a long time. A good account on this is the increasing number of experimental realizations for the study of such one dimensional systems, involving quantum wires and dots [1, 2, 3, 4]. The study of transport in such systems constitutes one of the most active lines of research in condensed matter physics at present.

In the mid thirties of the past century, it was discovered [5] that some transition metals develop a minimum in their resistivity when cooled down. A first attempt to fit the experimental data by using known phonon-scattering formulas failed in platinum [6]. This change in the properties of a material due to interactions is one of the main examples of *collective behaviour*, where correlations between constituents give rise to new phenomena otherwise hidden. It was recognized later that the underlying mechanism of this minimum in the resistivity had to come from something else than phonon scattering, which is rapidly suppressed at low temperatures. The attention turned to magnetic impurities and their survival inside a metallic environment.

It took almost thirty years to understand these experimental results from a fundamental point of view. The first approach was pioneered by Anderson [7] in 1961, and has to do with the concept of *virtual bound states* and the effect of Coulomb interactions between electrons. His proposed model is equivalent to the Fano model [8], but it includes a local Coulomb interaction between electrons occupying the impurity site. The appearance of this interacting term is based on physical arguments. Most of magnetic moments belong to *d* or *f* orbitals of elements from the periodic table. In these orbitals, the wavefunction is very *localized* within the nucleus. Therefore, when two electrons are occupying the same orbital, there must be an associated cost in energy. The inclusion of this interacting term in the hamiltonian gives rise to new interesting phenomena. Anderson was unable to explain the appearance of the resistivity minimum, but gave a lot of insight to the physics of impurity models, concretely about how a local magnetic moment develops inside the material. This formation of a local moment manifests in the appearance of a Curie term in the susceptibility, which is absent in the Fano model. He later deduced that the coupling between the spin density of conduction electrons and the magnetic moment should be antiferromagnetic. Based on this idea, Jun Kondo [9] approached the problem in 1964, working with the antiferromagnetic coupling between the local moment and the surrounding spin density. The model he used is now known as the s-d exchange model (called the *Kondo model* after him). Although the hamiltonian

of such a model is different from the Anderson model, both prove to be equivalent in the appropriate parameter regime. Kondo developed a perturbative calculation till third order, showing the appearance of a temperature dependent logarithm, and explaining the minimum in the resistivity, thus solving the long outstanding problem. The formal equivalence between the Anderson and Kondo models was shown soon after by Schrieffer and Wolff [10]. This proved that both Anderson's and the s-d exchange model describe the same low energy physics in some region of parameter space. Moreover, the Kondo model arises as a limiting case of the Anderson model.

However, from Kondo's calculation, there was still one big remaining question. The interaction between the electrons and the localized moment introduces a new energy scale in the problem, the so called Kondo temperature T_K . For $T > T_K$, the impurity survives in the surrounding environment, explaining the minimum observed in the resistivity. However, for $T < T_K$, perturbation theory breaks down and Kondo's calculation loses its validity due to the divergence in the logarithm as $T \rightarrow 0$. This motivated theorists to find new methods in order to understand the model in the low temperature sector. One first attempt to address this question was given by Anderson [11] in what is now called the "poor man's scaling" approach, and where the concepts of Renormalization Group and scaling started to emerge applied to impurity problems. This approach showed that under perturbative RG, a change in the cut-off of the theory involves a growth in the coupling constant between the impurity and the rest of electrons, but failed to explain what happened at $T \ll T_K$, in the so called *strong coupling* regime. However, the general belief was that this coupling continued growing as the energy scale is lowered down, something that would result in an infinite coupling between the localised moment and the environment, forming a singlet state between the magnetic moment and the conduction electrons (since the interaction parameter in the Kondo model is antiferromagnetic $J < 0$, see [10]). Therefore, it was expected that the local moment wouldn't survive at very strong interactions, or in other words, it is *screened* by the conduction electrons due to the strong coupling. In parallel, these renormalization group ideas were being applied to critical phenomena [12] of a range of different models in statistical physics [13].

Different approaches were taken by trying to find similarities between the Kondo problem and some other related models. A model to look at was the so called "X-ray edge problem", studied mainly by Mahan [14] and in a series of papers [15, 16, 17] by Nozières, Roulet, Gavoret and De Dominicis. This model describes the spontaneous change of potential scattering appearing in a metal when a hole is created by an X-ray. The electron is hit by the X-ray and promoted to the upper band, leaving a hole in the valence band. The effect of the generated hole is a reallocation of electrons in the Fermi sea, and introduces an interaction between the sea and the hole. Such a process is purely dynamical (time-dependent potential) and involves *time* correlations. Mahan was the first one to predict singularities in the correlation function, something that was also reproduced later by Nozières and Schotte and Schotte [18] employing different techniques. Nozières approach to solve the problem used the so called *parquet equations* [15], a set of complicated (coupled) integral

equations for the correlation functions. But the greatest achievement was to realise that the problem could be solved in an exact way as a single-particle problem [17]. This is because once the hole is created, it remains there, acting as a scatterer for conduction electrons, and therefore no record of all processes happening at the impurity is necessary. All one needs to study is the *response* of conduction electrons experiencing the potential change. In parallel, Schotte and Schotte introduced the method of *bosonization* applied to the X-ray [19]. Bosonization was known to provide exact results for the Tomonaga-Luttinger model [20, 21], and both approaches (Schotte, Nozières) are *exact*, they reproduce the exponents of correlation functions in an exact way, and confirm Mahan’s singularity at threshold in the absorption rate. The similarity of the X-ray edge problem and the Kondo model was captured in a series of papers by Anderson and Yuval [22, 23, 24]. Following Nozières method, Anderson and Yuval approached the Kondo problem by considering the flip of the localised magnet as a single X-ray process. Thus, every time an electron interacts with the impurity, a flip on the spin occurs, and this can be extended to infinite time by summing up all spin flips. In this sense, the approach is equivalent to a Feynman path integral for the conduction electrons reaching the impurity site, seeing an alternating potential scatterer. Anderson and Yuval approach is thus, a *time asymptotic* (large times) correlators method to study the Kondo problem. It provides exact results in the time domain, considering the Kondo problem as a sequence of X-ray edge problems.

With all these previous works, there was some basic knowledge to tackle the problem. The very big achievement of the application of such ideas to the Kondo problem was carried out by Wilson [25] in 1975, by developing a non-perturbative numerical method called the Numerical Renormalization Group (NRG). This work was worth the Nobel prize in 1982 “*for his theory for critical phenomena in connection with phase transitions*”. Wilson applied his method to solve the Kondo problem in the region $T \ll T_K$, demonstrating the finiteness of the solution at zero temperature. The so called “Wilson ratio”, relating the susceptibility and specific heat, proved to be for the impurity twice the result for a system of non-interacting electrons. This proved the fact that at very low temperatures, the magnet is *screened* by the surrounding electrons, forming a singlet and therefore, eliminating the impurity in an effective way. With this, the long-standing Kondo problem was solved by use of a non-perturbative technique, at least numerically.

The formidable work of Wilson served as a starting point for the theorists community to develop non-perturbative approaches to well known models, and the search of exactly solvable theories started to gain fame as opposed to previous perturbative methods. In particular, there was a strong interest in finding exact solutions for the Kondo problem in an analytic way. Wilson’s NRG provided accurate numerical results, but analytic approaches were also desirable. In an effort to do so, an old method to provide exact results began to be applied to impurity models. The method was first created in 1931 by Hans Bethe [26], to solve the antiferromagnetic spin 1/2 chain. The method is now known as the *Bethe ansatz*, and provides exact solutions of the many-body wavefunctions of certain interacting one dimensional

models. By the time, the Bethe ansatz had been applied to field theories that were known to be *integrable*, like the Massive Thirring model [27, 28, 29, 30] (MTM) and the Sine Gordon model [31] (SG). It was shown by Coleman [32] that both the MTM and the SG models are equivalent by a direct relation between the parameters of the theory, deduced from a perturbative treatment of the correlation functions. Thus, the relativistic fermions of the MTM are equivalent to the solitons of the SG model, another manifestation of the fermion-boson equivalence in (1+1) dimensions. Variations of these field theories include boundary value problems, which are intimately related to impurity models. One case is the boundary Sine-Gordon model, whose S matrix was firstly derived by Goshal and Zamolodchikov [33]. These results have been exploited later to study the boundary sine Gordon model (BSG) in depth [34], as well as finding application into out of equilibrium problems in nanowires [35].

Before an exact solution was developed for the Kondo model, Wiegmann and Finkelshtein [36] introduced the “Interacting Resonant Level Model” (IRLM), as a simpler model to study analytic properties of the s-d exchange model. By proper transformation of the fields, a direct relation of parameters between the IRLM and the anisotropic version of the Kondo model (AKM) is established, therefore both models are equivalent. In the IRLM, an impurity site or dot interacts with spinless fermions of the conduction channel, while at the same time conduction fermions can jump in and out of the impurity site. It is the interaction between the impurity and conduction electrons what makes the problem a *strongly correlated system*. The model will be described in more detail later. It is the aim of this thesis to develop a deep understanding and study of the IRLM, for reasons we will expose in the following. In [36], thermodynamic properties of the IRLM were calculated, like the impurity susceptibility and specific heat, and compared with the AKM. Although results prove Wilson’s ratio relation, some of the thermodynamic properties are not described in a complete way. As we shall see later, expressions in the model can be given in an *exact* way for the susceptibility, or what is the same, the associated energy scale in the problem. Another approach to the model was developed by Schlottman [37]. By directly bosonizing the AKM and fermionizing back all operators, one recovers the IRLM hamiltonian. His treatment of the model consists on perturbative Renormalization Group (RG) methods, in order to obtain dynamical quantities like the impurity Green’s function. Schlottman’s approach, being perturbative, is only valid for small values of interaction, and therefore has a short range of validity.

Several contributions have been done in order to gain a full understanding of the model, even with slightly variations like the attachment of more than one channel to the impurity site [38, 39, 40], in what is known as the multichannel IRLM (MIRLM). Other variations include the attachment of the resonant level coupled a Luttinger liquid [41, 42, 43]. There are many interesting questions to adress in the model, both in equilibrium and out of equilibrium, and that is why we believe in a revision of the theory, where deriving previous results becomes a necessary step for understanding the model in depth, while at the same time we provide new results that, to our knowledge, were not known previously. In this thesis, we will only focus

on equilibrium aspects of the model, since, as we will see, has a lot to offer by itself. We can divide our study into three main categories: some questions concerning the thermodynamics of the model, some concerning the dynamics and finally its integrability and exact solution. We want however to motivate the non-equilibrium problem briefly. The last two of the three above mentioned categories are intimately related to address one big question: the successful application of non-perturbative methods to out of equilibrium strongly correlated systems, something that has already been tried in the IRLM [44]. It has also been reported that this method fails to agree with numerical simulations by DMRG [45]. Other approaches to the model out of equilibrium have been proposed, by employing different techniques like Conformal Field Theory [46], study of the shot noise [47], and full-counting statistics [48]. Concretely in [46, 48], the model is solved out of equilibrium only at a single value of the interaction parameter, the so called *self-dual* point. A complete theory for any value of interaction in the non-equilibrium situation has not been developed yet, and therefore, it stands as an outstanding problem. One approach would be to attack directly the non-equilibrium problem, by assuming all results from previous works in the model. This has proved to lead to disagreement between theory and numerics, being [44] one example. The second approach would consist on a careful checking of these previous solutions and the construction of a full theory of the equilibrium IRLM, by fixing possible inconsistencies found in our way. Is this second approach the one we believe to offer insight into the model. Once a full theory of the equilibrium IRLM has been established, these results could well serve to understand the situation far from equilibrium (in the two channel version of the model). This is then the main motivation of the work presented here. Even for the simplest case, the single channel IRLM, the construction of such theory proves to be a challenging task.

We begin by the description of thermodynamics, where previous studies [38, 49, 50] reproduce the susceptibility exponent for the new energy scale Γ by use of bosonization, perturbative RG (only to first order in the coupling constant) and Anderson-Yuval methods [39]. However, the value of such exponent differs with the one found in other publications [51]. With regards to the energy scale Γ , the situation is somewhat more worrying. Analytic results start to differ from numerics as soon as interaction is slightly increased [38, 50]. Moreover, in the two channel version of the model, lattice treatment has been reported to offer different results from the field theory approach [51] at very strong values of interaction. In particular, it is argued [51] that those results depend on the *regularization* of the continuum version of the model. This constitutes one of the central points of discussion of this thesis, which will in turn try to prove that the theory cannot be dependent on any regularizations when taken to the continuum limit. In other words, both the lattice and the field treatment have to offer the same low-energy description of the model, showing results independent on regularization schemes employed. The main questions to address are as follows: I. *What is the true value of the thermodynamic exponent α ?*, II. *Is there any way to find a **exact** expression for the thermodynamic energy scale Γ ?*, III. *Can one obtain such exact expressions when there is more than one channel attached to the impurity site?*, IV. *Are lattice results in the model in accordance with those of a continuous (field) description?*

Respect to dynamics, the most interesting quantity to compute is the impurity density of states or spectral function. This is intimately related with dynamical processes where particles jump in and out of the impurity site. Previous works [38, 39] assume the scale of the density of states to be the same that the one obtained for thermodynamics by perturbative RG. In other words, it is believed that Γ dominates both thermodynamic and dynamic quantities. For this same Γ , it is also predicted a decrease in the density of states width as interaction is increased. However, it has been shown [52] that for the two channel IRLM, the width in the spectral function (the dynamic energy scale) grows monotonically as interaction is increased, contradicting the cited results. More than that, reference [53] shows a different behaviour of the dynamic energy scale as opposed to the thermodynamic one. For the two channel case, the thermodynamic width decreases to a zero value at infinite interaction. On the other hand, the dynamic energy scale shows a monotonic increase with interaction even at very big values of interaction. Such a strong coupling in the dynamic quantities needs to be better understood. The analytic formula at zero hybridization for the impurity correlation function has been given by Giamarchi et.al [54] (which corresponds exactly to the critical point, the non-Fermi liquid point). As interaction is switched on, the model is expected to behave as a non-Fermi liquid, developing a singularity in the zeroth energy sector. We will observe later that this is not the case when NRG simulations are carried out. In a different approach to study the dynamics, recent works [55] show the application of Continuous Time Quantum Monte Carlo methods in order to calculate the impurity spectral function. All of these motivate the following questions concerning dynamics of the model: I. *Are there two different energy scales in the problem, one for thermodynamics and another for dynamics?* II. *If both scales are different, what are the physical processes separated by the dynamic energy scale?* III. *What is the exact dynamical exponent of the theory, and how to calculate it?* IV. *What is the exact form of the spectral function on the dot as interaction is increased?*

To conclude, we look at the integrability of the IRLM, and its solution by the Bethe Ansatz method. It was shown by Filyov and Wiegmann [56] that the IRLM is integrable, and therefore, an exact expression of its many-body wavefunction can be given. Since the IRLM is obtained directly from the s-d exchange model, the main point of Filyov and Wiegmann's paper is to illustrate the integrability of the Kondo model, something that was done afterwards by Wiegmann [57, 58] and Andrei [59], and in later collaboration with Tsvelick [60], where several impurity models are solved by the Bethe ansatz technique, including the IRLM (see supplement of [60]). There is however a big problem on this solution. When the thermodynamic exponent for the susceptibility is calculated by bosonization, a second order term in the coupling constant g appears (that is, the exponent contains a term g^2). This turns out to be very important since, when one goes to the multichannel description of the model, this second order term g^2 transforms to Ng^2 , being N the total number of leads attached to the impurity. Surprisingly, when the Bethe ansatz method is applied, Filyov and Wiegmann's solution doesn't reproduce the g^2 term, and only does to first order in g . Since both bosonization and Bethe ansatz are *exact* meth-

ods, the same answer must be given by both. The fact that the term that cannot be reproduced is the one that distinguishes between different versions of the model is very worrying. For instance, that would imply no change between the two-channel version of the model and the single channel when using the exact solution. This motivates a revision of the method step by step, to discover the origin of such second order contributions. The main questions to address in this line are: I. *Why doesn't the Bethe ansatz method reproduce bosonization results?* II. *What is the origin of the second order terms, and the physical processes relevant to its description?* III. *Can one reproduce the exact prefactor for the thermodynamic energy scale by the Bethe ansatz method?*

The thesis is structured as follows. Chapter I presents an introduction to the main impurity models in the area of strongly correlated electronic systems, presenting the Interacting Resonant Level Model (IRLM) as one of them. Chapter II is devoted to the presentation of fundamental techniques in Quantum Field Theory (QFT) in impurity models that will be employed in the thesis, leaving specific treatment for further reading in the literature. In Chapter III we build in a unified way the main thermodynamics at zero temperature of the one channel IRLM. Different limits of the theory are explored and original results are presented. Chapter IV deals with general aspects of the multichannel version of the IRLM. Concretely, the two channel version of the model is contrasted respect to the one channel one, and main differences between both models are pointed out. This section also includes open questions to address in the N channel IRLM. Chapter V describes the dynamical properties of the single channel IRLM, with special attention to the local density of states on the impurity site. Original results are presented and discussed. Finally, Chapter VI presents the application of the Bethe ansatz technique to the IRLM, reproducing some known results and identifications between different field theories and the model are presented. At the moment, we are still working on the main questions in this area.

Acknowledgements

First I would like to thank my supervisor Sam T. Carr for taking me as a PhD student, giving me one of the best opportunities in my life, and for his continuous support and guidance throughout my studies. I can fairly say this has been a very exciting and stimulating project, and I will never forget how much I have learned here. I also want to thank Jorge Quintanilla, whom apart from being my second supervisor, was my first contact before arriving at the university, and has always been a good support at Kent. I also thank Peter Schmitteckert for being in close collaboration with us during the project.

I thank the University of Kent for funding during my studies, and in particular the School of Physical Sciences, all staff, administrative, technical and academic, for any help provided in any sort of circumstances, as well as for any other moments shared together. Special thanks go to my office mates in room 114 and vicinities, with whom I have shared the PhD journey these last years. I have enjoyed the comfortable work environment with them, as well as nice moments outside the office.

During these years, I have had the opportunity to meet people outside my working environment, with whom I have shared very special moments. Special thanks go to Emilio, Mariona, Silvia, Ander, Patricia, Inés, María, Pablo, Jon, Ben, and many others I have had the chance to spend time with, surely you made this trip more enjoyable and interesting.

It is not easy to leave your friends when you go abroad, but it is nice to see that you still keep them. That is why I want to thank my old friends from Spain, with whom I've always enjoyed my time, and have proved to be an invaluable support to me. Regardless of circumstances, you have always made me feel like home when I needed it. Special thanks go to Álvaro, Juan, Borja, Manu, Álvaro, Jose, Alex, Kike, Juan, Guti, Miguel and Jesús. I also want to give special thanks to Verena, for her patience and care, becoming a very important person in my life during all these years here.

Finally, but most important, I want to thank all my family, for their unconditional love and support, with a very special mention to mum, dad and my sister Carmen. I consider myself very lucky to have you around. Without a doubt, you have made this possible.

Notation and conventions

During most of this thesis, there are several conventions adopted in order to simplify things. Here are some tips to follow:

- Throughout all the thesis, Planck's constant is set $\hbar = 1$, as well as the Fermi velocity $v_F = 1$, in accordance with natural units convention. The lattice spacing $a = 1$ unless specified.
- We will be working with a one dimensional model, therefore all expressions (integrals, Fourier transforms, coordinates etc...) are taken to be one dimensional.
- Unless specified, we will be working at $T = 0$ most of the time, since we are interested in the ground-state properties of the model. This sets the Fermi distribution as $n_F(T = 0) = \theta(\varepsilon)$, with θ representing a step function:

$$\theta(\varepsilon_F) = \begin{cases} 1 & \text{if } \varepsilon \leq \varepsilon_F \\ 0 & \text{if } \varepsilon > \varepsilon_F \end{cases} \quad (1)$$

where ε_F is the Fermi energy.

- We will use the greek letter Λ in field theory to describe the cut-off, that is, the biggest energy scale present in the problem. This shouldn't be confused with the parameter Λ used later in NRG calculations. The reason for leaving both quantities with the same notation is purely conventional from bibliography, since the parameter Λ is an important number when performing NRG calculations. In addition, the use of Λ for the cut-off is the conventional approach when working with field-theories.
- Most operators will be written without the caret $O = \hat{O}$ to simplify notation. Operators involving time are Heisenberg operators, i.e: $O(t) = e^{iHt} O e^{-iHt}$.

Contents

| | |
|--|-------------|
| Introduction | i |
| Acknowledgements | viii |
| Notation and conventions | ix |
| List of Figures | xiii |
| 1 Impurity models | 1 |
| 1.1 The Fano and Anderson models | 1 |
| 1.2 The X ray edge problem | 4 |
| 1.3 The Kondo (s-d exchange) model | 8 |
| 1.4 The Interacting Resonant Level Model | 10 |
| 2 Quantum Field Theory methods | 14 |
| 2.1 Perturbation theory and correlators | 14 |
| 2.1.1 IRLM: Perturbation theory $U = 0$ | 15 |
| 2.1.2 IRLM: Perturbation theory $U \neq 0$ | 17 |
| 2.2 Bosonization: A field theory technique in (1+1) dimensions | 19 |
| 2.2.1 Bosonization basics | 19 |
| 2.2.2 Bosonization of the massive Thirring model (MTM) | 20 |
| 2.3 Wilson's Numerical Renormalization Group (NRG) | 23 |
| 2.3.1 NRG basics | 24 |
| 2.3.2 NRG algorithm: iterative diagonalization | 24 |
| 2.3.3 Dynamical quantities computation within NRG | 26 |
| 2.3.4 Application example: The Anderson model | 27 |
| 2.4 The Anderson-Yuval method | 29 |
| 2.5 The Schrieffer-Wolff transformation | 31 |
| 2.5.1 Kondo model derived from the Anderson model | 32 |
| 2.6 The Bethe ansatz method | 34 |
| 2.6.1 Bethe ansatz basics | 35 |
| 2.6.2 Understanding the Bethe equations: Rapidities representation | 38 |
| 2.6.3 Bethe ansatz for the Massive Thirring Model | 39 |
| 3 The single channel IRLM: Thermodynamics | 42 |
| 3.1 The single channel IRLM | 42 |
| 3.1.1 Bosonization of the IRLM | 44 |

| | | |
|----------|---|------------|
| 3.1.2 | Scaling dimensions of operators and thermodynamic exponent α | 46 |
| 3.1.3 | The thermodynamic energy scale Γ | 48 |
| 3.1.4 | NRG for the $N = 1$ IRLM | 50 |
| 3.1.5 | The Toulouse point | 54 |
| 3.2 | Lattice treatment of the IRLM | 55 |
| 3.2.1 | Strong coupling limit | 55 |
| 3.2.2 | Coupling to a bath of fermions: $1/U$ corrections | 57 |
| 3.2.3 | Bosonization of the strong coupling hamiltonian | 61 |
| 3.2.4 | Mean Field Theory in the strong coupling limit | 62 |
| 3.3 | Brief summary of results | 64 |
| 4 | N channel IRLM: General features | 66 |
| 4.1 | Two channel ($N = 2$) IRLM | 66 |
| 4.1.1 | Bosonization and thermodynamic exponent: Duality | 67 |
| 4.1.2 | The prefactor $f(\alpha)$: Broken duality | 69 |
| 4.1.3 | Field vs lattice descriptions | 70 |
| 4.1.4 | Strong coupling limit in the lattice | 71 |
| 4.2 | General thermodynamics in the IRLM | 73 |
| 4.2.1 | Multichannel ($N > 1$) IRLM | 73 |
| 4.2.2 | Scaling dimensions of operators and thermodynamic exponent α | 74 |
| 4.2.3 | Discussion of quantum phase transitions | 75 |
| 4.3 | Brief summary | 79 |
| 4.3.1 | Results | 79 |
| 4.3.2 | Open questions | 79 |
| 5 | The IRLM: Dynamics | 81 |
| 5.1 | Interesting behaviour of dynamical quantities | 82 |
| 5.2 | Analytical approach to the problem | 84 |
| 5.2.1 | The IRLM as a sequence of X-ray processes: $U = 0$ solution | 84 |
| 5.3 | NRG dynamics in the IRLM | 87 |
| 5.3.1 | Dynamics at $g = 0$ | 87 |
| 5.3.2 | Dynamics at $g \neq 0$ | 89 |
| 5.3.3 | The dynamical exponent | 94 |
| 5.3.4 | Universal scaling at fixed g | 97 |
| 5.4 | Summary of main results | 100 |
| 6 | The IRLM: Bethe ansatz solution | 101 |
| 6.1 | The Filyov-Wiegmann solution | 102 |
| 6.1.1 | Single particle states: $U = 0$ | 103 |
| 6.1.2 | Single particle states: $U \neq 0$ | 105 |
| 6.1.3 | Two particle states: Scattering phase-shift | 105 |
| 6.1.4 | The Bethe ansatz: N particle wavefunction and rapidities representation | 108 |
| 6.1.5 | Calculation of rapidities distribution | 111 |
| 6.1.6 | Thermodynamic exponent by Bethe ansatz in FW solution | 112 |
| 6.2 | Relation of the IRLM to (1+1) integrable field theories | 114 |
| 6.2.1 | Relation to the Massive Thirring model | 114 |

| | | |
|----------|---|------------|
| 6.2.2 | Relation to Boundary Sine Gordon theory | 115 |
| 6.2.3 | S matrix of solitons | 116 |
| 6.2.4 | Connection to the IRLM | 118 |
| 6.3 | Lattice solution | 121 |
| 6.3.1 | One particle states | 121 |
| 6.3.2 | Two particle states | 122 |
| 6.3.3 | The unfolded picture in the lattice | 123 |
| 6.4 | Multichannel IRLM | 124 |
| 6.5 | Summary of main results | 126 |
| 7 | Conclusions and outlook | 127 |
| A | Ground state of the Massive Thirring Model by Bethe ansatz | 131 |
| B | Bosonization in the IRLM | 135 |
| C | RG treatment and the Sine Gordon model | 142 |
| D | Strong coupling in the $N = 2$ IRLM | 146 |
| E | The IRLM as a sequence of X-ray processes: $U \neq 0$ | 151 |
| F | Bethe ansatz calculations | 154 |
| | Bibliography | 178 |

List of Figures

| | | |
|-----|---|----|
| 1.1 | Absorption process in the X-ray edge problem. An X-ray hits the Fermi sea exactly at $t = 0$, leaving a hole behind which acts as a scattering point for subsequent times. The surrounding Fermi sea reallocates, and one studies the <i>response</i> of the system due to the abrupt change in the scattering potential. | 5 |
| 1.2 | Schematic view of the antiferromagnetic Kondo model. At temperatures higher than the Kondo temperature T_K , the impurity site is free. Interacting with surrounding electrons results in spin flips. When temperatures are below T_K , the local moment is <i>screened</i> by the surrounding electrons by formation of a singlet at the impurity site, therefore no local moment exists in this regime. | 9 |
| 1.3 | Schematic representation of the IRLM on its lattice version (a) for $N = 1$ channel and (b) for $N = 3$ channels. The impurity site in red, interacts with the nearest neighbours of the chain by Coulom like interaction U . The hybridization parameter t' is essential in describing physical processes. | 12 |
| 2.1 | The self-consistent approximation, where all Fock diagrams are included to infinite order by replacing the non-interacting propagator G_0^{dc} by the <i>dressed</i> propagator G^{dc} (double line). This is equivalent to summing all first order diagrams to infinite order. | 18 |
| 2.2 | Schematic view of the NRG method. The initial hamiltonian is composed by the impurity site (red) and the last site of the chain. When this part is diagonalized, a new site is added to the system with a tunneling probability t_n , then the system is diagonalized again and the process is repeated. The addition of more and more sites eventually leads to the construction of a chain that resembles the initial hamiltonian of the model at low energies. | 24 |
| 2.3 | NRG flow for the many-body eigenvalues of the Anderson model with 800 kept states and $\Lambda = 1.5$, $\varepsilon_0 = -0.05$, $V = 0.1$, $U = 0.1$, and a total of $N = 112$ sites. After some iterations, the flows converge to steady values representing the approximate low energy eigenstates. | 28 |
| 2.4 | NRG simulation for the Anderson model, with hybridization $V = 0.1$, for $U = 0$ and $\varepsilon_0 = 0$ (left) and $U = 0.1$ and $\varepsilon_0 = -0.05$ (right). We observe the appearance of the Kondo resonance when $\varepsilon_0 < 0$ and the local interaction on the impurity site is strongly repulsive (Kondo limit). Dashed lines are included as a guide to the eye. | 28 |

| | | |
|-----|---|----|
| 2.5 | Kondo problem as a succession of X-ray problems, where the impurity spin is flipped at subsequent times. The conduction electrons see an alternating potential, which corresponds to a set of absorption/emission Nozières processes for each spin. | 30 |
| 2.6 | Virtual processes in the Anderson model when the hybridization parameter $V \neq 0$, and $\varepsilon_0 < 0$ and $U \gg \varepsilon_0 $. The left process flips the impurity spin by passing through the high-energy state $ 0\rangle$, therefore the electron on the impurity makes a virtual jump to the surrounding bath. On the right hand side, an electron from the surrounding bath jumps virtually to the impurity site, so that the state $ \uparrow\downarrow\rangle$ is visited. In both processes, there is some energy exchange in order to allow for the spin flip. | 32 |
| 2.7 | A pictorial representation of the Yang-Baxter's equation. The order on which three particles (a,b,c) scatter from each other is irrelevant, and all processes have the same amplitude given by the factorised S matrix. | 36 |
| 2.8 | Rapidities plane representing two different states on the system. On the left side, the state with all negative energies occupied ($\text{Im}(\beta) = 0$) is represented. When one particle is added with positive energy ($\text{Im}(\beta) = \pi$), the configuration on the plane changes, and one has to take that into account to construct the true physical vacuum of the theory. | 38 |
| 2.9 | The MTM ground state fills all negative energies below the mass m_0 . When the limit $m_0 \rightarrow 0$ is taken, two different branches appear, each of them describing either right (red) or left (blue) movers. Such a description is important when the fields are unfolded. | 40 |
| 3.1 | NRG simulations for the calculation of the relevant energy scale Γ , for different values of the hybridization parameter t' . The vertical axis is in log scale. The discretization parameter $\Lambda = 1.5$ and the system size is of a total of $N = 82$ lattice sites. Analytical curves correspond to equation (3.36). | 51 |
| 3.2 | NRG simulations for the prefactor of equation (3.37)(continuous curve). All data points collapse on the same curve for different values of the hybridization parameter t' | 52 |
| 3.3 | NRG simulations for the thermodynamic exponent and the occupation number of the dot. (a) NRG data points for the thermodynamic exponent α as a function of the interaction parameter g . A very good agreement between numerics and the analytical formula equation (3.24) is shown. (b) NRG simulations for the occupation of the dot $\langle d^\dagger d \rangle$ as a function of the local chemical potential ε_0 . As interaction is increased, the width in the $\varepsilon_0 \sim 0$ grows. | 53 |

| | | |
|-----|---|----|
| 3.4 | Calculation of the Toulouse point in the IRLM/AKM by DMRG simulations. The Toulouse point happens when both curves intersect each other. For that specific value of the coupling J^z , the AKM maps to the Resonant Level Model (RLM), the non-interacting version of the IRLM. (Graph courtesy of Peter Schmitteckert) | 54 |
| 4.1 | Numerical data for the thermodynamic energy scale in the 2 channel IRLM. The data was directly extracted from [53]. The red curve shows the proposed form for Γ given in equation (4.11), where a good agreement with numerics is found. Note the numerical oscillations developed close to the self-dual point. | 69 |
| 4.2 | DMRG calculation for the thermodynamic exponent α as a function of the interaction parameter g , for $N = 1$ (red) to $N = 4$ (purple) channels. For the $N = 4$ channel case, higher values of g are avoided, since one gets closer to the quantum phase transition. Graph courtesy of Peter Schmitteckert. | 74 |
| 4.3 | Low-energy subspace states in the strong coupling regime of the IRLM for $N = 1$ channels (left) and $N = 3$ channels (right). The geometry of the model is responsible of all phase transitions encountered. . . . | 76 |
| 5.1 | Calculation of the renormalized hybridization Γ_d by perturbative RG (left, after [38]), and numerically by DMRG (right, after [52]). The perturbative RG procedure is known to fail to give accurate analytical predictions when compared with NRG numerics in [38]. Note how for the $N = 2$ channel case, $V \equiv \Gamma_d$ is shown to decrease as the interaction U is increased, whereas the same quantity is shown to increase in [52] when performing DMRG numerics. | 83 |
| 5.2 | NRG results for the non-interacting case $g = 0$ (a) NRG data points for a value of $J = 0.01$ in the IRLM. The continuous curve represents the Lorentzian function that fits the data. (b) NRG data points for several values of J , with the corresponding fitting Lorentzian functions. Note the log scale in both axis. In both figures, Λ represents the logarithmic discretization parameter of the band, whereas S_k is the total number of states kept after truncation of the hamiltonian. | 88 |
| 5.3 | Values for the hybridization parameter Γ_0 as a function of J . Data points correspond to the fitting performed over NRG data, where the function to fit was a Lorentzian of width Γ_0 | 89 |
| 5.4 | NRG data for the weak-coupling limit of the IRLM. (a) Data points have been presented here for different values of interaction g . Lines are inserted between points as a guide to the eye. Notice how as g is increased in value, the width of the resonance increases. (b) Logarithmic plot of NRG points and the corresponding fitting functions (5.22). | 91 |

| | | |
|-----|---|----|
| 5.5 | NRG data for different values of interaction g . (a) Representation of the spectral function on the impurity site at different values of interaction. Data points have been joined by lines in order to make the graph more visible. Note how at values of $g > 0.4$, a splitting in the central region starts to emerge (b) Spectral functions in the region of $g \in [0.4, 0.5]$ where the splitting starts to appear. | 93 |
| 5.6 | NRG calculation of the dynamical exponent. (a) Scaling of J with interaction parameter g . All data points correspond to NRG simulations, where values of $J = 0.01, 0.03, 0.05, 0.07, 0.09$ were used for the fitting. Note the deviation from the thermodynamic exponent α , which means J scales with a different exponent in the spectral function. (b) Different data points collected for small values of g , showing the deviation of numerical data from the analytical expression of α | 95 |
| 5.7 | NRG data for the prefactor $F(U)$ as a function of the bare interaction parameter U , showing that as U is increased, data points grow, leading to a divergence at big interactions. | 97 |
| 5.8 | NRG calculation of the impurity spectral functions. (a) Spectral functions calculated by NRG and scaled by $\pi(J^\gamma)$ as a function of the dimensionless $\tilde{\omega} = \omega/\Gamma$. NRG data points have been omitted in order to make the graph more visible. (b) Scaled spectral functions for different values of J , at interactions $g = 0$ (black), $g = 0.3$ (blue), $g = 0.5$ (red) and $g = 0.7$ (green). Note how, regardless of the value of J , all data points collapse onto the same curve, showing universality at fixed value of g | 98 |

Chapter 1

Impurity models

*“What makes the desert
beautiful - said the little prince -
is that somewhere it hides a
well”*

The little prince, Antoine de
Saint-Exupéry

The beauty about impurity models is that from apparently simple hamiltonians, very rich physics can be extracted from them. Many-body effects manifest through interactions between constituents of a system, but when an impurity or defect is inserted, some new interesting phenomena arise due to the interaction of the impurity with the surrounding environment. In this chapter we will briefly present some of the most important impurity models, with emphasis on their physics. In particular, we will also present the main model this thesis deals with, the Interacting Resonant Level Model (IRLM). For further reading, I recommend to follow [61], and the introductory part of [60], as well as chapter 16 of [62]. Also, Giamarchi [63] is an excellent reference to study such systems.

1.1 The Fano and Anderson models

One of the simplest impurity models was first introduced by Fano [8] in 1961. In this model, an impurity site is inserted in the material, and electrons from the surrounding bath can jump in and out the impurity site, since there is a non-zero probability amplitude for this tunneling effect to happen. It can occur that the system minimizes its energy by allowing a *hybridization* of the impurity electrons with the rest of the system, that is, the impurity doesn't survive as an isolated defect; instead, it becomes part of the surrounding environment. Therefore one of the main questions is: under which conditions can we observe a survival of the impurity site? This has to do with the concept of *emergent energy scale*. Due to the hybridization process described above, the system develops a relevant energy scale that separates two different behaviours; one where the local impurity survives apart from the environment, the other being the one with the impurity hybridized.

On its lattice version, the hamiltonian for the Fano model describing the process above is written in second quantised notation:

$$H_F = \sum_{k,\sigma} \varepsilon_k c_{k,\sigma}^\dagger c_{k,\sigma} + \varepsilon_0 \sum_{\sigma} d_{\sigma}^\dagger d_{\sigma} + \sum_{k,\sigma} V_k (d_{\sigma}^\dagger c_{k,\sigma} + \text{h.c.}) \quad (1.1)$$

where d_{σ}^\dagger represents an orbital or impurity creation (fermionic) operator with spin σ . The parameter ε_0 is the local chemical potential associated to the impurity site. When $\varepsilon_0 < 0$ it favours occupation of the impurity, whereas $\varepsilon_0 > 0$ makes the opposite. The parameter V_k is known as *hybridization* because it allows a hopping between the impurity and the surrounding bath, and usually is taken to be independent of k , which can be done within a good level of approximation. This is the same as considering a spherically symmetric potential, where only s waves interact with the potential. The problem is then reduced to a one dimensional problem, the dimension being determined by the distance to the impurity. Due to this hybridization with the surrounding sea, a new energy scale appears in the problem, which we will call Γ_0 . For $V_k = V$ independent of k , this scale is $\Gamma_0 \sim V^2$. The appearance of a new energy scale due to this hybridization term is called *resonance*, and it is a signature of *virtual bound state*, with timelife of order $\tau \sim \Gamma_0^{-1}$ (*virtual states* are not eigenstates of the hamiltonian, therefore they have finite lifetime). This means that because of the allowed hopping between the impurity and the rest of the environment, the local density of states on the impurity site is spreaded, so more excitations with energies in a range of width $\Delta\omega \sim \Gamma_0$ are allowed.

Notice that the hamiltonian is independent of spin, in the sense that each spin configuration can be treated separately from the other. The two main interesting quantities to calculate for this model are the *occupation number* of the impurity site and the *density of states* associated, which we will present here for $T = 0$. Both have well known formulas:

$$n_{d,\sigma} = \frac{1}{2} - \frac{1}{\pi} \arctan \left(\frac{\varepsilon_0}{\Gamma_0} \right) \quad A_d(\omega) = \frac{1}{\pi} \frac{\Gamma_0}{(\omega - \varepsilon_0)^2 + \Gamma_0^2} \quad (1.2)$$

It is worth noting that each of these quantities, although related between them, are different due to the *time dependence*. To be clear, the occupation number n_d is a *thermodynamic* quantity, since its computation doesn't require for the impurity operators to change with time. However, the impurity density of states is a *dynamical* quantity, since in order to calculate it, operators act on the state at different times. It is also of relevance since spectral functions can always be measured by ARPES technique. However, from the theoretical point of view, calculation of dynamical quantities proves to be a more challenging task.

For the Fano model, the impurity density of states has a Lorentzian shape, characteristic of resonant processes. Physically, it represents the probability of finding an excitation with energy ω . When the hybridization term is absent ($V = 0$), the spectral function on the impurity is a Dirac delta centered at $\omega = \varepsilon_0$. As hybridization is switched on, the delta function is spreaded, being the width equal to the new energy scale Γ_0 . However, the hamiltonian (1.1) doesn't develop a Curie term in

the susceptibility, and therefore, no local moment forms in the metallic environment. In order to account for this effect, the hamiltonian above needs some modification.

It was P.W.Anderson [7] the first one to propose a variant of the model as a possible explanation of the local moment survival. In his model, a Hubbard-like repulsive interaction is included between electrons occupying the impurity site:

$$H_A = \sum_{k,\sigma} \varepsilon_k c_{k,\sigma}^\dagger c_{k,\sigma} + \varepsilon_0 \sum_{\sigma} d_{\sigma}^\dagger d_{\sigma} + \sum_{k,\sigma} V_k (d_{\sigma}^\dagger c_{k,\sigma} + \text{h.c.}) + U n_{\uparrow} n_{\downarrow} \quad (1.3)$$

Note the new added term, where the operators $n_{\uparrow,\downarrow}$ represent the number operator for spin up/down on the impurity site respectively. This interacting term U is the one that allows for the local moment to survive, being the explanation simple: a double occupancy of the dot site costs energy $U > 0$, therefore single occupation is favoured. The reason for adding this new term to the hamiltonian is that for f or d orbitals magnetic impurities are usually associated with transition metals, where the d and f levels are partially occupied, therefore these materials are more likely to develop local moments, the wavefunctions being very localized within the nucleus region. Therefore, a double occupation on the impurity might have a large Coulomb repulsion between electrons.

There are two basic limits to study the Anderson model. One has been described already, and corresponds to the case when the Coulomb interaction $U = 0$ (see above). The other limit is the one that accounts for very strong repulsive interactions between the impurity electrons, but when there is no hybridization $V = 0$. In this limit, also called the *atomic limit*, there is a zero probability for an electron to jump from the impurity to the surrounding bath. The electron bath and the impurity site can then be treated as independent quantum systems. Therefore, the d or f orbital on the impurity has four possible states, all of them eigenstates of the hamiltonian:

$$H_{\text{atomic}} = \varepsilon_0 \sum_{\sigma=\uparrow,\downarrow} d_{\sigma}^\dagger d_{\sigma} + U n_{\uparrow} n_{\downarrow} \quad (1.4)$$

There is then the question about the formation of a local moment. In order for this to happen, the double and empty states of the orbital must correspond to excited states, so that the amount of energy needed to pass from one state to another is:

$$\begin{aligned} |\uparrow(\downarrow)\rangle &\rightarrow |\uparrow\downarrow\rangle & \Delta E &= \varepsilon_0 + U > 0 \\ |\uparrow(\downarrow)\rangle &\rightarrow |0\rangle & \Delta E &= -\varepsilon_0 > 0 \end{aligned} \quad (1.5)$$

where $|\uparrow(\downarrow)\rangle$ represents and either up or down quantum spin state. It is clear that when $\varepsilon_0 < 0$ and U is sufficiently large, the low-energy part of the hamiltonian (1.4) is given by the single spin states. This limit is called the *Kondo limit*, and it is the limit one has to work with in order to observe Kondo physics.

Here there has been a rough approximation to show the similarity between the Anderson and Kondo models, since V has been taken to be zero in the atomic limit. However, the connection between the Anderson and Kondo hamiltonians is even

more general ($V \neq 0$), as it can be shown by low energy arguments. From Anderson's model, it is deduced that at strong values of interaction U , an antiferromagnetic coupling between the conduction electrons and the localised magnet occurs. This is the essence of the work developed by Schrieffer and Wolff [10], which will be discussed in the next chapter. When one takes into account the situation $U \neq 0$ and $V \neq 0$, Mean Field Theory can still provide good information about the model. It can be shown that the energy scale associated with the resonance (Γ_0) divides now two regions, depending on the values of interaction: when $U < \pi\Gamma_0$, the impurity site is likely to be doubly occupied or empty, whereas as soon as $U > \pi\Gamma_0$, a local moment forms. When the impurity site is hybridized with the rest of the system (region $U < \pi\Gamma_0$), this manifests in a resonance centered around ε_0 as in the Fano model. However, as $U > \pi\Gamma_0$, this central resonance splits, giving rise to two other resonances now at energies ε_0 and $\varepsilon_0 + U$, which are called *Hubbard bands* (see [62] for details on this). They correspond to the high-energy part of the spectrum. There is more to say on the spectral function, since Langreth [64] theorem states that the local density of states of the impurity site must be pinned at $\omega = 0$:

$$A_d(\omega = 0) = \frac{1}{\pi\Gamma_0} \quad \forall U \quad (1.6)$$

and independent of interaction. This forces that, even when the splitting occurs, there has to be a very narrow resonance of height $\sim \Gamma_0^{-1}$. The width of such a narrow resonance is given by the *Kondo temperature*, that we will define later. This very narrow resonance is the *Kondo resonance*, or sometimes also called the *Abrikosov-Suhl resonance*.

There are many good reviews on the Anderson model, and I recommend [65, 62, 61] in the literature. Here we will limit ourselves to this short introduction to the model, but it already serves to illustrate the point that, from apparently simple-looking hamiltonians, many physical effects can be extracted. In fact, Anderson's model has been a cornerstone to understand most effects associated with the formation of local moments in metals.

1.2 The X ray edge problem

The X-ray edge problem was very actively studied in the late sixties and beginning of seventies, mostly by Nozières and others [15, 16, 17, 18, 19]. The theory of the X-ray edge problem was started by Mahan [14], as a way to understand X-ray interband transitions between electrons. Its popularity was also linked to a bigger problem: the Kondo problem and its developed singularities in the low energy sector. It was thought by the time that a deep understanding of such X-ray processes would shed some light into Kondo physics, as we will shortly see.

When a metal is kicked by an X-ray photon, an electron is promoted to the conduction band leaving a deep hole behind, in what is called the *absorption* process. Naturally, the emission process describes the opposite, where the electron

recombines with the system. After promotion of the electron, the Fermi sea reallocates and interacts with the remaining hole. This process is described in figure (1.1).

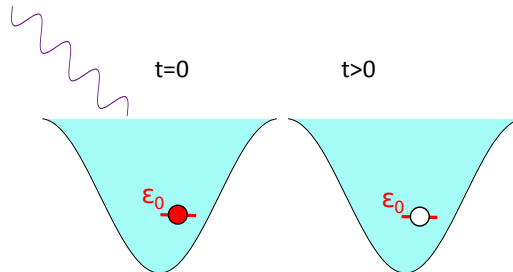


Figure 1.1: Absorption process in the X-ray edge problem. An X-ray hits the Fermi sea exactly at $t = 0$, leaving a hole behind which acts as a scattering point for subsequent times. The surrounding Fermi sea reallocates, and one studies the response of the system due to the abrupt change in the scattering potential.

In metals, these absorption and emission processes develop a threshold in their spectrum, due to the sharpness of the Fermi distribution. Mahan's [14] main result was to show, by perturbation theory, that the transition rate of the absorption process displays a divergent power-law behaviour in the low-energy sector near the threshold ω_0 . He conjectured for these divergences to sum up to a power law behaviour, so that the absorption rate has the form:

$$S(\omega) \sim \left(\frac{\xi_0}{\omega - \omega_c} \right)^{2\Delta} \theta(\omega - \omega_c) \quad (1.7)$$

where ξ_0 needs to be inserted as a cut-off in order to prevent the logarithms to diverge. The merit of Nozières et.al was to develop an alternative theory apart from perturbative expansions, in order to explain such singular behaviour. Moreover, they showed that the problem can be solved in an *exact* way by considering a single particle scattering off a time dependent potential [17]. The fact that the X-ray problem can be treated in the single particle picture comes from the non-dynamics of the hole. That is, the hole can either be created or destroyed, but nothing else, it cannot fluctuate between different states, as a quantum spin will do. Therefore, it is not necessary to keep track of the different stories of the impurity, in contrary to the Kondo problem, where one has to account for all possible spin configurations in time.

The total hamiltonian of an X-ray process is:

$$\begin{aligned} H &= H_x + \sum_k \varepsilon_k c_k^\dagger c_k + \varepsilon_0 d^\dagger d + V \sum_{kk'} c_k^\dagger c_{k'} d d^\dagger \\ H_x &= \sum_k W_k c_k^\dagger d e^{-i\omega t} + \text{h.c} \end{aligned} \quad (1.8)$$

The term H_x describes the coupling to the X-ray field. Note that the scattering term with V is absent when the deep hole is filled. In fact, this term is only present

suddenly after the X-ray has been absorbed (absorption process). In an emission process, this term is suddenly cancelled after emission, since the deep level gets filled again. Electrons in the metal experience a *transient* behaviour in such process.

Let us describe the absorption process, following Nozières [17]. The main quantity to compute is the transition rate between the ground state with no hole and that with the formed one after absorption. The transition rate is proportional to the imaginary part of the Fourier transform of the following response function [66]

$$S_{k,k'}(t-t') = \langle 0|T\{H_x(t)H_x(t')\}|0\rangle \quad (1.9)$$

where the curly brackets should *not* be confused with the anticommutation of operators. They just indicate the action of the time ordering operator T . The state $|0\rangle$ represents the initial state, before the creation/destruction of the hole takes place.

In the absorption process, the conduction electrons don't see a single impurity potential, therefore the Green's function takes the non-interacting form:

$$G_{kk'}(t) = \langle 0|T\{c_k(t)c_{k'}(0)\}|0\rangle = -\delta_{k,k'}e^{-i\varepsilon_k t}\theta(-t) \quad \varepsilon_k < 0 \quad (1.10)$$

The two important correlators to be found are the deep hole propagator, which in the absorption case is:

$$G^d(t) = \langle 0|T\{d(t)d^\dagger(t')\}|0\rangle = -e^{-i\varepsilon_0 t}\theta(-t) \quad (1.11)$$

and the correlator given by (1.9), so that knowing it we can extract the transition rate easily. Note that all correlators, as written, should carry a factor of $-i$ in the front, which can be reinserted later. When one passes from the many-body problem to the single particle time dependent problem, all diagrams for the deep hole are composed by loops at some times. This is the so called *linked-cluster expansion* [17, 66]. The contribution of these loops to $S_{kk'}$ is the aim of study in the paper by Nozieres and De Dominicis. Making use of the linked cluster theorem, the two correlators are expressed as:

$$\begin{aligned} S_{kk'} &= L_{kk'}(t)e^{C(t)} \\ G^d(t) &= e^{C(t)} \end{aligned} \quad (1.12)$$

Where the function $L_{kk'}(t)$ is related with the *bulk* conduction electrons propagator:

$$L_{kk'}(t) = -\varphi_{kk'}(t', t) \quad (1.13)$$

where this last correlator satisfies Dyson's equation, and is defined as:

$$\varphi_{kk'}(t', t) = \langle T\{c_k(t)c_{k'}^\dagger(t')\} \rangle \quad (1.14)$$

This is the total conduction electrons correlator, where the average is now respect to the ground state of the whole interacting system (That is, after the hole has been created in absorption, therefore the scattering potential in (1.8) is present).

All quantities above are then integrated for all possible modes k, k' , so that we are interested in calculating:

$$S^a = \int \frac{dkdk'}{(2\pi)^2} S_{k,k'}^a \quad (1.15)$$

The total conduction electron Green's function obeys Dyson's equation (in the absorption case):

$$\varphi^a(\tau, \tau', t, t') = G^a(t - t') + iV \int_t^{t'} d\tau'' G^a(\tau - \tau'') \varphi^a(\tau'', \tau', t, t') \quad (1.16)$$

where the initial propagator reduces to the non-interacting one (1.10), but taking into account all k modes:

$$G^a(t) = \int d\epsilon \nu(\epsilon) e^{-i\epsilon t - |\epsilon|\xi_0} = \frac{\nu_0}{it + (1/\xi_0)\text{sign}(t)} \quad (1.17)$$

and where we have taken the wide-band limit, so that $\nu_0 = \text{const}$. The asymptotic form of G^a can then be used when all time intervals are long compared to ξ_0^{-1} . The final result of all processes carried out in the paper [17] later gives the expression for the correlators:

$$\varphi_{kk'}^a(t, t') = G^e(t) \left(\frac{(t' - \tau')(\tau - t)}{(t' - \tau)(\tau' - t)} \right)^{\delta/\pi} \quad G^e(\omega) = \frac{G^a(\omega)}{1 - iV G^a(\omega)} \quad (1.18)$$

where the parameter δ comes from the following relations (see [17]):

$$\tan(\delta) = \frac{\pi g}{1 - \pi g \tan(\theta)} \quad \tan \theta = \frac{1}{\pi} \int_{-\infty}^{+\infty} d\epsilon P(1/\epsilon) e^{-2|\epsilon|/\xi_0} \quad (1.19)$$

Now it is clear that the transient behaviour of conduction electrons is given by the term in brackets in (1.18). When one takes the limit $t' \rightarrow -\infty$ and $t \rightarrow +\infty$, the correlator for the absorption case is that of the emission one, that is, when the scattering potential was present.

The exact result¹ for the $S_{k,k'}$ correlator is also given in terms of this parameter δ . By taking (1.18) and the limiting cases $\tau = t'$ and $\tau' = t$, a divergence occurs. The time cut-off ξ_0^{-1} needs to be introduced in order to make the expression finite:

$$L^a(t) = (i\nu_0/t)(i\xi_0 t)^{2\delta/\pi} \theta(-t) \quad (1.20)$$

Let us stop here to interpret this result. The correlation function still preserves its power law behaviour for long times. However, due to the appearance of the scattering potential, the exponent of the decay is different. This power law decay of correlation functions is intimately related with Anderson's orthogonality catastrophe effect [67]. The total correlator is then:

$$S^a(t) = (i\nu_0/t)(i\xi_0 t)^{2\delta/\pi - (\delta/\pi)^2} e^{i\omega_0 t} \theta(-t) \quad (1.21)$$

¹Here the term *exact* is meant within *logarithmic accuracy*, since the asymptotic form of correlators has been used. For details on this see [17].

In the case $\delta > 0$, that is, repulsive interaction with the scattering point, the decay is *slower*. Now let's look at the deep hole's correlator, which for the absorption case has the form [17]

$$G^d(t) = -(i\xi_0 t)^{-(\delta/\pi)^2} e^{-i\varepsilon_0 t} \theta(-t) \quad (1.22)$$

If we compare this expression with the non-interacting case (1.11), we see that the long time (low-energy) behaviour of the deep hole develops a power law. Such a power law decay is related with the total life-time of the hole, before electrons of the surrounding sea recombine.

The detailed analysis of this problem, carried out by Nozieres and De Dominicis is quite broad to show in detail here, so we have mentioned only the main physical results of their paper. The reader is referred to [15, 16] for a perturbative treatment of the X-ray problem, whereas [17], which is the method we just described, solves the problem in an *exact* way as a one body problem. We also cite [63, 65, 66] for reviews.

1.3 The Kondo (s-d exchange) model

The study of local moments inside metallic environments brought up the idea that the coupling between the magnet and the rest of electrons should be antiferromagnetic. One then needs a hamiltonian describing such a process, which on its simpler version, implies an *exchange* term in the energy between the alignment of the isolated spin and the spin of the surrounding electrons. Such a model is known as the *s-d exchange model*, or sometimes called the *Kondo model*. On its isotropic form, it is written in second quantized notation:

$$H_{s-d} = \sum_{k,\sigma} \epsilon_{k,\sigma} c_{k,\sigma}^\dagger c_{k,\sigma} + J \sum_{k,k',\sigma,\sigma'} c_{k,\sigma}^\dagger c_{k',\sigma} \vec{\sigma}_{\sigma,\sigma'} \cdot \vec{S} \quad J > 0 \quad (1.23)$$

The model is sometimes conveniently written in terms of the upper/lower spin operators. In this general case, there is also the possibility that the parallel coupling (the one in the z direction) is different from the perpendicular one (the one flipping the impurity and conduction electron spin). If this happens, this is the *anisotropic Kondo model*, whose hamiltonian is written as:

$$H_{AKM} = H_0 + J_\perp \sum_{k,k'} \left(c_{k,\uparrow}^\dagger c_{k',\downarrow} \sigma^- S^+ + c_{k,\downarrow}^\dagger c_{k',\uparrow} \sigma^+ S^- \right) + \frac{J_\parallel}{2} \sum_{k,k',\sigma=\pm} c_{k,\sigma}^\dagger c_{k',\sigma} \sigma^z S^z \quad (1.24)$$

where the first term H_0 is the non-interacting part in (1.23). In the anisotropic version of the model, one of the terms results in an energy cost when the spin flips both in the impurity and the electron of the band. The energy cost associated with this process is J_\perp . The existence of this term is what makes the Kondo problem difficult

to treat. In the case $J_{\perp} = 0$, the problem is trivial, as the hamiltonian can be divided into the up and down spin sectors, each of them containing a scattering potential given by the sign of S^z . This is the process described by the term proportional to J_{\parallel} .

It took time to understand the real physics described by hamiltonian (1.23). One of the main reasons has been discussed previously: When perturbation theory is applied, a divergent logarithm in temperature is found in the resistivity, as shown by Kondo [9] in 1964. The nature of this logarithmic divergences must be found in a low energy description of the model, and of course, as $T \rightarrow 0$ the solution must be finite. The method to study such a scaling behaviour was developed by Anderson [11] in the so called *poor man's scaling* in 1970. Anderson's scaling treatment of the Kondo problem is supported by the concept of renormalization : Under variations of the cut-off energy of the system, coupling parameters change. In other words, the coupling constants J_{\parallel} and J_{\perp} depend on the cut-off energy Λ in some way. The variation of these parameters with Λ is what defines trajectories in parameter space, allowing for a good understanding of the system's behaviour. The main result in Anderson's paper [11] is that it proves the existence of only one relevant energy scale, separating two regions, one where the local moment exists apart from the surrounding environment, and one where the spin is totally screened by the surrounding electrons (strong coupling limit). The energy scale separating both limits has a well defined dependence on the coupling parameter $J > 0$:

$$T_K \sim e^{-1/\nu J} \quad (1.25)$$

where ν is the electron density of states of the metal. This energy scale is called the *Kondo temperature*. For temperatures higher than this value, the local moment survives in the surrounding environment, and therefore, a Curie like term appears in the susceptibility. This is called the *weak coupling* limit of the model. On the other hand, as temperature is lowered, the strong coupling regime is reached, and a perturbative treatment of the model is not possible. This is because the equations defining the *running* of the coupling constants present, above the isotropic line, escaping trajectories for every value $J\nu \ll 1$. Therefore, in the antiferromagnetic Kondo model, interaction strength increases at lower energies (larger distances). This is an example of *asymptotic freedom*, where low-energy properties of a system are described by strong couplings.

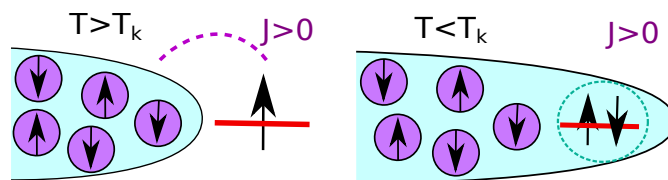


Figure 1.2: Schematic view of the antiferromagnetic Kondo model. At temperatures higher than the Kondo temperature T_K , the impurity site is free. Interacting with surrounding electrons results in spin flips. When temperatures are below T_K , the local moment is screened by the surrounding electrons by formation of a singlet at the impurity site, therefore no local moment exists in this regime.

Therefore, Anderson's paper was unable to calculate exactly what happens at $T < T_K$ in the antiferromagnetic case, but gave an insight of the underlying mechanism. It is now known that due to this strong antiferromagnetic coupling, the impurity spin *hybridizes* with the conduction electrons at temperatures below T_K . In this regime, the impurity doesn't exist on its own anymore, and a singlet state is formed [68, 69], therefore no Curie term is found on the impurity susceptibility. Due to this, the system behaves as a Fermi liquid, with renormalized quasiparticle masses. This renormalization of the parameters is found in the thermodynamic properties of the model at $T = 0$. In his famous paper in 1975, Wilson [25] proved numerically the following relationship:

$$\lim_{T \rightarrow 0} \frac{C_V(T)}{T\chi(T)} = \frac{1}{2} \frac{4\pi^2 k^2}{3} = \frac{1}{2} \lim_{T \rightarrow 0} \frac{C_V^0(T)}{T\chi^0(T)} \quad (1.26)$$

Thus, in the $T \rightarrow 0$ limit, the ratio between the specific heat and the susceptibility (called the *Wilson ratio*) is half that of a system of non-interacting electrons. This proved both the singlet formation and the Fermi liquid nature of the Kondo model in the strong coupling regime.

There is a vast and varied study of the Kondo problem in the literature, which almost every book on many-body physics contains [62, 65, 63, 70]. We summarize here the most important features of the Kondo model:

- There is only one relevant energy scale in the problem, called the Kondo temperature and given by $T_K \sim e^{-1/\nu J}$.
- This energy scale separates two regimes, the weak and strong coupling sectors. In the weak coupling sector, the impurity survives as a local moment inside the metal, whereas in the strong coupling, the local moment forms a singlet with conduction electrons, and gets *screened*.
- Perturbative methods fail to describe the low-energy physics of the Kondo model in the antiferromagnetic strong coupling regime. A quantitative treatment must involve non-perturbative calculations, either numerical (Wilson's NRG), or analytical (Anderson-Yuval, Bethe ansatz, see [22, 23, 24, 57, 60]).

The Kondo model is, once again, the great example about *top down approach* models. From its apparently simple looking, very fundamental physics can be extracted, and Kondo physics have found applications in different branches of physics, for example, in quark confinement theories.

1.4 The Interacting Resonant Level Model

We introduce now the model we will deal with throughout thesis, known as the Interacting Resonant Level Model (IRLM), or sometimes called Resonant Level Model (RLM) in the literature. Here we will use the RLM to refer to the IRLM in the absence of interaction, so that the RLM is the spinless version of the Fano model

(1.1) described before. The IRLM was first proposed by Wiegmann and Finkel'shtein [36] in 1978, as a toy model to search for an exact solution of the Kondo model. The model can be directly extracted from the anisotropic Kondo model by an exact relation between parameters [36, 37], and both partition functions are shown to be equivalent. Much of the previous work done in the model has mostly been presented in the introduction, so we will cite each work individually when convenient to compare results.

The *simplicity* of the IRLM lays on its non-spin dependence. The meaning of having spinless fermions corresponds to the situation where a magnetic field is applied to the system, so that spin is *polarized*. Nevertheless, these spinless fermions arise naturally from the transformation of the AKM. The model describes an isolated spinless impurity hybridizing with a bath of spinless fermions. Although it might look fairly similar to the X-ray edge problem (see equation (1.8)), this is a different model. First because it is directly extracted from the anisotropic Kondo model, by exact manipulations between operators. Secondly, the X-ray edge problem describes a dynamic situation where the dot is created in the metallic environment, and one studies how the system reallocates due to this sudden potential change. In other words, the X-ray problem describes a transient behaviour of conduction electrons due to a sudden creation/annihilation of a hole. In contrast, the impurity is *dynamic* in the IRLM, and therefore, allows fluctuations on the dot's occupancy within time.

The main difference between this model and the Fano (or non-interacting Anderson) model, is that apart from the hybridization, there is an interacting term between the impurity site and the last site of the surrounding bath. The schematic view of such a model is shown in figure (1.3).

On its lattice version, the single channel IRLM is represented by the following hamiltonian:

$$H = -t \sum_{i=1}^N c_{i+1}^\dagger c_i + \text{h.c} - \varepsilon_0 d^\dagger d + t'(d^\dagger c_0 + \text{h.c}) + U(d^\dagger d - 1/2)(c_0^\dagger c_0 - \rho) \quad (1.27)$$

Here ρ represents the *vacuum* expectation value of conduction electrons at the origin. Since we will be working in the particle-hole symmetric case, this is usually taken to be $\rho = 1/2$. There are four different contributions to this hamiltonian. The first part of the r.h.s corresponds to a simple non-interacting tight binding chain, which is diagonal in momentum space:

$$H_0 = -t \sum_{i=1}^N c_{i+1}^\dagger c_i + \text{h.c} = \sum_k \varepsilon_k c_k^\dagger c_k \quad \varepsilon_k = -2t \cos(k) \quad (1.28)$$

Thus, the non-interacting part of the system corresponds to a cosine band where different k levels are filled according to Pauli's exclusion principle. Since our fermions are spinless, that means each k state can be occupied only by one single fermion. It is also worth mentioning the limit we will be dealing with throughout this thesis. Being interested in *low-energy excitations*, the so called *wide-band limit* consists

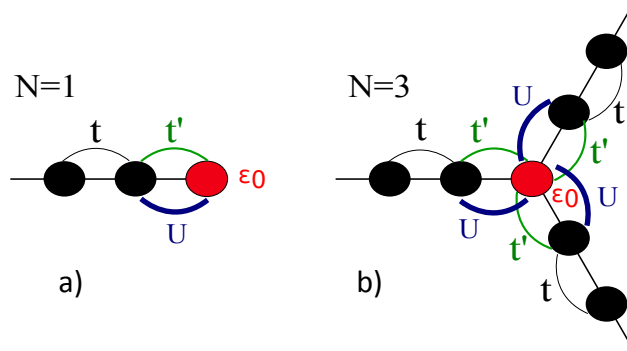


Figure 1.3: Schematic representation of the IRLM on its lattice version (a) for $N = 1$ channel and (b) for $N = 3$ channels. The impurity site in red, interacts with the nearest neighbours of the chain by Coulomb like interaction U . The hybridization parameter t' is essential in describing physical processes.

on considering a constant density of states associated with the dispersion relation (1.28). This corresponds to study the system considering only excitations close to the Fermi surface, which in this case is located at $k_F = \pm\pi/2$. This is equivalent to a *linearization of the spectrum*. Then, in this limit, the *bulk* density of states is a constant independent of energies:

$$\nu(\varepsilon) = \text{cont.} \quad (1.29)$$

We consider now the *hybridization part*, proportional to t' . This describes the tunneling process between electrons in the metal and the impurity site, with probability amplitude t' . Throughout the study of the model, this value of t' remains small as compared to the bandwidth, that is $t'/t \ll 1$. In this limit, it is then assumed that electrons move inside the material hopping from one place to another (tight-binding) with the same probability, whereas hopping from the metal to the impurity site carries a smaller probability amplitude for the process to occur. This is also the case in the Anderson model (1.3), where a similar hybridization term is present in the system. In fact, we will see later that this hybridization defines an *energy scale* Γ separating two different regions: for $T < \Gamma$, the impurity site is *hybridized with the system*, whereas at $T > \Gamma$ the impurity is decoupled and isolated from the rest of the environment.

The part including the parameter ε_0 represents the local chemical potential of the impurity. When the impurity is filled ($d^+d = 1$), this term contributes with an energy ε_0 . The limit where $\varepsilon_0 \rightarrow 0$ represents the *particle-hole* symmetry in the model, which is the main limit we will be dealing with. In this limit, the system is said to be *at resonance*. Finally, the interacting term is written in the normal ordered version of operators, where the subtracted quantities are the vacuum expectation values of the impurity and chain site. Note that this term involves an interaction between the impurity and *the last site of the chain*, as opposed to Anderson's model where the interaction occurs between two fermions occupying the impurity (see 1.3).

The continuum limit is the field theory version of the model. In this version, the

hamiltonian for the IRLM is:

$$\begin{aligned}
H = & -i \int_{-\infty}^0 dx \left(\psi_R^\dagger(x) \partial_x \psi_R(x) - \psi_L^\dagger(x) \partial_x \psi_L(x) \right) \\
& + \varepsilon_0 d^\dagger d + t' \sum_{i=L,R} \int_{-\infty}^0 dx \delta(x) d^\dagger \psi_i(x) \\
& + \text{h.c} + U \sum_{i=R,L} \int dx \delta(x) (d^\dagger d - 1/2) (\psi_i^\dagger(x) \psi_i(x) - \rho) \quad (1.30)
\end{aligned}$$

Notice that the x coordinate represents a half line, since it indicates the distance to the central scatterer point. It is then convenient to *unfold* the fields in order to map the problem onto the whole line $(-\infty, +\infty)$. In this unfolding, left movers in the negative semiaxis can be interpreted as right movers in the positive semiaxis due to the shared boundary conditions, that is:

$$\psi_L(x < 0) = \psi_R(x > 0) \quad (1.31)$$

With this, the above hamiltonian takes the form:

$$\begin{aligned}
H = & -i \int_{-\infty}^{+\infty} dx \psi^\dagger(x) \partial_x \psi(x) + \varepsilon_0 d^\dagger d + t' \int_{-\infty}^{+\infty} dx \delta(x) (d^\dagger \psi(x) + \text{h.c}) \\
& + U \int_{-\infty}^{+\infty} dx \delta(x) (d^\dagger d - 1/2) (\psi^\dagger(x) \psi(x) - \rho) \quad (1.32)
\end{aligned}$$

where now all fermionic fields are right-movers on the entire line. The problem is then reduce to a single species of fermions (right-movers) in the whole dimension. We will refer to these lines as *channels* or *leads* attached to the impurity site. Variants of the model are introduced, for example, if one attaches more than one channel to the impurity. The multichannel version of the model includes M total channels:

$$\begin{aligned}
H_{MIRLM} = & -t \sum_{\alpha=1}^M \sum_{i=1}^N c_{\alpha,i+1}^\dagger c_{\alpha,i} + \text{h.c} - \varepsilon_0 d^\dagger d + t' \sum_{\alpha=1}^M (d^\dagger c_{\alpha,0} + \text{h.c}) \\
& + U \sum_{\alpha=1}^M (d^\dagger d - 1/2) (c_{\alpha,0}^\dagger c_{\alpha,0} - \rho) \quad (1.33)
\end{aligned}$$

In order to get the continuum version of the multichannel case, one proceeds in a similar way as in the single channel version [40]. Of particular interest is the *two-channel* version of the model, since it is the one where *transport* properties can be studied.

Throughout this thesis, an intense study of the IRLM will be done. Although one would wish to have a complete theory of such a model, regardless of the total number of channels attached, we will suddenly discover that this represents by itself a great task. In particular, one needs first to understand the importance of the single channel case, since most of the fundamental physics of the model can be extracted from there. One of the main goals of this thesis is to illustrate all the rich physics that can be extracted from the IRLM.

Chapter 2

Quantum Field Theory methods

*“I learned very early the
difference between knowing the
name of something and knowing
something”*

Richard P. Feynman

In this chapter, some fundamental techniques for the study of quantum many-body problems are discussed, in application to impurity models. Without going into technical details, an introduction to these methods is aimed to provide the reader a good starting point to follow future calculations. Further reading is always indicated when convenient.

2.1 Perturbation theory and correlators

The easiest way to treat an interacting problem is by assuming that interactions between constituents are *weak* in comparison with the individual energies of each particle. This approximation, although it might seem a bit rough in principle, provides a good understanding for many macroscopic properties of materials. In fact, Landau’s theory of metals, what is called the *Fermi liquid theory*, rests on the idea of treating interactions as perturbations. When treating an interacting system, sometimes going to first or second order of perturbation accounts for a good description of the fundamental physics. However, this is rarely the case in *strongly correlated systems*, where perturbation theory can be considered a poor approach to treat the problem. Nonetheless, the method has been applied to the IRLM previously [37, 38], and it is worth to reproduce some of its results by a slightly different approach apart from perturbative RG. Some results from [49] are reproduced in this fashion.

2.1.1 IRLM: Perturbation theory $U = 0$

The desired quantity to calculate is the time-ordered Green's function:

$$G(x, x', t, t') = -i\langle \hat{T}\psi(x, t)\psi^\dagger(x', t') \rangle \quad G(\omega, k) = \int dx dt e^{i(\omega t + kx)} G(x, t) \quad (2.1)$$

where \hat{T} is the time ordering operator. This quantity is of interest, since one of its components, the *retarded* one, is related to the spectral density, which can be measured experimentally. To calculate the retarded Green function from the time ordered one, one chooses that part of the function which is analytic in the upper half plane of ω . The retarded Green function and the spectral function are related to each other:

$$A(\omega) = -\frac{1}{\pi} \sum_k \text{Im} G_R(\omega, k) \quad G_R(\omega, k) = \int dx dt e^{i(\omega t + kx)} G_R(x, t) \quad (2.2)$$

The spectral density is of relevance since it can be measured experimentally by ARPES techniques. One of the main questions in this area is how to provide a good approximation for the spectral function on the impurity site, since perturbation theory offers a poor description. The development of methods for the calculation of such quantities is then very desirable. Chapter 5 of this thesis is concerned with the calculation of such quantities, therefore understanding the fundamentals here is essential.

The total change on the Green function by interactions is encoded in Dyson's equation:

$$G(\omega, k) = G_0(\omega, k) + G_0(\omega, k)\Sigma(\omega, k)G(\omega, k) \quad (2.3)$$

The quantity $\Sigma(\omega, k)$ is the *self-energy*, and it includes all *compact* and different interacting diagrams. The calculation of the self-energy is the main problem to deal with, since in some cases, diagrams depend on the excitation energies ω . Dyson's equation states that by knowing the self-energy, one can compute the total Green's function of the interacting system in the simple way written above. The computation of Σ in an exact way is in most cases impossible, therefore the problem is only worth to be solved by this method if perturbation theory accounts for a good description of the system. Strongly correlated systems are not, in general, well described by this perturbative approaches.

Let us apply perturbation theory methods to the IRLM. We can divide the hamiltonian in two parts:

$$\begin{aligned} H &= H_0 + H_U \\ H_0 &= -t \sum_i c_i^\dagger c_{i+1} + \text{h.c} + \varepsilon_0 d^\dagger d + \underbrace{t'(d^\dagger c_0 + \text{h.c})}_{H_V} \\ H_U &= U(d^\dagger d - 1/2)(c_0^\dagger c_0 - 1/2) \end{aligned} \quad (2.4)$$

Let us forget first about H_U and H_V . Then the system consists on an isolated impurity with local chemical potential ε_0 and a non-interacting bath of electrons. The corresponding Green functions are easily calculated:

$$G_0^d(\omega) = \frac{1}{\omega - \varepsilon_0 \pm i0^+} \quad \mathcal{G}_0^L(\omega) = \frac{1}{\omega - \varepsilon_k \pm i\delta} \quad (2.5)$$

The second term in (2.5) is the Green function corresponding to a non-degenerate electron gas. We are interested in this propagator but happening exactly at the impurity site $x = 0$. Thus, a summation over all momenta is carried out:

$$G_0^L(\omega) = \int \frac{dk}{2\pi} \mathcal{G}_0^L(k, \omega) = \int d\varepsilon \nu(\varepsilon) \mathcal{G}_0^L(\varepsilon, \omega) = \int d\varepsilon \nu(\varepsilon) \frac{1}{\omega - \varepsilon + i\delta \text{sign}(\varepsilon)} \quad (2.6)$$

This term will have both real and imaginary parts; however, if we consider a flat (constant) density of states ν , the real part can be neglected since it is a principal value integral and the result gives 0. So we have to deal with the imaginary part at the end:

$$G_0^L(\omega) = i \int d\varepsilon \nu \lim_{\delta \rightarrow 0} \frac{-\delta \text{sign}(\varepsilon)}{(\omega - \varepsilon)^2 + \delta^2} = -i\pi \nu \text{sign}(\omega) \quad (2.7)$$

The first perturbative treatment is done in the parameter t' of the IRLM, which can be done till infinite order of perturbation, due to the form of the diagrams. Therefore we first take the case $U = 0$. The diagrams involved are, indeed, non-interacting in this case. We can write the Green functions in matrix form:

$$\mathbf{G}_0(\omega) = \begin{pmatrix} G_0^d(\omega) & 0 \\ 0 & G_0^L(\omega) \end{pmatrix}$$

Here, off-diagonal terms represent the *anomalous* correlators $G^{cd} = G^{dc}$. Every time there is a scattering process in the system, is between the wire (c) and the dot (d), that means that we can consider the scattering matrix as a non-diagonal 2×2 matrix, with the same scattering amplitude going from the dot to the channel than the one going from the channel to the dot. This is a consequence of Wick's theorem for the system at $U = 0$, therefore:

$$\Sigma = \begin{pmatrix} 0 & t' \\ t' & 0 \end{pmatrix}$$

is the *self-energy* matrix. The total Green function of the system is given by Dyson's equation in matrix form:

$$\mathbf{G}(\omega) = \mathbf{G}_0(\omega) + \mathbf{G}_0(\omega) \Sigma \mathbf{G}(\omega) \quad (2.8)$$

This is exactly equivalent as developing each of the Green's functions individually using the diagrammatic expansion. In fact, this is done when the diagrammatic expansion is taken to infinite order, and we complete the Dyson series. Inverting Dyson's equation we get the total Green function for $U = 0$:

$$\mathbf{G}(\omega) = \begin{pmatrix} \frac{1}{\omega - \varepsilon_0 + i\Gamma_0 \text{sign}(\omega)} & \frac{J \text{sign}(\omega) \nu_L}{-\Gamma_0 \text{sign}(\omega) + i(\omega - \varepsilon_0)} \\ \frac{J \text{sign}(\omega) \nu_L}{-\Gamma_0 \text{sign}(\omega) + i(\omega - \varepsilon_0)} & \frac{\text{sign}(\omega) \nu_L (\omega - \varepsilon_0)}{-\Gamma_0 \text{sign}(\omega) + i(\omega - \varepsilon_0)} \end{pmatrix} \quad (2.9)$$

Here the quantity $\Gamma_0 = \pi\nu t^2$ appears for the first time. This defines the hybridization energy scale of the system in the absence of interaction. This is natural since, having summed all diagrams to infinite order, the problem is trivial and corresponds to the Fano model we discussed earlier in chapter 1. Thus, in the limit $U = 0$, all physics of the IRLM are exactly equivalent to the Anderson model at $U = 0$. In particular, the impurity density of states is given by a Lorentzian of width Γ_0 :

$$A(\omega) = \frac{1}{\pi} \frac{\Gamma_0}{(\omega - \varepsilon_0)^2 + \Gamma_0^2} \quad (2.10)$$

which is easily seen by taking the *retarded* form of the Green function (2.9).

2.1.2 IRLM: Perturbation theory $U \neq 0$

Having calculated the correlators in the $U = 0$ case, one can start building up a perturbative solution when $U \neq 0$. Thing is, now there are *crossed* propagators like G_0^{dc} (the non-diagonal terms in (2.9)), whose physical significance is also not clear. This manifests in more possible terms when working out Wick contractions, therefore going to second order of perturbation adds enough complexity in the diagrammatic expansion. One can however, start by the simplest treatment considering only first order contributions. We then consider the first order diagrams contributing to the self-energy, those called Fock diagrams. The total interacting Green function is now called $\mathbf{G}(\omega)$. In a similar way as in the $U \neq 0$ case, Dyson's series is solved in matrix form:

$$\mathbf{G}(\omega) = \mathbf{G}_0(\omega) + \mathbf{G}_0(\omega)\mathbf{\Sigma}\mathbf{G}(\omega) \quad (2.11)$$

where $\mathbf{\Sigma}$ is the self-energy matrix, and G_0 is given by (2.9). The form for the self-energy matrix $\mathbf{\Sigma}$:

$$\mathbf{\Sigma} = \begin{pmatrix} \Sigma^d & \Sigma^{dc} \\ \Sigma^{cd} & \Sigma^c \end{pmatrix} \quad (2.12)$$

with $\Sigma^{dc} = \Sigma^{cd}$. The appearance of off-diagonal terms has to do with the fact that $G^{dc} \neq 0$, therefore contractions between impurity and lattice operators can be performed now in the $U \neq 0$ case. The total Green function can be calculated by just inverting Dyson's equation. Of particular interest is the impurity Green's function G^d , which has the following form:

$$G^d(\omega) = \frac{1}{(\omega - \varepsilon_0 - \Sigma^d) + i\text{sign}(\omega)\Gamma_0(1 + (\Sigma^{dc}/t')^2)(1 + i\nu\Sigma^c)^{-1}} \quad (2.13)$$

Here, all self-energies have real and imaginary part, and they can depend on ω . Note that if the self-energies depend on ω , the imaginary part of the *retarded* Green function doesn't remain as a Lorentzian anymore, thus changing the local density of states at the impurity.

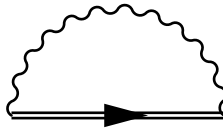


Figure 2.1: The self-consistent approximation, where all Fock diagrams are included to infinite order by replacing the non-interacting propagator G_0^{dc} by the dressed propagator G^{dc} (double line). This is equivalent to summing all first order diagrams to infinite order.

One of the easiest assumptions is to let $\Sigma^d = \Sigma^c = 0$. After all, Σ^d can be absorbed in a renormalization of ε_0 , whereas the Σ^c renormalizes the density of states of conduction electrons. In this approximation, the lead and dot-lead propagators are:

$$G^{dc}(\omega) = -i(\Sigma^{dc} + J)\nu \text{sign}(\omega)G^d(\omega) \quad G^L(\omega) = -i\nu(\omega - \varepsilon_0)\text{sign}(\omega)G^d(\omega)$$

In first order of perturbation, only Fock diagrams contribute to the crossed terms Σ^{cd} . By use of Feynman's rules [65], this contribution is given by the following integral:

$$\Sigma^{dc} = iU \int_{-\Lambda}^{\Lambda} \frac{d\epsilon}{2\pi} e^{i\epsilon 0^+} G_0^{dc}(\epsilon) \quad (2.14)$$

where a cut-off Λ needs to be inserted in order to prevent divergences. The self-consistent calculation then consists on replacing G_0^{dc} (the non-diagonal terms in (2.9)) by the total interacting Green function G^{dc} , which is given from (2.11). The self-consistency equation determines the self-energy when all first order diagrams are taken into account:

$$x = \frac{\Sigma^{dc}}{t'} = \frac{U\nu(1+x)}{2\pi} \log\left(\frac{\Lambda^2}{\varepsilon_0^2 + \Gamma^2}\right) \quad \Gamma = \Gamma_0(1+x)^2 \quad (2.15)$$

Thus, the first order correction to the hybridization is given by ($\varepsilon_0 = 0$):

$$\Gamma = \frac{\Gamma_0}{\left(1 - U\nu \log(\Lambda/\Gamma)\right)^2} \quad (2.16)$$

This result agrees with [37, 38, 39, 49] calculations, and is only valid when $U\nu \ll 1$. Due to interaction with the surrounding sea, the hybridization parameter t' scales with a new exponent:

$$\Gamma \sim (t')^{\frac{2}{1+2g}} \quad g = U\nu \quad (2.17)$$

Within this approximation, the spectral function preserves the Lorentzian shape like in (2.10), but with a renormalized width Γ :

$$A_{\text{SC}}(\omega) = \frac{1}{\pi} \frac{\Gamma}{(\omega - \varepsilon_0)^2 + \Gamma^2} \quad (2.18)$$

where SC stands for *self-consistent*. This is a first order result, and as such, it shouldn't be taken too seriously to describe the actual renormalization of t' , nor the exact form of the spectral function on the impurity site. The key point to illustrate here is twofold: First, that all first order diagrams don't alter the functional form of $A(\omega)$. This is because first order diagrams don't depend on excitation energies ω . The second has to do with complex nature of Σ , which accounts for different contributions to the impurity spectral function. Different diagrams can depend on ω in a non-trivial way. Furthermore, these diagrams can develop *logarithmic divergences* in higher order of perturbation. For instance, if that will happen in Σ^d (which we neglected in our treatment here), this will indicate the appearance of a *non-Fermi liquid* exponent in ω (i.e. the spectral function might depend on ω^γ , with $\gamma \neq 2$). The preservation of an exponent $\gamma = 2$ in the low ω sector of an impurity spectral function is a signature of Fermi liquid behaviour (see [71]).

2.2 Bosonization: A field theory technique in (1+1) dimensions

In one dimension, there is an analogy between fermions and bosons. This analogy makes the solution of some one dimensional models much simpler, since an initially complicated fermionic problem can be reduced to a non-interacting bosonic hamiltonian, whose solution is well known. The method is non-perturbative, since it provides *exact* operator relationships between bosonic and fermionic fields, and accounts for the exact calculation of exponents in correlation functions. However, this technique is quite extensive, and we won't expose it here in detail, so we refer the reader to the literature for study. Recommended references for this are those by [63, 66, 72, 73, 74].

2.2.1 Bosonization basics

In one dimension, and close to the Fermi level, density fluctuations have a well defined energy-dispersion:

$$\rho_q = \sum_k c_{k+q}^\dagger c_k \quad \varepsilon(q) = vq \quad (2.19)$$

where v is the Fermi velocity, and ρ_q represents a particle-hole excitation, being q the transferred momentum. This means that they can be considered as the *actual* excitations of the system. Moreover, the commutation relations satisfy:

$$[\rho_q, \rho_{q'}^\dagger] \sim \delta_{q,q'} \rightarrow \rho_q \sim b_q \quad (2.20)$$

The term ρ_k represents a *particle-hole* excitation, and b_k is a boson destruction operator. Thus, a particle-hole excitation behaves like a boson due to these commutation rules. If one chooses this basis to represent the new operators of the problem, the

(initially fermionic) hamiltonian can be rewritten as:

$$H \sim \sum_q \varepsilon_q b_q^\dagger b_q \quad (2.21)$$

that is, a hamiltonian of non-interacting bosons, representing the density waves of the system. The hamiltonian (2.21) is diagonal in the k basis, therefore its properties can be computed in an easy way. If everything can be expressed as a set of free bosons, the free boson model (also called *gaussian* model) is of relevance:

$$S = \int dx d\tau \left((\partial_\tau \varphi)^2 + (\partial_x \varphi)^2 \right) \quad (2.22)$$

where $\varphi(x, t)$ represents a Bose field, and $\tau = it$. Note that the action is Euclidean in (1+1) dimensions, and we have set $v = 1$. In a one dimensional theory, the Bose field can be decomposed into *right* and *left* moving bosons:

$$\varphi(z, \bar{z}) = \phi(z) + \bar{\phi}(\bar{z}) \quad (2.23)$$

It can be proved that the correlation function of bosonic exponents is equal to that of fermionic fields if the following relationships hold [72]

$$\psi(z) = \frac{\eta}{\sqrt{2\pi a}} e^{-i\sqrt{4\pi}\beta\phi(z)} \quad \bar{\psi}(z) = \frac{\eta}{\sqrt{2\pi a}} e^{i\sqrt{4\pi}\beta\bar{\phi}(\bar{z})} \quad (2.24)$$

where \pm represents right and left movers, respectively, and the complex coordinates $z = v\tau - ix$ and $\bar{z} = v\tau + ix$. The factors η are Klein factors, whose only function is to ensure that anticommutation relations hold in these fermionic operators. We will now work with these relations in an application example: a (1+1) relativistic fermionic theory.

2.2.2 Bosonization of the massive Thirring model (MTM)

To apply the bosonization approach described above, let us use an example of a specific fermionic field theory. The massive Thirring model (MTM) represents the interaction between two relativistic fermionic fields in (1+1) dimensions [27]. The model has been extensively studied, due to its integrability, by Bethe ansatz methods [28, 29, 30], and it is a cornerstone in understanding exactly solvable one dimensional systems.

The fact that the fermions are relativistic is because they obey a Dirac-like hamiltonian. The total hamiltonian is:

$$H = \int dx \left\{ i\Psi^\dagger \sigma^z \partial_x \Psi + m_0 \Psi^\dagger \sigma^x \Psi + 2\xi \psi^\dagger(x) \bar{\psi}^\dagger(x) \bar{\psi}(x) \psi(x) \right\} \quad (2.25)$$

where the spinor ψ is defined as:

$$\Psi = \begin{pmatrix} \psi(x) \\ \bar{\psi}(x) \end{pmatrix} \quad (2.26)$$

$\psi(x)$ ($\bar{\psi}(x)$) representing right(left) moving spinless fermions, and σ are the Pauli matrices. We will use the bosonization for spinless fermionic fields, following Senechal [72]. The right and left movers have the bosonization representation:

$$\psi(x) = \frac{1}{\sqrt{2\pi}} e^{-i\sqrt{4\pi}\phi(x)} \quad \bar{\psi}(x) = \frac{1}{\sqrt{2\pi}} e^{i\sqrt{4\pi}\bar{\phi}(x)} \quad (2.27)$$

where the Klein factors are not dynamical objects, so their representation can be chosen freely as in this case. The massive Thirring model can be written in terms of the fermionic components:

$$H = \int dx \left\{ i \left(\psi^\dagger(x) \partial_x \psi(x) - \bar{\psi}^\dagger(x) \partial_x \bar{\psi}(x) \right) + m_0 \left(\psi^\dagger(x) \psi(x) + \text{h.c.} \right) + 2\xi \psi^\dagger(x) \bar{\psi}^\dagger(x) \bar{\psi}(x) \psi(x) \right\} \quad (2.28)$$

We will now express the hamiltonian above in this representation. Also, for the vertex operators, we bear in mind that:

$$e^A e^B = e^{A+B} e^{[A,B]/2} \rightarrow e^{i\alpha\phi(x)} e^{i\beta\phi(x')} = e^{i\alpha\phi(x)+i\beta\phi(x')} e^{-\alpha\beta\langle\phi(x)\phi(x')\rangle} \quad (2.29)$$

We will go through all the bosonization procedure explicitly. The non-interacting part of the hamiltonian is representing a single free boson:

$$H_0 = \int dx \frac{1}{2} \left((\partial_t \varphi)^2 + (\partial_x \varphi)^2 \right) \quad (2.30)$$

with units of $v = 1$. To evaluate expressions of the form $\psi^\dagger(x) \partial_x \psi(x)$, we follow Senechal [72] and we take the limit:

$$: \psi^\dagger(x) \partial_x \psi(x) := -i \lim_{\varepsilon \rightarrow 0} \left(\psi^\dagger(z + \varepsilon) \partial_z \psi(z) - \langle \psi^\dagger(z + \varepsilon) \partial_z \psi(z) \rangle \right) \quad (2.31)$$

This process is known as *normal ordering*, and it is essential to avoid divergences. The relation above is taken by substitution of $\partial_x = -i(\partial_z - \partial_{\bar{z}})$, and $\varepsilon = z' - z$. The relation between z and x coordinates was previously defined in (2.24). The following identities are always useful (see [72]):

$$\langle \psi^\dagger(z) \psi(z') \rangle = \frac{1}{2\pi} \frac{1}{z - z'} \quad \langle \phi^\dagger(z) \phi(z') \rangle = -\frac{1}{4\pi} \log(z - z') + \text{const.} \quad (2.32)$$

After normal ordering, and taking care of the product of exponential operators, the fermionic currents have the form:

$$J(z) = i \frac{1}{\sqrt{\pi}} \partial_z \phi = i \frac{1}{\sqrt{\pi}} \partial_z \varphi \quad \bar{J}(\bar{z}) = -i \frac{1}{\sqrt{\pi}} \partial_{\bar{z}} \phi = -i \frac{1}{\sqrt{\pi}} \partial_{\bar{z}} \varphi \quad (2.33)$$

with $\varphi = \phi(z) + \bar{\phi}(\bar{z})$. All time ordered products must then be taken into account in this way, when treating interacting terms specially.

The mass term can be easily written, since the fields $\phi(x), \bar{\phi}(x)$ commute, and it is:

$$\frac{2m_0}{\sqrt{2\pi}} \cos(\sqrt{8\pi}\varphi(x, t)) \quad (2.34)$$

We are then left with bosonizing the interacting term. We see that it is composed by an interaction over densities in normal order, that is:

$$: \rho_R(x)\rho_L(x) := \lim_{\varepsilon \rightarrow 0} \left(\psi^\dagger(z + \varepsilon)\psi(z)\bar{\psi}^\dagger(\bar{z} + \bar{\varepsilon})\bar{\psi}(\bar{z}) - \frac{1}{(2\pi)^2\varepsilon\bar{\varepsilon}} \right) \quad (2.35)$$

After expansion of the products, there is only one remaining term, characteristic from forward scattering:

$$: \rho_R(z)\rho_L(\bar{z}) := \frac{1}{\pi} \partial_z \varphi \partial_{\bar{z}} \varphi \quad (2.36)$$

Thus, the bosonized version of the MTM reads:

$$H_{MTM} = \int dx \frac{1}{2} \left((\partial_t \varphi)^2 + (\partial_x \varphi)^2 \right) + \frac{2m_0}{\sqrt{2\pi}} \cos(\sqrt{4\pi}\varphi(x, t)) + \frac{2\xi}{\pi} \partial_z \varphi \partial_{\bar{z}} \varphi \quad (2.37)$$

In terms of the real coordinates (x, t) , the hamiltonian is bosonized and given by:

$$H_{MTM} = \int dx \frac{1}{2} \left((\partial_t \varphi)^2 + (\partial_x \varphi)^2 \right) + \frac{2m_0}{\sqrt{2\pi}} \cos(\sqrt{4\pi}\varphi(x, t)) - \frac{\xi}{2\pi} \left((\partial_t \varphi)^2 - (\partial_x \varphi)^2 \right) \quad (2.38)$$

Now if we take a look at the expression, we see that the non-interacting part can be written in a similar way as for a free boson field:

$$H_0 = \frac{v^*}{2} \int dx \left(K(\partial_t \varphi)^2 + (1/K)(\partial_x \varphi)^2 \right) \quad (2.39)$$

with new renormalized Fermi velocity and K defined as:

$$v^* = \sqrt{1 - (\xi/\pi)^2} \quad K = \sqrt{\frac{1 - (\xi/\pi)}{1 + (\xi/\pi)}} \quad (2.40)$$

From here, we can rescale the fields as:

$$\Pi \rightarrow (1/\sqrt{K})\Pi' \quad \varphi \rightarrow \sqrt{K}\varphi' \quad (2.41)$$

After this scaling, we are left with the Sine-Gordon hamiltonian:

$$H = \frac{v^*}{2} \int dx \left((\partial_t \varphi')^2 + (\partial_x \varphi')^2 \right) + \frac{2m_0}{\sqrt{2\pi}} \cos(\sqrt{4\pi K}\varphi') \quad (2.42)$$

Then one obtains the scaling dimension β of the operator:

$$\beta = \sqrt{4\pi K} \rightarrow \frac{\beta^2}{4\pi} = \sqrt{\frac{1 - (\xi/\pi)}{1 + (\xi/\pi)}} \sim 1 - (\xi/\pi) \quad (2.43)$$

This establishes an important relationship between the MTM and the Sine-Gordon model (SG): the one dimensional fermions can be mapped directly to a Bose field obeying a SG model. The relationship (2.43) between parameters of both models is *exact* in $\xi/\pi \ll 1$. This was first derived by Coleman [32], and can be extracted as well from Korepin's work [28, 30] on the MTM.

2.3 Wilson's Numerical Renormalization Group (NRG)

The Numerical Renormalization Group (NRG) was developed by Wilson [25] in 1975, as a method to understand the ground state (i.e zero temperature) properties of the antiferromagnetic Kondo model. Although being mostly used for $T = 0$ cases, it can also be used for any finite temperature $T \neq 0$. The approach is based on a *logarithmic discretization* of the band, by which a continuum model can be mapped to a discrete one (*tight-binding*), to successfully describe all *low-energy* (infrared) properties of the system, therefore it can be applied to any kind of impurity models. Since it does not involve any perturbative calculations, the method is non-perturbative, and therefore, very robust for the study of such systems. We must remember that most condensed matter systems deal with big system sizes, where the thermodynamic limit is taken (the system size is taken to infinity when compared to the shortest length scale). As the system size increases, the low-energy description of the model becomes the appropriate one. Although there are possibly many good reviews on the NRG method, we will mostly follow the one from Bulla et.al [75] in this thesis.

In such a discrete model, the tight-binding parameters undergo some *renormalization*. This renormalization makes the hopping parameters to decrease in value with distance to the impurity site, a consequence of the *logarithmic discretization* of the band. The result is the addition of weaker hoppings amplitudes with each iteration, ensuring convergence of the method. The addition of more sites, with smaller hopping amplitudes as we get away from the impurity, constitutes the so called *Wilson chain*. The mathematical details of discretization are out of scope in this thesis, and we refer to Wilson's original paper [25] for further reading on this. However, one should not be too worried about these discretization steps, since after all, one is interested in a direct application of the method for the specific model under consideration. Therefore, understanding its basic concepts as opposed to its mathematical technicality is more beneficial.

2.3.1 NRG basics

We consider a one dimensional tight binding model, with hopping amplitudes t_n , and a single impurity site at the end of the chain. This picture is schematically represented in figure (2.2).

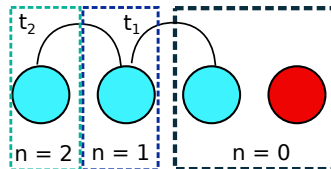


Figure 2.2: Schematic view of the NRG method. The initial hamiltonian is composed by the impurity site (red) and the last site of the chain. When this part is diagonalized, a new site is added to the system with a tunneling probability t_n , then the system is diagonalized again and the process is repeated. The addition of more and more sites eventually leads to the construction of a chain that resembles the initial hamiltonian of the model at low energies.

If we have already managed to logarithmically discretize the band, the different hopping amplitudes will depend on a discretization parameter Λ in a way that $t_{n+1}(\Lambda) < t_n(\Lambda)$, that is, the hopping amplitudes decrease with further distance to the impurity site. The discretization parameter $\Lambda > 1$ is chosen conveniently, usually in ranges $\Lambda \sim 1.5 - 2.5$, but it really depends on the model under consideration. The limit $\Lambda \rightarrow 1$ recovers the *continuum* nature of the model, where no discretization has taken place. The general form of a transformed hamiltonian by discretization of the band is:

$$H = \sum_{n=1}^{+\infty} t_n (c_n^\dagger c_{n+1} + \text{h.c.}) + \sum_{n=1}^{+\infty} \varepsilon_n c_n^\dagger c_n + H_{\text{imp}} \quad (2.44)$$

Spin has been ignored. Otherwise, an spin index σ must follow each of the operators. Here H_{imp} represents the part of the hamiltonian containing all impurity-related operators, so it will include the interacting terms as well as possible *hybridization* terms. The other parts of the hamiltonian form the resulting tight-binding model for the band. The NRG method provides a way to calculate both thermodynamic quantities (such as charge susceptibility on the impurity site, entropy, specific heat...) and dynamic quantities (spectral functions, self-energies [76]). We move now to describe briefly the NRG algorithm, and later we give important tips for the calculation of dynamical quantities within the NRG method, which will be relevant for the understanding of results in chapter 5.

2.3.2 NRG algorithm: iterative diagonalization

For now, consider only the hamiltonian given by H_{imp} in (2.44) as the zeroth order step NRG. This can be the $n = 0$ box in figure (2.2). That is, initially our system will consist only on the impurity site plus the last site of the tight binding chain

($n = 0$).

Suppose now that after logarithmic discretization, we find our hopping amplitudes to have the following dependence with Λ : $t_n \sim \Lambda^{-n/2}$. Mathematically, the exact identity states that the total hamiltonian of the system is defined as the limiting case when the number of steps (iterations) N tends to infinity:

$$H = \lim_{N \rightarrow \infty} \Lambda^{\frac{-(N-1)}{2}} H_N \quad (2.45)$$

where, in order to keep things unchanged, from (2.44) we have to include a prefactor [75]

$$H_N = \Lambda^{(N-1)/2} \left(\sum_{n=1}^N t_n (c_n^\dagger c_{n+1} + \text{h.c.}) + \sum_{n=1}^N \varepsilon_n c_n^\dagger c_n + H_{\text{imp}} \right) \quad (2.46)$$

The prefactor has been chosen to cancel the N dependence of the t_N hopping parameters. This is because we assumed that $t_N \sim \Lambda^{-N/2}$, but this is not always the case¹. The reason to choose a prefactor that cancels the n th dependence is that, at each iteration, the eigenvalues are of $O(1)$, and the identification of fixed points becomes easier. Now two consecutive hamiltonians are related by the following recursion [75, 61]:

$$H_{N+1} = \sqrt{\Lambda} H_N + \Lambda^{N/2} \varepsilon_N c_N^\dagger c_N + \Lambda^{N/2} t_N c_{N+1}^\dagger c_N + \text{h.c.} \quad (2.47)$$

At iteration step N , the hamiltonian is diagonalized:

$$H|r\rangle_N = E_N^r |r\rangle \quad (2.48)$$

therefore all eigenstates and eigenvalues are computed. When going to the next step $N + 1$, the hamiltonian needs to be expressed in the new basis $\{|r\rangle \otimes |s\rangle\}$, where the states $\{|s\rangle\}$ add the new degree of freedom to the system (added site, see figure (2.2)). Then the hamiltonian is expressed in this new basis and diagonalized again, and the procedure is repeated.

The problem with the above method is that, after some iterations, the hamiltonian becomes of unmanageable size. When a sufficiently large hamiltonian has been created, truncation is imposed. This means that, out of all possible eigenstates of the diagonalized hamiltonian, only those with the lowest energy eigenvalues (say S_K of them) are taken. These now constitute the new *truncated* basis $|\tilde{r}\rangle$, from where the hamiltonian at step $N + 1$ can be built. Usually, the total number of kept states varies depending on the model, and more importantly, on the parameter Λ . For typical values of $\Lambda \sim 1.5 - 2.5$, it is sufficient to keep $S_K = 500 - 1000$ states after truncation. However, as $\Lambda \rightarrow 1$, and therefore the continuous limit is approached, a bigger number of kept states is usually needed. Nonetheless, system specification

¹For each model, the dependence on n can be different for the hopping parameters. In such a case, the prefactor has to be chosen accordingly. Luckily, all models we will be considering have this n dependence on the hopping parameters, so we can work with this specific construction of H .

plays an important role, and systems with low enough dimensionality allow for a small value of Λ while the number of kept states is still $S_K = 500 - 1000$.

We want to make a remark in this last part of the algorithm. The NRG method can be *improved* in order to account for those discarded states [77] that were neglected after truncation. That means that, when truncation is done, the discarded states for the next step can still have some usage to calculate some physical quantities at step N . Methods like these are out of scope here, as they offer poor qualitative behaviour differences in the computation of physical quantities, since they are mostly used for numerical accuracy.

2.3.3 Dynamical quantities computation within NRG

The computation of dynamical quantities is much more difficult than that of thermodynamic ones. The main reason has to do with the *energy scaling* within each NRG step: at different NRG steps, we are working at different energy scales. This is a consequence of the logarithmic discretization we presented before. Since dynamical quantities depend *explicitly* on excitation energies ω , one needs to take care to work in the appropriate range of energies.

The method we are about to describe can be found in detail in [75, 78] for its basic understanding. For improvement of numerical accuracy or alternative discretization methods, we refer to [77, 79, 80], as these methods are not considered here. We are interested in calculating the impurity density of states:

$$A_\sigma(\omega) = \sum_r |\langle \text{GS} | f_\sigma | r \rangle|^2 \delta(\omega - (E_r - E_{\text{GS}})) \quad (2.49)$$

This is the discrete representation of the impurity spectral function in terms of energy eigenvalues, where each excitation energy $\omega_N^r = E_r - E_{\text{GS}}$ is weighed by the matrix element of the impurity operator between the many-body ground state $|\text{GS}\rangle$ and excited states. The problem is that we have no clue about the *true* many-body states of the system, since after some NRG steps, truncation must be applied, keeping only the lowest eigenstates from the whole hamiltonian. Therefore, we can only think about getting an approximate solution for the above quantity. It can be argued that at step N , the spectral function can be approximated by all the N kept states as [75]

$$A_\sigma(\omega) \approx A_\sigma^N(\omega) = \sum_{\tilde{r}} |\langle \tilde{r}_0 | f_\sigma | \tilde{r} \rangle|^2 \delta(\omega - \omega_N^r) \quad (2.50)$$

where $|\tilde{r}\rangle$ are the approximate eigenstates of the many-body system. Another problem has to do with the delta functions involved. To obtain a valid numerical result, these peaks must be *broadened* [75]. The broadening of delta functions by other functions is varied, but offers non significant differences on the qualitative behaviour of the model. Concretely, we will be working with the gaussian representation of delta functions:

$$\delta(\omega - \omega_N^r) \rightarrow \frac{1}{\sigma\sqrt{2\pi}} e^{-\frac{(\omega - \omega_N^r)^2}{2\sigma^2}} \quad (2.51)$$

where $\sigma = b\omega_N$, with $b \sim 0.2 - 0.8$ (see [75] for details).

After N steps, the hamiltonian of the model H_N has a characteristic energy scale that depends on the parameter Λ as:

$$\omega_N = \frac{1}{2}(1 + \Lambda^{-1})\Lambda^{-(N-1)/2} \quad (2.52)$$

Notice that this includes a $\sqrt{\Lambda}$ factor as compared with the hopping amplitudes. It is customary to include this factor proportional to the whole hamiltonian H_N with each iteration, therefore suppressing the dependence of t_n on n . In this way, each NRG step corresponds to a different energy scale, but its eigenvalues are always of $O(1)$. Due to the truncation of the spectrum, the range of excitations is in the window $0 < \omega < M\omega_N$, with M being a constant depending on the value of Λ . For typical values, this sets $M = 2$, and therefore only excitation energies $\omega \leq 2\omega_N$ contribute. One usually chooses to evaluate the spectral function at the concrete point $\pm 2\omega_N$. Therefore, an NRG implementation with N total steps will have $2N$ points in total, if we take into account negative excitations ($\omega < 0$) as well. There are plenty of publications about NRG methods applied to calculate these quantities, the most relevant selected to be followed here [78, 81, 82]

A final remark must be made here. We have talked about obtaining NRG points for the spectral function at each NRG step. However, we have to make a distinction between a chain with *even* number of sites and another with *odd*. Concretely, all points collected to describe the spectral function need to belong to the same type of chain. If all points were represented (that is, a point for each NRG step), then oscillations are observed between neighbouring points in the spectral function. This is due to a finite size effect. What one usually does is to discard those points calculated for an odd number of sites chain, keeping only those points calculated when the total number of added sites is even.

2.3.4 Application example: The Anderson model

Consider the single impurity Anderson model defined earlier in Chapter 1. The logarithmic discretization of the band gives the following hamiltonian [75]

$$H_A = \sum_{n=1}^{+\infty} t_n (c_{n+1}^\dagger c_n + \text{h.c.}) + \varepsilon_n c_n^\dagger c_n + H_{\text{imp}} + t' \sum_{\sigma} (f_{\sigma}^\dagger c_0 + \text{h.c.}) \quad (2.53)$$

For practical purposes, and due to the form of ε_n , we can take $\varepsilon_n = 0$ for all values n , and the hopping parameters satisfy:

$$t_n = \frac{1}{2}(1 + \Lambda^{-1})\Lambda^{-n/2} \quad (2.54)$$

The algorithm is implemented to calculate the impurity spectral function or *density of states*, as well as the energy flow of the lowest many-body eigenvalues. In figure (2.3), the energy flow is represented for the Anderson model. We observe that,

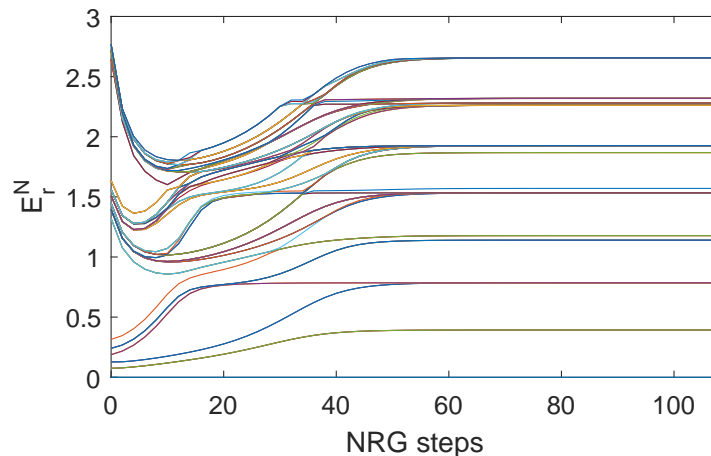


Figure 2.3: NRG flow for the many-body eigenvalues of the Anderson model with 800 kept states and $\Lambda = 1.5$, $\varepsilon_0 = -0.05$, $V = 0.1$, $U = 0.1$, and a total of $N = 112$ sites. After some iterations, the flows converge to steady values representing the approximate low energy eigenstates.

after some steps, different eigenvalues converge to a *steady* value of the energy. After the NRG process is repeated, the lowest eigenvalues don't change. This makes sense since, adding a site with large n only introduces a very weak coupling of the chain with the added site. In particular, these steady values of the energy flow represent *fixed points* of the hamiltonian. This means that, no matter how many times we apply a renormalization step to the system, the value of its parameters will remain constant.

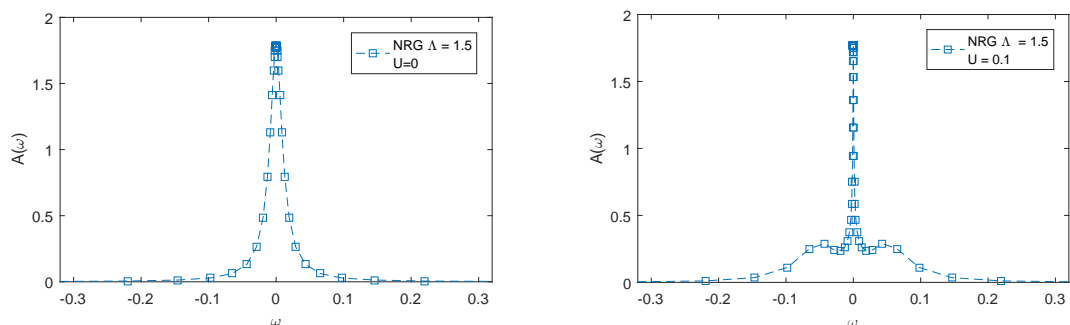


Figure 2.4: NRG simulation for the Anderson model, with hybridization $V = 0.1$, for $U = 0$ and $\varepsilon_0 = 0$ (left) and $U = 0.1$ and $\varepsilon_0 = -0.05$ (right). We observe the appearance of the Kondo resonance when $\varepsilon_0 < 0$ and the local interaction on the impurity site is strongly repulsive (Kondo limit). Dashed lines are included as a guide to the eye.

The spectral function for the single impurity Anderson model is represented in figure (2.4). Here both sectors of the hamiltonian, with spin up and down, have been taken into account to contribute. That is, what is actually represented in figure (2.4) is the sum of both the spin up and down density of states. The left side corresponds to the trivial case of the Fano model, that is, when $U = 0$. The right

figure represents the Anderson model in the Kondo limit. Notice how two shoulders appear at both sides of $\omega = 0$. The spectral function is pinned at $\omega = 0$, as it should be according to Langreth theorem [64].

We have also selected ε_0 for the following reason: the parameter ε_0 acts as a local chemical potential on the impurity site. This can also be regarded as a magnetic field applied in the z direction on the impurity site. One knows that, when $\varepsilon_0 \neq 0$, the spectral function in the Anderson model is a Lorentzian centered at ε_0 . However, since the NRG method works on different energy scales with each iteration, whenever the value of the characteristic energy scale $\omega_n \sim \varepsilon_0$, accuracy is lost. In other words, and following [75, 83], we cannot resolve a very narrow width when values of ε_0 are big enough above the characteristic energy scale ω_c . We refer to [83] for details.

2.4 The Anderson-Yuval method

We turn our look now to analytical approaches in the computation of time correlations. In a series of papers [22, 23, 24], Anderson and Yuval proposed a method to calculate exact results in the Kondo problem. The idea is based on Feynman's path integral for a time history of the impurity magnet (see [70] for details), and in the X-ray edge problem analysis carried out by Nozières and De Dominicis [17]. The fact that the X-ray problem can be treated as a single particle problem with a transient potential, allows for a similar calculation in the Kondo problem. We describe briefly the essence of the method here, and refer the reader to Anderson's papers [22, 23, 24, 70] for details.

Consider the Kondo hamiltonian:

$$\begin{aligned}
 H &= H_0 + H_I \\
 H_0 &= \sum_{k,\sigma} \varepsilon_{k,\sigma} c_{k,\sigma}^\dagger c_{k,\sigma} + JS^z \sum_{k,k',\sigma,\sigma'} \sigma^z c_{k,\sigma}^\dagger c_{k',\sigma'} \\
 H_I &= J \sum_{k,k',\sigma,\sigma'} S^+ \sigma_{\sigma,\sigma'}^- c_{k,\sigma}^\dagger c_{k',\sigma'} + S^- \sigma_{\sigma,\sigma'}^+ c_{k,\sigma'}^\dagger c_{k',\sigma} \quad (2.55)
 \end{aligned}$$

For the non-interacting part H_0 , we have two types of eigenstates, those with the spin on the impurity up ($|\psi_\uparrow\rangle$), and those where the impurity spin is down ($|\psi_\downarrow\rangle$). Consider the state of this set with the *lowest* eigenvalue $|\psi_{0\uparrow}\rangle$, and where the impurity spin is up. Then the Anderson-Yuval (AY) method applies the following: at $t = 0$, the interacting term H_I is switched on, evolving the state to a later time t . In the mean process, a complete (even) set of up and down switches occurs on the impurity site due to the action of H_I . At time t , the state comes back to its original form $|\psi_{0\uparrow}\rangle$. One is then interested in the *response* of the system (the conduction electrons) due to these spin-flip processes. The amplitude of the process described above is given by:

$$F(t) = \langle \psi_{0\uparrow} | e^{iHt} | \psi_{0\uparrow} \rangle = \langle \psi_{0\uparrow} | e^{iH_0 t} e^{i \int_0^t dt' H_I(t')} | \psi_{0\uparrow} \rangle \quad (2.56)$$

which can be immediately identified as a partition function.

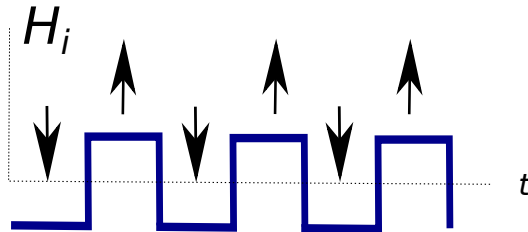


Figure 2.5: Kondo problem as a succession of X-ray problems, where the impurity spin is flipped at subsequent times. The conduction electrons see an alternating potential, which corresponds to a set of absorption/emission Nozières processes for each spin.

The interaction representation has been used in formula (2.56). One can then expand the exponential in its series form, realising that every time H_I acts, it flips the spin. Therefore, in a normal term of order n of the expansion, there are $2n$ spin flips. Here is where the connection between the X-ray problem and the Kondo problem manifests, since each of these spin flips can be regarded as a single X-ray process in the finite time (t_{i+1}, t_i) , and therefore, Nozières-De Dominicis formulas can be used. To be clear, a typical second order term is of the type:

$$F^{(2)}(t) \sim J^2 \int_0^t dt_1 \int_0^{t_1} dt_2 S_{\uparrow N}(t_1 - t_2) S_{\downarrow N}(t_1 - t_2) \quad (2.57)$$

where the Nozières correlation function $S(t)$ has been defined previously in chapter 1. However, it has to be taken into account that every time there is a flip, the scattering phase shift changes from $\delta \rightarrow -\delta$. For the Kondo problem, these correlators take the form (see [22]):

$$S_{\pm}(t) = (it\xi_0)^{-\pi^{-2}(\pm\pi+2\delta_{\pm})^2} \quad \delta_{\pm} = \pm = \arctan\left(\frac{J\pi\nu}{4}\right) \quad (2.58)$$

Then all possible allowed paths for conduction electrons in $[0, t]$ must be taken into account. The AY method generalises Nozières-De Dominicis method by adding three contributions to the propagator. Basically, the total amplitude (2.56) is calculated as:

$$F_{2n}(t) = G_{2n}^0 \phi(\delta, t) e^{C(t, \delta)} \quad (2.59)$$

The first term corresponds to *all* possible diagrams for the non-interacting conduction electrons. This has the form of a Cauchy determinant when all time orderings are taken into account, and each of the product terms represents the *transient* behaviour in conduction electrons found by Nozières-De Dominicis. The solution has a determinant form because alternating sign appears whenever the order of fermionic

operators is interchanged. The other two terms correspond to single-particle scattering corrections. The first one $\phi(\delta, t)$ is calculated from Dyson's equation for the conduction propagators, and has a similar form of the first term, but with a different exponent. The second term corresponds to all closed loops contributions to the different paths. Such a term was also computed by Nozières and De Dominicis *for a single X-ray* problem.

With this, Anderson and Yuval found an interesting similarity between formula (2.56) and that of the classical partition function of a one dimensional Coulomb gas with charges distributed in the imaginary time axis. The final form of the partition function [22] is:

$$F(i\beta) = \sum_{n=0}^{+\infty} J^{2n} \int_0^\beta d\beta_{2n} \dots \int_0^{\beta_2} d\beta_1 \left((2 - 2\epsilon) \sum_{n>n'} (-1)^{n-n'} \log \left(\frac{\beta_n - \beta_{n'}}{\tau} \right) \right) \quad (2.60)$$

where $\epsilon \sim J\nu$ and τ is a time cut-off related to ν . The most important thing to note about this expression is that the result, being exact, relies on an infinite perturbation expansion on the parameter J . The AY method extracts information about the response in the system due to the spin flips of the local impurity. More important is that it proves, in some sense, the analogy between the Kondo model and the X-ray edge problem. The Kondo problem can be seen as an infinite sequence of X-ray processes, where conduction electrons in the metal experience spin flips at the impurity site. We also want to remark the importance of the method for calculating dynamical quantities in time domain. However, we note that the method allows the calculation of the *response* of conduction electrons, but does not provide an exact expression for the *transverse correlator*:

$$\langle \hat{T} S^-(t) S^+(0) \rangle \quad (2.61)$$

As we will see later, it is this second correlator the one we would be interested in when calculating dynamical quantities in the IRLM.

2.5 The Schrieffer-Wolff transformation

When studying strongly correlated systems, one has to deal with the fact that interactions don't allow to solve the hamiltonian in an exact way. However, sometimes we are not interested in diagonalizing the whole interacting hamiltonian, because this includes all possible energy ranges, and therefore, all fluctuations are taken into account. In practice, only dealing with a *low energy* description of the hamiltonian gives enough information about the system's behaviour when interactions are present. Loosely speaking, we are looking for a description that encodes all important features of the initial hamiltonian when interactions are strong enough, but when high energy states are not considered. In practice, this is equivalent to a *renormalization* of our original hamiltonian into another where high-energy degrees of freedom have been integrated out. This is the essence of the Schrieffer and Wolff

(SW) transformation.

The Kondo problem is the best example of a very strongly correlated system. Anderson's impurity model, described in chapter 1, has very similar characteristics than the Kondo model when one works in the appropriate parameters regime, and both models are related to each other. This relationship was already known at the time when Anderson first proposed his model [7], although the formal proof was given later by Schrieffer and Wolf [10]. In their paper, it was shown that a low-energy description of Anderson's model in the strong coupling regime (large U) leads to an equivalent hamiltonian with antiferromagnetic coupling developed between an impurity magnet and the local conduction electrons. The most relevant references to follow such calculations are [10, 62, 84].

2.5.1 Kondo model derived from the Anderson model

We have seen previously Anderson's impurity model:

$$H = \sum_{k,\sigma} \varepsilon_k c_{k,\sigma}^\dagger c_{k,\sigma} + \varepsilon_0 \sum_{\sigma} d_{\sigma}^\dagger d_{\sigma} + \sum_{k,\sigma} V_k (d_{\sigma}^\dagger c_{k,\sigma} + \text{h.c.}) + U n_{\uparrow} n_{\downarrow} \quad (2.62)$$

In the specific case of $V = 0$ (no hybridization), then the impurity site and the electrons bath are totally decoupled from each other. If we consider $U > 0$ and $\varepsilon_0 < 0$, the ground state of the impurity site is degenerate, since now $|\uparrow\rangle$ and $|\downarrow\rangle$ have the same eigenvalue ε_0 . It is then obvious that in this situation, the ground state of the whole system includes a localised magnet.

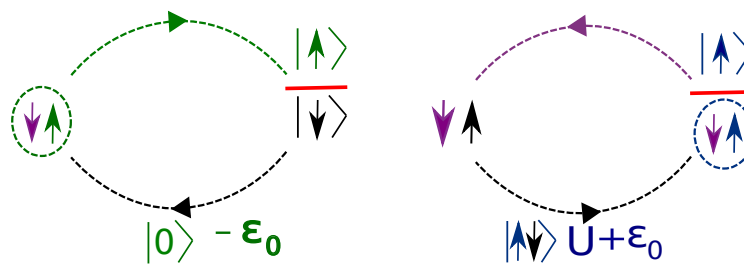


Figure 2.6: Virtual processes in the Anderson model when the hybridization parameter $V \neq 0$, and $\varepsilon_0 < 0$ and $U \gg |\varepsilon_0|$. The left process flips the impurity spin by passing through the high-energy state $|0\rangle$, therefore the electron on the impurity makes a virtual jump to the surrounding bath. On the right hand side, an electron from the surrounding bath jumps virtually to the impurity site, so that the state $|\uparrow\downarrow\rangle$ is visited. In both processes, there is some energy exchange in order to allow for the spin flip.

However, when the hybridization parameter V is switched on, electrons from the surrounding bath start to jump in and out from the impurity site. These are called *virtual processes*, where electrons migrate from/to the lead for a short period, involving an energy shift associated with spin-exchange processes. This is schematically shown in figure (2.6). Therefore the high energy manifold is visited shortly during

these virtual processes. At this stage, the local moment is likely to be suppressed under some conditions. In order to get an idea of when this might happen, one could treat the parameter V perturbatively, however this results in divergences in high orders of V . The alternative method proposed by SW is to isolate the relevant degrees of freedom dominating the dynamics by applying a canonical transformation to the hamiltonian:

$$\bar{H} = e^S H e^{-S} \quad (2.63)$$

where the condition is to clear out all dependence on V in first order. The fact that S needs to be antihermitian is clear since we have:

$$U^\dagger U = I \rightarrow e^{S^\dagger} e^S = e^{S+S^\dagger} e^{\frac{1}{2}[S,S^\dagger]} = I \quad (2.64)$$

therefore $S^\dagger = -S$. The hamiltonian (2.62) can be divided into an exactly diagonal part and a non-diagonal one:

$$H = H_0 + V \quad V = \sum_{\sigma k} V_{k\sigma} c_{k,\sigma}^\dagger d_\sigma + \text{h.c} \quad (2.65)$$

The way to suppress the first order dependence on V is by use of the Baker-Campbell-Hausdorff (BCH) formula. The appropriate choice of S is then given by:

$$[H_0, S] = V \quad (2.66)$$

Therefore, to second order in V (first in S) we have in (2.63):

$$\bar{H} = H_0 + \frac{1}{2}[S, V] + O(S^2) \quad (2.67)$$

The H_0 part of the hamiltonian is diagonal, and we can divide it into a low energy subspace and a high energy one (see [62]):

$$H_0 = \begin{pmatrix} H_0^L & 0 \\ 0 & H_0^H \end{pmatrix} \quad S = \begin{pmatrix} 0 & -S^\dagger \\ S & 0 \end{pmatrix} \quad (2.68)$$

S can be obtained easily from (2.66):

$$S = \frac{V}{E^H - E^L} \quad -S^\dagger = \frac{V^\dagger}{E^L - E^H} \quad (2.69)$$

As a result, one ends up with a renormalized hamiltonian H^* under such canonical transformation. The interesting part of this new hamiltonian is the one projected onto the low-energy subspace:

$$H_L^* = P_L H^* P_L \quad H^* = H_0 - \frac{1}{2}(V^\dagger S + S^\dagger V) \quad (2.70)$$

The important point to illustrate is that, from a canonical transformation of our original hamiltonian, a new, renormalized version has been derived. In this new

version, new interacting terms appear. At the end, the most relevant one is the so called *s-d exchange* term [10]

$$H_{s-d} = \sum_{k,k'} J_{k,k'} c_{k,\alpha}^\dagger \vec{\sigma}_{\alpha\beta} c_{k',\beta} \vec{S} \quad (2.71)$$

where \vec{S} is the impurity spin operator, and σ represent the Pauli matrices. The most relevant result of the SW transformation is the confirmation of an antiferromagnetic exchange interaction:

$$J_{k,k'} = V_k V_{k'} \left(\frac{1}{U + \varepsilon_0} + \frac{1}{-\varepsilon_0} \right) > 0 \quad (2.72)$$

This result, which was predicted by Anderson in his paper [7], proves to be very important at very low temperatures, since an antiferromagnetic interaction between the impurity and the surrounding sea is the cause for the local moment to be *screened*. The screening of the local moment occurs when the impurity spin and a surrounding electron form a singlet state. To all practical effects, this is equivalent to a metallic system in an absence of impurity. The fact that the impurity doesn't survive as a local moment at very low temperatures was later proved by Wilson [25], as it has been discussed previously.

After application of the SW transformation to the Anderson model, one ends up with the following hamiltonian:

$$H_L^* = \sum_{k,\sigma} \varepsilon_k c_{k,\sigma}^\dagger c_{k,\sigma} + \sum_{k,k'} J_{k,k'} c_{k,\alpha}^\dagger \vec{\sigma}_{\alpha\beta} c_{k',\beta} \vec{S} \quad (2.73)$$

This result proves that both the Anderson and Kondo hamiltonians are related. More concretely, the Kondo hamiltonian provides a good low-energy description of the Anderson model in some region of parameter space. Although the SW transformation was originally used in the Anderson model, the method can be extrapolated to more general hamiltonians.

2.6 The Bethe ansatz method

We will introduce now a very powerful method to solve one dimensional problems, known as the *Bethe ansatz*. The method was introduced in 1929 by Hans Bethe [26], in order to study the one dimensional Heisenberg antiferromagnet. Although initially created to solve isotropic systems, it was later applied to impurity models [36, 60], concretely to give an exact analytical solution of the anisotropic Kondo model [57, 58]. We will just give the conceptual introduction to the method, leaving detailed description to be found in the literature [30, 85, 86].

The Bethe ansatz is applied to those systems that are said to be *integrable*, that is, they contain an infinite number of conservation laws in a field theory. In a lattice version model, the number of conservation laws is discrete, but both approaches

must give the same low energy description in the thermodynamic limit. In essence, the method allows to calculate in an *exact* way all possible eigenvalues of an interacting one dimensional system.

2.6.1 Bethe ansatz basics

The most important concept to introduce is that of *scattering matrix*, usually represented by S . A scattering matrix represents the *amplitude* of a scattering process between an *in* and *out* state of N particles when interactions are taken into account:

$$S(p_1 \dots p_n) = {}_{\text{out}} \langle p'_1 \dots p'_n | p_1 \dots p_n \rangle_{\text{in}} \quad (2.74)$$

As a result, the general N body wavefunction experiences a phase-shift. In general:

$$S = e^{i\Phi(\varepsilon_1 \dots \varepsilon_N)} \quad (2.75)$$

In a one dimensional system, particles are very likely to meet at some point in space-time. When this happens, they are said to *scatter* from each other. Due to an infinite number of conservation laws, in some $(1 + 1)$ dimensional theories, the scattering matrix *factorises* into products of scattering pairs, therefore the complexity of the problem is reduced (since now, instead of an N -interacting bodies problem, we have a set of 2 body-problems). This symmetry property is reflected in the Yang-Baxter's equations:

$$S_{12}(\theta_1 - \theta_2) S_{13}(\theta_1 - \theta_3) S_{23}(\theta_2 - \theta_3) = S_{23}(\theta_2 - \theta_3) S_{13}(\theta_1 - \theta_3) S_{12}(\theta_1 - \theta_2) \quad (2.76)$$

which states that the order of scattering between three particles is irrelevant, and each order is equivalent [86]. This has been represented schematically in figure (2.7). By induction, if this is true for any three particles, it can be proved to be true for N .

In general, there are two approaches to calculate the S matrix of a $(1 + 1)$ dimensional model. One of them [87] is based on a more axiomatic approach, taking into account the unitarity and crossing symmetries that the S matrix must satisfy. The other method relies on a regularisation of the theory, by direct computation of the S matrix solving the Schrodinger equation for a two-particle problem. It is this latter approach the one we will follow here. The computation of the S matrix by the second method seems at first sight more laborious, however it proves to be convenient *when the regularization scheme employed is fundamental in the theory we are about to study*. This justifies our use of the later method instead of the more conventional axiomatic approach.

Here θ represents the physical *rapidities* of the model, which we will discuss soon. An integrable system must satisfy the Yang-Baxter's equations.

We will now describe the essence of the Bethe ansatz method, referring to [30, 85] for a detailed description. A hamiltonian can be given in the continuum (field

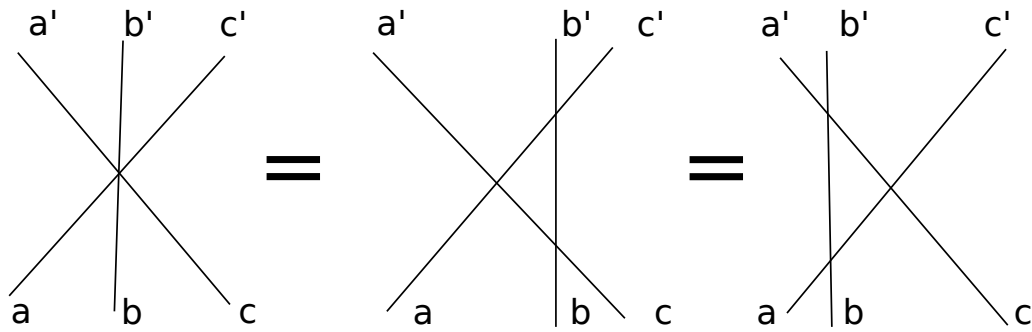


Figure 2.7: A pictorial representation of the Yang-Baxter's equation. The order on which three particles (a, b, c) scatter from each other is irrelevant, and all processes have the same amplitude given by the factorised S matrix.

theory) or its lattice version. When given on its field theory version, we must find the operators constituting the equivalent (quantum-mechanical) N body problem. A possible form of the N body state is written in terms of the field operators:

$$|\Psi_N\rangle = \mathcal{N} \int \prod_{i=1}^N dx_i \Psi(x_1 \dots x_N) \psi^\dagger(x_N) \dots \psi^\dagger(x_1) |0\rangle \quad \psi(x) |0\rangle = 0 \quad (2.77)$$

where \mathcal{N} is a normalization constant. This does not represent the most general N body state that can be written, since it depends on the system, but introduces two important concepts in the method, the wavefunction Ψ and the state $|0\rangle$. The wavefunction $\Psi(\{x_i\})$ represents the wavefunction that satisfies the equivalent N -body interacting hamiltonian, therefore:

$$H_N \Psi(x_1 \dots x_N) = E \Psi(x_1 \dots x_N) \quad (2.78)$$

The state $|0\rangle$ belongs to the Fock space and it is called the *pseudovacuum*, which must be distinguished from the *vacuum* of the theory, since the former one includes interactions. The state $|0\rangle$ only represents a vacuum in the non-interacting system. It is the state annihilated by any destruction operator.

We describe now the *coordinate* Bethe ansatz. The aim is the calculation of all possible eigenvalues of the interacting system. First one solves the Schrodinger equation for the single particle problem, calculating the form of the single particle states $\phi_1(\varepsilon_1, x_1)$. After this, one calculates the two body problem from the Schrodinger equation:

$$H |\Psi_{N=2}\rangle = (\varepsilon_1 + \varepsilon_2) |\Psi_{N=2}\rangle \quad (2.79)$$

that is, taking into account states with only two particles, and $\varepsilon_{1/2}$ being the single particle eigenvalues. It is important to mention that, in one dimensional Lorentz invariant theories, we don't distinguish between energy and momentum, since $\varepsilon = \pm p$.

When considering two particles, scattering between the two must be taken into account in the wavefunction. This changes the total wavefunction only by a phase

factor, called the *scattering phase shift*. Due to this, and in the case of a fermionic system, the Slater determinant incorporates this phase factor:

$$\Psi(x_1, x_2) = \phi(x_1, \varepsilon_1)\phi(x_2, \varepsilon_2)e^{i\Phi(\varepsilon_1-\varepsilon_2)} - \phi(x_1, \varepsilon_2)\phi(x_2, \varepsilon_1)e^{-i\Phi(\varepsilon_1-\varepsilon_2)} \quad (2.80)$$

The wavefunction Ψ has to preserve the statistics of the particles in the model under consideration. For a fermionic system, this implies Ψ to be antisymmetric under exchange of two particles. The single particle states $\phi(x)$ depend on the system under consideration, therefore they can be free states $\phi \sim e^{i\varepsilon x}$ or states derived from a potential felt by the particle. The two-particle scattering phase shift $\Phi(\varepsilon_1 - \varepsilon_2)$ is only a function in the difference of energies, due to energy conservation.

Everything explained to this point has nothing to do with the Bethe ansatz method, since so far we have only solved a two-particle problem. However, one must know the two scattering phase shift beforehand in order to introduce the ansatz for the general N body wavefunction. The so called **Bethe ansatz** arrives when a solution of the following form is proposed (again, for a fermionic system):

$$\Psi(x_1 \dots x_N) = \mathcal{N} \sum_{\{\mathcal{P}_{ij}\}} (-1)^{\mathcal{P}} \phi(x_1, \varepsilon_1) \dots \phi(x_N, \varepsilon_N) \prod_{i \neq j} e^{i\Phi(\varepsilon_i - \varepsilon_j) \text{sign}(x_i - x_j)} \quad (2.81)$$

where \mathcal{P}_{ij} denotes all possible permutations of the single particle indices i, j , and \mathcal{N} is a normalization constant. With this *ansatz* for the N body wavefunction, one introduces it into Schrodinger equation, and checks that it is verified. In the expression above, there is a product of exponentials, each carrying a different phase shift. This is a consequence of the S matrix factorisation we discussed before.

In order to compute different properties, we place our system on a ring of length L , imposing periodic boundary conditions. The wavefunction must then be periodic on each of the coordinates, so that:

$$\Psi(x_1 \dots x_i \dots x_N) = \Psi(x_1 \dots x_i + L, \dots x_N) \quad \forall i \quad (2.82)$$

This periodicity condition is actually very important, since it leads to the *Bethe equations*, a set of N coupled non-linear equations. In general, they have the form:

$$2\pi n_i = \varepsilon_i L + \sum_{i \neq j} \Phi(\varepsilon_i - \varepsilon_j) \quad (2.83)$$

These equations determine uniquely the eigenvalues of the interacting system. The $\{n_i\}$ is a set of integer quantum numbers for each i index. The values of these integers depends on the state we are considering. For example, for the case where interaction is switched off, all scattering phase-shifts on the r.h.s are cancelled. Then, we can build up the ground state of the system by ordering the eigenvalues $n_1 < n_2 < \dots < n_i < n_{i+1} \dots < n_N$ in the Bethe equations. When interactions are switched on, usually one has to check that this ordering of the integers indeed reproduces the ground state.

2.6.2 Understanding the Bethe equations: Rapidities representation

At this stage, it is useful to introduce the physical rapidities of the system, related to the energy eigenvalues and momentum:

$$\varepsilon(\beta) = m_0 \cosh(\beta) \quad p(\beta) = m_0 \sinh(\beta) \quad (2.84)$$

where m_0 represents some *mass* associated to the field. The reason to do this is that most two particle scattering phase-shifts depend only on the rapidities difference under this mapping:

$$\Phi(\varepsilon_1, \varepsilon_2) \rightarrow \Phi(\beta_1 - \beta_2) \quad (2.85)$$

For reasons we will discover later, this representation becomes much more transparent for subsequent calculations. In order to specify the state, the set $\{\beta_i\}$ is calculated from equations (2.83). Usually, such a set is big, and it is more convenient for later purposes to introduce the *rapidities distribution*, which is defined for the long L (thermodynamic) limit as:

$$\rho(\beta) = \frac{1}{L} \frac{1}{(\beta_i - \beta_{i+1})} > 0 \quad (2.86)$$

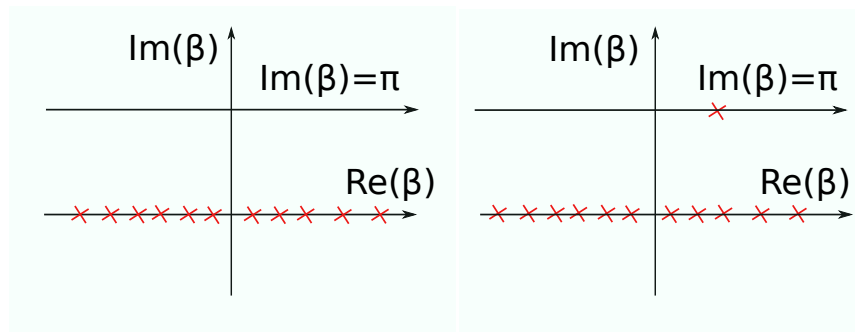


Figure 2.8: Rapidities plane representing two different states on the system. On the left side, the state with all negative energies occupied ($\text{Im}(\beta) = 0$) is represented. When one particle is added with positive energy ($\text{Im}(\beta) = \pi$), the configuration on the plane changes, and one has to take that into account to construct the true physical vacuum of the theory.

This distribution is dense in such a limit, and represents how all different rapidities (eigenvalues/momentum) are distributed for the state under consideration. Therefore, if one calculates this function, one knows exactly what are the values of all the energies in the interacting system. Usually, the rapidities distribution for the interacting system is calculated by solving an integral equation of second kind:

$$\rho(\beta) = \rho^0(\beta) + \int d\alpha \rho(\alpha) K(\beta - \alpha) \quad (2.87)$$

Here $K(\beta - \alpha)$ represents the kernel of the integral equation, which is related to the two particle scattering phase shift $\Phi(\beta - \alpha)$. The relation will be explored later.

The fundamental equations we have written are essential to derive all physical properties in the thermodynamic limit, that is, when the size of the system $L \rightarrow \infty$. It allows one to compute the spectrum of the hamiltonian in an *exact* way. The best way to clarify how the method works is by introducing an specific example.

2.6.3 Bethe ansatz for the Massive Thirring Model

The Massive Thirring Model (MTM) was introduced previously when describing the bosonization technique (section 2 of this chapter). The model has been solved by Bethe ansatz [28, 29], and its exact solution is well known. We will give here the steps in the calculation of the physical vacuum of the theory, following [28].

Consider the following hamiltonian:

$$\begin{aligned} H &= \int dx \left(i\Psi^\dagger \sigma_z \partial_x \Psi(x) + m_0 \Psi^\dagger \sigma_x \Psi(x) + 2\xi \psi^\dagger(x) \bar{\psi}^\dagger(x) \bar{\psi}(x) \psi(x) \right) \\ \Psi &= \begin{pmatrix} \psi(x) \\ \bar{\psi}(x) \end{pmatrix} \end{aligned} \quad (2.88)$$

representing spinless fermions interacting in (1+1) dimensions. There are two species, one associated with *right* movers, the others being *left* movers. The hamiltonian preserves the total number of particles, and the discrete operators for the total energy and momentum are:

$$H_N = \sum_{i=1}^N i\sigma_z^i \partial_{x_i} + m_0 \sigma_x^i + 2\xi \sum_{j \neq i} \delta(x_i - x_j) \quad P_N = -i \sum_{i=1}^N \partial_{x_i} \quad (2.89)$$

One then looks for common eigenfunctions of these operators. The appropriate single-particle wavefunctions are given by [28, 30]:

$$\phi(x|\beta) = e^{ixm_0 \sinh(\beta)} \begin{pmatrix} e^{-\beta/2} \\ e^{\beta/2} \end{pmatrix} \quad (2.90)$$

The total N particle wavefunction is given by:

$$\Psi(x_1 \dots x_N) = \sum_{\mathcal{P}} (-1)^P \phi(x_{1\mathcal{P}}|\beta_{1\mathcal{P}}) \dots \phi(x_{N\mathcal{P}}|\beta_{N\mathcal{P}}) e^{i \sum_{j < k} \Phi(\beta_j - \beta_k)} \quad (2.91)$$

Here \mathcal{P} represents all possible permutations, and the two particle scattering phase shift is known before hand.

In the MTM, one has to distinguish between different scattering processes, depending on the sign of the energy. For two negative energy pseudoparticles, the scattering phase shift is [28, 29, 30]:

$$\Phi(\beta) = i \log \left(\frac{\sinh(i\omega - \beta/2)}{\sinh(i\omega + \beta/2)} \right) = -2 \arctan \left(\cot(\omega) \tanh(\beta/2) \right) \quad (2.92)$$

where $\omega = \frac{\pi - \xi}{2}$. Here β is a simplification to represent the rapidities difference, so that $\beta \equiv \beta_i - \beta_j$. It is important to mention that given different pseudoparticles, this

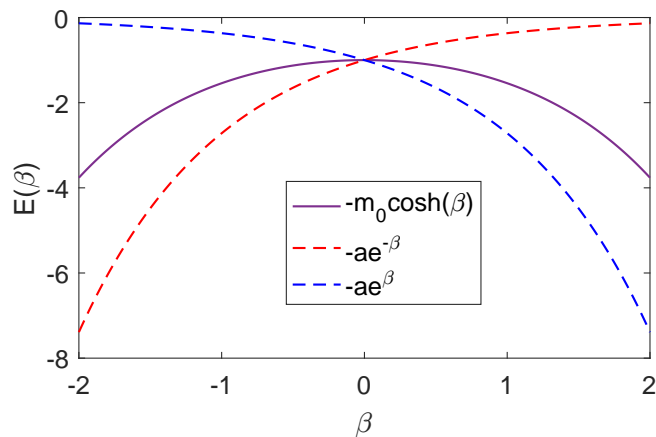


Figure 2.9: The MTM ground state fills all negative energies below the mass m_0 . When the limit $m_0 \rightarrow 0$ is taken, two different branches appear, each of them describing either right (red) or left (blue) movers. Such a description is important when the fields are unfolded.

scattering phase shift is different (for example, when considering a pseudoparticle with negative energy scattering from one with positive energy). All these expressions can be found in detail in [28]. From now on, β is to be understood as a real number only. Since in the ground state all pseudoparticles have negative energies, the Bethe equations have the form:

$$m_0 L \sinh(\beta_i) = 2\pi n_i + \sum_{i \neq j} \Phi(\beta_i - \beta_j) \quad n_{i+1} - n_i = 1; \quad (2.93)$$

The total energy of this state is $E = -m_0 \sum_j \cosh(\beta_j)$. If one takes the $i+1$ equation in (2.93) and subtracts the i th one, and using the definition (6.55), the following integral equation specifies the ground state distribution of rapidities:

$$m_0 \cosh(\beta) = 2\pi\rho(\beta) + \int_{-\Lambda}^{+\Lambda} d\alpha \rho(\alpha) \partial_\beta \Phi(\beta - \alpha) \quad (2.94)$$

Importantly, a rapidity cut-off Λ has been inserted here. This cut-off is necessary in order to keep the ground state energy bounded. Here we observe the relation between the kernel and the scattering phase shift:

$$K(\beta - \alpha) = -\frac{1}{2\pi} \partial_\beta \Phi(\beta - \alpha) = \frac{1}{2\pi} \frac{\sin(2\omega)}{\cos(2\omega) - \cosh(\beta - \alpha)} \quad (2.95)$$

which will become important later. The solution of (2.94) can be found by solving the equation by standard techniques [88]. However, this would not represent the actual value of the distribution of rapidities in the *physical vacuum*.

Consider, for instance, the case were all excitations over that vacuum preserve the total number of rapidities (particles). This corresponds to the *zero-charge* sector of the model. In this case, removing a particle from the vacuum and adding it with a

positive energy above destabilizes the pseudoparticles sea by pushing some of them apart from the cut-off. In other words, due to the addition of such excitation, a *renormalization* of the mass parameter occurs, therefore one is interested in obtaining $m_0(\Lambda)$. This is illustrated in figure (2.8). Detailed description of this process is written in the appendix. The final form of m_0 and the rapidities distribution is [28]

$$m_0 = ae^{-\frac{\xi\Lambda}{\pi+\xi}} \quad \rho(\beta) \sim \cosh\left(\frac{\pi}{\pi+\xi}\beta\right) \quad (2.96)$$

Therefore, as compared to a purely free system, the true physical vacuum of the system has *renormalized* the rapidities. The so called *physical rapidities* are then defined as:

$$\theta = \frac{\pi}{\pi+\xi}\beta \quad (2.97)$$

The procedure of obtaining such a vacuum might appear confusing at first, but once it has been constructed, different excited states of the system can be computed. The procedure of renormalizing quantities like rapidities or scattering phase shifts is known as *dressing*. Dressed functions are the ones that provide the actual physical results of the theory, therefore understanding how to compute them is fundamental in the method.

Chapter 3

The single channel IRLM: Thermodynamics

*“Nothing is boring if you look at
carefully”*

Freeman John Dyson

This chapter is devoted to condense the theory of thermodynamic properties of the single channel IRLM. The single channel IRLM was the first variant of the model as proposed originally by Wiegmann and Finkelshtein [36], something that makes it fundamental to study in detail. It is also important due to its direct relation to the anisotropic Kondo model (AKM).

In order to study cases for arbitrary values of U , we use the bosonization [66, 72] technique. This being a field theory technique, still has to reproduce the same low energy description of the lattice model hamiltonian (3.1). The technique has been applied previously to the IRLM [39], in order to compute the exact expression for the thermodynamic exponent α . Although the final form of the exponent given in [39] is correct, it does not include a correct interpretation of the scattering phase shift associated to U . Our approach here will prove to differ from previous studies [38, 39, 50, 55] as we will see shortly. All results presented here for the single channel IRLM are *exact*, and moreover, an important connection to an integrable field theory will be established.

3.1 The single channel IRLM

Since we are dealing with thermodynamic quantities, we focus exclusively on properties where the operators are evaluated at equal times. We recall here the form of

the IRLM on its lattice version:

$$\hat{H} = \varepsilon_0 d^\dagger d - t \sum_{i,\delta} c_i^\dagger c_{i+\delta} + t'(c_0^\dagger d + h.c.) + U \left(c_0^\dagger c_0 - \frac{1}{2} \right) \left(d^\dagger d - \frac{1}{2} \right) \quad (3.1)$$

where N specifies the total number of channels attached to the lead, and the c_i represent fermionic operators in the lattice. The operator d represents the impurity annihilation operator.

Since we are interested in the behaviour of the system at the impurity site, the most important quantity to compute is the *hybridization* Γ . This defines a new energy scale in the system separating two different regions, one where the dot is decoupled from the surrounding bath, the other describing the dot hybridized. It is important to say that, in our wide band limit, this energy scale satisfies $\Gamma \ll 2t$, thus much smaller than the bandwidth. As we have seen previously, for the non-interacting case $U = 0$, the hybridization is given by $\Gamma_0 = \pi\nu(t')^2$ for $N = 1$ channels. As one switches on interactions, we found in chapter 2 by perturbation theory that the hybridization parameter t' scales with interaction as:

$$\Gamma_{\text{pert.}} \sim (t')^{\frac{2}{1+2g}} \quad g = U\nu \quad (3.2)$$

This chapter is devoted to find an *exact* (non-perturbative) solution for the hybridization scale. Perturbative calculations fail to describe the model away from the *weak coupling* regime [38], that is, for large values of U , when compared to numerics. We explore here this issue. The problem we deal with is to find the (exact) expression for Γ in the form:

$$\Gamma = f(\alpha)(t')^\alpha \quad (3.3)$$

where α will be called from now on the *thermodynamic exponent*. We will calculate this exponent in an exact way for an arbitrary number of channels, and compare with numerical results. The exponent α represents the scaling of t' with interaction U . The quantity $f(\alpha)$ represents a prefactor that depends non-trivially on α . This dependence on α turns out to be very important, since it is what determines the change in the energy scale as interaction is increased. One can clearly see that the inclusion of such prefactor is necessary in the theory in order to account for a full match with numerics. It will be seen later that for the case $N = 2$ case, such prefactor reveals even more surprising properties over the calculation of physical quantities. Once this exact expression is given, different limits of the theory are explored and shown to match with the exact result.

3.1.1 Bosonization of the IRLM

In the bosonization picture, the parameter t' is treated as a perturbation. For $N = 1$, the hamiltonian (3.1) has the following version in the field description:

$$H = \sum_{\alpha=R,L} \mp \frac{iv_F}{2} \int_{-\infty}^0 dx (\psi_{\alpha}^{\dagger}(x) \partial_x \psi_{\alpha}(x)) + \varepsilon_0 d^{\dagger} d + t' (d^{\dagger} \psi_{0,\alpha}(x) + \text{h.c.}) \\ + U : \psi_{\alpha}^{\dagger}(0) \psi_{\alpha}(0) : \left(d^{\dagger} d - \frac{1}{2} \right) \quad (3.4)$$

where α described right (R) or left (L) moving one dimensional fermions, and v_F is the Fermi velocity. Most of the results collected here will correspond to the *particle-hole* symmetric case, therefore we will set $\varepsilon_0 = 0$ from now on. The operators between $::$ symbols are normal ordered, so that $: A := A - \langle A \rangle$. We recall that the IRLM is a spinless fermionic model. It is useful to introduce the unfolded representation of the fields, so that:

$$\psi_L(x < 0) = \psi_R(x > 0) \quad (3.5)$$

and express the hamiltonian (3.4) in terms of right-moving fields only:

$$H = -iv_F \int_{-\infty}^{+\infty} dx (\psi_R^{\dagger}(x) \partial_x \psi_R(x)) + \varepsilon_0 d^{\dagger} d + t' (d^{\dagger} \psi_R(0) + \text{h.c.}) \\ + U : \psi_R^{\dagger}(0) \psi_R(0) : \left(d^{\dagger} d - \frac{1}{2} \right) \quad (3.6)$$

We use the usual definition for fermionic fields in terms of bosons [72]

$$\psi(x) = \frac{\eta}{\sqrt{2\pi}} e^{i\sqrt{4\pi}\phi(x)} \quad (3.7)$$

Here η are Klein factors, which are not important in the following calculations, since they are not dynamical variables, therefore its representation is free to choose so long as they preserve the anticommutation relations of the operators $\psi(x)$.

The impurity operators are identified with spin operators:

$$S^z = d^{\dagger} d - \frac{1}{2} \quad d^{\dagger} = \eta S^+ \quad d = \eta S^- \quad (3.8)$$

Note that the non-interacting part of (3.4) is a Dirac hamiltonian when we linearize the spectrum (in the vicinity of the Fermi surface), characteristic of one dimensional fermionic systems.

With the above considerations into account, the bosonized version of the IRLM reads ($v_F = 1$):

$$H = \frac{1}{2} \int_{-\infty}^{+\infty} dx (\partial_x \phi(x))^2 + \frac{t'}{\sqrt{2\pi}} \left(S^+ e^{i\sqrt{4\pi}\phi(x)} + \text{h.c.} \right) + \\ U \frac{S^z}{\sqrt{\pi}} \partial_x \phi(0) \quad (3.9)$$

Here one takes into account the limit of $t' = 0$. In this limit, the model is exactly solvable, since both the impurity and the lead are decoupled from each other. The situation is equivalent to a right-moving boson scattering off a point-like potential at $x = 0$:

$$V(x) = U\delta(x) \quad (3.10)$$

Therefore, the N body problem is reduced in this limit to a single particle scattering problem. The scattering phase shift experienced by the scattered particles is given by:

$$\delta = \arctan\left(\frac{U\pi\nu}{2}\right) \quad g = \frac{2\delta}{\pi} \in [-1, 1] \quad (3.11)$$

where ν represents the density of states on the lead. Equation (3.11) will prove to be one of the most important identities in this thesis. It is convenient to define the parameter g as the actual interacting parameter in the theory. Since α in (3.3) will depend only on the interaction, the relevant thermodynamic energy scale Γ is a function of this parameter only. The mapping $U\nu \rightarrow 2\delta$ makes a direct identification between the actual parameter of the model U and the phase shift experienced by a free boson arriving at the impurity.

The hamiltonian (3.9) is now rotated under a unitary transformation of the form:

$$\bar{H} = \mathcal{U}^\dagger H \mathcal{U} \quad \mathcal{U} = e^{i\sqrt{4\pi}\rho S^z \phi(0)} \quad (3.12)$$

The parameter ρ is to be determined, so that the rotation changes the scaling dimension of the vertex operators $\beta \rightarrow \beta'$ (see appendix for details). The unitary transformation allows to absorb the boundary term of 2δ , so that we have:

$$\bar{H} = H_0 + \frac{t'}{\sqrt{2\pi}}(S^+ e^{i\sqrt{4\pi}(1-\rho)\phi(0)} + \text{h.c}) \quad \rho = \frac{2\delta}{\pi} \equiv g \quad (3.13)$$

Under such rotation of the fields, the new scaling dimension of the exponential operator depends on the interaction parameter g :

$$2d = \frac{\beta^2}{4\pi} = (1-g)^2 \quad (3.14)$$

We summarize the key points of the transformation above:

- The term proportional to U in the original hamiltonian can be substituted by the scattering phase shift 2δ experienced by a free boson in the $t' \rightarrow 0$ limit.
- The scaling dimension of the new vertex operators is changed and depends on the interacting parameter g .

3.1.2 Scaling dimensions of operators and thermodynamic exponent α

Here we explore the change on the scaling dimension of the operators, as well as we show explicit calculation of the thermodynamic exponent α for the single channel case. We have seen previously how, under a certain unitary transformation, the scaling dimension of operators changes, that is, it becomes dependent on the interaction. For the single channel case we obtained equation (3.14) as the main result.

After explicit calculation of the scaling dimension, we need to see how the parameter t' behaves under renormalization. In other words, how does the parameter t' scale in the IRLM as interaction g is changed. Ultimately, we are interested in getting the expression of α , which is in relation with the correlation length:

$$\xi \sim (t')^\alpha \quad (3.15)$$

The exponent α will be called the *thermodynamic exponent* from now on.

In order to get such exponent, we will make use of the Renormalization Group (RG) procedure. One then expects the theory to be similar to another renormalizable theory of moving bosons with an added boundary condition. A well known renormalizable theory is the Sine Gordon Model, which we discussed previously on the introduction. The Sine Gordon Model (SGM) is given by the action (in (1+1) dimensions):

$$S_{\text{SGM}} = \int d^2x \left((\partial_t \varphi)^2 - (\partial_x \varphi)^2 + g \cos(\beta \varphi) \right) \quad (3.16)$$

The cosine term accounts for the non-linearity of the corresponding equation. The parameter β is directly related with the scaling dimension of operators by:

$$2d = \frac{\beta^2}{4\pi} \quad (3.17)$$

A variant of the SGM is the Boundary Sine Gordon Model (BSGM) [34], which includes a boundary term in addition. The BSGM is described by the action [89]:

$$S = \frac{1}{2} \int dx^2 (\partial_\mu \phi)^2 + G \cos(\beta \phi) + g \cos\left(\frac{\beta}{2} \phi(0)\right) \quad (3.18)$$

Note the factor 1/2 in the boundary term, which is important for integrability of the model. The SGM has a well known spectrum. When a perturbation is included, it develops a mass gap with scaling dimension:

$$m \sim G^{\frac{(1+\lambda)}{2\lambda}} = G^{\frac{1}{2-2d}} \quad \lambda = \frac{8\pi}{\beta^2} - 1 = \frac{1}{d} - 1 \quad (3.19)$$

For the IRLM in (3.13) we will choose a generalised version of the sine-Gordon model, where the Euclidean (imaginary time) action is:

$$\bar{S} = \bar{S}_0 + z \int \frac{dx d\tau}{a^2} \cos(\beta' \phi(x)) \delta(x) \quad (3.20)$$

where a is introduced to preserve the dimensions and its taken as the inverse of lattice spacing ($\Lambda \sim 1/a$). Notice that the parameters β' and β refer to different scaling dimensions. It is important to clarify this: β will always correspond to the bulk parameter in the SGM, whereas β' corresponds to a boundary version of it. The parameter z is the one whose flow we want to study under renormalization. More concretely, $z \sim t'$ for the IRLM, since t' represents a small perturbation. The method we are about to develop thus works for small values of t' , but for any value of interaction U on the IRLM.

We move now to map our IRLM to a generalised SGM in the massless limit, that is, where only the boundary term is considered. For that, we follow a Renormalization Group procedure, which is detailed in the appendix. By changing the cut-off of the theory $\Lambda \rightarrow \Lambda'$ and integrating out the high-energy degrees of freedom, one ends up with an equivalent action where the parameter z has been *renormalized*. To understand how this works, it is important to understand the renormalization of the SGM. This is well known and following [66], one finds that the relevant energy scale appearing is that related to the correlation length by:

$$\xi^{-1} \sim \Lambda z^{\frac{1}{1-2d'}} \quad 2d' = \frac{\beta'^2}{4\pi} \quad (3.21)$$

We should not confuse this d' with the one on (3.14). This is the scaling dimension associated to a general SGM in (3.20), and it is easy to obtain the relation between β and β' from here:

$$\beta' = \frac{\beta}{\sqrt{2}} \quad (3.22)$$

Therefore, for the IRLM the *thermodynamic* energy scale is estimated as:

$$\frac{\Gamma}{\Lambda} \sim \left(\frac{t'}{\Lambda}\right)^{1/1-2d'} \quad 2d' = \frac{1}{2}(1 - 2g + g^2) \quad (3.23)$$

where Λ here represents the cut-off of the theory. Thus, we have an exact formula of the thermodynamic exponent α in terms of the interaction parameter g :

$$\alpha = \frac{2}{1 + 2g - g^2} \quad (3.24)$$

Note that for the non-interacting case $g = 0$, the thermodynamic exponent is $\alpha = 2$, as one would expect. We also identify in this case a quantum critical point, happening where the thermodynamic exponent $\alpha \rightarrow \infty$. This happens for:

$$g_c = 1 - \sqrt{2} \sim -0.4142 \quad (3.25)$$

Notice that the other solution has been discarded because it lies outside the interval $[-1, 1]$ where g belongs. We identify a quantum phase transition with this point in the attractive ($U < 0$) regime. At this point, the correlation length becomes infinite. We will discuss later the significance of these quantum phase transitions

for an arbitrary number of leads N .

We also recognise here the first order correction from perturbation theory exposed in chapter 2. When $U \sim 0$ we get:

$$g = \frac{2}{\pi} \arctan\left(\frac{U\pi\nu}{2}\right) \sim U\nu + O(U^2) \rightarrow \alpha \sim \frac{2}{1+2U\nu} \quad (3.26)$$

The result (3.24) agrees with previous studies [39, 38, 50], however some comments need to be added. In references [38, 39], it is not clear that this exponent relates to the *thermodynamic* exponent, since explicit mention to the local density of states (a dynamical quantity) is done. The exponent α is clearly associated to the correlation length. Also in [50], this result is recovered for $N = 1$, but without mentioning that this is an *exact* result. Both points need to be clarified here, and understand that expression (3.24) is the actual thermodynamic exponent in the theory, and that it is not related to dynamical quantities of the model.

Another comment to make on expression (3.23) is that the expression is approximate, but not *exact*¹. Therefore one raising question is what is the exact form of the prefactor appearing on the thermodynamic scale. To further explore this, the connection with the BSGM we have already seen here is exploited.

3.1.3 The thermodynamic energy scale Γ

Although the thermodynamic exponent α has been calculated in an exact way, there is a missing proportionality factor in the expression of Γ , which describes the energy scale of the system. We will give now an *exact* formula for Γ in the form:

$$\frac{\Gamma}{\Lambda} = f(\alpha) \left(\frac{t'}{\Lambda}\right)^\alpha \quad (3.27)$$

Here $f(\alpha)$ is called the *prefactor*. When equation (3.23) was derived, a direct mapping of the IRLM into a generalised (boundary) SGM was done. It is then worth considering if *exact results on the theory of the BSGM can be equally applied to the IRLM*.

It is important to make a clear definition of Γ in the IRLM. Such an energy scale relates to observables of the theory. In the non-interacting case ($g = 0$), the energy scale Γ_0 is related to the impurity occupation number:

$$n_d = \frac{1}{2} - \frac{1}{\pi} \arctan\left(\frac{\varepsilon_0}{\Gamma_0}\right) \quad \Gamma_0^{-1} = -\pi \left(\frac{\partial n_d}{\partial \varepsilon_0}\right) \Big|_{\varepsilon_0=0} \quad (3.28)$$

¹To avoid confusion here, note that what is exact is the exponent α , however the expression for the thermodynamic energy scale Γ misses a prefactor that might depend on g in a non-trivial way. The RG method doesn't allow to calculate the exact form of this prefactor.

When interactions are switched on, one can still adopt this definition for the thermodynamic energy scale, so that the value of Γ is determined for any interacting value g by just changing $\Gamma_0 \rightarrow \Gamma$ in equation (3.28). Thus, the thermodynamic energy scale is directly related with the microscopic parameters of the theory, more concretely, with small variations of ε_0 around the point $\varepsilon_0 = 0$.

Now we will match both definitions of Γ eqns (3.23),(3.28). The following result is recovered from the exact expression given in [35] for the *boundary temperature* on the BSGM. The boundary temperature T_B represents the relevant energy scale in the Boundary Sine Gordon Model, as Γ does for the IRLM. The exact expression is given in [35] by:

$$\lambda_1 \Lambda^{-\nu} = \frac{2^\nu}{4\pi} \Gamma(\nu) \nu^{1-\nu} T_B^{1-\nu} R(\lambda)^{1-\nu} \quad \nu = \frac{\beta^2}{8\pi} \quad (3.29)$$

where $\Gamma(x)$ represents the gamma function, Λ represents an energy cut-off, and $R(\lambda)$ is defined as:

$$R(\lambda) = \frac{2\sqrt{\pi}(1+\lambda)\Gamma(\frac{1}{2} + \frac{1}{2\lambda})}{\Gamma(\frac{1}{2\lambda})} \quad \lambda = \frac{1}{\nu} - 1 \quad (3.30)$$

The β in the expression above corresponds to the bulk term in the SGM. For the IRLM, we make the following identification of parameters:

$$\lambda_1 = t' \quad T_B = \pi\Gamma \quad (3.31)$$

The parameter ν , which represents the scaling dimension in the BSGM, is then related to the scaling dimension of operators in the IRLM, so that:

$$\nu = 2d' = \frac{1}{2}(1-g)^2 \quad (3.32)$$

By some manipulations of equation (3.29), we identify $f(\alpha)$ in equation (3.27) as:

$$f(\alpha) = \frac{2^\alpha \pi^{\alpha-\frac{3}{2}} \Gamma(\frac{\alpha-1}{2})}{[\Gamma(\frac{\alpha-1}{\alpha})]^\alpha \Gamma(\frac{\alpha}{2})} \quad (3.33)$$

In order to recover the non-interacting limit, the cut-off of the theory Λ must be chosen in a consistent way, moreover, it depends on the bandwidth of the lead fermions (density of states of the bulk). Equation (3.27) has the limit:

$$\Gamma_{\lim \alpha \rightarrow 2} = \Gamma_0 = \pi\nu(t')^2 \quad (3.34)$$

We should not confuse this ν with the one used in (3.32). Here ν represents the bulk density of states in the IRLM. To recover the correct non-interacting limit, the appropriate value of Λ is chosen as:

$$\Lambda = \frac{4}{\pi\nu} \quad \nu = \frac{1}{\pi t} \quad (3.35)$$

We arrive then at the final form of the thermodynamic energy scale:

$$\Gamma = \frac{2^{2-\alpha} \pi^{2\alpha-5/2} \Gamma\left(\frac{\alpha-1}{2}\right)}{\left[\Gamma\left(\frac{\alpha-1}{\alpha}\right)\right]^\alpha \Gamma\left(\frac{\alpha}{2}\right)} \nu^{\alpha-1} (t')^\alpha \quad (3.36)$$

The above expression is *exact*, and represents the thermodynamic energy scale on the single channel IRLM as a function of the thermodynamic exponent α , the hybridization parameter t' and the bulk density of states ν . Such expression works in the limit $t'/t \ll 1$ considered here.

The same expression can be written in a more convenient way. One is usually interested in comparing how the hybridized Γ scales in ratio with Γ_0 of the non-interacting case, in which case equation (3.36) is written as:

$$\frac{\Gamma}{\Gamma_0} = \Omega(\alpha) (\nu t')^{\alpha-2} = \frac{2^{2-\alpha} \pi^{2\alpha-7/2} \Gamma\left(\frac{\alpha-1}{2}\right)}{\left[\Gamma\left(\frac{\alpha-1}{\alpha}\right)\right]^\alpha \Gamma\left(\frac{\alpha}{2}\right)} (\nu t')^{\alpha-2} \quad (3.37)$$

The identification of the IRLM with the boundary Sine Gordon Model has not been justified yet. The reader might think that we have only managed to identify two different models by making direct substitution of their parameters into one known formula, since equation (3.29) has been derived exclusively in [35] for the Boundary Sine Gordon Model. As we will show in the next section, we prove numerically equation (3.36) to be correct one for the IRLM.

3.1.4 NRG for the $N = 1$ IRLM

In this section we will prove numerically the analysis carried out previously. The method we use is the Numerical Renormalization Group (NRG), which was described before on chapter 2. The code used to run simulations was written in Matlab[®].

There are two thermodynamic properties we will focus on: the impurity occupation number and the associated thermodynamic scale Γ .

The thermodynamic scale is defined as in (3.28) by just substituting $\Gamma_0 \rightarrow \Gamma$. Numerical simulations are performed for the IRLM, by choosing carefully the parameters. A standard value of the discretization parameter $\Lambda = 1.5$ in NRG². A total system size of $N = 82$ sites has been chosen, meaning that a total of 80 lattice sites are added to the initial hamiltonian (that contains only the impurity and the last site of the chain). Since system's size grows with each added site, truncation

²Again, we make a bit abuse of notation here. Λ represents the discretization parameter in the NRG method, it is not to be confused with the field theory cut-off we discussed earlier. The reason to keep both quantities with the same letter is purely conventional and standard from the literature.

needs to be done, keeping only the lowest eigenstates of the hamiltonian. We take this truncation of the hamiltonian for a total of 500 states when the system size is $N = 11$ sites, meaning the hamiltonian is a 2048×2048 matrix. Thus, at each iteration step after truncation the hamiltonian matrix is of size 1000×1000 .

To calculate all data points, several values of ε_0 are chosen in the region $\varepsilon_0 \in [-a, a]$, with $a \sim 10^{-5} - 10^{-4}$. When the occupation number has been recorded for these values, we proceed to a standard fitting to calculate the slope near $\varepsilon_0 = 0$, which gives a direct value for Γ according to the definition in (3.28). This procedure is then repeated for several values of the interaction parameter g (that is, of U in the IRLM hamiltonian). Note that different values of the interaction parameter have been chosen for different t' .

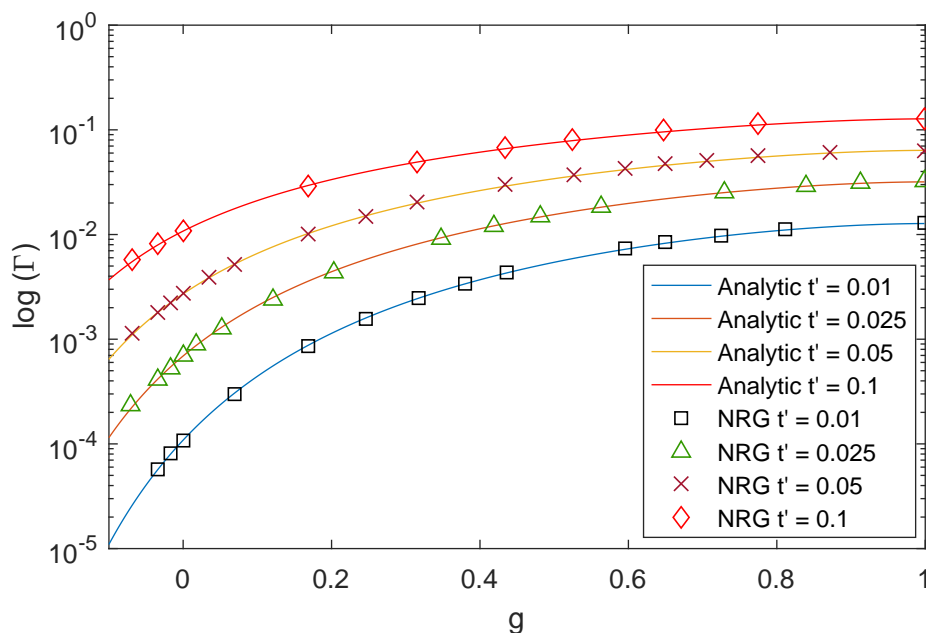


Figure 3.1: NRG simulations for the calculation of the relevant energy scale Γ , for different values of the hybridization parameter t' . The vertical axis is in log scale. The discretization parameter $\Lambda = 1.5$ and the system size is of a total of $N = 82$ lattice sites. Analytical curves correspond to equation (3.36).

Figure (3.1) represents all NRG data simulated for the IRLM. The continuous lines are given by formula (3.36). The value of the bulk density of states ν was calculated from the $U = 0$ case, and inserted into the analytical formula (3.36). An excellent agreement between numerics and the analytical formula is shown. The most surprising feature is that the IRLM, being a model with microscopic parameters described in a lattice, can equally well be described by a bosonic field theory with a boundary term. This equivalence has not been established previously in the literature, although previous studies have explored the relationship between both models by their integrability [46]. Here we prove this equivalence supported by numerical simulations, which leads us to the conclusion that equation (3.36) is an exact expression for the one channel IRLM. More over, the IRLM and the SGM are related

models, whose relation between parameters is then given by:

$$\frac{\beta^2}{4\pi} = (1 - g)^2 \quad (3.38)$$

where again β makes reference to the bulk sine Gordon Model. This relation between the parameters of both models will be useful later in chapter 6, but it is worth to mention now.

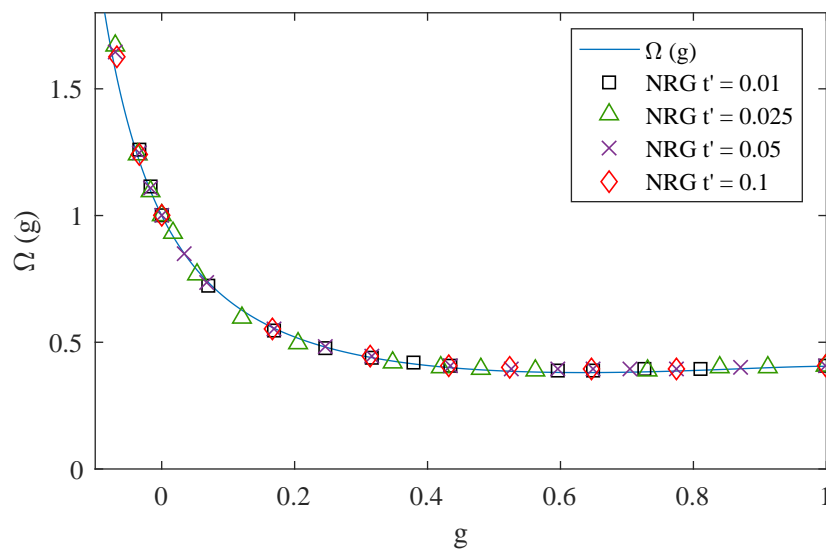


Figure 3.2: NRG simulations for the prefactor of equation (3.37)(continuous curve). All data points collapse on the same curve for different values of the hybridization parameter t' .

On figure (3.2) is represented the prefactor $\Omega(g)$ of equation (3.37). We see how all data points collapse onto the same curve, providing evidence once again for equation (3.37) for the IRLM. The attractive region $g < 0$ contains few points since, as soon as one starts getting closer to the quantum critical point, accuracy in the method is lost.

The thermodynamic exponent α is also obtained from NRG simulations.

For this, we have used a value of $\Lambda = 1.5$ as the discretization parameter. Values of the interaction parameter $g \in [0, 1]$ in steps of 0.1. Three different values of the hybridization parameter $t' = 0.01, 0.025, 0.05$ were used. For each value of g and t' , values of $\varepsilon_0 \in [-1e - 5, +1e - 5]$ where taken (11 values in total). The total size of the chain was $N = 82$ and a total of 500 lowest energy states were kept after truncation of the hamiltonian. The analytic formula represented by the continuous red line is that of equation (3.24). We observe a very good agreement between numerics and the analytical results. It is worth mentioning that this exponent hasn't been calculated numerically in the literature, although the correct analytic formula can be found in [39, 50, 55]. It was believed that NRG should only provide good numerical results for the model in the *weak coupling limit*, this being due to the lack

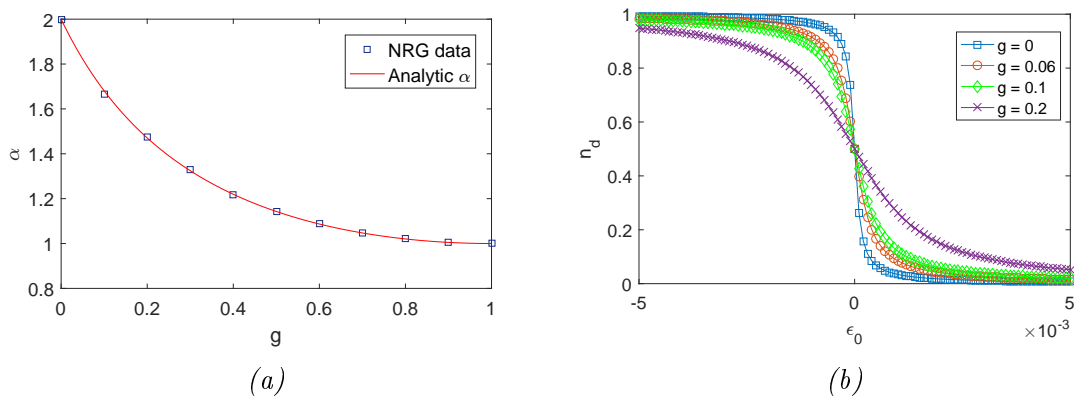


Figure 3.3: NRG simulations for the thermodynamic exponent and the occupation number of the dot. (a) NRG data points for the thermodynamic exponent α as a function of the interaction parameter g . A very good agreement between numerics and the analytical formula equation (3.24) is shown. (b) NRG simulations for the occupation of the dot $\langle d^\dagger d \rangle$ as a function of the local chemical potential ϵ_0 . As interaction is increased, the width in the $\epsilon_0 \sim 0$ grows.

of an exact expression. In this sense, a confirmation of (3.24) has been made for any value of interaction U .

We also consider to give a graph of the occupation number as a function of ϵ_0 for different values of interaction. For positive (repulsive) interaction, the occupation number undergoes a broadening of the width as one would expect. The following points were calculated by NRG for a value of $\Lambda = 1.5$ and a system size of $N = 82$ total sites, by keeping a total of 500 lowest energy states after truncation of the hamiltonian.

3.1.5 The Toulouse point

We want to close this section with the important analogy between the IRLM and the Anisotropic Kondo Model (AKM). For a single value of the parameter J^z in the AKM, the model is exactly solvable, since it maps directly to the $U = 0$ limit of the IRLM. This is known as the *Toulouse point* [66]. This was important at the time of the Kondo problem, since it allows one to map the model exactly to a non-interacting one (at least for a single value of the parameter J). The AKM hamiltonian is:

$$H = H_0 + \frac{J_{\perp}}{2}(s^+ J^- + \text{h.c.}) + J s^z S^z \quad (3.39)$$

with fermionic currents:

$$J^+ =: \psi_{\uparrow}^{\dagger}(x)\psi_{\downarrow}(x) : \quad J^z = \frac{1}{2} : (\psi_{\uparrow}^{\dagger}(x)\psi_{\uparrow}(x) - \psi_{\downarrow}^{\dagger}(x)\psi_{\downarrow}(x)) : \quad (3.40)$$

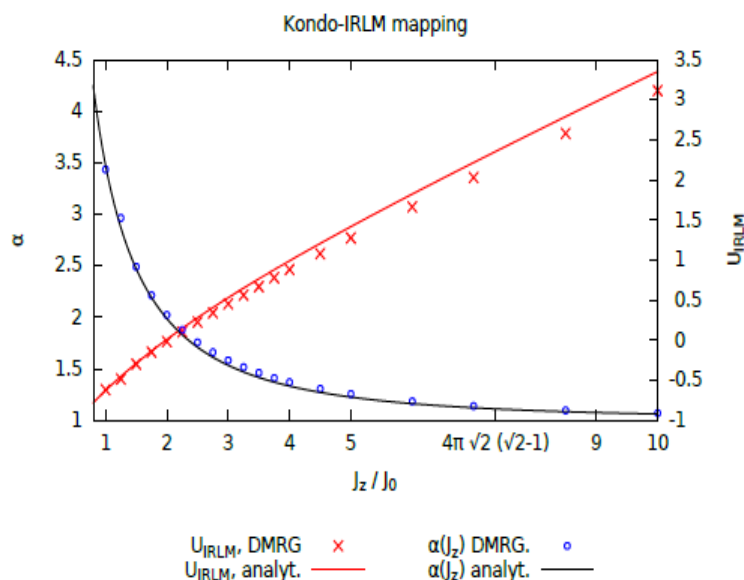


Figure 3.4: Calculation of the Toulouse point in the IRLM/AKM by DMRG simulations. The Toulouse point happens when both curves intersect each other. For that specific value of the coupling J^z , the AKM maps to the Resonant Level Model (RLM), the non-interacting version of the IRLM. (Graph courtesy of Peter Schmitteckert)

If one bosonizes the above hamiltonian, one *spin* degrees of freedom contribute, so that the hamiltonian (3.39) only includes the field:

$$\phi(x) = \frac{1}{\sqrt{2}}(\phi_{\uparrow}(x) - \phi_{\downarrow}(x)) \quad (3.41)$$

The AKM has the bosonized form:

$$H[\phi] = H_0[\phi] + \frac{J_{\perp}}{4\pi}\eta(s^+ e^{i\sqrt{8\pi}\phi(0)} + \text{h.c.}) + \frac{\sqrt{2}J}{\sqrt{\pi}}s^z \partial_x \phi(0) \quad (3.42)$$

One proceeds now in the same way as before (3.12) by applying a unitary transformation \mathcal{U} . In this case, the parameter ρ in (3.12) is chosen so that the scaling dimension of the vertex operators is $d = 1/2$, that is, they are *fermionic*. Similarly, the coupling constant J can be substituted by the scattering phase-shift on the $J_{\perp} = 0$ limit. In this case, because there are two channels (one for spin up and another for spin down), the scattering phase shift contains an extra $1/2$ factor as compared with the IRLM case:

$$\delta_K = \arctan\left(\frac{J\pi\nu}{4}\right) \quad g_T = \frac{2\delta_K}{\pi} \quad (3.43)$$

The Toulouse point is obtained for a value of:

$$g_T = 1 - \frac{1}{\sqrt{2}} \sim 0.29 \rightarrow J^* = \frac{4}{\pi\nu} \tan\left(\frac{\pi g_T}{2}\right) \quad (3.44)$$

We report here this result to be incorrect in [66], however it is obtained correctly in [90]. Notice that although the numerical value of g_T is known, the value of the corresponding coupling still depends on one microscopic parameter, the bulk density of states ν .

3.2 Lattice treatment of the IRLM

We have considered so far the IRLM as described by a field theory of fermionic operators, which ended being bosonized. It is also well known that the low-energy sector of any given model is to be described either by a field or by its lattice version. Both methods provide the same answers, and here we will explore these analogies by applying different techniques to study the single channel IRLM on its lattice version. Moreover, we will be interested in computing expressions useful to study the *strong coupling* limit of the theory, when the interaction parameter U is pushed far away from the original cut-off of the theory (the bandwidth describing the bulk electrons).

3.2.1 Strong coupling limit

We will study now the strong coupling limit of the theory, where the system becomes strongly correlated. In such a limit $U\nu \gg 1$ for the IRLM. In fact, we will be now interested in studying the limit of the model when the parameter $g \sim 1$. Because we are dealing with strong values of interaction, one can first consider the *atomic* part of the hamiltonian to be isolated from the rest of the environment. That is, given the IRLM hamiltonian (3.1), we consider the part:

$$H_{\text{atomic}} + U/4 = \varepsilon_0 d^\dagger d + t'(d^\dagger c_0 + \text{h.c.}) + U\left(c_0^\dagger c_0 - \frac{1}{2}\right)\left(d^\dagger d - \frac{1}{2}\right) + U/4 \quad (3.45)$$

The reason to lift the origin of energies by $+U/4$ is that this makes the low-energy subspace to be independent on the interaction parameter U . In the many-particle basis, the situation is equivalent to a two level system, with four possible binary states on it: $\{|00\rangle, |01\rangle, |10\rangle, |11\rangle\}$. In such a basis, the hamiltonian (3.45) is given by:

$$H_{\text{atomic}} = \begin{pmatrix} U/2 & 0 & 0 & 0 \\ 0 & \varepsilon_0 & t' & 0 \\ 0 & t' & 0 & 0 \\ 0 & 0 & 0 & \varepsilon_0 + U/2 \end{pmatrix} \quad (3.46)$$

We note that the low-energy subspace is that formed by the states $|10\rangle, |01\rangle$, states with a total number of particles equal to 1, where the impurity is filled or empty, respectively. We are working here in the limit $U \gg \varepsilon_0$, and also in the strong coupling limit $g \rightarrow 1$. We just need to diagonalize the middle 2×2 matrix (which is the low energy sector) to get the new ground state as:

$$\begin{aligned} |GS\rangle &= \frac{\varepsilon_0 - \xi}{N_1} |10\rangle + \frac{2t'}{N_1} |01\rangle \\ |ES\rangle &= \frac{\varepsilon_0 + \xi}{N_2} |10\rangle + \frac{2t'}{N_2} |01\rangle \end{aligned} \quad (3.47)$$

with corresponding eigenvalues:

$$\lambda^- = \frac{\varepsilon_0 - \xi}{2} \quad \lambda^+ = \frac{\varepsilon_0 + \xi}{2} \quad (3.48)$$

and where we have defined for convenience:

$$\begin{aligned} \xi &= \sqrt{\varepsilon_0^2 + (2t')^2} \\ N_1 &= \sqrt{(2t')^2 + (\varepsilon_0 - \xi)^2} \\ N_2 &= \sqrt{(2t')^2 + (\varepsilon_0 + \xi)^2} \end{aligned} \quad (3.49)$$

The occupation number of the impurity site is now calculated in the atomic limit to be:

$$\langle GS | d^\dagger d | GS \rangle = \left(\frac{\varepsilon_0 - \xi}{N_1} \right)^2 \quad (3.50)$$

or using the above definitions:

$$\langle d^\dagger d \rangle = \frac{(\varepsilon_0 - \sqrt{\varepsilon_0^2 + (2t')^2})^2}{(2t')^2 + (\varepsilon_0 - \sqrt{\varepsilon_0^2 + (2t')^2})^2} \quad (3.51)$$

The occupation number is given by the following expression:

$$n_d = 1 - \frac{1}{1 + (x - \sqrt{1 + x^2})^2} \quad x = \frac{\varepsilon_0}{2t'} \quad (3.52)$$

Note that the density of states of the bulk ν does not appear here, since both last sites of the chain are decoupled from the rest of the bath. By expanding the expression around $x \sim 0$, we get:

$$n_d \sim \frac{1}{2} - \frac{x}{2} + O(x^2) \quad (3.53)$$

and by use of equation (3.28) (the definition of Γ), we have that:

$$\Gamma(g = 1) = \frac{4t'}{\pi} \quad (3.54)$$

The strong coupling limit $g \rightarrow 1$ corresponds to a value of the thermodynamic exponent $\alpha = 1$. If we now take a look at the expression (3.36), and take the limit $\alpha \rightarrow 1$, we see that:

$$\lim_{\alpha \rightarrow 1} \Gamma = \lim_{\alpha \rightarrow 1} \frac{2^{2-\alpha} \pi^{2\alpha-5/2} \Gamma\left(\frac{\alpha-1}{2}\right)}{\left[\Gamma\left(\frac{\alpha-1}{\alpha}\right)\right]^\alpha \Gamma\left(\frac{\alpha}{2}\right)} \nu^{\alpha-1} (t')^\alpha = \frac{4t'}{\pi} \quad (3.55)$$

With that, we have proved that both limits agree in the strong coupling case, for an expression directly taken from the field theory (actually, from the Boundary Sine Gordon Model), and another expression taken from the microscopic parameters in the lattice. Once again, this proves the validity of the mapping between both the BSGM and the IRLM, and more important, *that both the lattice and field theory descriptions of the model reproduce the same low-energy properties*. We remind the reader that equation (3.36) was taken directly from [35], where no explicit mention to the IRLM is done. This strong coupling limit also agrees with the NRG simulations in figures (3.1) and (3.2).

3.2.2 Coupling to a bath of fermions: $1/U$ corrections

In previous calculations, we have treated just the two level system of an impurity and the last site of the wire. This was justified by the strong value of interaction $U = +\infty$ present in the system, when both last sites of the chain can be isolated. However, the true situation is that these two sites, for any other value of $U \neq \infty$ but strong, are still coupled to a surrounding environment. Therefore the term of the hamiltonian:

$$t(c_1^\dagger c_0 + h.c) \quad (3.56)$$

is the term that allows for first order corrections in the $1/U \sim 0$ parameter. We can express the new operators in terms of the old basis ones:

$$\begin{aligned} a &= \frac{\varepsilon_0 - \xi}{N_1} d + \frac{2t'}{N_1} c_0 & d &= \frac{-N_1}{2\xi} a + \frac{N_2}{2\xi} b \\ b &= \frac{\varepsilon_0 + \xi}{N_2} d + \frac{2t'}{N_2} c_0 & c_0 &= \frac{(\varepsilon_0 + \xi)N_1}{4t'\xi} a + \frac{(\xi - \varepsilon_0)N_2}{4t'\xi} b \end{aligned} \quad (3.57)$$

And therefore, the low-energy hamiltonian is expressed:

$$H_L^{eff} = H_0^L + t\hat{P}_L(c_1^\dagger c_0 + h.c)\hat{P}_L + \lambda_- a^\dagger a + \lambda_+ b^\dagger b \quad (3.58)$$

We have to calculate the operator of the coupling projected to the low energy subspace. However, we see that clearly this operator takes us to the high-energy manifold because the number of particles is changed when we apply it. More formally:

$$\hat{P}_L c_1^\dagger c_0 \hat{P}_L = c_1^\dagger (|a\rangle\langle a| + |b\rangle\langle b|) |0\rangle\langle b| = 0 \quad (3.59)$$

Thus the low energy effective hamiltonian here is:

$$H_L^{eff} = H_0^L + \lambda_- a^\dagger a + \lambda_+ b^\dagger b \quad (3.60)$$

which is a totally decoupled hamiltonian. The way to calculate the effect of the surrounding bath into the impurity+site system is by allowing virtual fluctuations between the low energy subspace and the high-energy one. It is here where the Schrieffer-Wolff transformation [10] is applied.

The case of interest appear when we allow virtual exchange hopping between the high-energy manifold and the low energy one. The idea is recovered from the Schrieffer-Wolff transformation that we described earlier in chapter 2. The first order correction to the low energy hamiltonian is given by:

$$H^* = \frac{1}{2} \hat{P}_L [S, V] \hat{P}_L \quad (3.61)$$

where V is the exchange term $t(c_1^\dagger c_0 + h.c)$, and S is antihermitian and arises from a canonical transformation. These corrections are of order $1/U$, so that is why in the limit of $U \rightarrow \infty$ they are not considered. When these terms are taken into account, the low energy hamiltonian (with first order corrections) can be expressed as:

$$\boxed{H_L^{eff} \sim H_0^L + \lambda_a a^\dagger a + \lambda_b b^\dagger b + \frac{2t^2}{U} c_1^\dagger c_1 (J_1^2 a^\dagger a + J_2^2 b^\dagger b + J_1 J_2 a^\dagger b + h.c) + C}$$

where the couplings are defined as:

$$\begin{aligned} J_{1/2} &= N_{1/2} \frac{(\xi \pm \varepsilon_0)}{4t'\xi} \\ J_1^2 + J_2^2 &= 1 \\ J_1 J_2 &= 2 \left(\frac{t'}{\sqrt{(2t')^2 + \varepsilon_0(\varepsilon_0 - \xi)^2}} \right) \left(\frac{t'}{\sqrt{(2t')^2 + \varepsilon_0(\varepsilon_0 + \xi)^2}} \right) \end{aligned} \quad (3.62)$$

The definitions of N_1, N_2, ξ are given by (3.49). We should note that the constant C is essential to come back to the original basis of operators expression. An analysis using perturbation theory can be carried out in the $1/U$ parameter.

We have seen that in this limit, the IRLM transforms into a two level system. The new basis the operators can be identified with spin operators [65], so that:

$$\begin{aligned} S^-/S^+ &= b^\dagger a/a^\dagger b \\ S^z &= \frac{a^\dagger a - b^\dagger b}{2} \\ a^\dagger a + b^\dagger b &= 1 \end{aligned} \quad (3.63)$$

where the last condition arrives since we cant have both levels occupied at the same time. We may want to transform the non-interacting part in an analogy with a spin in a magnetic field:

$$H_0 = h_z S^z + B \quad (3.64)$$

where B is a constant. For that, we have:

$$\lambda_a a^\dagger a + \lambda_b b^\dagger b = c(\lambda_a - \lambda_b)(a^\dagger a - b^\dagger b) + D \underbrace{(a^\dagger a + b^\dagger b)}_1 \quad (3.65)$$

Therefore:

$$\begin{aligned} c(\lambda_a - \lambda_b) + D &= \lambda_a \\ c(\lambda_b - \lambda_a) + D &= \lambda_b \end{aligned} \quad (3.66)$$

$$(3.67)$$

The solutions are easily found for the constants c and D :

$$D = \frac{1}{2}(\lambda_a + \lambda_b) \quad c = \frac{1}{2} \quad (3.68)$$

Neglecting the constant term, we can now express the non-interacting part of the hamiltonian as:

$$H_0 = H_0^{\text{bath}} + h_z S^z \quad (3.69)$$

with $h_z = -\xi < 0$, so the impurity is immersed in a magnetic field (thats why there are two possible energy levels, the ground state being the *spin* aligned parallel to the magnetic field). The interacting part is expressed in terms of the spin operators as:

$$H_{int} = -\frac{2t^2}{U} c_1^\dagger c_1 \left((2J_1^2 - 1)S^z + J_1 J_2 (S^+ + S^-) + \frac{1}{2} \right) \quad (3.70)$$

Recalling that:

$$S^+ + S^- = 2S^x \quad (3.71)$$

Then we can express the interacting part of the low-energy effective hamiltonian as:

$$H_{int} = K_1 c_1^\dagger c_1 \left(S^z + \Delta S^x + g \right) \quad (3.72)$$

where we define:

$$\begin{aligned}
K_1 &= -\frac{2t^2}{U}(2J_1^2 - 1) \\
\Delta &= \frac{2J_1J_2}{(2J_1^2 - 1)} \\
g &= \frac{1}{2}\left(\frac{1}{2J_1^2 - 1}\right) \\
h_z &= -\xi
\end{aligned} \tag{3.73}$$

The important parameter here is K_1 , which englobes the dependence with the interaction. The parameter t represents the hopping amplitude for the tight binding chain, and it is related to the bulk density of states by $\nu = (\pi t)^{-1}$. Thus, a low energy hamiltonian has been constructed in the spin-operator language:

$$H = H_0^{\text{bath}} + h_z S^z + K_1 c_1^\dagger c_1 \left(S^z + \Delta S^x + g \right) \tag{3.74}$$

This hamiltonian represents the IRLM in the sector where $g \sim 1$. Although we managed to express the hamiltonian in the diagonal basis of states $|a\rangle, |b\rangle$, we see that a transverse field appears in the interacting term. This makes the above hamiltonian difficult to treat. If we come back to our original basis, our hamiltonian in the low energy sector is described by:

$$H_{eff} = H_0^L + \varepsilon_0 S^z + 2t' S^x + \frac{2t^2}{U} \hat{P}_L (c_1^\dagger c_0 + h.c.) (c_1^\dagger c_0 + h.c.) \hat{P}_L \tag{3.75}$$

Notice the factor of 2 in the above expression, which accounts for the fact that the high-energy manifold is expanded by two states. Therefore, there are a total of 2 possible virtual fluctuations between the low and the high-energy manifold. This specific form of the SW transformation is allowed when the energy difference between the low and high energy states is big compared to the bulk's characteristic energy scale t .

If we expand the interacting part of this expression, we are left with:

$$\frac{2t^2}{U} \left(c_1^\dagger c_0 c_0^\dagger c_1 + c_0^\dagger c_1 c_1^\dagger c_0 \right) \tag{3.76}$$

Since these are the only operators that are non-zero acting over a state. Taking into account that:

$$\begin{aligned}
c_0^\dagger c_0 &= 1 - c_0 c_0^\dagger \\
S^z &= \frac{d^\dagger d - c_0^\dagger c_0}{2}
\end{aligned} \tag{3.77}$$

Applying anticommutation rules, the hamiltonian can be written as:

$$\boxed{H_{eff} = H_0^L + \varepsilon_0 S^z + 2t' S^x + \frac{4t^2}{U} \left(c_1^\dagger c_1 - \frac{1}{2} \right) S^z} \tag{3.78}$$

This hamiltonian is known as the *resonant tunneling model*, studied previously by Caldeira and Leggett [63]. It gives the strong coupling corrections for the IRLM in the low-energy sector.

3.2.3 Bosonization of the strong coupling hamiltonian

The hamiltonian given by equation (3.78) represents the low energy physics of the IRLM in the strong coupling limit, where the microscopic parameter $U \gg t$. Being a lattice hamiltonian, one can go to the continuum limit by making the lattice spacing $a \rightarrow 0$. In this limit, the lattice operator for the channel becomes:

$$c_1^\dagger c_1 - \frac{1}{2} \rightarrow: \psi^\dagger(x)\psi(x): \quad (3.79)$$

When written in a field theory version, the hamiltonian (3.78) can be bosonized by the same procedure we described before. By making the same identifications between fermionic/bosonic operators, its bosonized form reads ($\varepsilon_0 = 0$):

$$H_{eff} = \frac{1}{2} \int dx (\partial_x \phi(x))^2 + t'(S^+ + S^-) + \frac{K}{\sqrt{\pi}} \partial_x \phi(x) \quad K = \frac{4t^2}{U} \quad (3.80)$$

Applying a canonical transformation of the form similar to (3.12), the model maps onto a bosonized version similar to (3.9):

$$\begin{aligned} U^\dagger H_{eff} U &= \frac{1}{2} \int dx (\partial_x \phi(x))^2 + t'(S^+ e^{-i\sqrt{4\pi}\tau\phi(0)} + \text{h.c.}) \\ \tau = \frac{K}{\pi t} &= K\nu = \frac{4t}{\pi U} \end{aligned} \quad (3.81)$$

The scaling dimension of vertex operators is:

$$2d = \frac{\beta^2}{4\pi} = \frac{(\sqrt{4\pi}\tau)^2}{4\pi} = \tau^2 = \left(\frac{4t}{\pi U}\right)^2 \quad (3.82)$$

Now we take a look at our exact expression for the scaling dimension in the general U field theory, which was derived in (3.14). A $1/U$ expansion gives:

$$g = \frac{2}{\pi} \arctan\left(\frac{U}{2t}\right) \sim 1 - \frac{4t}{\pi U} + O((1/U)^2) \quad (3.83)$$

Therefore, the scaling dimension of vertex operators in the field theory (3.9) in the large U limit is given by:

$$2d = (1 - g)^2 \sim \left(\frac{4t}{\pi U}\right)^2 \quad (3.84)$$

which matches with equation (3.82). Thus, we have proved the general field theory for the IRLM in the large U sector to match the field theory derived from a strong

coupling expansion in $1/U$ in the lattice. This proves one very important result: No matter how big the value of U is, we can always derive our field theory results from the lattice construction of the model, and viceversa. This was proved already with numerical simulations in figure (3.1), where an equivalence between the model on its lattice version (depending on the microscopic parameters) and the equivalent field theory (Boundary Sine Gordon Model) is shown. A conclusion of this is that all low-energy properties of the model can be extracted either by its lattice version or its field description.

3.2.4 Mean Field Theory in the strong coupling limit

Usually, a Mean Field Theory treatment of a physical model can offer rich information about the qualitative behaviour of the model in some region of parameter space. This proves to be the case in the Anderson model. For the IRLM, we consider equation (3.78). A MFT treatment simplifies the problem by substituting some operator in the interacting part of a hamiltonian by an averaged value, which is to be calculated in a self-consistent way. We will see that with this method we do not reproduce the correct $1/U$ correction one would expect from an expansion of equation (3.23). Nevertheless, the method is quite general to be considered here and to serve as a point of reference for further work.

Consider the interacting term in (3.78), which is substituted by:

$$\langle c_1^\dagger c_1 \rangle = n_1 = \frac{1}{2} - \frac{1}{\pi} \arctan \left(\frac{\varepsilon'_0}{\nu t^2} \right) \quad (3.85)$$

which resembles the occupation number of the non-interacting Resonant Level Model. If we consider the relation:

$$S^z = n_d - \frac{1}{2} \rightarrow \langle S^z \rangle = \langle n_d \rangle - \frac{1}{2} \quad (3.86)$$

thus the local chemical potential ε'_0 equals:

$$\varepsilon'_0 = \frac{2t^2}{U} \left(\langle n_d \rangle - \frac{1}{2} \right) \quad (3.87)$$

Therefore, the occupation number on the first site of the tight-binding chain is:

$$\langle c_1^\dagger c_1 \rangle = \frac{1}{2} - \frac{1}{\pi} \arctan \left(\frac{\langle n_d \rangle - 1/2}{\nu U/2} \right) \quad (3.88)$$

Defining the following parameters:

$$\begin{aligned} \langle c_1^\dagger c_1 \rangle - 1/2 &= -\frac{1}{\pi} \arctan \left(\frac{\langle n_d \rangle - 1/2}{\nu U/2} \right) = \Delta \\ k_1 &= \frac{2t^2}{U} \end{aligned} \quad (3.89)$$

the hamiltonian in terms of d, c_0 operators is:

$$H_{MF} = \left(\frac{\varepsilon_0}{2} + k_1 \frac{\Delta}{2} \right) d^\dagger d - \left(\frac{\varepsilon_0}{2} + k_1 \frac{\Delta}{2} \right) c_0^\dagger c_0 + t'(c_0^\dagger d + d^\dagger c_0) \quad (3.90)$$

We diagonalize this to get the eigenvalues:

$$\lambda_{\mp} = \mp \frac{1}{2} \sqrt{(2t')^2 + (\varepsilon_0 + k_1 \Delta)^2} = \mp t' \sqrt{1 + x^2} \quad x = \frac{\varepsilon_0 + k_1 \Delta}{2t'} \quad (3.91)$$

The eigenvector associated with the lowest eigenvalue (i.e, the ground state) is:

$$|GS\rangle = \frac{1}{N_1} \left(-1, x + \sqrt{1 + x^2} \right) \quad (3.92)$$

where the normalization constant is:

$$N_1 = \sqrt{2} \sqrt{1 + x^2 + x \sqrt{1 + x^2}} \quad (3.93)$$

Since the ground-state $|GS\rangle$ is:

$$|GS\rangle = \alpha|10\rangle + \beta|01\rangle \quad (3.94)$$

Then we have an expression for the occupation of the dot:

$$\langle n_d \rangle = \alpha^2 = \frac{1}{2(1 + x^2 + x \sqrt{1 + x^2})} \quad (3.95)$$

where we must keep in mind that τ depends on $\langle n_d \rangle$ through Δ . This is then a self consistent equation for the occupation number on the impurity site. For $x = 0$, we find $\langle n_d \rangle = 1/2$ as expected. We now define the quantity:

$$\zeta = \langle n_d \rangle - \frac{1}{2} \quad k_1 \Delta = -\frac{k_1}{\pi} \arctan \left(\frac{k_1 \zeta}{\nu t^2} \right) \quad (3.96)$$

Since we are interested in the large U limit of this expression, we perform an expansion in the parameter k_1 . Expanding to first order we have:

$$\zeta \sim -\frac{y}{2\sqrt{1+y^2}} + \zeta \frac{(\Lambda/U)^2}{16\pi\nu t'} \frac{1}{(1+y^2)^{3/2}} \quad y = \frac{\varepsilon_0}{2t'} \quad (3.97)$$

In terms of the cut-off of the theory, $\Lambda = 4t$, then:

$$\zeta \sim \frac{\beta y(1+y^2)}{2((\Lambda/U)^2 - \beta(1+y^2)^{3/2})} \quad \beta = 16\pi\nu t' \quad (3.98)$$

It is at this stage when we make use of the formula for the definition of the thermodynamic energy scale used in (3.28). The value of the charge susceptibility is calculated by taking the derivative respect to y :

$$\chi = \frac{1}{2t'} \frac{\partial \zeta}{\partial y} = \frac{\beta}{4t'} \left(\frac{(\Lambda/U)^2(1+3y^2) - \beta(1+y^2)^{3/2}}{((\Lambda/U)^2 - \beta(1+y^2)^{3/2})^2} \right) \quad (3.99)$$

which provides directly the value of the width, for small values of y :

$$\Gamma \sim -\frac{1}{\pi} \frac{4t'((\Lambda/U)^2 - \beta\kappa^3)^2}{\beta\left((\Lambda/U)^2(1 + 3y^2) - \beta\kappa^3\right)} \quad \kappa = (1 + y^2) \quad (3.100)$$

The minus sign comes from the definition of Γ equation (3.28). We see that the limit of $U \rightarrow +\infty$ is recovered here. In this concrete limit:

$$\Gamma_{U=\infty} = \frac{4t'}{\pi}(1 + y^2)^{3/2} \quad (3.101)$$

For the value $y = 0$, that is, when the local chemical potential $\varepsilon_0 = 0$, this expression is:

$$\lim_{g \rightarrow 1} \Gamma = \frac{4t'}{\pi} \quad (3.102)$$

which matches with the limit of (3.36) for $g \rightarrow 1$. The MFT allows to calculate the first order correction in $1/U$ for the susceptibility, so that for $\kappa = 1$:

$$\Gamma_{MF} \sim \frac{4t'}{\pi} - \frac{1}{4\pi^2\nu} \left(\frac{\Lambda}{U}\right)^2 \quad (3.103)$$

Notice that this correction doesn't depend on the parameter t' , which is surprising at first sight. Thus, we believe the MFT approach exposed here to be incomplete; although it does not reproduce the expected corrections, the method is quite general and can serve as a starting point for further work on the model.

3.3 Brief summary of results

In this chapter, we have built up a theory for *exact* thermodynamics in the single channel version of the IRLM. Analytical results have been compared with NRG numerics, resulting in very good agreement between both. We summarize here the most important results found:

- By use of bosonization, the IRLM in the one channel case is mapped to a Boundary Sine Gordon Model (BSGM), where the parameters of both models are related by:

$$\frac{\beta^2}{8\pi} = \frac{1}{2}(1 - g)^2 \quad (3.104)$$

where β is the bulk parameter in the standard Sine Gordon theory, and g is related to the phase-shift experienced by the single boson arising from the bosonized version of the IRLM.

- From this mapping, an standard RG procedure allows to calculate the *correlation length*, which will determine the relevant energy scale $\Gamma \sim (t')^\alpha$. This allows to calculate in an *exact* way the thermodynamic exponent α . The analytical result is then confirmed by NRG simulations.
- To further prove correspondence between both models, an *exact* relation between the boundary temperature T_B in the BSGM and the thermodynamic energy scale of the IRLM Γ is given. The relation *between microscopic parameters of the model* and the field theoretic description ($U\nu \rightarrow 2\delta$) is proved carrying out NRG simulations. These simulations match analytical results with a very good agreement.
- Correct identification of the so called Toulouse point, where the Anisotropic Kondo Model (AKM) maps to the $U = 0$ IRLM.
- Strong coupling treatment of the model *in the lattice* proves to give the same answers as its field theory version. Within this description, we give an effective low-energy hamiltonian, with coupling in $1/U$ order. The bosonized version of the strong coupling hamiltonian (worked out from the lattice) is in agreement with the field theory carried out for all values of U .
- We study $1/U$ corrections in the large U limit by Mean Field Theory. We recover the exact result at $U = +\infty$, but the method fails to provide the correct next order corrections away from this point.

Chapter 4

N channel IRLM: General features

*“All human wisdom is contained
in these two words - Wait and
Hope”*

Alexandre Dumas, The Count
of Monte Cristo

Whereas a complete thermodynamic theory of the single channel IRLM has been discussed in the previous chapter, further generalization of the model to its multichannel version presents interesting questions to address. Even being the same model, attaching one extra channel to the impurity site changes drastically the physics, as we will shortly see. A complete theory of the model for an arbitrary number of leads constitutes a major challenge to be completed in the equilibrium IRLM. However, some general features of the model can still be computed following a similar analysis as for the one channel case. In this chapter, we will describe these general features, pointing out in our way all open questions arising in the model, which can serve as a starting point for further investigation.

4.1 Two channel ($N = 2$) IRLM

We pass now to describe some general thermodynamic features of the two channel IRLM. Although we won't treat non-equilibrium properties of the IRLM in this thesis, we want to motivate its introduction briefly. The two channel version of the IRLM is of great importance from the point of view of its transport (non-equilibrium) properties. It has been studied out of equilibrium under several methods [44, 46, 47, 48, 49, 51]. Of particular interest is the extension of the Bethe ansatz method [44] applied to the model, the so called *open Bethe ansatz*. The method claims to be quite general to solve for the non-equilibrium steady state of strongly correlated systems, allowing an exact solution for every value of the interaction parameter. However, performed numerics [45] disagree with the claimed exact solution, and thus the method, despite of being a pioneering one, still undergoes revision. The two channel IRLM has only been solved in an exact way at the self-dual point [48], when $U = 2t$, where it has proved to agree with performed numerics. One

of the main quantities to be computed is the *noise* related to the current. This has also been studied at the self-dual point (SDP) of the model, where very good agreement between numerics and analytics has been found [91]. In this line of research, extension of analytical approaches to solve the model for an arbitrary interaction value are desirable.

Instead, we will focus on some of its equilibrium properties, in a similar fashion as we made with the single channel case. Despite its apparent simplicity as compared to its non-equilibrium counterpart, we find the two lead IRLM in equilibrium to offer rich physics, which may serve as a good starting point when treating the problem out of equilibrium.

4.1.1 Bosonization and thermodynamic exponent: Duality

Following our last treatment for the one channel IRLM, we will bosonize the two channel case in the same way. The unfolding of the fields can be done in the similar way as in (3.5). Thus the two channel IRLM is equivalent to two single channel IRLM in the whole line:

$$H = -i \sum_{i=\pm} \int_{-\infty}^{+\infty} dx (\psi_i^\dagger(x) \partial_x \psi_i(x)) + \varepsilon_0 d^\dagger d + t' \sum_{i=\pm} (d^\dagger \psi_i(0) + \text{h.c.}) + U \sum_{i=\pm} : \psi_i^\dagger(0) \psi_i(0) : (d^\dagger d - \frac{1}{2}) \quad (4.1)$$

where \pm represent the right and left leads respectively, and each lead carries only right-moving fermions. The bosonization expressions now work for every field, so we have two bosonic fields ϕ_\pm representing each channel. The hamiltonian transforms to ($\varepsilon_0 = 0$):

$$H = \frac{1}{2} \sum_{\pm} \int dx (\partial_x \phi_\pm(x))^2 + \frac{t'}{\sqrt{2\pi}} \left(\eta_\pm S^+ e^{i\sqrt{4\pi}\phi_\pm(0)} + \text{h.c.} \right) + \frac{2\delta}{\sqrt{\pi}} \sum_{\pm} \partial_x \phi_\pm(0) \quad (4.2)$$

where again, we have substituted the microscopic parameter $U\nu \rightarrow 2\delta$ as in (3.11). Now one needs to perform a proper rotation of the fields in order to eliminate the part proportional to 2δ . For that, we choose:

$$U = e^{i\sqrt{4\pi}S^z \rho \frac{1}{\sqrt{2}}(\phi_+(0) + \phi_-(0))} \quad (4.3)$$

where ρ is to be determined. Applying the unitary transformation over the above hamiltonian, we obtain:

$$H = H_0 + \frac{t'}{\sqrt{2\pi}} \sum_{\pm} \eta_\pm S^+ e^{i\sqrt{4\pi}(1-\rho/\sqrt{2})\phi_\pm(0)} e^{-i\sqrt{4\pi}\rho/\sqrt{2}\phi_\mp} + \text{h.c.}$$

$$\rho = \frac{2\delta\sqrt{2}}{\pi} \quad (4.4)$$

In analogy with the treatment for the one channel case, now we can take a look at the scaling dimension of the vertex operators. In this case, since each field is independent, the scaling dimension is just the sum of both. Thus:

$$2d = \frac{\beta_+^2}{4\pi} + \frac{\beta_-^2}{4\pi} = 1 - 2g + 2g^2 \quad (4.5)$$

Notice the analogy with the one lead channel (3.14), but a factor of 2 (the number of leads) now follows for the g^2 term. It is worth understanding the importance of this g^2 term, since in fact, its where all difference between the IRLM with different number of channels lies.

By generalizing to a boundary Sine Gordon Model, and carrying out the same analysis as before, one finds that the relevant energy scale for the two channel IRLM has to be of the form:

$$\Gamma \sim f(\alpha)(t')^\alpha \quad \alpha = \frac{2}{1 + 2g - 2g^2} \quad (4.6)$$

This result has also been obtained in [39, 50], although no explicit mention to the prefactor $f(\alpha)$ is done, which turns out to be essential as we will shortly see. We want to make an important analysis of the result found for α .

The model develops a *duality*, in the sense that a change in the phase shift:

$$\delta \rightarrow \frac{\pi}{2} - \delta \quad (4.7)$$

keeps the scaling dimension unchanged. In the two dimensional case, this duality happens exactly at the infinite interaction point $g = 1$ so that:

$$\delta = \frac{\pi}{2} \rightarrow d = \frac{1}{2} \quad (4.8)$$

Therefore, exactly at this point, the vertex operators correspond to fermions again. This duality represents a relation between the small U values of the model and strong values of U , so that $U \leftrightarrow 1/U$ are equivalent for the exponent α . This has been pointed out in [51], and can be seen if one represents α against g . The point $g = 0.5$, which corresponds to $U = 2t$, is called the *self-dual* point. We have thus found the first peculiarity between the one channel case and the IRLM when an extra channel is attached to the impurity site: the thermodynamic exponent α in the two channel version of the model *presents a duality* between the weak coupling limit and the strong coupling limit of the theory.

It is curious to see that at this concrete value of infinite interaction, the model maps itself onto another non-interacting fermionic problem. When we *refermionize* at $g = 1$, we get a hamiltonian similar to:

$$H_{U=\infty} = H_0 + \varepsilon_0 d^\dagger d + J'(d^\dagger \psi_+^\dagger(0) + d^\dagger \psi_-^\dagger(0) + \text{h.c.}) \quad (4.9)$$

Notice that this hamiltonian doesn't contain an interaction between the leads and the dot, nor represents an hybridization between the impurity and the channels,

therefore its physical interpretation is unclear. It is a remarkable fact that for infinite interaction between the leads and the impurity, the system behaves as that of free fermionic fields.

4.1.2 The prefactor $f(\alpha)$: Broken duality

We have seen previously that the two channel IRLM develops a duality, in the sense that there is a correspondence $U \leftrightarrow 1/U$ in the thermodynamic exponent. Moreover, we have shown that at infinite interaction $U = +\infty$, the model maps again to a non-interacting model of fermions.

One would expect this duality to hold in the relevant thermodynamic scale Γ , that is, not only the exponent, but the value of Γ itself, to be subjected to the correspondence $U \leftrightarrow 1/U$. If at $U = 0$ the thermodynamic scale is $\Gamma_0 = 2\pi\nu(t')^2$, one would expect that, exactly at $U = +\infty$, this same value of Γ is recovered due to the duality. As we will see shortly, this proves *not* to be the case, reflecting once again another surprising feature of the model.

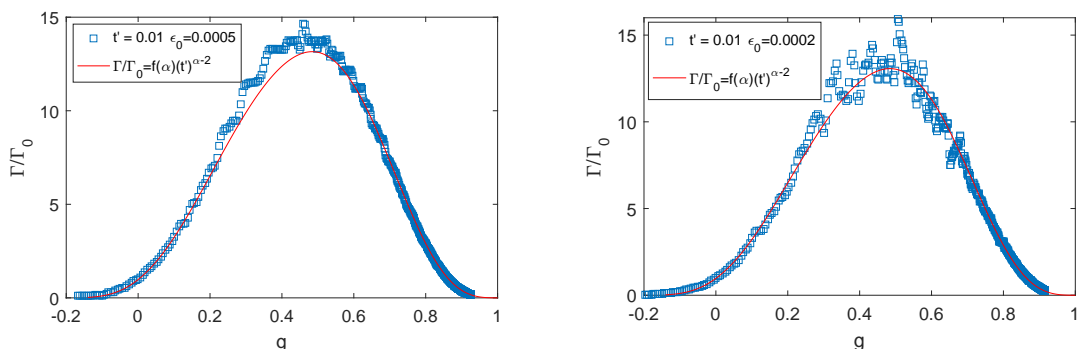


Figure 4.1: Numerical data for the thermodynamic energy scale in the 2 channel IRLM. The data was directly extracted from [53]. The red curve shows the proposed form for Γ given in equation (4.11), where a good agreement with numerics is found. Note the numerical oscillations developed close to the self-dual point.

Numerical data on the occupation number for the two lead IRLM was obtained from [53] and the thermodynamic width Γ was extracted in the similar way as for the one channel IRLM. The values of $\varepsilon_0 = 2e - 4, 5e - 4$, so that the width can be extracted from the occupation number n_d as:

$$\Gamma = \varepsilon_0 \tan(\pi n_d(g)) \quad g = \frac{2}{\pi} \arctan\left(\frac{U\pi\nu}{2}\right) \quad (4.10)$$

In order to fit the numerical data, a proposed form for the prefactor is taken, with two fitting parameters, a, b . It is only the ratio Γ/Γ_0 what can be compared with the analytic result, since we are using different values of ε_0 . The proposed form for

the analytical formula for Γ is:

$$\frac{\Gamma}{\Gamma_0} = \frac{1}{\Gamma_0} f(\alpha) (t')^\alpha \quad f(\alpha) = \left(\frac{b\Lambda_0}{\tanh(a(\Lambda_0/U)^2)} \right)^{1-\alpha} \quad (4.11)$$

The reason to choose this function is that it recovers nicely the weak and strong coupling limits of the theory. The parameters $a = 8$ and $b = 0.5$ prove to be the convenient values for the function to fit the numerical data. The numerical data is plotted against this proposed analytical form in figure (4.1). We notice that, as opposed to the exponent α , the duality is broken when the prefactor for the expression is taken into account. In other words, as interaction is increased and we approach the $g \rightarrow 1$ limit, $\Gamma \rightarrow 0$ and not to Γ_0 . At the moment, we are still working on possible explanations of this effect. This is shown in figure (4.1). It can be seen how as $g \rightarrow 1$, the thermodynamic energy scale Γ vanishes. If $\Gamma = 0$ at infinite interaction, this means that now the correlation length in the system becomes infinite, that is, fluctuations work now at all length scales. At this specific point, the model experiences *something similar*¹ to a quantum phase transition (QPT). Notice that the hamiltonian described exactly at $g = 1$ does not conserve particle number, which at first sight is surprising, and might hint why such broken duality occurs. In order to gain some clarity on this effect, we turn now to discuss the model onto its lattice version.

4.1.3 Field vs lattice descriptions

We want now to discuss one of the main points of the above results, which is in relationship with what was shown before in chapter 3 for the single channel version of the model. It has been argued [51] that different behaviours can be expected in the strong coupling limit of the $N = 2$ IRLM, depending on whether the continuous (field) or discrete (lattice) versions are considered. One of the conclusions in [51] is that the apparent broken duality for the thermodynamic scale Γ we have just shown, is a purely lattice effect.

In a lattice version of the model, the energy cut-off of the theory is related to the bandwidth of the model, since the natural distance cut-off is given by the lattice spacing. In a field theory description, a cut-off Λ might depend on the regularization scheme employed. When working on the lattice version of the $N = 2$ IRLM, one always observes a decreasing value of Γ , the thermodynamic width, as we approach the infinite interaction limit $g \rightarrow 1$. This can be shown by a strong coupling treatment we are about to develop. On the other hand, in the continuous version (field theory), the cut-off is subjected to regularization schemes, and therefore, one can recover $\Gamma = \Gamma_0$ at $U = +\infty$, preserving the duality both in α (the thermodynamic exponent) and Γ , the relevant low-energy scale. Therefore, one of the main conclusions of [51] is that, for the $N = 2$ version of the IRLM in the strong coupling limit,

¹We want to be a bit careful here when talking about QPT in the model. As we will see in the next section, these are determined by the relevancy or irrelevancy of operators describing the low-energy physics in the model in some region of parameter space.

the duality $U \leftrightarrow 1/U$ can be preserved when going to a continuous description of the model, but not in the lattice version. In this sense, one just needs to select the appropriate cut-off dependence on interaction, and regularize the theory accordingly.

At this point, we need to show our discrepancy on that, supported by our previously shown results in chapter 3. It is hard to imagine that both, the lattice and the field versions of a model, can still provide different answers when going to the low-energy description of a model. Moreover, the fact that this differences have origin in the regularization schemes employed (for the field theory version), introduces some arbitrariness when computing *exact expressions of relevant physical quantities*.

We look now at expression (3.36) in chapter 3. As it is shown in figures (3.1) and (3.2), the exact expression for the thermodynamic energy scale Γ can be very well reproduced by the discrete version of the model. What is shown here is that, even when expression (3.23) is computed from the field theory, no regularization scheme or similars are needed to describe the low-energy physics of the lattice version of the IRLM. In other words, what was shown for the single channel IRLM is that both treatments (field/lattice) provide identical answers, as one would expect working at large length scales.

We therefore believe that *the computation of exact results has to be independent of the regularization scheme employed by the field theory*. Thus, the cut-off Λ is always kept fixed, described by the bandwidth of the model. In this fashion, we believe the broken duality shown in figure (4.11) to be a *real* effect that can be recovered from both the lattice and the field description. Moreover, we believe that the prefactor $f(\alpha)$ can be computed in an exact way from the field theory, in a similar way as it is done for the $N = 1$ version of the model (by direct mapping to a Boundary Sine Gordon theory). The correct way to identify again such analogies is at the moment unclear to us.

4.1.4 Strong coupling limit in the lattice

We will study the strong coupling limit of the two channel case in the lattice, in a similar fashion as we did before for the single lead. For the two channel IRLM, the non-interacting width (what we have been calling Γ_0) is:

$$\Gamma_0 = 2\pi\nu t'^2 \quad (4.12)$$

where ν is the bulk density of states for one of the leads.

For a strong coupling between the leads and the impurity, the initial hamiltonian matrix consists on 8×8 elements in the many-body basis (see appendix D for details). In the low energy sector, two energy states appear:

$$\begin{aligned} |GS\rangle &= a|100\rangle + b|001\rangle + c|010\rangle \\ |ES\rangle &= n|110\rangle + p|011\rangle + m|101\rangle \end{aligned} \quad (4.13)$$

where the letters are parameters depending on t', U . Notice that these states correspond to the subspace of $N = 1$ total particles in the system and $N = 2$, but they expand the low-energy subspace of the initial hamiltonian. Defining the following parameters:

$$\begin{aligned} \xi &= \sqrt{8t'^2 + (\varepsilon_0 - U/2)^2} & \chi &= \sqrt{8t'^2 + (\varepsilon_0 + U/2)^2} \\ \alpha &= \varepsilon_0 - U/2 & \beta &= \varepsilon_0 + U/2 \\ \zeta &= \sqrt{16t'^2 + 2(\alpha + \xi)^2} & \gamma &= \sqrt{2(\beta - \chi)^2 + 16t'^2} \\ \zeta' &= \sqrt{16t'^2 + 2(\alpha - \xi)^2} & \gamma' &= \sqrt{2(\beta + \chi)^2 + 16t'^2} \end{aligned} \quad (4.14)$$

One finds the coefficients to satisfy the following relations:

$$\begin{aligned} a &= \frac{\alpha + \xi}{\zeta} = b & n &= \frac{\beta - \chi}{\gamma} = p \\ c &= -\frac{4t'}{\zeta} & m &= \frac{4t'}{\gamma} \end{aligned} \quad (4.15)$$

When we work out the projector, we can apply this to the coupling between the last site of the chain and that of the leads as we did before, then:

$$\hat{P}_L \left(t \sum_{i=L/R} (c_{i,1}^\dagger c_{i,0} + h.c.) \right) \hat{P}_L \quad \hat{P}_L = |GS\rangle\langle GS| + |ES\rangle\langle ES| \quad (4.16)$$

becomes the operator describing the low-energy sector of the model in the strong-coupling regime, where L/R represent the left or right channel, respectively. The new coupling constant can be worked out in the limit of $U \gg \varepsilon_0$ and $U \gg t'$, resulting to be:

$$J = t(nc + am) = t \frac{4t'}{\zeta\gamma} (-U + \xi + \chi) \sim 4t \frac{t'}{U} \quad (4.17)$$

in agreement with what is found in [51]. We refer to appendix D for details on the calculation. Therefore, in the strong coupling case, the width decreases to 0 as observed from the collected numerical data in figure (4.1). Therefore, in this limit:

$$\Gamma(g \sim 1) \sim \frac{1}{U^2} \quad (4.18)$$

This reflects the fact that as $U \rightarrow +\infty$, the thermodynamic width $\Gamma \rightarrow 0$ in the two channel version of the model. At this point, fluctuations work at all length scales, since $\Gamma \sim \xi^{-1}$, the correlation length in the system.

Compare this behaviour with the one found in the single channel case, equation (3.102). Whereas in the single channel version the thermodynamic energy scale goes to a finite value proportional to the hybridization parameter t' , the two channel case is totally different: the value of Γ at infinite interaction vanishes, regardless of the value of the hybridization parameter t' .

4.2 General thermodynamics in the IRLM

In this section, the multichannel IRLM is treated in the field theory by bosonization. We will compute the value of the thermodynamic exponent α for any number of leads N attached to the impurity site. We present DMRG results on this, in agreement with the general formula for the N channel case. After this, we will give an explanation of all possible quantum phase transitions we encounter in the model, which represent separation between two regions where operators behave in a different way under renormalization.

4.2.1 Multichannel ($N > 1$) IRLM

We consider now the IRLM when more than one channel is attached to the impurity site. Such a hamiltonian is written as:

$$H = -i \sum_{j=1}^N \int_{-\infty}^{+\infty} dx (\psi_{Rj}^\dagger(x) \partial_x \psi_{Rj}(x)) + \varepsilon_0 d^\dagger d + t' \sum_{j=1}^N (d^\dagger \psi_{R,j}(0) + \text{h.c.}) + U \sum_{j=1}^N : \psi_{Rj}^\dagger(0) \psi_{Rj}(0) : (d^\dagger d - \frac{1}{2}) \quad (4.19)$$

where the sum is running for all different leads (fields). Again, we will work on the particle-hole symmetric limit $\varepsilon_0 = 0$ unless specified. The identification of each fermionic operator with a bosonic one in the form (3.7) leads to a bosonized hamiltonian of N independent Bose fields:

$$H = H_0 + \sum_{j=1}^N \frac{t'}{\sqrt{2\pi}} (S^+ e^{i\sqrt{4\pi}\phi_j(0)} + \text{h.c.}) + \frac{2\delta}{\sqrt{\pi}} \sum_{j=1}^N S^z \partial_x \phi_j(x) \quad (4.20)$$

where again we have substituted $U\nu \rightarrow 2\delta$. The procedure is the same as in the $N = 1$ case, except that now all bosonic fields must be taken into account in the rotation. We choose the unitary transformation:

$$\mathcal{U} = e^{i\sqrt{4\pi}\rho S^z \frac{1}{\sqrt{N}} \sum_{j=1}^N \phi_j(0)} \quad (4.21)$$

to perform the rotation of the fields. With that, the transformed hamiltonian $\bar{H} = \mathcal{U}^\dagger H \mathcal{U}$ is:

$$\bar{H} = \bar{H}_0 + \frac{t'}{\sqrt{2\pi}} \sum_j^N (S^- e^{i\beta_j \phi_j(0)} e^{-i\beta_l \phi_l(0)} + \text{h.c.}) \quad \rho = \frac{2\delta\sqrt{N}}{\pi} = g\sqrt{N} \quad (4.22)$$

and the non-interacting part being:

$$\bar{H}_0 = \sum_{j=1}^N \frac{1}{2} \int_{-\infty}^{+\infty} dx (\partial_x \phi_j(x))^2 \quad (4.23)$$

Note that the value of ρ has been chosen in a way that the term proportional to 2δ in (4.20) disappears. In expression (4.20) we have defined for notation convenience:

$$\beta_l \phi_l = \sum_{l \neq j} \sqrt{4\pi} \frac{\rho}{\sqrt{N}} \phi_l(0) = \sum_{l \neq j} \sqrt{4\pi} g \phi_l(0) \quad (4.24)$$

Therefore, a full bosonized version of the IRLM has been developed for an arbitrary number of channels N .

4.2.2 Scaling dimensions of operators and thermodynamic exponent α

Here we explore the change on the scaling dimensions of the operators, as well as we show explicit calculation of the thermodynamic exponent α . We have seen previously how, under a certain unitary transformation, the scaling dimension of operators changes, that is, it becomes dependent on the interaction. For the single channel case we obtained equation (3.14) as the main result.

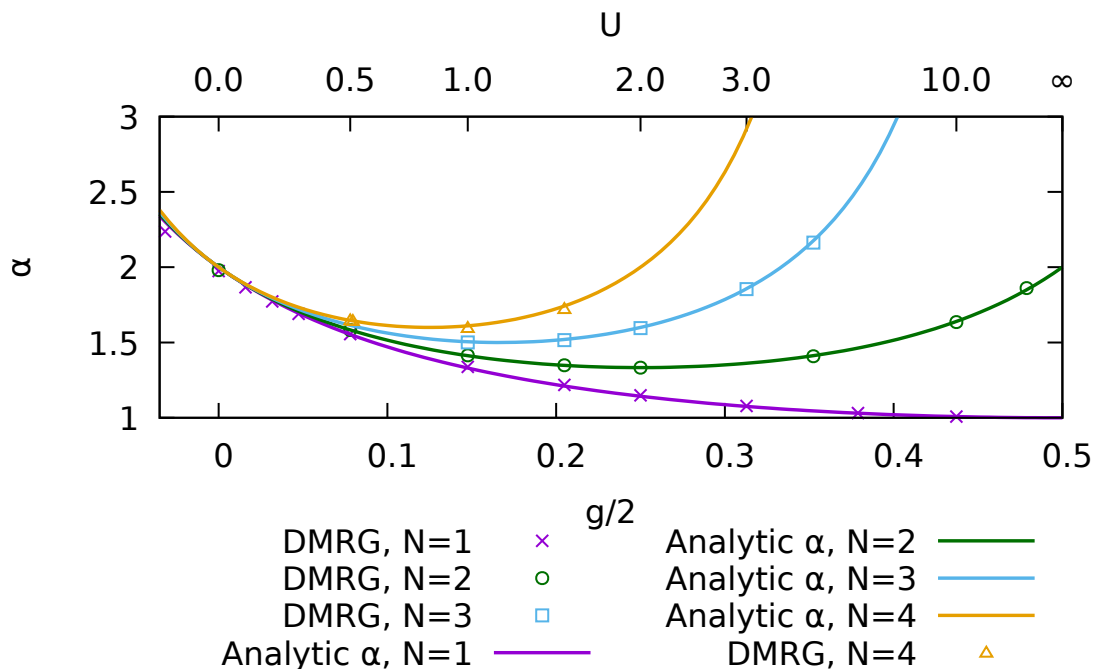


Figure 4.2: DMRG calculation for the thermodynamic exponent α as a function of the interaction parameter g , for $N = 1$ (red) to $N = 4$ (purple) channels. For the $N = 4$ channel case, higher values of g are avoided, since one gets closer to the quantum phase transition. Graph courtesy of Peter Schmitteckert.

For the N channel IRLM, the total scaling dimension of the operator in equation (4.22) is just the sum of all the scaling dimensions of vertex operators:

$$2d = \frac{\beta_j^2}{4\pi} + (N-1) \frac{\beta_{l \neq j}^2}{4\pi} \quad (4.25)$$

For the field j , this was previously calculated to have scaling dimension of the form (see (3.14)):

$$\frac{\beta_j^2}{4\pi} = (1 - g)^2 \quad (4.26)$$

By taking this into consideration, the scaling dimension for the N channel IRLM is:

$$\boxed{2d = 1 - 2g + Ng^2} \quad g \in [-1, 1] \quad (4.27)$$

It is important to note the appearance of N in the g^2 term. This means that significant results between different number of leads on the IRLM start to appear in second order. This term will be *extremely important* when the exact solution by Bethe ansatz is developed in chapter 6. We also see that the scaling dimension of the operators is unchanged under the following shift:

$$\delta \rightarrow \frac{\pi}{N} - \delta \quad (4.28)$$

therefore, a *duality* is found for any $N \geq 2$. Coming back to the RG procedure in analogy with a generalised (boundary-type) Sine Gordon Model (BSGM), the thermodynamic exponent is found for the N channel case by making the following identifications:

$$\frac{\beta^2}{8\pi} = \frac{1}{2}(1 - 2g + Ng^2) \quad \alpha = \frac{1}{1 - d} = \frac{2}{1 + 2g - Ng^2} \quad (4.29)$$

The values of the thermodynamic exponent α have been represented in figure (4.2). In general, the thermodynamic energy scale (related to the Boundary Temperature in the BSGM) will be of the form:

$$\Gamma_N = f_N(\alpha)(t')^\alpha \quad (4.30)$$

As we have seen previously, the calculation of the prefactor $f_N(\alpha)$ still remains an open question whenever $N > 1$. For the one lead case, we found this prefactor to match that of the boundary temperature of the BSGM found in [35], but generalisation of such result to more leads is outstanding. We have also seen the importance of this prefactor, which might depend on α in a non-trivial way, being the responsible to drive the thermodynamic energy scale into a zero value in the $N = 2$ channel case. Thus we see that, for different values of N in the model, we expect to have different prefactors in the exact form of Γ .

4.2.3 Discussion of quantum phase transitions

Further analysis can be done in the multichannel IRLM for thermodynamics. If we take a look at expression (4.29), we can identify the quantum critical points (QCP) of the theory, where the correlation length $\xi \rightarrow \infty$. These have been identified in [50], but no physical interpretation is shown for them. We will show here the nature

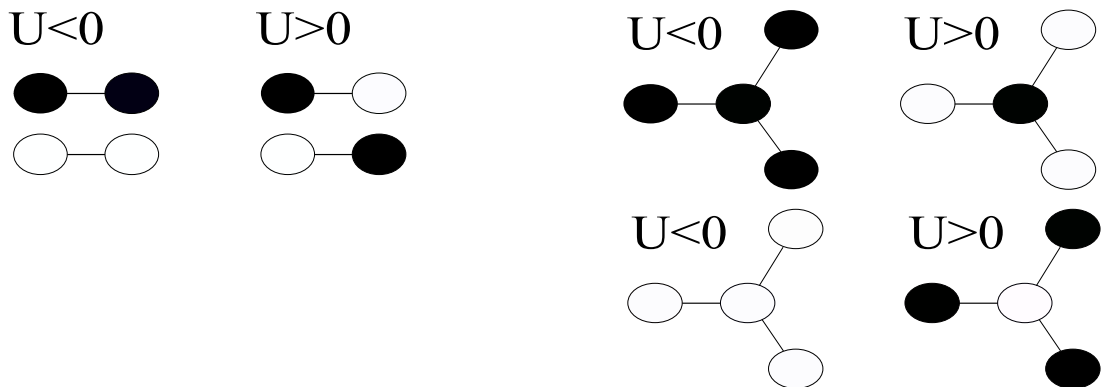


Figure 4.3: Low-energy subspace states in the strong coupling regime of the IRLM for $N = 1$ channels (left) and $N = 3$ channels (right). The geometry of the model is responsible of all phase transitions encountered.

of these QCP, and their relation with the geometry of the model.

QCP appear when, for a finite value of t' , the scaling of the parameter goes to ∞ . In this case, we have:

$$\Gamma \sim \xi^{-1} \sim (t')^\alpha \quad (4.31)$$

where ξ is the *correlation length* of the system. Whenever $\xi \rightarrow \infty$, we have a signature of a Quantum Phase Transition (QPT) in our system. In the IRLM, we are always considering values of t' very small compared to the bandwidth, therefore $t'/t \ll 1$. Thus, when $\alpha \rightarrow \infty$ a phase transition occurs. By taking a look at the equation of α , we identify these QCP to be at:

$$g_{QCP} = \frac{1 \pm \sqrt{1 + N}}{N} \quad (4.32)$$

We recall that $g \in [-1, +1]$, therefore some of the solutions above lie beyond the physically acceptable range. Concretely, for the $N = 1, 2$ channels case, we only discover QPT at a points where $U < 0$, that is, in the attractive regime, but not when $U > 0$. In fact, a QPT is always encountered in the region $U < 0$, no matter how many leads we attach to the impurity.

The situation changes when we have $N \geq 3$. Apart from the QCP encountered in the attractive region $U < 0$, we also find QCP in the repulsive region ($U > 0$). For instance, in the case $N = 3$, a QPT appears exactly at infinite interaction $g_{QCP} = 1$, and for $N > 3$ all QCP in the repulsive region belong to the interval $[0, 1]$. To understand the nature of these phase transitions, we have to look at the strong coupling regime. Moreover, we will show how these phase transitions occur due to the geometry of the model.

To begin with, consider the single channel IRLM in the region $U < 0$. In the strong coupling limit, the hamiltonian matrix can be represented as a 4×4 matrix.

The low energy subspace is then formed by two energy states, which are depicted to the left in figure (4.3). We call these states $|00\rangle$ and $|11\rangle$. On the other hand, the high energy subspace needs to be diagonalised, resulting in the following two eigenstates:

$$|+\rangle = \frac{1}{\sqrt{2}}(|10\rangle + |01\rangle) \quad |-\rangle = \frac{1}{\sqrt{2}}(|01\rangle - |10\rangle) \quad (4.33)$$

The Schrieffer Wolff (SW) transformation allows to pass from one state of the low-energy subspace to the other by virtually visiting the high-energy states. Exactly at the phase transition point, there has to be a change in the ground state of the system, which is precisely driven by the effective operator calculated by the SW transformation. We know how this happens in the one lead case, since for the electrons to pass from the state $|00\rangle \rightarrow |11\rangle$, both electrons need to jump onto the wire. Therefore, the resulting operator describing such low energy process will look similar to:

$$\psi^\dagger(j = -1)\psi^\dagger(j = -1)S^- \quad (4.34)$$

where $j = -1$ refers to the last site of the chain attached to the impurity. Bosonizing the operator by the usual transformations, one gets the following scaling dimension:

$$d = \frac{(2\sqrt{4\pi})^2}{8\pi} = 2 \quad (4.35)$$

For a field theory in (1+1) dimensions *with a boundary*, all operators satisfying $d > 1$ are said to be *irrelevant*, whereas for $d < 1$ they are *relevant*. This has to do with how the couplings run under a Renormalization Group (RG) step. If the operator is irrelevant, applying an RG step to the system drives the coupling to the critical point, therefore no growth or change is observed on its correlation functions.

We have thus seen why the phase transition occurs in the $U < 0$ sector for the $N = 1$ IRLM: The low-energy effective hamiltonian that drives the ground state into a new one in the phase transition contains *irrelevant operators*. In other words, when crossing the QCP, we pass from the *relevant phase* $g > g_{QCP}$ to the *irrelevant phase*, where $g < g_{QCP}$.

The reason why this doesn't happen in the $U > 0$ sector is presented now. Looking at figure (4.3), we see that the low-energy subspace in the strong coupling sector is formed by the states $|10\rangle$ and $|01\rangle$. Now, in order to pass from one state to the other, it is clear that there is no need to visit the high-energy manifold (now formed by the states $|00\rangle$ and $|11\rangle$). This is why no phase transition is observed in the sector $g > 0$ for $N = 1$ channels.

The same analysis can be done when an arbitrary number of leads N are attached to the impurity site. We first focus on the attractive regime $U < 0$ for the N channel case. In such a case, the low-energy sector is always described by either all sites close to the impurity (and the impurity itself) filled or empty. We have represented

this situation in figure(4.3) for $N = 3$ channels. In such a low-energy description, a change in the ground state only occurs when two electrons jump onto the same channel. Thus, the operator describing this low-energy process is given by:

$$\psi_\alpha^\dagger(j_\alpha = -1)\psi_\alpha^\dagger(j_\alpha = -1)\prod_{\gamma \neq \alpha}\psi_\gamma^\dagger(j_\gamma = -1)S^- \quad (4.36)$$

whose scaling dimension is calculated:

$$2d = \frac{(2\beta_\alpha^2)}{4\pi} + (N-1)\frac{\beta_\gamma^2}{4\pi} \rightarrow d = 2 + \frac{N-1}{2} \quad (4.37)$$

We see now that for $N \geq 1$, the scaling dimension of this operator makes it *irrelevant*, being always $d > 1$. Thus, when the quantum critical point is reached in the $U < 0$, the operator describing a change in the ground state is always irrelevant: the phase transition happens from the relevant sector to the irrelevant one. Here we see the importance of the geometry involved in the multichannel case.

Things are different when we look at the $U > 0$ sector. In this case, the low-energy subspace is formed by states alternating an impurity filled (empty) with empty (filled) nearest neighbours. In such a case, passing from one ground state to another only requires $N - 1$ operators acting directly on channels, since the impurity site is flipped by the S^+ or S^- operator. This change in the ground state happens by allowing virtual fluctuations between the low and high energy manifolds (a Schrieffer-Wolff process). Thus, the required operator for that will be of the form:

$$\prod_{\alpha}^{N-1}\psi_\alpha(j_\alpha = -1) \quad (4.38)$$

whose scaling dimension is:

$$d = \frac{N-1}{2} \quad (4.39)$$

It is clearly seen now why no phase transition occurs in the $U > 0$ sector when $N < 3$. For the one and two channel models, this scaling dimension is always representing *relevant* operators being $d < 1$. Thus, for these two models, no critical point is reached in the $U > 0$ sector, and this sector always corresponds to a relevant phase.

Things are different for the $N = 3$ channel case, where we notice a quantum critical point happening exactly at $U = +\infty$ ($g = 1$). For the $N = 3$ channel case, the scaling dimension of the operator describing low-energy processes to change the ground state is $d = 1$, that is, the *marginal* case. In this case, we cannot tell if a theory is renormalizable in the vicinity of a critical point, since its parameters undergo logarithmic variations, thus a sum of all orders of perturbed terms is necessary.

For $N > 3$, the situation is somewhat similar to that of the $U < 0$ sector, where the operator changing the ground state drives the system in a irrelevant phase. Thus we always identify two quantum phase transitions for $N > 3$, that bring the system from the relevant phase to the irrelevant phase. The QCP where this happens are given by equation (4.32).

4.3 Brief summary

4.3.1 Results

Here we have treated some fundamental properties of the IRLM when the number of channels attached to the impurity site is $N > 1$. We also worked out results for the two channel case, which is the most interesting one to study its transport (out of equilibrium) properties [44, 46, 48, 47, 91] The key results of this chapter summarize as follows:

- For the $N = 2$ channel IRLM, an *exact* expression is given for the thermodynamic exponent α . In contrast with the $N = 1$ channel case, the thermodynamic energy scale Γ proves to decrease after the self-dual point ($U = 2$) is reached.
- The most important feature of the $N = 2$ channel is its *duality* in the thermodynamic exponent α , for which a mapping $U \leftrightarrow 1/U$ develops. This has been explored already in [51], where a distinction between the strong coupling in the lattice and different regularizations in the field theory is made.
- The prefactor $f(\alpha)$ breaks the duality for the thermodynamic width Γ in the two channel IRLM. Contrary to the thermodynamic exponent α , which recovers the value $\alpha = 2$ in both the $U = 0$ and the $U = +\infty$ points, at $U = +\infty$ the value of $\Gamma = 0$, instead of being $\Gamma_0 = 2\pi\nu(t')^2$, which corresponds to the non-interacting point $U = 0$. This effect is a *real effect*, and shouldn't depend on any regularizations carried out in the continuum. In this sense, the cut-off of the theory is fixed and does not vary with U . It is the exact form of the prefactor $f(\alpha)$ what makes the energy scale Γ to vanish at infinite interaction.
- For a different number of channels N , we have shown the thermodynamic exponent to differ in order g^2 . This term Ng^2 is one of the main reasons that makes different channel models to have different physics.
- All quantum phase transitions happening in the model have been identified, with the corresponding low-energy explanation in the strong coupling picture.

4.3.2 Open questions

In order to construct a full thermodynamic theory of the IRLM for an arbitrary number of channels N , we need to know the exact form of the prefactor $f(\alpha)$ in all cases. We have proved this prefactor to be of essential importance to describe the main features of the model. For the $N = 2$ channel, the formula presented in (4.11) is a guess which proves to fit numerical data with some considerable accuracy. However, alternative ways to calculate such prefactor are needed. For instance, one could ask if the mapping to the BSGM done in the $N = 1$ channel case can be extrapolated here as well. Therefore, the two main questions to ask here are:

- In the two channel case, does that correspond to a two-bosonic field theory subject to boundaries?
- Is there a way to generalize the form of the prefactor $f(\alpha)$ when N channels are attached to the impurity site? In other words, can all relevant thermodynamic energy scales Γ be calculated in an *exact* way as for the $N = 1$ channel case?
- Does cut-off regularization really present a problem to compute exact thermodynamic quantities?

These questions reflect the fact that, even in the equilibrium situation, the IRLM possesses interesting features.

We want to emphasize that, although no satisfactory *field theory* description of the $N = 2$ has been carried out in the strong-coupling regime, we believe the answer to the last question to be negative. We support this argument with our previous results of chapter 3. As we have shown for the $N = 1$ channel IRLM, there is no dependence on cut-off regularization in order to compute exact thermodynamic quantities like the prefactor $f(\alpha)$. Correct answers are derived by considering an equivalent field theory where these quantities are computed, and proved to be equivalent to the microscopic lattice version of the model. Thus, we have reasons to think that this is also the case when more channels are attached to the model. The fact that the prefactor $f(\alpha)$ drives the thermodynamic width to zero (i.e breaks the *duality*) in the two channel case, has been argued [51] to happen due to cut-off regularization. Instead, we believe this to happen due to missed fundamental physics, which require further investigation.

Chapter 5

The IRLM: Dynamics

“I wish it need not have happened in my time,” said Frodo. “So do I,” said Gandalf, “and so do all who live to see such times. But that is not for them to decide. All we have to decide is what to do with the time that is given us.”

J.R.R. Tolkien, The Lord of the Rings

In this chapter, we explore the dynamics of the single channel IRLM. When we talk about dynamics, we refer to quantities involving operators that vary over time. There are various reasons to look at such quantities in the equilibrium situation. Firstly, these are *harder* to compute as compared to its thermodynamics counterparts, since now time evolution of the operators is involved. The fact that finite order perturbation theory breaks down for one dimensional strongly correlated systems [63] motivates the search of new robust analytical methods. Some of these have been proposed in other impurity models like the Anderson model [71] and the mixed valence problem [92], but their generalisation to different models is far from obvious.

Secondly, equilibrium dynamical quantities are important, since they can help to understand the steady state of the non-equilibrium problem. In particular, this non-equilibrium situation happens in the two channel version of the model, where current flows from one lead to another. The study of non-equilibrium transport in strongly correlated systems constitutes an active field of research at present [35, 44, 45, 46, 47, 48]. Although we cannot perform transport in the $N = 1$ version of the model, studying its dynamical properties will help to understand the physics involved in the two channel version. It is worth mentioning that even in the equilibrium case, there is not a complete understanding of the dynamics. The computation of analytical forms of the impurity spectral function proves to be extremely difficult, and one usually has to approach the problem by perturbation theory. As we will see shortly, this approach offers a poor understanding of the physical effects developing

in the system as interaction is increased.

This chapter studies in depth the impurity spectral function in the IRLM:

$$A(\omega) = \frac{1}{\pi} \text{Im}(G^d(\omega)) \quad (5.1)$$

Original results will be presented and discussed. The chapter is mainly devoted to numerical data obtained by simulations carried out by NRG in the model, although an analytical approach to the problem is also described, but no satisfactory results on this approach have been found yet. First, we want to motivate the reader by a brief introduction to some interesting features of the dynamics in the model found in the literature.

5.1 Interesting behaviour of dynamical quantities

The main reason to study the dynamics of the IRLM is twofold. We recall the model at $U \sim 0$, which has been discussed in chapter 2. The impurity local density of states is, according to first order of perturbation, given by:

$$A(\omega) = \frac{1}{\pi} \frac{\Gamma_d}{\omega^2 + \Gamma_d^2} \quad \Gamma_d \sim (t')^{\frac{2}{1+2g}} \quad (5.2)$$

where, at small values of interaction U we have:

$$g \sim U\nu \quad (5.3)$$

Here Γ_d is the renormalized hybridization. If we look at energies higher than this, the impurity is decoupled from the surrounding bath. However, when energies are below Γ_d , the impurity site *hybridizes* with the surrounding environment, and thus a virtual bound state (resonance) is observed.

Exactly at zero interaction $U = 0$ ($g = 0$), we have $\Gamma_d = \Gamma_0 = \pi\nu(t')^2$, therefore:

$$\Gamma_d(g = 0) = \Gamma_0 = \Gamma(g = 0) \quad (5.4)$$

where Γ was given in (3.36). The result (5.2) matches with what was found in previous publications [37, 38]. It also reveals the Fermi liquid nature of the model in the *weak coupling limit*, where one always expects to find a Lorentzian shape for the impurity density of states as shown in (5.2).

One of the main results of [37, 38] is the calculation of this *hybridization* Γ_d . In [38], it is argued that this quantity is an increasing function for $U\nu \sim 0$, but decreases to a zero value as interaction is increased, therefore a maximum is observed in the graph $\Gamma_d(U)$. Moreover, this is said to happen for the general multichannel case, no matter how many channels are attached to the impurity site. The values of $\Gamma_d(U)$ in [38] are shown in (5.1).

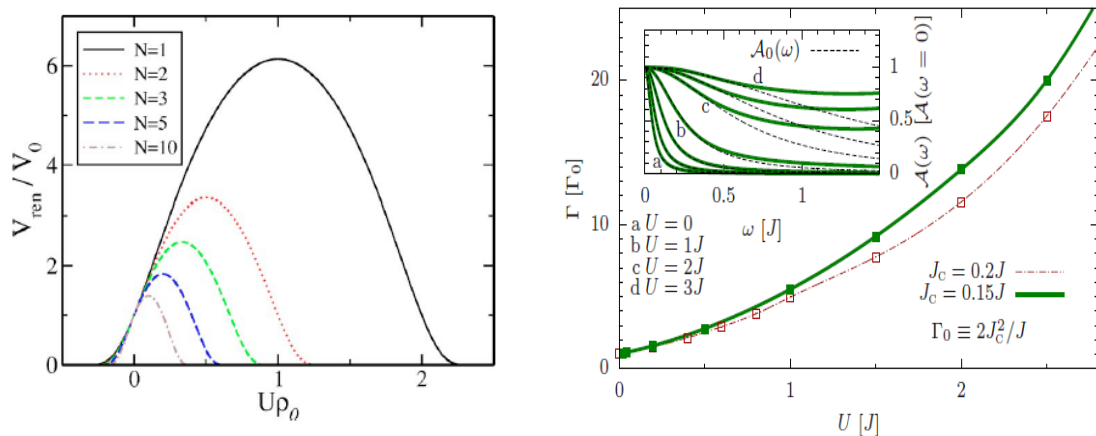


Figure 5.1: Calculation of the renormalized hybridization Γ_d by perturbative RG (left, after [38]), and numerically by DMRG (right, after [52]). The perturbative RG procedure is known to fail to give accurate analytical predictions when compared with NRG numerics in [38]. Note how for the $N = 2$ channel case, $V \equiv \Gamma_d$ is shown to decrease as the interaction U is increased, whereas the same quantity is shown to increase in [52] when performing DMRG numerics.

A different result has been reported by A. Braun and P. Schmitteckert [52] for the two channel version of the IRLM. In [52], the local (impurity) density of states is shown to spread as U is increased. This is shown in figure (5.1). The graph of the hybridization $\Gamma_d(U)$ is shown to be a monotonic increasing function, where no maximum is reached. This reveals in principle a surprising feature of the two channel IRLM, but also poses the question about if something similar happens in the single channel version of the model. More interesting is the fact that this result differs from the one we already described for the *thermodynamic* energy scale Γ shown in figure (4.1) for the two channel IRLM. As we have already discussed before, for the two channel version of the model, the thermodynamic energy scale Γ starts to reduce its value after reaching the *self-dual* point at $U = 2t$. This different behaviour motivates a careful check of the theory when discussing dynamical quantities, and moreover, the definition of such energy scales in the problem.

It is known that the IRLM appears as a direct mapping from the Anisotropic Kondo Model (AKM) [36]. In the Kondo model, a single energy scale appears, the so called Kondo temperature T_K . This energy divides two regions with well differentiated physics: at temperatures $T < T_K$ (strong coupling), the impurity is screened by the surrounding electrons, and therefore a Fermi liquid forms [25]. For higher energies, the impurity survives in the surrounding environment as a quantum spin, independent of the environment. The energy scale T_K manifests in the impurity spectral function as a very narrow resonance around the $\omega = 0$ sector. This is called the *Abrikosov-Suhl* resonance, which is a signature that, in the strong coupling regime, the Kondo model behaves like a Fermi liquid [62, 63, 66, 90]. Despite the narrow resonance whose width is T_K , the spectral function is pinned at $\omega = 0$ in the Kondo model, due to Langreth theorem [64]. Thus, no matter how big the

coupling, the spectral function at $\omega = 0$ maintains its value.

For the two channel version, the situation is different. The two channel *isotropic* Kondo model can be solved by a proper transformation to the Resonant Level Model, as was done by Emery and Kivelson [93]. Due to the isotropy of the channels, the impurity site is overscreened in the strong coupling regime, and therefore a non-Fermi liquid behaviour manifests. This differs considerably from the anisotropic case. The anisotropy of the channel couplings moves the system away from the non-trivial fixed point [66, 90], and the Fermi liquid nature of the model is recovered, since now the impurity hybridizes with the channel having the strongest coupling value. Thus, due to the relation of the IRLM to the AKM, we would expect an equivalence between both low-energy descriptions of the models.

All these considerations lead us to think that the IRLM presents some new fascinating physics when we look at dynamic properties. Moreover, we believe this to be a fundamental way to understand dynamical properties of the AKM.

5.2 Analytical approach to the problem

In this section, we describe briefly the analytical approach carried out for the computation of the impurity spectral function in the IRLM. The range of applicability of such methods in the model is still under investigation, and we have not managed to make it work for the whole interacting problem. The generalization of the AY method to the IRLM has been proposed in [90], however it deals with the calculation of the partition function in the system, which is related to the response of conduction electrons due to a change of sign in the scatterer point.

5.2.1 The IRLM as a sequence of X-ray processes: $U = 0$ solution

Here we will attempt to solve the IRLM in a non-perturbative way, by using the Anderson-Yuval approach [22, 23, 24, 39, 90]. applied to the IRLM. Although the exact partition function of the model has been calculated [90] in analogy with the AKM, this only leads to the calculation of *bulk* properties. Instead, we are interested in computing an exact expression for the time-history of the dot as a sequence of X-ray edge problems. That is we seek an exact expression of the correlator:

$$G^d(t) = -i\langle Td(t)d^\dagger(0) \rangle \quad (5.5)$$

when the perturbation t' is introduced in the model. Let us first start by the non-interacting case $U = 0$. In this case, the IRLM hamiltonian is ($\varepsilon_0 = 0$):

$$H_{U=0} = H_0 + (t')(\psi_0^\dagger(0)d + \text{h.c}) \quad (5.6)$$

The expression of $G^d(\omega)$ is well known to us in this limit (see chapter 2). Now we want to do a time treatment of the dot dynamics. The $t' = 0$ and $U = 0$ propagators

of the dot and the bulk electrons are:

$$G_0^d(t) = -i\text{sign}(t) \quad G_0^c(t) = \frac{-i\nu_0}{it + \text{sign}(t)\tau} \quad (5.7)$$

where a time(energy) cut off $\tau = \xi_0^{-1}$ has been inserted to regularize the theory. Such expressions are then valid when $t/\tau \gg 1$, that is, when $\tau \rightarrow 0^+$. In time domain, it is important to set a direction of time propagation. In this case, we will choose $t > 0$, and results can be derived in a similar way for $t < 0$. Thus $\text{sign}(t) = +1$ in the above expressions. The correlator of conduction electrons can then be written as:

$$\lim_{\tau \rightarrow 0^+} G_0^c(t) = -i\pi\nu_0\delta(t) - \frac{\nu_0}{t} \quad (5.8)$$

Note that $t = 0$ is a singular point in the theory, and one needs to be careful in order to treat such divergences. For the moment, let us forget about the real part of this expression, and prove that the method gives the appropriate spectral function for the impurity density.

For $t' \neq 0$, we use perturbation theory. The first order term corresponds to a term with $(t')^2$, since the first order in t' term does not allow to construct non-zero Wick contractions. Also, note that the Green functions carry a minus sign under time reversal, that is:

$$G_0^d(t) = -G_0^d(-t) \quad G_0^c(t) = -G_0^c(-t) \quad (5.9)$$

However, both processes have the same probability amplitude. Thus, we can choose only one time direction (say $t > 0$), and multiply our result by a factor of two in order to account for negative time propagations. The first order term of the expansion is:

$$G_{(1)}^d(t) \sim 2(t')^2 \int_0^t dt_2 \int_0^{t_2} dt_1 G_0^d(t - t_2) G_0^c(t_2 - t_1) G_0^d(t_1) \quad (5.10)$$

with a possible overall normalization factor. The process is composed by three probability amplitudes, describing a single hybridization process, where the impurity electron jumps to the wire for a short time, and comes back again at a later time. The time ordering is $t > t_2 > t_1 > 0$. We need to emphasize here that our approach differs from the one employed in [22, 90], since we are not interested in the response of conduction electrons due to a impurity flip. Here we are trying to calculate the *impurity* Green's function, which is the sum of all probability amplitudes taking place during a hybridization process. Substituting (5.7) into (5.10), we get:

$$G_{(1)}^d(t) \sim i2\pi\nu_0(t')^2 \int_0^t dt_2 \int_0^{t_2} dt_1 \delta(t_2 - t_1) \quad (5.11)$$

We now make use of the following property:

$$\int_0^b dx \delta(x - b) = \frac{1}{2} \quad (5.12)$$

Thus, the first order correction reads:

$$G_{(1)}^d(t) = -i(-\Gamma_0 t) \quad \Gamma_0 = \pi\nu(t')^2 \quad (5.13)$$

Let us calculate the second order contribution. In this case:

$$G_{(2)}^d(t) \sim 2\pi\nu_0(t')^2 \int_0^t dt_4 \int_0^{t_4} dt_3 \delta(t_4 - t_3) G_{(1)}^d(t_3) = (-i) \frac{(\Gamma_0 t)^2}{2!} \quad (5.14)$$

We then extrapolate the result and realise that the n th term has the form:

$$\begin{aligned} G_{(n)}^d &= 2 \int_0^t dt_{2n} \int_0^{t_{2n}} dt_{2n-1} G^d(t - t_2) G^c(t_2 - t_1) G_{(2n-1)}^d(t_{2n-1}) \\ &= -i(-1)^n \frac{(\Gamma_0 t)^n}{n!} \end{aligned} \quad (5.15)$$

Therefore, the total impurity Green's function is calculated by summing to all orders of perturbation:

$$G^d(t) = -i \sum_{n=1}^{+\infty} (-1)^n \frac{(\Gamma_0 |t|)^n}{n!} = -ie^{-\Gamma_0 |t|} \quad (5.16)$$

where we have taken $|t|$ since both processes $t < 0$ and $t > 0$ have been taken into account as described above. Up to a normalization constant, this expression is the Fourier transform of a Lorentzian centered at $\omega = 0$ whose width is Γ_0 :

$$\int dt e^{-\Gamma_0 |t|} \sim \frac{\Gamma_0}{\omega^2 + \Gamma_0^2} \quad (5.17)$$

Thus, the non-interacting impurity density of states has been recovered with the method above. We want to emphasize three main points of discussion here: First, the real part of conduction electrons $\text{Re}(G_0^c(t))$ presents divergences when the method is applied. One needs to re-insert a cut-off $a \rightarrow 0^+$ in the integral limits in order to make things finite. Whether these contributions cancel out to all orders of perturbation or not is something we still have under investigation.

Secondly, the AY method, as it stands, allows for an exact calculation *in the time propagation of conduction electrons*, that is, it calculates the exact result for the single-particle Green function of conduction electrons at the origin (where the impurity is). The calculation of such Green's function has been done in several papers [19, 22, 90]. It gives the exact expression of the partition function, from where different thermodynamic properties can be extracted (see [24]). However, the method does not explicitly allow calculation of the *impurity propagator*, which in principle, requires a different treatment.

Finally, we have tried to generalise the method for the $U \neq 0$ case, by substituting the bare correlators by those from the X-ray edge problem, so that the problem can be treated as a sequence of X-ray problems, where the impurity fluctuates between a filled and empty state. This is equivalent to the Anderson-Yuval approach

[22, 23, 24] to the Kondo problem. To much of our regret, the method has not provided satisfactory results yet due to divergences encountered in the $g \rightarrow 0$ limit of the expressions, and thus, we consider not to include such solutions here. However, we have included results on this in the appendix, for the interested reader, which might also serve as an starting point towards a refinement of the approach.

5.3 NRG dynamics in the IRLM

This section constitutes the main results of this chapter. NRG simulations are carried out, and computation of dynamical quantities is performed as it was described in chapter 2. All different values of parameters employed are described when necessary. Due to peak resolving restrictions, all results presented are for $\varepsilon_0 = 0$. For a better understanding of the effect of a local magnetic field in the computation of dynamical quantities, we refer the reader to the literature [75, 79, 81, 82]

5.3.1 Dynamics at $g = 0$

In this part, we prove the NRG code to represent the analytical results expected for the spectral function on the impurity site, as in (5.17). Although this result is well known, it provides evidence of the reliability of numerics. All NRG computations for the spectral function were carried out as described previously in chapter 2.

It is worth mentioning that parameters need to be chosen in a careful way. For instance, the hybridization parameter of the IRLM shouldn't be too large when compared to the bandwidth parameter, which is taken to be $t = 1$. Therefore, we restrict ourselves to a range of values of $t' \sim t/100$. Thus, in this limit, t' is regarded as a small perturbation in the system. For notational convenience, we have changed $t' \equiv J$ in all graphs.

As one would expect, as the value of ω is increased, the NRG method loses accuracy. We remember that, due to the logarithmic discretization, the NRG method works well to reproduce low-energy properties of the system, however computation of features in the high-energy region proves to be more challenging (see [75] for detailed discussion). Note that as energy is decreased, more data points are calculated. All data points in figure (5.2) have been represented in comparison with their associated Lorentzian functions:

$$A(\omega) = \frac{1}{\pi} \frac{\Gamma_0}{\omega^2 + \Gamma_0^2} \quad (5.18)$$

If one calculates the associated widths Γ_0 from the fitting, then we find the value not to differ considerably when compared with the theoretical value. For a bulk density of states of $\nu = 1/\pi$ (that is $t = 1$ in the tight-binding chain), results for Γ_0 are represented in figure (5.3).

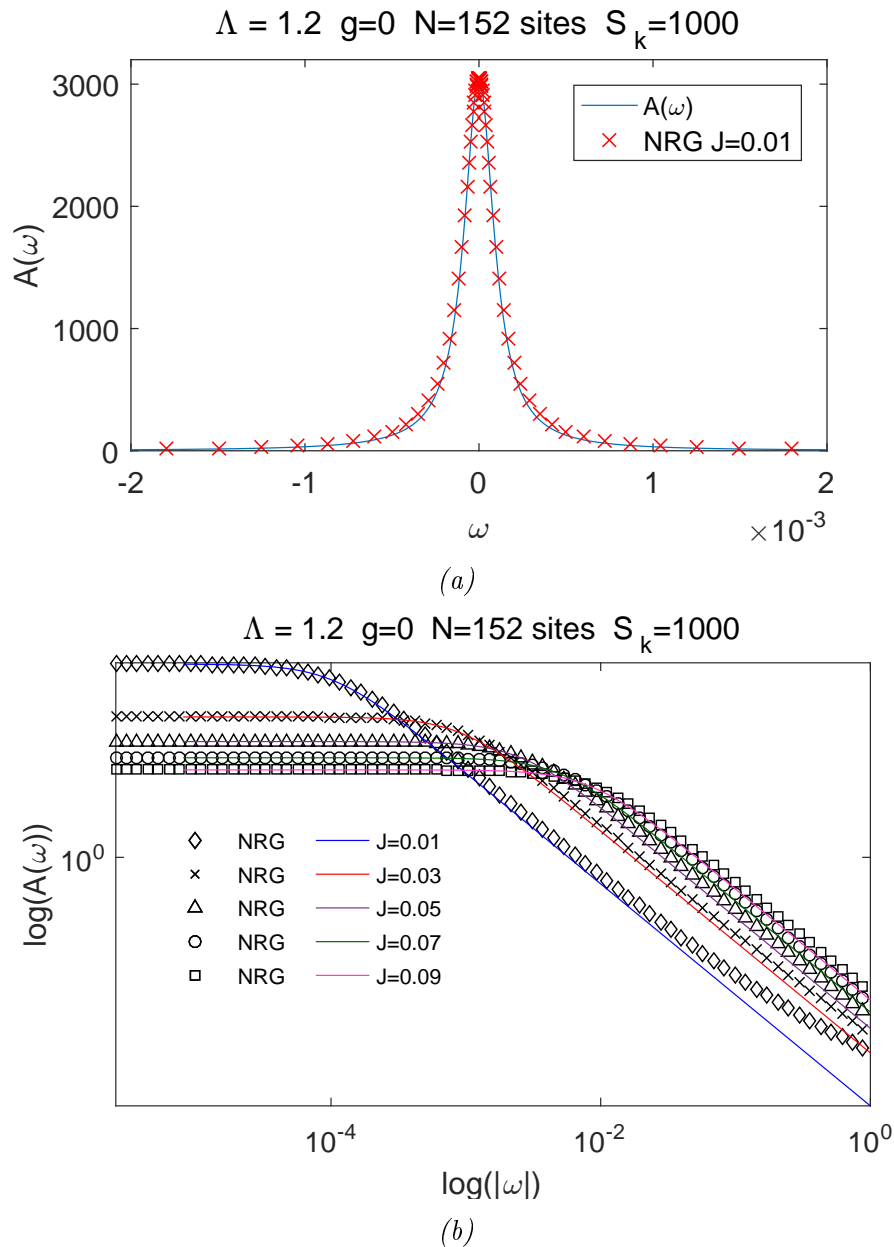


Figure 5.2: NRG results for the non-interacting case $g = 0$ (a) NRG data points for a value of $J = 0.01$ in the IRLM. The continuous curve represents the Lorentzian function that fits the data. (b) NRG data points for several values of J , with the corresponding fitting Lorentzian functions. Note the log scale in both axis. In both figures, Λ represents the logarithmic discretization parameter of the band, whereas S_k is the total number of states kept after truncation of the hamiltonian.

We could ask why choosing a value of $\Lambda = 1.2$ should give such accurate results. Usually, NRG simulations have been performed with values of $\Lambda \in 1.5 - 2.5$ when 1000 states are retained [75] after truncation. The reason is that, as Λ is lowered, one gets closer to the continuum limit of the model ($\Lambda \rightarrow 1$), and we need to keep more states as this happens. The IRLM presents a nice low-dimensionality (spinless model) that allows one to get close enough to the continuum limit, without the

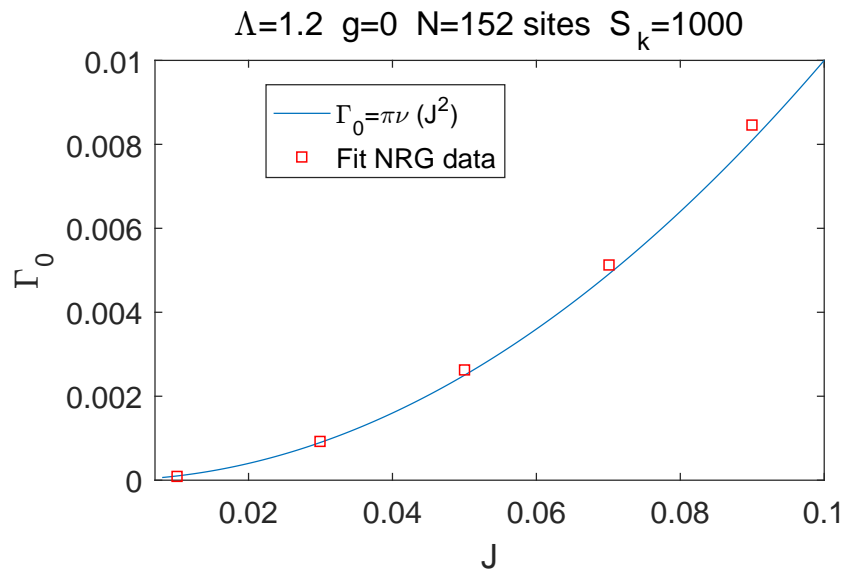


Figure 5.3: Values for the hybridization parameter Γ_0 as a function of J . Data points correspond to the fitting performed over NRG data, where the function to fit was a Lorentzian of width Γ_0 .

necessity of keeping more states than the ones needed for other models, even when we get closer to this limit. Therefore, a smaller value of Λ provides more numerical data in the whole spectrum.

One more thing to add here is that of the definition of an *energy scale* in the problem. Since $A(\omega)$ has units of ω^{-1} , the associated energy scale in this problem is precisely Γ_0 as one would expect. This matches with the result found in chapter 3, where the relevant (thermodynamic) energy scale is Γ_0 at $g = 0$. Therefore, we can conclude that at $g = 0$, both the dynamic and thermodynamic properties of the model are dominated by Γ_0 .

In the next section, we will explore the evolution of the spectral function as the interaction parameter $g(U)$ is changed. It should be pointed out that, in the construction of the initial hamiltonian for the NRG treatment, it is the bare parameter U what is inserted as an input. Nevertheless, a relation between g and U has been established previously, and therefore, we will consider switching to the g parameter, which can only take values $g \in [0, 1]$ for repulsive U .

5.3.2 Dynamics at $g \neq 0$

The most interesting situation happens when we switch on the interaction between the impurity and the rest of the system. We remember that this interaction involves a term:

$$U : \psi^\dagger(0)\psi(0) : \left(d^\dagger d - \frac{1}{2} \right) \quad (5.19)$$

in the hamiltonian, where $: O :$ stands for normal ordering of the operator. In the NRG case, the vacuum expectation value of fermionic operators at $x = 0$ corresponds to:

$$\langle \psi^\dagger(0)\psi(0) \rangle = \frac{1}{2} \quad (5.20)$$

in the *particle-hole* symmetric case, which is the one we focus on. When the term (5.19) is considered, the system becomes strongly correlated, and therefore, any attempt to solve it by perturbation theory fails giving accurate results.

In what follows, we shall distinguish two well differentiated regimes: one we call the *weak coupling*, where values of $U\nu \ll 1$, and this limit has been studied in the literature by the same NRG methods [38] or even time-dependent Monte Carlo [55]; the other limit is the *strong coupling*, and we can consider this limit to start when $U\nu \sim 1$. In the weak coupling limit, that is, for very small values of U , one still expects to recover a Lorentzian shape in the density of states. This was already anticipated in chapter 2 by perturbation theory arguments, where to first order in U , the hybridization parameter J is renormalized as:

$$\Gamma \sim (J)^{\frac{2}{1+2g}} \quad g = U\nu \quad (5.21)$$

Thus, in the weak coupling limit, the spectral function of the impurity can be well approximated as:

$$A_{\text{wc}}(\omega) = \frac{1}{\pi} \frac{\Gamma}{\omega^2 + \Gamma^2} \quad (5.22)$$

We must however give a warning here, which has to do with the exact form of Γ . It has previously mentioned how important is to determine the *prefactor* appearing in Γ , thus, the above expression should be taken with a bit of care, and Γ should *not* be confused with the one we showed in chapter 3.

To restore analogies with the Kondo problem, we remember that in the Kondo and Anderson models, no matter how big the interaction is, the spectral function of the impurity remains pinned at $\omega = 0$, therefore satisfying Langreth's theorem [64]. One of the fundamental questions to answer is then what is the effect of increasing interaction over dynamical quantities in the IRLM. Analytically, this is a difficult problem to solve, however, the advantage of NRG is that, because all bare parameters enter in the initial hamiltonian, one can in fact go beyond the bandwidth, and still recover the essential low-energy properties of the model. In fact, this is what happens in the Anderson model, when one takes the value of U sufficiently large above the bandwidth, approaching the Kondo limit [10, 61, 76].

We start by showing results for the spectral function in the *weak coupling* limit. In this case, we observe the NRG data to be well represented by the usual Lorentzian shape, as first order perturbation theory predicts. This has been represented in figure (5.4). Note that the peak is well resolved (very small energies), whereas at higher energy values, data points deviate respect to the analytical formulas. As the

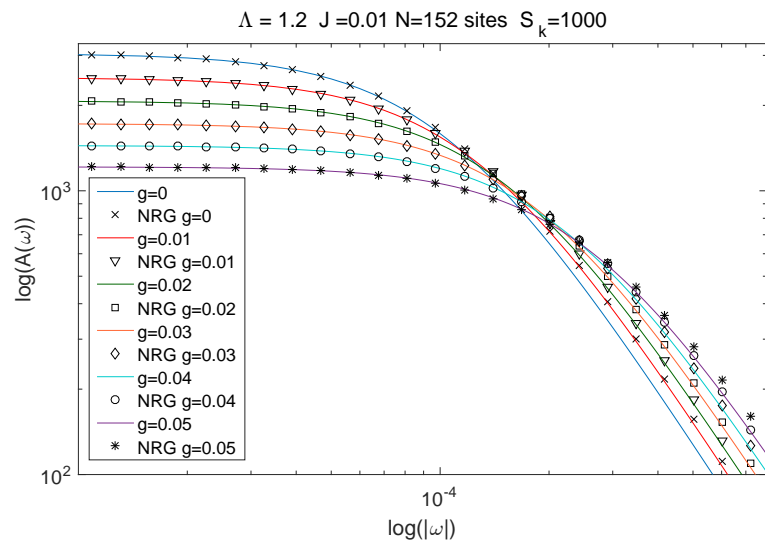
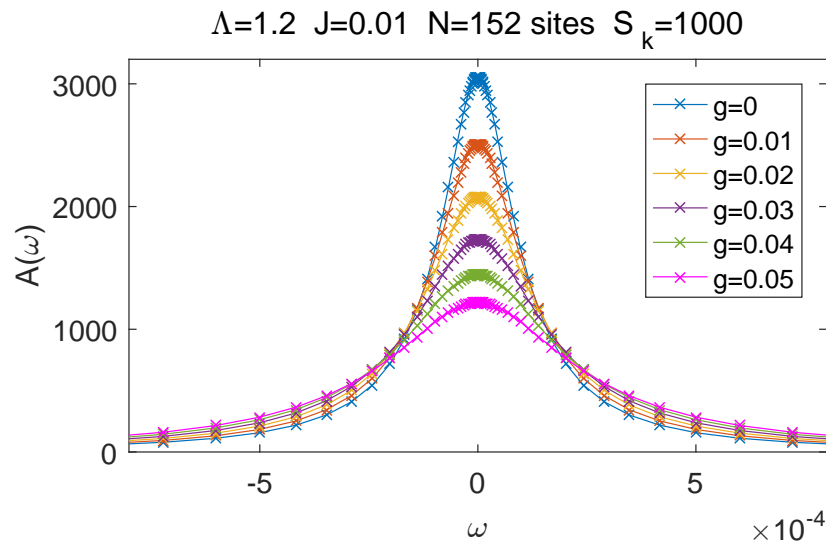


Figure 5.4: NRG data for the weak-coupling limit of the IRLM. (a) Data points have been presented here for different values of interaction g . Lines are inserted between points as a guide to the eye. Notice how as g is increased in value, the width of the resonance increases. (b) Logarithmic plot of NRG points and the corresponding fitting functions (5.22).

value of g is increased, one would expect the spectral function to broaden, therefore the resonance being suppressed. We will shortly see that, this being true, something more interesting starts to happen at stronger values of interaction.

The spectral function has been represented in figure (5.5) for several values of interaction g . We have not use data markers in this case in order to make the figure more visible. Instead, all data points have been joined by lines. As interaction is increased, we observe a split of the central peak in the spectral function, which

is a hint of non-Fermi liquid behaviour. Notice that, as interaction is increased, the spectral function gets broadened, therefore the width gets infinitely broad when we reach the limit $g \sim 1$; however, its height is reduced as subsequent values of interaction. Since the spectral function must satisfy the sum rule:

$$\int_{-\infty}^{+\infty} A(\omega) d\omega = 1 \quad (5.23)$$

that means part of the spectral weight has been displaced into higher energy regions. Such high energy peaks are the so called *Hubbard bands*, and they also appear in the Anderson and Kondo models in the strong coupling limit. Here, due to the limitation imposed by NRG to study low-energy properties of the model, they prove to be quite difficult to observe.

It is clear from figures (5.4) and (5.5) that the model does not satisfy Langreth theorem [64]. This has to do with the fact that interaction, as opposed to the Anderson and the Kondo models (which we know are equivalent in a certain limit), is not purely local. In the Anderson model, electrons interact with energy U only by sitting into the same d impurity state, therefore they are forced to have opposite spin due to Pauli exclusion principle. On the other hand, the IRLM includes an interaction in the hamiltonian between electrons in the d level with *bulk* electrons at the origin. In both the Kondo and Anderson models, the $\omega = 0$ is pinned, no matter how big the interaction is. The IRLM is directly related to the anisotropic version of the Kondo model (AKM) [36, 66, 90], therefore we expect similar physics to happen in the AKM. This has already been reported for the $s = 3/2$ AKM [94] in the presence of an external magnetic field, and such a splitting of the central peak can be also found in [95].

From all results presented above, it is clear that the Lorentzian shape of the density of states is lost as g starts to increase. Moreover, the central peak in the spectral function is not pinned at $\omega = 0$ as one would expect in a Fermi liquid. These are, we believe, signatures that the system is not a Fermi liquid anymore, but we want to be cautious about such claims. As it has been reported by Giamarchi et al. [54], the $J = 0$ point in the model presents a non-trivial fixed point, where the dot correlator is given by:

$$G^d(t) \sim t^{-g^2} \quad (5.24)$$

manifesting the non-Fermi liquid behaviour concretely at this point. We also see this result to match with that of the X-ray edge singularity problem as worked out by Nozières-De Dominicis [17]. As $J \neq 0$, one moves away from this fixed point, and, being the perturbation relevant, one expects the parameter J to renormalize in the same way as it was presented in chapter 3 at low energies. The result we are about to present studies such renormalization of J with the interaction parameter g .

Finally, we want to mention that, due to the form of the impurity correlator (5.24), the Fourier transform has an ω dependence with an exponent different from

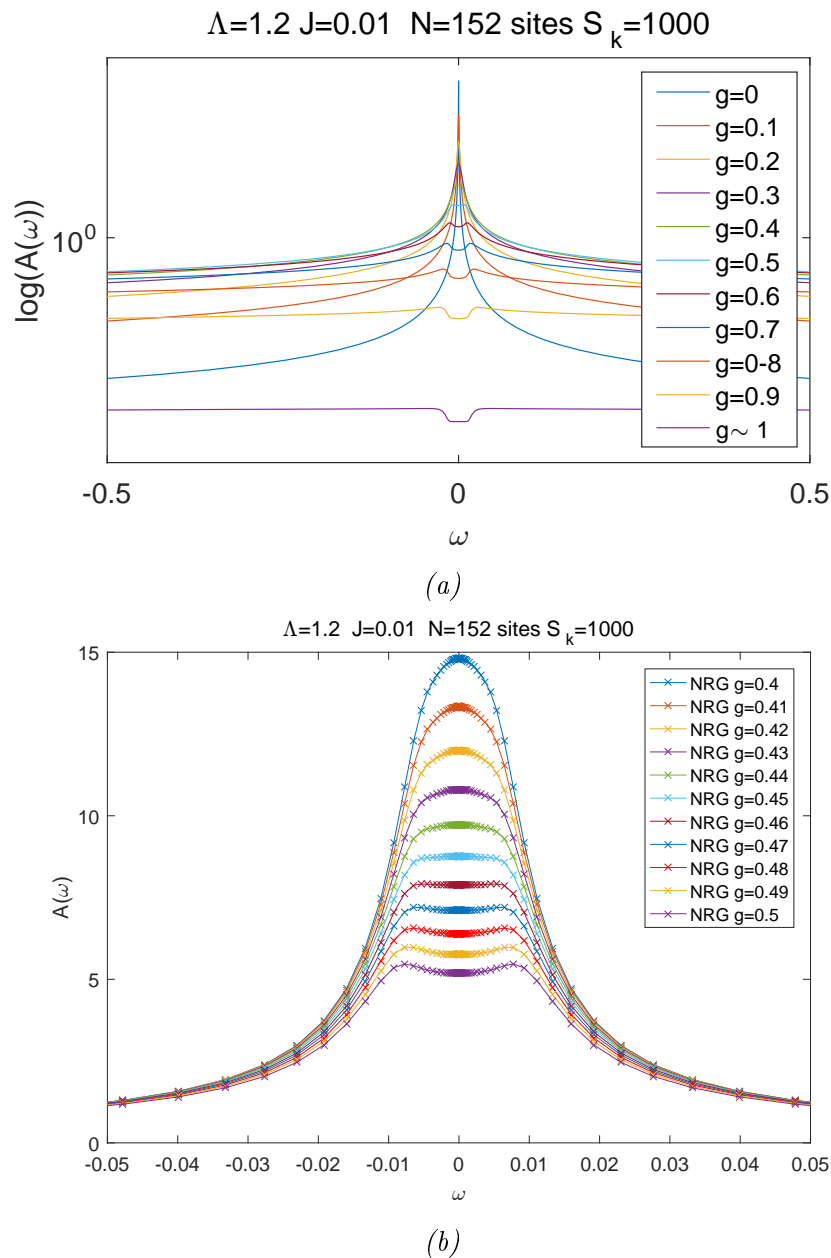


Figure 5.5: NRG data for different values of interaction g . (a) Representation of the spectral function on the impurity site at different values of interaction. Data points have been joined by lines in order to make the graph more visible. Note how at values of $g > 0.4$, a splitting in the central region starts to emerge (b) Spectral functions in the region of $g \in [0.4, 0.5]$ where the splitting starts to appear.

2, that is, we believe that at $J \neq 0$:

$$A(\omega)^{-1} \sim \omega^{s(g)} \quad (5.25)$$

so that such exponent has a non-trivial dependence on g . The computation of such exponent proves to be a challenging task with our performed numerics, and further refined and more accurate approaches could serve in order to study this. The fact that ω has a different exponent of 2 is also a signature of non-Fermi liquid behaviour

in the system [71]. This change in the exponent of ω would manifest in logarithmic singularities in the impurity self-energy:

$$\Sigma^{dd}(\omega) \sim g^2 \omega \log\left(\frac{\omega}{\Lambda}\right) \quad (5.26)$$

The fact that this is a second order effect in the dynamical quantity $G^d(\omega)$ is quite clear, since all first order diagrams are independent of excitation energies ω . Unfortunately, the computation of such terms from perturbation theory presents added difficulties, regarding the analytic properties of all propagators in the problem and all possible Wick contractions that can be formed, involving too many different diagrams contributing.

5.3.3 The dynamical exponent

As it has been already mentioned, the point $J = 0$ in the model corresponds to a non-Fermi liquid [54]. This is because when interactions g are present, the impurity correlator decays with a non-universal exponent. The overlap between the two ground states, one without a scatterer and the other one with a scatterer point, proves to be zero [67] only in the thermodynamic limit $N \rightarrow \infty$. Hence the non-universal decay of the correlation function on the impurity site.

The situation as $J \neq 0$ is different. Now, due to the hybridization between the lead and the impurity site, the occupation on the dot is highly fluctuating in time. From the RG treatment, we observed how the hybridization parameter scales with interaction, being the behaviour:

$$J^\alpha \quad \alpha = \frac{2}{1 + 2g - g^2} \quad (5.27)$$

where we called α the thermodynamic exponent. Here, when computing dynamical properties of the model, we considered the low energy sector to be described by:

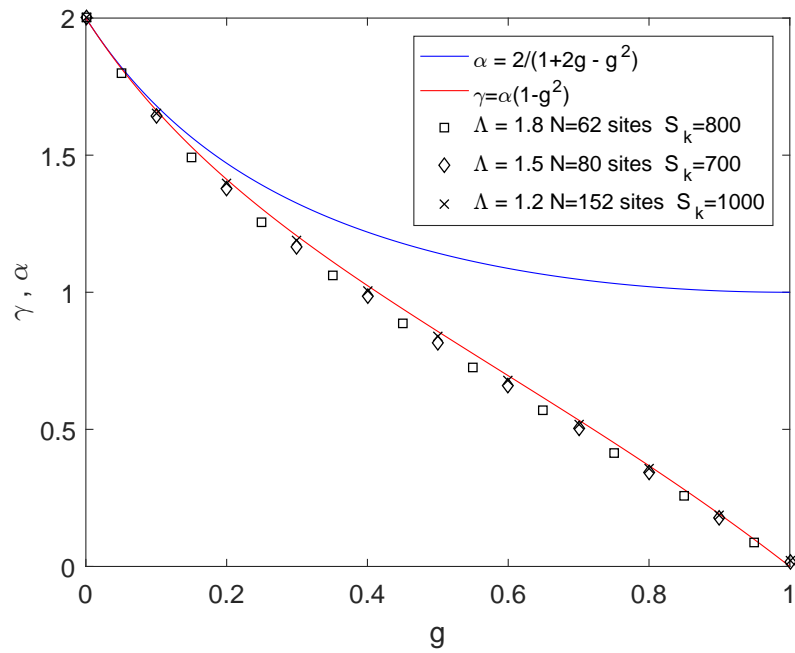
$$A(\omega) \sim \frac{\Gamma}{\omega^2 + \Gamma^2} \quad \Gamma \sim (J)^{\frac{2}{1+2U\nu}} \quad (5.28)$$

only at small values of interaction $U\nu \sim 0$. We have already seen from previous numerics that as interaction is increased, this picture is no longer valid. One way to study how the parameter J renormalizes in the low energy sector is by defining the *energy* quantity:

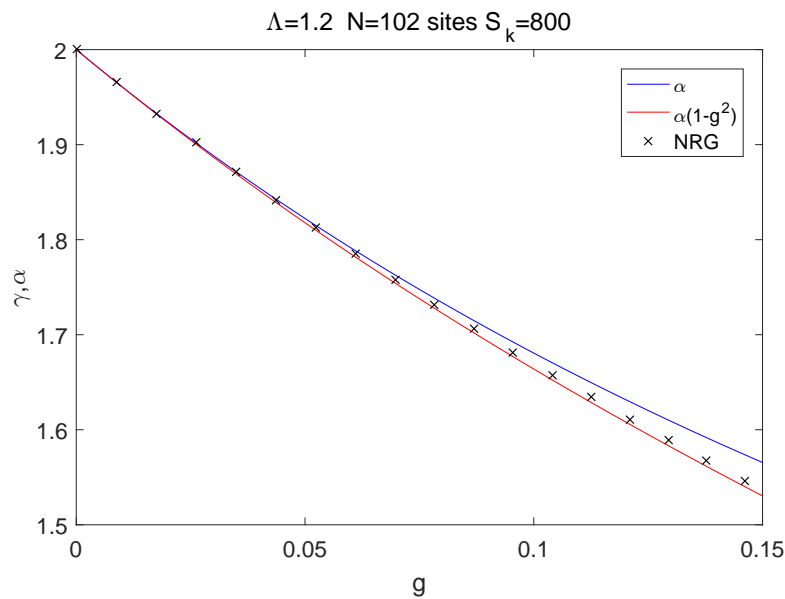
$$\Gamma_d = A(\omega = 0)^{-1} \quad (5.29)$$

Due to the dimensions of $A(\omega)$, Γ_d has dimensions of energy. Such definition of energy makes an analogy with the conserved quantity in Langreth's theorem [64], which states that $A(\omega = 0) = 1/(\pi\tilde{\Gamma})$ for any value of interaction. Let us now take NRG data points for different values of J . Then, at a single value of interaction g , we can compute the scaling of the J parameter with g by the following relation:

$$\log(A(\omega = \omega_N)^{-1}) = a + \gamma \log(J) \quad (5.30)$$



(a)



(b)

Figure 5.6: NRG calculation of the dynamical exponent. (a) Scaling of J with interaction parameter g . All data points correspond to NRG simulations, where values of $J = 0.01, 0.03, 0.05, 0.07, 0.09$ were used for the fitting. Note the deviation from the thermodynamic exponent α , which means J scales with a different exponent in the spectral function. (b) Different data points collected for small values of g , showing the deviation of numerical data from the analytical expression of α .

where ω_N is the lowest energy scale reached in Wilson's chain. Our aim is then the calculation of γ from our NRG numerics. In principle, one would expect this

exponent to be equivalent to the thermodynamic exponent we have previously calculated. We will prove now this not to be the case, and highlight the fact that, in the IRLM, two different exponents coexist, and one of them (what we shall call the *dynamical* exponent γ) dominates the scaling of the spectral function height, whereas our known α (thermodynamic exponent) relates to excitation energies ω . Therefore, it is essential to understand that *the computation of dynamical quantities in the model requires two exponents in order to describe them correctly*, as opposed to thermodynamic quantities which are entirely dominated by α .

The values of γ computed from the fitting equation (5.30) have been represented in figure (5.6). The thermodynamic exponent α has also been represented for comparison. As we can see, all data points deviate from α as interaction is increased. Moreover, they start to differ at second order in g , since at very small values of g , both exponents match. At large values of interaction, the exponent $\gamma \rightarrow 0$ as $g \rightarrow 1$. This suggests that data follows an equation of the type:

$$\boxed{\gamma = \frac{2(1 - g^2)}{1 + 2g - g^2} = \alpha(1 - g^2)} \quad (5.31)$$

In figure (5.6), numerics prove to agree well with the above equation. To much of our regret, the origin of such expression is at the moment unknown to us. Therefore, equation (5.31) is not a derived result, but rather phenomenological. The derivation of such scaling from analytics is the next step in order to understand such an unexpected scaling for the parameter J . This poses the question on whether dynamical quantities involve two different *energy scales* as opposed to thermodynamic ones, which only involve Γ . The apparent appearance of two different behaviours, one for thermodynamic quantities and another for dynamics, has been reported in the literature [42, 43]. In fact, in these works it is claimed that the IRLM possesses universal thermodynamics even when coupled to a Luttinger liquid [42]. That is, regardless of the interaction between electrons in the bulk, the form of thermodynamic properties remains the same. We do not adventure ourselves here to extrapolate this result onto dynamical quantities, and we believe further research in this arena is necessary in order to account for a satisfactory theory. Dynamical quantities prove to be much more complicated to compute, and the lack of analytic approaches as compared to thermodynamic quantities make these properties much less tractable.

We have then shown, at least numerically, that such scaling of the parameter J differs from the one found in the thermodynamic energy scale:

$$\Gamma_d \sim J^\gamma \quad \Gamma \sim (J)^\alpha \quad (5.32)$$

In chapter 3, the relevant (boundary) energy scale was defined as Γ , and an exact expression was found for it. The energy Γ_d , though not representing an energy scale, represents the behaviour of the spectral function in the $\omega = 0$ sector. An outstanding problem is then the computation of the prefactor, which we know has to be dependent on g only:

$$\Gamma_d = F(g)(J^\gamma) \quad \lim_{g \rightarrow 1} F(g) \rightarrow \infty \quad (5.33)$$

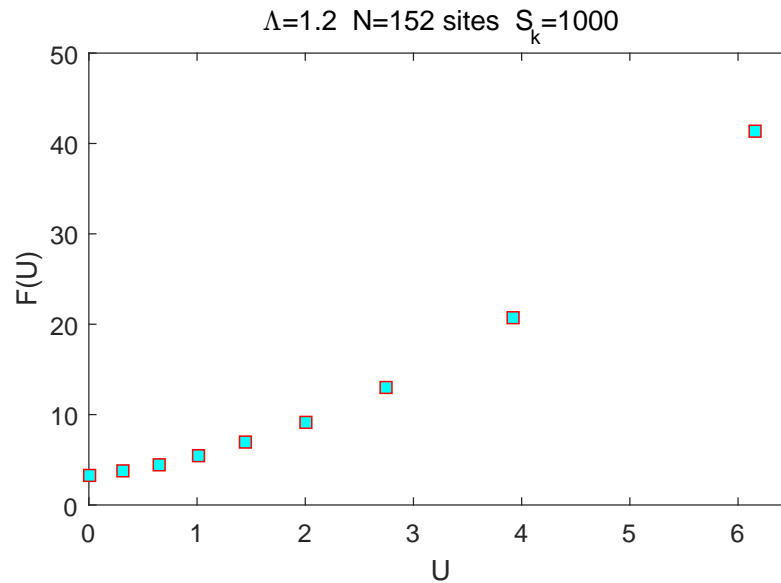


Figure 5.7: NRG data for the prefactor $F(U)$ as a function of the bare interaction parameter U , showing that as U is increased, data points grow, leading to a divergence at big interactions.

Such a prefactor is also given by equation (5.30). The fact that the prefactor presents a divergence as U is increased, is what makes the spectral density to vanish in the $\omega = 0$ sector for very big interactions. This has been represented in figure (5.7), where a clear increase of the prefactor with the bare interaction parameter U is observed.

The parameter J , which is known to be a relevant perturbation from RG (see chapter 3) scales differently for thermodynamic and dynamic properties, which is at first, very surprising. To our knowledge, these results have not been reported elsewhere in the IRLM. The next section is devoted to understand the role of each of these different scalings when applied to the spectral density for several values of interaction g .

5.3.4 Universal scaling at fixed g

In order to get a clearer view of the behaviour of $A(\omega)$, it is useful to *scale* our numerical data. In what follows, we will represent the following scaled data:

$$y = \pi A(\omega)(J)^\gamma \quad x = \omega/\Gamma \quad (5.34)$$

where the definition of γ was given in (5.31) and Γ is the exact expression for the thermodynamic energy scale we encountered in chapter 3, that we rewrite here for reference:

$$\Gamma = \frac{2^{2-\alpha} \pi^{2\alpha-5/2} \Gamma\left(\frac{\alpha-1}{2}\right)}{\left[\Gamma\left(\frac{\alpha-1}{\alpha}\right)\right]^\alpha \Gamma\left(\frac{\alpha}{2}\right)} \nu^{\alpha-1} (J)^\alpha \quad (5.35)$$

being ν the *bulk* density of states. Notice how the parameter J scales with a different exponent in both expressions.

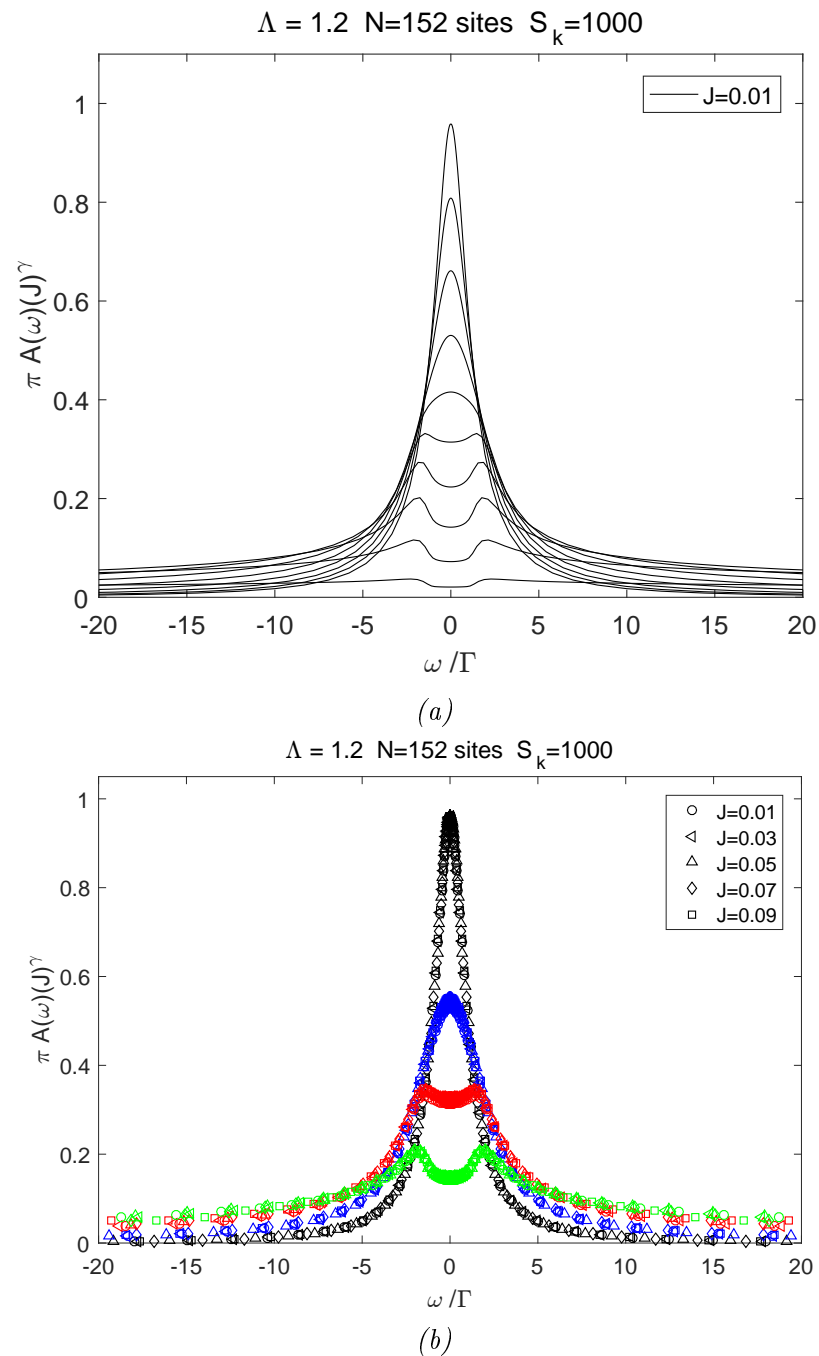


Figure 5.8: NRG calculation of the impurity spectral functions. (a) Spectral functions calculated by NRG and scaled by $\pi(J^\gamma)$ as a function of the dimensionless $\tilde{\omega} = \omega/\Gamma$. NRG data points have been omitted in order to make the graph more visible. (b) Scaled spectral functions for different values of J , at interactions $g = 0$ (black), $g = 0.3$ (blue), $g = 0.5$ (red) and $g = 0.7$ (green). Note how, regardless of the value of J , all data points collapse onto the same curve, showing universality at fixed value of g .

We now represent y against x on a graph. Having done these scalings, we relate

each exponent to a different quantity: γ is associated with the spectral function, that is, the actual probability density of an excitation of energy ω , whereas the thermodynamic exponent α is related to all possible energy excitations. The scaled spectral function is represented for $J = 0.01$ in figure (5.8). Values of $g \in [0, 0.9]$ in increments of 0.1. In the scaled picture, the split of the central peak is much more visible than before. We have avoided using markers for data points, joining them by lines instead, in order to make the graph clearer.

The most surprising feature comes when one represents curves like (5.8a) for different values of the hybridization parameter J . If we put all of them together, we see that *all data points, regardless of the value of J used, collapse onto the same curve for a fixed value of g* . This shows that, when scaled properly, the spectral function is a function of only two quantities: x and g . Such behaviour shows a *universal* shape for the density of states on the impurity site for a fixed value of interaction g . In other words, under proper scaling of the quantities, one obtains a curve independent of J . This evidences that, when computing these dynamical quantities, two exponents must be taken into account. The thermodynamic exponent α proves to be the relevant one to scale all excitation energies, and thus, controls the *width* of the spectral function. On the other hand, the dynamical exponent (γ) controls the scaling of the height, which is related to the probability of having an excitation of energy ω .

This universal scaling forms have been represented in figure (5.8b). In order to differentiate data points, different colors have been used for each different value of g . These numerical data strongly suggests the dependence of dynamical quantities on two different exponents. Even when both exponents γ and α are related to each other (see equation (5.31), the way such relation is established is at the moment unknown to us.

Finally, let us conclude the section by mentioning the equivalence of the Anisotropic Kondo Model (AKM) with the IRLM. Since both models are related by their coupling constants [36], one would expect a similar behaviour to occur in the *transverse* spin correlation function of the AKM, that is, if we compute:

$$S(t) = -i\langle TS^-(t)S^+(0) \rangle \quad (5.36)$$

and we Fourier transform, by taking the imaginary part of $S(\omega)$ a similar behaviour should be expected. The analytical calculation of such quantity is an outstanding point in the theory, since usually what is calculated in the Kondo model is the correlator for the z spin component:

$$\langle TS^z(t)S^z(0) \rangle \quad (5.37)$$

the so called *spin-relaxation* function. Universal scaling of thermodynamic properties of the AKM, as well as for the spin-relaxation function, has been reported previously [95]. We believe these results to be in relation with the observed phenomena exposed here.

5.4 Summary of main results

To conclude, we want to summarize the main results obtained so far in this chapter:

- The spectral function of the local impurity site in the IRLM changes in the low ω sector as interaction is increased. A split of the central peak is observed at sufficiently strong interactions, which hints a possible non-Fermi liquid behaviour of the model.
- When looked in the $\omega \sim 0$ sector, the hybridization parameter J shows a different scaling as the one showed by RG. Numerical data on this *dynamical* exponent shows a relation with the thermodynamic exponent α , and how such relation is established is still outstanding.
- The spectral function at the impurity site shows *universal scaling* curves for a fixed value of interaction g .
- Strong evidence that dynamical quantities, as opposed to thermodynamic ones, require the determination of *two different exponents*, one of them (γ) resulting from a purely dynamical effect in the system. Under these scalings, dynamical quantities develop *universal curves* independent of J for a fixed value of interaction.

Chapter 6

The IRLM: Bethe ansatz solution

"You have your way. I have my way. As for the right way, the correct way, and the only way, it does not exist"

Friedrich Nietzsche

In this chapter, integrability of the IRLM will be discussed based on the coordinate Bethe Ansatz technique. First, a detailed treatment of the solution developed by Filyov and Wiegmann (FW) [56] is followed. The main problem with the FW solution of the IRLM is that the g^2 term appearing in the thermodynamic exponent α is *not* present in the Bethe ansatz method, whereas the term arises naturally by bosonization, as we have already seen in chapter 3 equation (3.24). The result for the charge susceptibility in the model is given in [56] by:

$$\chi^{-1} \sim (t')^{\frac{2}{1+U/\pi}} \quad (6.1)$$

Since χ is directly related with Γ , the thermodynamic energy scale we studied in chapter 3, we see that the FW solution does not reproduce the correct exponent α . We have proved this exponent to be correct numerically by the Numerical Renormalization Group, a non-perturbative technique *in the lattice version of the model*, as well as by DMRG. It was also remarkable that such a lattice description describes very accurately results from the field theory, without any *regularization* taken into account. Being both methods *exact* (bosonization and Bethe ansatz), an agreement must hold between different ways to calculate the same quantity, in this case, the thermodynamic exponent α .

As we will shortly see, one has to face more difficulties when trying to calculate such term by the Bethe ansatz method. The search of this g^2 term is not only a pure (and tedious) mathematical exercise by itself. As we have seen previously, the g^2 term is of extreme importance, since it is proportional to the total number of leads N attached to the dot. It is therefore the term relevant to give rise to different physics in the IRLM when different number of leads are considered.

More worrying is the fact that this g^2 term hasn't been reproduced in the generalised multichannel version of the model [40], treated as well by the coordinate Bethe ansatz approach. A recent publication [96] has dealt with solving the single lead problem of the dot attached to a Luttinger liquid (where interactions between electrons in the bulk are considered) by the same Bethe ansatz technique, however we have noticed this term to be absent here too. Moreover, previous studies [42, 43] of the IRLM attached to a Luttinger liquid have shown universality of thermodynamic properties, even when interactions between fermions in the bulk are present (Luttinger liquid), therefore no changes should be observed here.

Before proceeding, we warn the reader about the high level of detail required here, mostly regarding analytical expressions. This *heavy* mathematical treatment of the problem can sometimes push ourselves in the direction where physics are missed. A good account to this is that, till today, we have not managed to solve the problem yet. Nevertheless, the Bethe ansatz problem in the IRLM, although being mostly a mathematically focused one, will provide a better insight into the physics of these systems once solved.

6.1 The Filyov-Wiegmann solution

As we have discussed earlier, the solution by Bethe ansatz of the IRLM in [56] does not contain the g^2 on the thermodynamic exponent α . Initially, the Bethe ansatz solution of the IRLM was done to prove the equivalence between the IRLM and the Anisotropic Kondo Model (AKM) by direct relation of their susceptibilities. The charge susceptibility, which is directly related to Γ in the IRLM, is the quantity calculated in [56].

It is important to develop the solution step by step here. We will proceed now to calculate the two-particle scattering matrix for the IRLM. The IRLM for a single channel has the following hamiltonian:

$$\begin{aligned}
 H &= H_d + H_l + H_V + H_U \\
 H_d &= -\varepsilon_0 d^\dagger d \\
 H_l &= -i \int dx \psi^\dagger(x) \partial_x \psi(x) \\
 H_{t'} &= t' \int dx \delta(x) (\psi^\dagger(x) d + \text{h.c.}) \\
 H_U &= U \int dx \delta(x) (\psi^\dagger(x) \psi(x) - \langle \psi^\dagger(x) \psi(x) \rangle) (d^\dagger d - \langle d^\dagger d \rangle)
 \end{aligned} \tag{6.2}$$

Note that everything is written in units $v_F = 1$ and thus, all microscopic parameters are divided by a factor $v_F = 2t$. The Dirac delta functions express the locality of the hybridisation/interaction. All position integrals belong to the interval $(-\infty, +\infty)$, since only one species of fermions is considered (say, right movers) after unfolding of the fields. The above hamiltonian conserves particle number, and therefore

$[N, H] = 0$, where the total particle number operator is $N = \int dx \psi^\dagger(x) \psi(x) + d^\dagger d$.

Since particle number is conserved, the many-body wavefunction can be written in general terms in the form:

$$|\Psi\rangle = \left(\int \phi(x_1, x_2, \dots, x_N) \prod_{i=1}^N \psi^\dagger(x_i) dx_i + \int \zeta(x_1, \dots, x_{N-1}) d^\dagger \prod_{i=1}^{N-1} \psi^\dagger(x_i) dx_i \right) |0\rangle \quad (6.3)$$

Notice that these states represent different situations, one where the impurity is empty and another where the impurity is filled. The aim of the Bethe ansatz method is to determine the functions $\phi(x_i), \zeta(x_i)$. If we consider first the non-interacting limit $U = 0$, then the wavefunction factorizes, and each mode of the hamiltonian is calculated independently.

6.1.1 Single particle states: $U = 0$

In a non-interacting system, the many-body wavefunction is just the product of each of the individual modes of the system. Consider then the associated wavefunction for a single particle (a single mode in k space):

$$|\Psi\rangle_k = (c_k^\dagger + \zeta_k d^\dagger) |0\rangle = \left(\int dx \phi_k(x) \psi^\dagger(x) + \zeta_k d^\dagger \right) |0\rangle \quad (6.4)$$

The general solution in this $U = 0$ case comes from the product of the individual solutions for each mode,

$$|\Psi\rangle = \prod_k |\Psi\rangle_k = \prod_k \left(|k\rangle + \zeta_k |1\rangle \right) \quad (6.5)$$

Here we have defined $|1\rangle = d^\dagger |0\rangle$ and $|k\rangle = c_k^\dagger |0\rangle$. The single particle Schrödinger equation is satisfied:

$$H |\Psi\rangle_k = \epsilon_k |\Psi\rangle_k \quad (6.6)$$

At this stage the following relations are useful:

$$\begin{aligned} c_k^\dagger &= \int dx \phi_k(x) \psi^\dagger(x) dx & \psi^\dagger(x) &= \int (dk/2\pi) \phi_k^*(x) c_k^\dagger \\ c_k &= \int dx \phi_k^*(x) \psi(x) dx & \psi(x) &= \int (dk/2\pi) \phi_k(x) c_k \end{aligned} \quad (6.7)$$

therefore defining:

$$\int dk \phi_k(x) \phi_{k'}^*(x) = 2\pi \delta(x) \quad (6.8)$$

With that transformation and the above definition of the state, we have:

$$\begin{aligned}
H_0|\Psi\rangle_k &= -i \int dx dk_2 \phi_{k_2}^*(x) \partial_x \phi_k(x) |k_2\rangle \\
H_d|\Psi\rangle_k &= -\varepsilon_0 \zeta_k |1\rangle \\
H_{t'}|\Psi\rangle_k &= V \int dx \delta(x) \phi_k(x) |1\rangle + V \int dx dk_2 \delta(x) \phi_{k_2}^*(x) \zeta_k |k_2\rangle
\end{aligned} \tag{6.9}$$

which has to equal $\varepsilon_k |k\rangle + \varepsilon_k \zeta_k |1\rangle$ from equation (6.6). Equating the corresponding terms on both sides and using the closure relation $\int |x\rangle\langle x| = 1$, we have the two equations:

$$\begin{aligned}
(\varepsilon_0 + \varepsilon_k) \zeta_k &= t' \phi_k(x=0) \\
-i \partial_x \phi_k(x) + t' \delta(x) \zeta_k &= \varepsilon_k \phi_k(x)
\end{aligned} \tag{6.10}$$

which combined reduce to the single equation:

$$-i \partial_x \phi_k(x) + \frac{t'^2 \delta(x) \phi_k(x=0)}{\varepsilon_0 + \varepsilon_k} = \varepsilon_k \phi_k(x) \tag{6.11}$$

In order to obtain a solution, one has to be careful treating the delta function. The function admits a solution of the form:

$$\phi_k(x) = e^{i\varphi \text{sign}(x)} e^{i\varepsilon_k x} \tag{6.12}$$

where there is a phase-shift experienced by electrons when reaching the boundary. Here we have dealt with the $\delta(x)$ by imposing the condition:

$$\lim_{x \rightarrow 0^+} \phi_k(x) = e^{i\varphi} \quad \lim_{x \rightarrow 0^-} \phi_k(x) = e^{-i\varphi} \tag{6.13}$$

By integrating equation (6.11) above we find:

$$-i(e^{i\varphi} - e^{-i\varphi}) + (\varepsilon_k/2)(e^{i\varphi} + e^{-i\varphi}) = 0 \tag{6.14}$$

where we have used that:

$$\int dx \delta(x) \phi_k(x) = \frac{1}{2} (e^{i\varphi} + e^{-i\varphi}) \tag{6.15}$$

From here we obtain the phase shift as in [56] to be:

$$\Delta(\varepsilon_k) = \arctan \left(\frac{t'^2}{2(\varepsilon_k + \varepsilon_0)} \right) \tag{6.16}$$

so that the function representing single particle scattering states is:

$$\phi_k(x) = \phi_k(x=0) e^{i\varepsilon_k x + i\Delta(\varepsilon_k) \text{sign}(x)} \tag{6.17}$$

Since this constitutes the individual solutions of the non-interacting case, we will call these solutions

$$\boxed{\phi_k^0(x) = C e^{i\varepsilon_k x + i\Delta(\varepsilon_k) \text{sign}(x)}} \tag{6.18}$$

to differentiate from the interacting case. Here C is an arbitrary constant, usually chosen by normalization.

6.1.2 Single particle states: $U \neq 0$

We now look at the solution for single particle states when $U \neq 0$. This comes from applying the interacting part of the hamiltonian to the state:

$$U \int dx \delta(x) (\rho(x) - \rho) (n_d - 1/2) (|k\rangle + \zeta_k |1\rangle) \quad (6.19)$$

We omit the constant part of the hamiltonian coming from $\rho/2$. The contributions of both the dot and wire are:

$$-U \rho \zeta_k |1\rangle \quad -(U/2) \int dx \delta(x) \phi_k(x) |x\rangle \quad (6.20)$$

The interacting part has zero contribution, since there are not two particles in this case. The two equations we obtained before are slightly changed now:

$$\begin{aligned} (\varepsilon_0 + \varepsilon_k + U\rho)\zeta_k &= t' \phi_k(x=0) \\ -i\partial_x \phi_k(x) + t' \delta(x) \zeta_k - (U/2) \delta(x) \phi_k(x=0) &= \varepsilon_k \phi_k(x) \end{aligned} \quad (6.21)$$

As before, we end up with an equation for $\phi_k(x)$, which now accounts for the interaction parameter U :

$$-i\partial_x \phi_k(x) + \left(\frac{t'^2}{\varepsilon_k + \varepsilon_0 + U\rho} - (U/2) \right) \delta(x) \phi_k(x=0) = \varepsilon_k \phi_k(x) \quad (6.22)$$

The solution is immediately found from the previous result:

$$\boxed{\phi_k(x) = C e^{i\varepsilon_k x + i\Delta_U(\varepsilon_k) \text{sign}(x)}} \quad (6.23)$$

where the phase shift is changed as:

$$\boxed{\Delta_U(\varepsilon_k) = \arctan \left(\frac{t'^2}{2(\varepsilon_0 + \varepsilon_k + U\rho)} - \frac{U}{4} \right)} \quad (6.24)$$

where the number ρ is:

$$\rho = \langle \psi^\dagger(0) \psi(0) \rangle \quad (6.25)$$

The single particle states when the impurity is filled, ζ_k are easily found as:

$$\boxed{\zeta_k = \frac{t'}{\varepsilon_0 + \varepsilon_k + U\rho} \cos(\Delta_U(\varepsilon_k))} \quad (6.26)$$

6.1.3 Two particle states: Scattering phase-shift

In the previous section, we solved the *one-body* problem, since the system being non-interacting can be solved by only knowing information of one single particle's behaviour. We now turn our look to the two-body description of the problem. Here,

two particles scatter from each other in the one dimensional world. When this happens, a *scattering phase shift* Φ occurs in the two-body wavefunction. This is the main quantity we will calculate here.

A general eigenstate of the total (two particle) hamiltonian is written as:

$$|\Psi\rangle_2 = \left(\int \phi(x_1, x_2) \psi^\dagger(x_2) \psi^\dagger(x_1) dx_2 dx_1 + \int dx_1 \zeta(x_1) d^\dagger \psi^\dagger(x_1) \right) |0\rangle \quad (6.27)$$

The state with the two-body wavefunction $\phi(x_1, x_2)$ belongs to a *bulk* state, where particles are located inside the channel. The state proportional to $\zeta(x)$ is the state where the impurity site is filled, the other particle belonging to the wire. This is written more conveniently in position basis as:

$$|\Psi\rangle_2 = \int dx_2 dx_1 \phi(x_1, x_2) |x_2, x_1\rangle + \int dx_1 \zeta(x_1) |1, x_1\rangle \quad (6.28)$$

Now we want to calculate:

$$H|\Psi\rangle_2 = E|\Psi\rangle_2 \quad (6.29)$$

in order to get the corresponding equations for $\phi(x_1, x_2)$ and $\zeta(x_1)$. Here $E = \varepsilon_1 + \varepsilon_2$ is the sum of energies of particles. Since the model only accounts for two body interactions, calculation of the associated phase shift for this case constitutes something enough to build up Bethe's hypothesis later. The action of hamiltonian (6.2) over the state $|\Psi\rangle_2$ has several contributions:

$$H|\Psi\rangle_2 = (H_0 + H_{\varepsilon_0} + H_{t'} + H_U)|\Psi\rangle_2 \quad (6.30)$$

Detailed calculation of these terms can be found in the appendix. Equation (6.29) then reduces to the following two equations to determine $\phi(x_1, x_2)$ and $\zeta(x)$:

$$\begin{aligned} -i(\partial_{x_1} + \partial_{x_2})\phi(x_1, x_2) + \frac{t'}{2} \left(\delta(x_1)\zeta(x_2) - \delta(x_2)\zeta(x_1) \right) \\ - \frac{U}{2} \left(\delta(x_1) + \delta(x_2) \right) \phi(x_1, x_2) = E\phi(x_1, x_2) \\ -i\partial_x \zeta(x) + 2t'\phi(x, 0) + \frac{U}{2} \delta(x)\zeta(x) = (E + \varepsilon_0 + U\rho)\zeta(x) \end{aligned} \quad (6.31)$$

Here, the total energy is the sum $E = \varepsilon_1 + \varepsilon_2$. We now look for solutions in the form:

$$\begin{aligned} 2!\phi_\varepsilon(x_1, x_2) &= \phi_{\varepsilon_1}(x_1)\phi_{\varepsilon_2}(x_2)f(x_1 - x_2) - \phi_{\varepsilon_1}(x_2)\phi_{\varepsilon_2}(x_1)f(x_2 - x_1) \\ \zeta(x) &= \zeta_{\varepsilon_1}\phi_{\varepsilon_2}(x)f(-x) - \zeta_{\varepsilon_2}\phi_{\varepsilon_1}(x)f(x) \end{aligned} \quad (6.32)$$

which resembles the definition of a Slater determinant, but including an antisymmetric function $f(x_1 - x_2)$ in each term. Here we recall the form of the single particle wavefunctions as defined in the previous section:

$$\begin{aligned} \phi_\varepsilon(x) &= C e^{i\varepsilon x + i\Delta_U(\varepsilon)\text{sign}(x)} \\ \Delta_U(\varepsilon) &= \arctan \left(\frac{t'^2}{2(\varepsilon_0 + \varepsilon + U\rho)} - \frac{U}{4} \right) \end{aligned} \quad (6.33)$$

The target is to determine this f function, depending only on the relative positions of the two interacting particles. When we insert these guesses for the functions, we have to keep in mind that the single-particle problem holds, which makes the first equation to be an identity by no additional condition. Thus, the function $f(x)$ is only determined by the second equation in (6.31).

By a set of manipulations, and taking into account the single particle equations (6.21), the second equation in (6.31) can be written as:

$$-i\frac{\phi_1(x)}{\zeta_1}\partial_x f(x) + i\frac{\phi_2(x)}{\zeta_2}\partial_x f(-x) = E_2\delta(x)f(-x) - E_1\delta(x)f(x) \quad (6.34)$$

where we have defined:

$$E_i = \frac{U(\varepsilon_0 + \varepsilon_i + U\rho)}{t'} \quad x = x_1 - x_2 \quad (6.35)$$

Since this equation represents the form of $f(x=0)$, some regularization of the delta function must follow. It is clear then that $f(x)$ suffers a discontinuity at $x=0$, so that we can define as in the one particle case:

$$f(x=0) = \frac{1}{2}(e^{i\Phi} + e^{-i\Phi}) \quad (6.36)$$

Then, equation (6.34) is integrated in an interval $[-\epsilon, +\epsilon]$. By doing this, we get the form satisfied by the scattering phase shift $\Phi(\varepsilon_1, \varepsilon_2)$, which is:

$$\boxed{\Phi(\varepsilon_2, \varepsilon_1) = \arctan\left(\frac{U}{2} \frac{\varepsilon_2 - \varepsilon_1}{\varepsilon_1 + \varepsilon_2 + 2(\varepsilon_0 + U\rho)}\right)} \quad (6.37)$$

and therefore, the final form of the function $f(x)$ is:

$$f(x_1 - x_2) = f(0)e^{i\Phi(\varepsilon_2, \varepsilon_1)\text{sign}(x_1 - x_2)} \quad (6.38)$$

Equation (6.37) is the most important formula of this section. It agrees with the one calculated by Mehta and Andrei [44]. It represents the exact scattering phase-shift between two particles scattering in the 1D world. Note that it depends on the microscopic parameters of the model U, ε_0, ρ . In practical terms, and in simulations carried out by NRG in chapter 3, we took the parameter $\rho = 1/2$, whereas the condition $\varepsilon_0 = 0$ represents the model in *resonance*, which is also the limit we are interested into. Also, by taking into account that $U/2t = \tan(\delta)$, we find the coefficient inside the argument to correspond to $\delta/2$.

In [56, 60], the coefficient inside the scattering phase shift is different:

$$\Phi(\varepsilon_2, \varepsilon_1) = \arctan\left(\tau \frac{\varepsilon_2 - \varepsilon_1}{\varepsilon_1 + \varepsilon_2 + 2(\varepsilon_0 + U\rho)}\right) \quad \tau = \tan\left(\frac{U}{2}\right) \quad (6.39)$$

although no explicit calculation of the regularization used for the delta function is given. Nevertheless, it is clear that both expressions (6.37) and (6.39) match at

small values of U . It is frequently mentioned [30, 44, 96] that the factor $U/2$ inside the scattering phase shift is a *bare* quantity, and that therefore its form strongly depends on the regularization scheme employed. We believe this not to be case for the IRLM, based on our previous exact results of chapter 3, where we showed the analogy of results obtained from both a lattice /field version of the model, without any regularization employed. Moreover, we showed the field description of the IRLM to correspond to the Boundary Sine Gordon Model, where a exact relation between parameters of the theory was given:

$$\frac{\beta^2}{4\pi} = (1 - g)^2 \quad g = \frac{2}{\pi} \arctan \left(\frac{U\pi\nu}{2} \right) \quad (6.40)$$

We therefore believe results like (6.39) cannot depend on how the delta functions are regularized in the theory. In fact, we will show in a later approach that result (6.68) can be derived without taking into account such regularizations.

We will see later that the factor inside Φ in equation (6.39) does not map in a correct way between other field theories. As we have already mentioned, it does not reproduce the g^2 term encountered in the thermodynamic exponent α , which is a term has been verified both analytically and numerically in chapters 3 and 4.

We will later propose a different factor τ for the IRLM, proving this to be the one making the correct mapping between two well known integrable field theories, being one of them the Boundary Sine Gordon Model, which was proved to be equivalent in chapter 3.

6.1.4 The Bethe ansatz: N particle wavefunction and rapidities representation

Having calculated the two-particle interaction processes, the so called *Bethe ansatz* consists on expressing the general N body wavefunction by taking into account only two-particle processes, due to integrability of the model.

The ansatz for the N particle wavefunction is then:

$$N! \phi(x_1 \dots x_N) = \sum_P (-1)^P \phi_{p_1}(x_1) \dots \phi_{p_N}(x_N) \prod_{i>j} e^{i\Phi(\varepsilon_{P_i}, \varepsilon_{P_j}) \text{sign}(x_i - x_j)} \quad (6.41)$$

where the index P makes reference to all possible permutations. One can verify that such solution satisfies indeed Schrodinger equation in the IRLM for N particles. The way to obtain information about the eigenvalues of the problem is by imposing periodic boundary conditions on a ring of size $2L$, so that N coupled equations are obtained:

$$\phi(x_1, \dots, x_i = -L, \dots, x_N) = \phi(x_1, \dots, x_i = +L, \dots, x_N) \quad (6.42)$$

Therefore, the *Bethe equations* are given by:

$$2L\varepsilon_i = 2\pi n_i - 2 \sum_k \Phi(\varepsilon_i, \varepsilon_k) - 2\Delta_U(\varepsilon_i) \quad (6.43)$$

The equations determine the eigenvalues spectrum in an unique way. Notice that different set of integers n_i give different states in the system. However, since we are looking at low-temperature properties of the model, it is enough for us to determine the appropriate form of the ground state. The total energy is then the sum of these equations, resulting in:

$$E = (\pi/L) \sum_i n_i - (1/L) \sum_i \Delta_U(\varepsilon_i) \quad (6.44)$$

where we have used the fact that:

$$\Phi(\varepsilon_i, \varepsilon_j) = -\Phi(\varepsilon_j, \varepsilon_i) \quad (6.45)$$

The second term in the equation above $E = E_0 + \delta E$ is a term due to the impurity, and represents a deviation respect to the Fermi-sea energy, where all levels in $[-\Lambda, 0]$ are occupied. This term needs to be determined in a self consistent way. One way to calculate its first order contribution is to neglect it in the single-particle equation, as it is done in [56].

The ground state corresponding to a non-interacting Fermi gas has associated quantum numbers:

$$n_{i+1} = n_i - 1 \quad (6.46)$$

with $n_1 = 0$. In this way, the next energy level is shifted by an integer and the Fermi sea is filled. We define now the density of states as:

$$\rho(\varepsilon) = \frac{1}{2L(\varepsilon_i - \varepsilon_{i+1})} > 0 \quad (6.47)$$

Note that in our units, this quantity has no dimensions, since $[\varepsilon] = [L]^{-1}$. Important enough, this quantity is, by definition, *dense* in the thermodynamic limit $L \rightarrow \infty$. Then, using equations for ε_i and ε_{i+1} , and neglecting the term with Δ_U for individual particles, we have:

$$2L(\varepsilon_i - \varepsilon_{i+1}) = 2\pi \underbrace{(n_i - n_{i+1})}_1 - 2 \sum_k \Phi(\varepsilon_i, \varepsilon_k) - \Phi(\varepsilon_{i+1}, \varepsilon_k) \quad (6.48)$$

and using the definition of the density of states, we can take the continuum limit. In such a limit, the spectrum of eigenvalues becomes *dense*, and the calculation of its distribution function $\rho(\varepsilon)$ is given by solving the following integral equation:

$$\rho(\varepsilon) = \frac{1}{2\pi} + \frac{1}{\pi} \int_{-\Lambda}^0 d\omega \rho(\omega) \frac{\partial \Phi(\varepsilon, \omega)}{\partial \varepsilon} \quad (6.49)$$

There is a comment to do here. In [56], all eigenvalues are shifted by an amount $-NU/2L$, in order to get rid of the *awkward* term inside the phase shift $U\rho$. However, this is done because of the term $\tan U/2$ inside expression (6.39), whereas we have proved this to be $U/2$ instead, being U the *actual* microscopic parameter.

We turn now to the rapidities representation, which proves to be more convenient for such systems [30, 28, 56, 60]. The scattering phase $\Phi(\varepsilon_i, \varepsilon_k)$ can be expressed as a function that only depends on the *rapidities* difference $\beta = \beta_i - \beta_k$. Notice how the term $\varepsilon_0 + U\rho$ in the denominator in expression (6.37) makes this difficult. One way to get rid of it is to shift all eigenvalues of the problem by a quantity $-\varepsilon_0 - U\rho$. Then we make the replacement:

$$\varepsilon_i \rightarrow \varepsilon_i - \varepsilon_0 - U\rho \quad (6.50)$$

so that the two-particle scattering phase is:

$$\Phi(\varepsilon_i, \varepsilon_k) = \arctan\left(\frac{U}{2} \frac{\varepsilon_i - \varepsilon_k}{\varepsilon_i + \varepsilon_k}\right) \quad (6.51)$$

The unfolding of fields use in (6.2) deals only with one kind of fermions, in this case, right-movers. The following mapping is standard in these systems:

$$\varepsilon_k = -\Lambda e^{-\beta_k} \quad (6.52)$$

Note that all negative energy particles must have $\text{Im}(\beta) = 0$. The mapping (6.52) is common to use in massless field theories. Thus the scattering phase shift depends solely on β :

$$\Phi(\beta) = -\arctan\left(\frac{U}{2} \tanh\left(\frac{\beta}{2}\right)\right) \quad \beta = \beta_i - \beta_k \quad (6.53)$$

which can also be expressed more conveniently as:

$$\Phi(\beta) = -\frac{i}{2} \log\left(\frac{1 - i(U/2) \tanh(\beta/2)}{1 + i(U/2) \tanh(\beta/2)}\right) \quad (6.54)$$

The integral equation (6.49) can then be written in the rapidities representation:

$$\rho(\beta) = \frac{\Lambda}{2\pi} e^{-\beta} + \int_0^{+\infty} d\alpha \rho(\alpha) K(\beta - \alpha) \quad (6.55)$$

where the *kernel* is the most important quantity to solve the integral equation:

$$K(\beta - \alpha) = -\frac{1}{2\pi} \frac{\partial(2\Phi)}{\partial\beta} = -\frac{1}{2\pi} \frac{\sin(2\omega)}{\cos(2\omega) - \cosh(\beta - \alpha)} \quad \cot(\omega) = \frac{U}{2} \quad (6.56)$$

Note the symmetry of the kernel, which allows for standard methods in the calculation of the above integral equation [88]. By solving equation (6.55), the exact spectrum of eigenvalues can be computed and therefore the problem is solved in an exact way.

6.1.5 Calculation of rapidities distribution

We solve now equation (6.55), this being not explicitly done in [56], but a similar calculation for the multichannel case can be found in [40].

The integral equation (6.55) can be solved by a standard Wiener-Hopf method. The equation is Fourier transformed to give [60, 88]:

$$\rho^-(p) + (1 - K(p))\rho^+(p) = \rho^0(p) \quad (6.57)$$

where we adopt the following definition of Fourier transforms:

$$\begin{aligned} \rho^0(p) &= \frac{\Lambda}{2\pi} \int_{-\infty}^{+\infty} d\alpha e^{ip\alpha} e^{-\alpha\theta(\alpha)} = \frac{i\Lambda}{2\pi(p+i)} \\ K(p) &= \int_{-\infty}^{+\infty} d\alpha K(\alpha) e^{ip\alpha} = \frac{\sinh(\pi p g)}{\sinh(\pi p)} \\ \rho^\pm(p) &= \pm \int_0^{\pm\infty} d\alpha \rho^\pm(\alpha) e^{i\alpha p} \end{aligned} \quad (6.58)$$

Here $\alpha \equiv \text{Re}(\beta)$. The parameter g is the interaction parameter of the IRLM we have already defined in previous sections. By use of the Wiener Hopf method [60, 35, 88], the next step is to factorise the $1 - K(p)$ factor into two analytic functions in the half complex plane p . This gives:

$$1 - K(p) = \gamma^+(p)\gamma^-(p) = \frac{\pi(1-g) \prod_{\pm} \Gamma(1 \pm ip)}{\prod_{\pm} \Gamma(1 \pm ip(1-g)/2) \Gamma(1/2 \pm ip(1+g)/2)} \quad (6.59)$$

Here $\gamma^+(p)$ ($\gamma^-(p)$) is analytic in the upper (lower) half plane of p . Curiously enough, we can establish a relation between this kernel and the one found in [35], where the S matrix of solitons in the sine Gordon theory eq.(6.88) is considered. The relation comes from a proper renormalization of the inverse rapidities:

$$p = \frac{\omega}{1+s} \rightarrow (1 - \tilde{\Phi}(p))^{-1} = (1 - K(p)) \quad (6.60)$$

Here, s is a parameter we will shortly define, for now we just need to understand that This fact, which is at first a surprising relation between the S matrix for the IRLM pseudoparticles and the S matrix of solitons in the Sine Gordon theory, needs to be explored further. We now refer to the appendix for details on the calculation. Solving equation (6.57) by the Wiener Hopf technique (appendix), we find for $\rho^+(p)$ the following solution:

$$\rho^+(p) = \frac{1}{a(2\pi)^2} \frac{i\Lambda}{(i+p)} \frac{\Gamma(1+a)\Gamma(1/2+b)\Gamma(1-ipa)\Gamma(1/2-ipb)}{\Gamma(1-ip)} e^{(1-ip)\Delta} \quad (6.61)$$

where we have defined for convenience $a = (1-g)/2$ and $b = (1+g)/2$. If one Fourier transforms back this expression, we obtain $\rho^+(\alpha)$ expressed as an infinite

series, since now the expression has multiple poles due to the gamma functions. This series is formed by two contributions:

$$\begin{aligned}\rho(\beta) &= \sum_{n=1}^{+\infty} A_n e^{-\frac{n\alpha}{a}} + B_n e^{-\frac{(2n-1)\alpha}{2b}} \\ A_n &= \frac{\Lambda}{2\pi} \frac{(-1)^n \Gamma(1/2 - na/b)}{n! \Gamma(2 - n/a)} \\ B_n &= \frac{\Lambda}{2\pi} \frac{(-1)^n \Gamma(1 - (2n-1)(a/2b))}{n! \Gamma(2 - (2n-1)/2b)}\end{aligned}\quad (6.62)$$

We are only interested in the most important contributions of such poles, that is, those that allow for a slower decay of the exponential function. Thus, an expression for the eigenvalues distribution can be obtained, giving:

$$\rho(\varepsilon) \sim \varepsilon^{-g/(1+g)} \quad \rho(\varepsilon) = -\varepsilon^{-1} \rho(\alpha) \quad (6.63)$$

Note that at $g = 0$, that is, in the non-interacting system, the distribution of eigenvalues is uniform as one would expect. We do not worry too much about prefactors from now on, since we would be interested in computing the scaling of the parameter t' with g .

6.1.6 Thermodynamic exponent by Bethe ansatz in FW solution

Once the function $\rho(\varepsilon)$ is known, one can calculate the impurity's contribution to the total energy. From equation (6.44) this is, following [56]

$$\delta E = \int_{-\Lambda}^0 d\varepsilon \rho(\varepsilon) \arctan \left(\frac{(t')^2}{2(\varepsilon + \varepsilon_0)} \right) \quad (6.64)$$

Note that the factor $-U/4$ inside the argument of the arctan is absent in [56]. Defining the occupation on the dot as [40]:

$$n_d = \frac{\partial \delta E}{\partial \varepsilon_0} \rightarrow \chi \sim \left. \frac{\partial n_d}{\partial \varepsilon_0} \right|_{\varepsilon_0=0} \quad (6.65)$$

then the charge susceptibility can be calculated. The calculation can be followed in detail in the appendix. The impurity contribution to the ground state energy of the system eq.(6.64) can be turned into another integral by standard change of variables. Defining $\Gamma_0 = (t'/\sqrt{2})^2$, we find:

$$\chi \sim \int_{-\Lambda}^0 \frac{d\varepsilon}{\varepsilon^2} \frac{(\Gamma_0/\varepsilon)}{(1 + (\Gamma_0/\varepsilon)^2)^2} (-\varepsilon/\Lambda)^{-g/(1+g)} \sim \Gamma_0^{\frac{-1-2g}{1+g}} \quad (6.66)$$

Therefore, we find:

$$\chi^{-1} \sim \Gamma \sim (t')^{\frac{2+4g}{1+g}} \quad (6.67)$$

Note that the exponent doesn't correspond with the previous calculated thermodynamic exponent α (although it does for $g = 0$), neither matches with the result derived in [56]:

$$\chi^{-1} \sim (t')^{\alpha_{FW}} \quad \alpha_{FW} = \frac{2}{1 + U/\pi} \quad (6.68)$$

According to this, and by inspection of the thermodynamic exponent α for the IRLM in equation (3.24), we can identify:

$$\alpha = \frac{2}{1 + 2g - g^2} \rightarrow \frac{U}{2} = 2\delta \quad (6.69)$$

In FW's solution. Note that in this fashion, the U employed in [56] *does not* correspond to the microscopic parameter of the theory U , but to some related phase-shift. In this case, and because the expression of α is known from (6.69) to be correct, we made this identification. The exponent we have just calculated is also not recovered in [40] when the model is generalised to the N lead case. The fact that one does not recover the exact thermodynamic exponent from the Bethe ansatz method, which is in nature non-perturbative, makes a sufficient argument to check the theory in further look for a solution that incorporates such term.

We make now connection with our previous results in chapter 3. It has been shown how the lattice version of the IRLM can well reproduce results from the field theory without any regularizations taken into account. The NRG numerics in the IRLM proved to work quite well when the field theory expression for the Boundary temperature in the Boundary Sine Gordon model is taken as the relevant energy scale. Thus, we incline ourselves to believe this to be the same when the Bethe ansatz (BA) is applied to the model. Whereas the thermodynamic exponent α is reproduced without difficulties by use of bosonization, here we see how the BA proves to be a much more complicated way to obtain such quantities. Regardless of which technique we decide to employ, the same physical answers need to be recovered.

Thus the big problem in the Bethe ansatz solution of the model has been presented, and we have attempted to derive the thermodynamic exponent α . The fact that we haven't been successful on this, we believe, has to do with the appropriate choice of the two-particle S matrix. We should note that equation (6.37) does not contain a g^2 term on it. However, we can analyse the appropriate value for the exponent in $\rho(\varepsilon)$ in order to reproduce the known result. Therefore we require:

$$\rho(\varepsilon) \sim \varepsilon^{-\kappa} \quad 1 + \kappa = \frac{1}{1 + 2g - g^2} \quad (6.70)$$

The appropriate exponent satisfying this is then:

$$\kappa = \frac{-(2g - g^2)}{1 + 2g - g^2} = -(2g - g^2) \frac{\alpha}{2} = -\frac{s}{1 + s} \quad (6.71)$$

where α is the thermodynamic exponent in (3.24) and we have defined $s = 2g - g^2$. We see later that this parameter is of importance to preserve the mapping to the

other (1+1) dimensional field theories.

Finally, to conclude this section, note that the change:

$$\rho(\varepsilon) \rightarrow \rho(\varepsilon)^{-1} \quad (6.72)$$

does indeed recover the solution from FW for the thermodynamic exponent. In this case:

$$\rho(\varepsilon) \sim \varepsilon^{\frac{g}{1+g}} \quad (6.73)$$

then by substituting in equation (6.66) we find:

$$\chi \sim (t')^{\frac{-2}{1+g}} \rightarrow \Gamma \sim (t')^{2/1+g} \quad (6.74)$$

If we remember that g is defined as:

$$g = 1 - \frac{2\omega}{\pi} \rightarrow \omega = \frac{\pi}{2}(1 - 2g + g^2) \quad (6.75)$$

would give the correct exponent. The fact that this is the appropriate value of g is not a simple coincidence, as we will explore in the next section. Thus we can conclude from here that, in order to get the appropriate thermodynamic exponent, one must work with a *renormalized set* of rapidities, instead of the bare one. We will explore these connections in the next section.

6.2 Relation of the IRLM to (1+1) integrable field theories

In this section we explore the connection between the IRLM and other integrable field theories in (1+1) dimensions. Concretely, we explore these connections for the massless limit of the Massive Thirring Model (MTM) we described in chapter 2, and the soliton solutions of the Sine Gordon Model (SGM). The relation between the MTM and the SGM was discovered by Sidney Coleman [32], and has been studied later by several authors in the field [28, 29, 30, 87].

6.2.1 Relation to the Massive Thirring model

The MTM was introduced in chapter 2. It can be solved in an exact way when a *mass* term m_0 is considered for the bulk fermions. Once the exact solution has been computed, one then takes the massless limit $m_0 \rightarrow 0$ of the theory. In this limit, the energy and momentum distributions are changed:

$$\varepsilon_k = -m_0 \cosh(\beta) \rightarrow \varepsilon_k = -ae^{\pm\beta} \quad (6.76)$$

These two new branches correspond now to massless pseudoparticles, representing right and left movers. Since the field theory of the IRLM is defined only for right

movers (after unfolding of the fields), then one identifies this mapping with the one used in (6.52). Massless fermions of the MTM behave as fermions of the IRLM. For a proper definition of the MTM and its parameters, we refer back to section (2.6.3) of this thesis.

The S matrix for two negative energy pseudoparticles in the MTM can be found in [28, 29]. We write it down here again:

$$\Phi_{MTM} = i \log \left(\frac{\sinh(i\omega - \beta/2)}{\sinh(i\omega + \beta/2)} \right) = -2 \arctan \left(\cot(\omega) \tanh(\beta/2) \right) \quad (6.77)$$

and $\omega = (\pi - \xi)/2$. It is then immediate to see the connection of this (bulk) field theory with the IRLM. We note that the following relation between scattering phase shifts holds for both models:

$$2\Phi_{IRLM} = \Phi_{MTM} \quad (6.78)$$

By inspection of equation (6.54), one could argue that the relation between microscopic parameters of the model is given by:

$$\cot(\omega) = \frac{U}{2} \rightarrow \xi = 2 \arctan \left(\frac{U}{2} \right) = 2\delta \quad (6.79)$$

In fact, from FW solution equation (6.68), this is not entirely true, since then we obtain:

$$\cot(\omega) = \tan(2\delta) \rightarrow \xi = 2(2\delta) \quad (6.80)$$

This factor of 2 proves to be of extreme importance when we relate different microscopic parameters between these models. For now, we will mention that relation (6.80) is the first order of what the actual relation between parameters should be. Nevertheless, it is worth noting that both kernels, that of the MTM and the one corresponding to the IRLM are identical. However, the integral equation to solve for both models is different. Whereas an integral equation of the form (6.55) can be calculated in a *symmetric interval* of rapidities $\beta \in [-\Lambda, +\Lambda]$ for the MTM (see [28, 30]), for the IRLM we have to solve the integral equation *in the half line*. The method to solve such equations is usually more complicated than simple Fourier transformation.

6.2.2 Relation to Boundary Sine Gordon theory

At this stage, it should be of no surprise to us that the BSGM plays a role, as we have already discovered in chapter 3. The sine-Gordon model has a well known scaling dimension of the mass gap developed in the solutions, which are composed by a soliton and an antisoliton. It is convenient to define a parameter λ directly related with the scaling dimension of the field:

$$\lambda = \frac{8\pi}{\beta^2} - 1 = \frac{1}{d} - 1 \rightarrow 2d = \frac{\beta^2}{4\pi} \quad (6.81)$$

where β is the bulk parameter in the sine Gordon lagrangian. The lagrangian describing the BSGM is given by [34, 89]:

$$\mathcal{L}_{BSG} = \int dx (\partial_\mu \phi)^2 + G \cos(\sqrt{2}\beta\phi) + g\delta(x) \cos((\beta/\sqrt{2})\phi) \quad (6.82)$$

This is the well known boundary sine Gordon model. Note the factor $\sqrt{2}$ inserted in both terms. This is because the bulk and boundary terms are related by a factor of two inside their scaling dimensions. The lagrangian 6.82 can be found in [35] in that concrete form. The estimated correlation length for the BSGM is:

$$m \sim G^{(1+\lambda)/2\lambda} \sim G^{1/2-2d} \quad (6.83)$$

which can be found in the literature [66, 86, 89], and we already came across this in chapter 3.

The important point to understand here is how does this model relate to the IRLM as seen in chapter 3. The massless limit $G \rightarrow 0$ must be taken in order to reproduce known results. That is, the BSGM maps onto the IRLM when only the boundary term (proportional to g above) is taken into account. As we show in chapter 3, for the IRLM we identify:

$$t' \cos((\beta/\sqrt{2})\phi(0)) = t' \cos(\beta'\phi(0)) \quad (6.84)$$

and this provides the correct exponent for t' , since now:

$$2d' = \frac{\beta'^2}{4\pi} = \frac{\beta^2}{2(4\pi)} = \frac{1}{2}(1-g)^2 \quad (6.85)$$

Here β represents the ordinary bulk term in the standard Sine Gordon Theory. Both the SGM and the MTM proved to be equivalent by Coleman [32] by the following relation of their parameters:

$$\frac{\beta^2}{4\pi} = \frac{1}{1 + \xi/\pi} \sim 1 - \xi/\pi + O(\xi^2) \quad (6.86)$$

The above expression is *exact* [66]. We will prove now that, by comparing the S matrix of solitons in [35, 33] with that of [28], the above relation between parameters is recovered.

6.2.3 S matrix of solitons

Here we compare the two S matrices of solitons in the sine Gordon theory, given by [28] and [35], and we establish a relation between all different parameters employed. The S matrix of solitons for the boundary sine-Gordon model is defined as [35]:

$$S_{BSG}(\theta) = \exp \left\{ i \int_{-\infty}^{+\infty} \frac{dy}{2y} \sin \left(\frac{2\theta\lambda y}{\pi} \right) \frac{\sinh((\lambda-1)y)}{\sinh(y) \cosh(\lambda y)} \right\} \quad (6.87)$$

whereas from Korepin's work it follows:

$$S_K(\theta) = \exp \left\{ - \int_0^{+\infty} \frac{dx}{x} \frac{\sinh \left(\left(\frac{4\pi}{\gamma'} - \frac{1}{2} \right) x \right) \sinh \left(\frac{i8\theta x}{\gamma'} \right)}{\sinh \left(\frac{x}{2} \right) \cosh \left(\frac{4\pi x}{\gamma'} \right)} \right\} \quad (6.88)$$

The integrand here is symmetric, so the limits can be extended to $(-\infty, +\infty)$ dividing by 2. Then using that $\sinh(iz) = i \sin(z)$ and inserting the minus inside the first sinh we obtain:

$$S_K(\theta) = \exp \left\{ i \int_{-\infty}^{+\infty} \frac{dx}{2x} \frac{\sinh \left(\left(\frac{1}{2} - \frac{4\pi}{\gamma'} \right) x \right) \sin \left(\frac{8\theta x}{\gamma'} \right)}{\sinh \left(\frac{x}{2} \right) \cosh \left(\frac{4\pi x}{\gamma'} \right)} \right\} \quad (6.89)$$

Now by the change of variable $x = 2y$, we obtain:

$$S_K(\theta) = \exp \left\{ i \int_{-\infty}^{+\infty} \frac{dy}{2y} \frac{\sinh \left(\left(1 - \frac{8\pi}{\gamma'} \right) y \right) \sin \left(2 \left(\frac{8\theta}{\gamma'} \right) y \right)}{\sinh(y) \cosh \left(\frac{8\pi y}{\gamma'} \right)} \right\} \quad (6.90)$$

where γ' is defined as:

$$\gamma' = \frac{8\pi\gamma}{8\pi - \gamma} \quad (6.91)$$

and γ is taken from the sine-Gordon lagrangian:

$$\mathcal{L} = \frac{1}{2\gamma} (\partial_\mu \phi)^2 - \frac{\mu^2}{\gamma} (1 - \cos(\phi)) \quad (6.92)$$

It is important to note the different normalizations used in the two papers. Here the rapidities θ in (6.88) are understood as the renormalized rapidities, relating to the bare ones as:

$$\theta = \frac{\pi\alpha}{2(\pi - \omega)} \quad (6.93)$$

where we have called the *bare* rapidities α in order to avoid confusion later on. If we now identify:

$$\gamma' = \frac{8\pi}{\lambda} \quad \frac{1}{\lambda} = \frac{\gamma}{8\pi - \gamma} \rightarrow \frac{\nu}{1 - \nu} = \frac{\gamma}{8\pi - \gamma} \rightarrow \gamma = 8\pi\nu \quad (6.94)$$

A relation between the parameter β of the Sine Gordon Model and ω in the MTM can be established. Thus the relation between the Sine Gordon model and the MTM parameters is given by:

$$\frac{8\pi}{\lambda} = \frac{8\pi\omega}{\pi - \omega} \quad \frac{\beta^2}{4\pi} = 1 - \frac{\xi}{\pi} \quad (6.95)$$

which agrees with Coleman's result to first order in ξ , where the relation of parameters between both theories is valid and written in (6.86). It is also clear that one of the definitions in the papers lacks a minus sign, for them to be exactly equivalent. The correct exact formulas for the soliton-soliton S matrix in the sine-Gordon theory are given by:

$$\begin{aligned}
 S_K(\theta) &= \exp\left\{ \int_0^{+\infty} \frac{dx}{x} \frac{\sinh\left(\left(\frac{4\pi}{\gamma'} - \frac{1}{2}\right)x\right) \sinh\left(\frac{i8\theta x}{\gamma'}\right)}{\sinh\left(\frac{x}{2}\right) \cosh\left(\frac{4\pi x}{\gamma'}\right)} \right\} \\
 S_{\text{BSG}}(\theta) &= \exp\left\{ -i \int_{-\infty}^{+\infty} \frac{dy}{2y} \sin\left(\frac{2\theta\lambda y}{\pi}\right) \frac{\sinh((\lambda-1)y)}{\sinh(y) \cosh(\lambda y)} \right\} \quad (6.96)
 \end{aligned}$$

Whereas these results have been reported in the literature [28, 35], it is worth comparing all expressions encountered and the relationship between different parameters employed, as notation differs from one publication to another as we have already seen.

6.2.4 Connection to the IRLM

It was shown in chapter 3 that the IRLM is mapped to a generalised boundary sine-Gordon theory by the following relation between parameters:

$$2d = \frac{\beta^2}{4\pi} = (1-g)^2 \quad (6.97)$$

The most surprising feature of such relation is that, whereas β represents a purely bulk term in a field theory, the parameter g for the IRLM is directly related to the microscopic parameter U of the model, which also accounts for a description in the lattice. Nevertheless, we have shown to be the scattering phase shift δ the relevant parameter to use. This was proved in chapter 3 by NRG, where the exact expression of the boundary temperature [35] for the BSGM was identified with the relevant thermodynamic scale of the IRLM. In [35], the scaling dimension of the model is represented by λ as:

$$\lambda = \frac{1}{d} - 1 = \frac{1}{\alpha - 1} = \frac{1 + (2g - g^2)}{1 - (2g - g^2)} = \frac{1 + s}{1 - s} \quad d = \frac{1}{2}(1 - g)^2 \quad (6.98)$$

where g is defined in (6.40), and note that s has been defined in equation (6.71). As we know from chapter 3, this value of g is then restricted to lie in $[-1, 1]$ interval.

In the Bethe ansatz treatment of the model, the scattering phase shift presents a term τ inside:

$$\Phi(\alpha - \beta) \sim \arctan\left(\tau f(\alpha - \beta)\right) \quad (6.99)$$

We calculated this value to be $\tau = U/2$, in agreement with [44], whereas in [56] this is substituted by $\tan U/2$, accounting for a different regularization of the Dirac delta in the field theoretic treatment.

It is worth to notice how both the IRLM and the MTM reproduce the same kernel $K(\alpha - \beta)$ in equation (6.56) by just a direct substitution of their parameters. We should also remember that the scattering phase shift between two negative energy pseudoparticles in the MTM is *not* equivalent to the S matrix of solitons. According to Korepin [28, 30], the S matrix of physical particles (*fermions* in the MTM) is equivalent to the S matrix of solitons in the Sine Gordon theory. The direct mapping of the IRLM to the MTM comes from the replacement $\tau = \cot(\omega)$, and the parameter ω relates to the MTM parameter ξ as [28]

$$\omega = \frac{\pi - \xi}{2} \quad (6.100)$$

defining a new parameter $s = 1 - (2\omega/\pi)$, the relation between the IRLM and the boundary sine Gordon model [89, 34] reads:

$$\lambda = \frac{1 + s}{1 - s} \quad (6.101)$$

from where we have:

$$s = 2g - g^2 = 1 - (2\omega/\pi) = \frac{2}{\pi} \arctan(\tau) \quad (6.102)$$

Therefore we argue that the *correct* relations between parameters of these models are given by:

$$\begin{aligned} \tau = \cot(\omega) = \tan(2\delta(1 - \delta/\pi)) = \tan(\pi s/2) & \quad \xi/\pi = \frac{2}{\pi} \arctan(\tau) = 2g - g^2 \\ \frac{\beta^2}{4\pi} = 1 - \xi/\pi = 1 - (2g - g^2) = 1 - s & \quad \omega = \frac{\pi - \xi}{2} \end{aligned} \quad (6.103)$$

The last equation relates both the microscopic (bulk) parameters of the MTM and the Sine Gordon theory, with the interaction parameter g of the IRLM. Notice the dependence of τ with a g^2 term. This term g^2 is of special interest, and could explain why it is absent in FW solution when calculating the thermodynamic exponent of the impurity susceptibility. After all, we have seen that the exponent for the distribution of eigenvalues in equation (6.71) depends solely on s . The FW solution only reproduces a value of $\tau = \tan(2\delta) = \tan(\pi g)$, that is, only the first order term. We conjecture that, in order to satisfy all known relations between parameters of the different theories, the term $(1 - \delta/\pi)$ should be recovered at some point in the calculation. We will come back to this later in section 3 of this chapter.

For now, we have to content ourselves with a conjecture. According to the above mentioned relations, we claim the *actual* form of the scattering phase shift between two negative energy pseudoparticles in the IRLM to be:

$$\boxed{\Phi = -\arctan\left(\tan(\pi g(1 - (g/2))) \tanh(\beta/2)\right)} \quad (6.104)$$

It is clearly seen that the field theoretic approach we developed for equation (6.37) does not reproduce the correct parameter, despite the fact that this form of the scattering phase shift has been used in the literature [44]. As we will see later, a description in the lattice is necessary, at least to get the first order term in g in the correct form.

The S matrix of solitons from the IRLM

We have seen that the kernels in equation (6.60) are related. We can then establish a relation between the S matrix of solitons in the Sine Gordon theory and the IRLM. From equation (6.87), it can easily be obtained the form of the kernel in the integral equation, satisfying [35]

$$\tilde{K}(\omega) = \mathcal{FT}\left[\frac{1}{2\pi}\partial_\theta S(\theta)\right] = -\int_{-\infty}^{+\infty} d\theta e^{i\omega\theta} \frac{1}{2\pi}\partial_\theta \log(iS(\theta)) \quad (6.105)$$

Working this out directly from equation (6.96), we find:

$$\tilde{K}(\omega) = -\frac{\sinh\left(\frac{(\lambda-1)\pi\omega}{2\lambda}\right)}{2\cosh\left(\frac{\pi\omega}{2}\right)\sinh\left(\frac{\pi\omega}{2\lambda}\right)} \quad (6.106)$$

where we have λ in equation (6.101). At this stage, the following relations prove to be useful:

$$\begin{aligned} 2\cosh\left(\frac{\pi\omega}{2}\right)\sinh\left(\frac{\pi\omega(1-s)}{2(1+s)}\right) &= \sinh\left(\frac{\pi\omega}{1+s}\right) - \sinh\left(\frac{\pi\omega s}{1+s}\right) \\ \frac{\lambda+1}{2\lambda} &= \frac{1}{1+s} \end{aligned} \quad (6.107)$$

Taking into account equation (6.60), we get:

$$(-\tilde{K}(\omega)) = \frac{K(\omega)}{1-K(\omega)} \rightarrow (-\tilde{K}(\omega)) = K(\omega) + (-\tilde{K}(\omega))K(\omega) \quad (6.108)$$

providing that the following relations hold between the bare rapidities β and the *physical* (renormalized) rapidities θ :

$$\theta = \frac{\beta}{1+s} \quad \omega = p(1+s) \quad (6.109)$$

As we can see, this leaves invariant the inner product $p\beta = \omega\theta$, and all Fourier transforms are constructed accordingly. Thus, we substitute in (6.58) the values $p \rightarrow \omega/(1+s)$. The above equation (6.108) can be identified with the Fourier transform of an integral equation:

$$\partial_\theta \tilde{\Phi}(\theta) = \partial_\theta \Phi(\theta) + \frac{1}{2\pi} \int_{-\infty}^{+\infty} d\theta' \partial_\theta \Phi(\theta - \theta') \partial_{\theta'} \tilde{\Phi}(\theta') \quad (6.110)$$

The equation can now be integrated in θ , so that we get the *dressing equation*:

$$\tilde{\Phi}(\theta) = \Phi(\theta) + \frac{1}{2\pi} \int_{-\infty}^{+\infty} d\theta' \partial_{\theta} \Phi(\theta - \theta') \tilde{\Phi}(\theta') \quad (6.111)$$

Equation (6.111) is the *dressing equation* for the two particle scattering phase shift [30, 28]. It basically relates how excitations over the physical vacuum (which now are the *physical particles*, carrying phase shift $\tilde{\Phi}$) relate to the original *pseudoparticle* picture. Being the pseudovacuum not bounded from below, i.e, containing an infinite number of states, it is necessary to construct a proper physical vacuum for the theory. For details on this, see appendix A as well as [28, 30] on the Massive Thirring Model.

6.3 Lattice solution

In this section, we try a different approach to the two body problem in the IRLM developed by Filyov and Wiegmann [56]. In particular, we describe the solution of the model *in the lattice*, in order to see is we can get a different value for τ in 6.103 that includes the g^2 term. The solution of the model in the lattice introduces a natural regularization, where now there is a minimum distance (lattice spacing) between sites, as opposed to the field theoretic description we have discussed earlier. In this section, we recover Filyov and Wiegmann's solution for the two-body scattering phase-shift with the correct parameter to first order in g .

6.3.1 One particle states

We consider the IRLM hamiltonian defined in the lattice:

$$H = -t \sum_{i=0}^{N-2} c_{i+1}^{\dagger} c_i - t \sum_{i=0}^{N-2} c_i^{\dagger} c_{i+1} - \varepsilon_0 d^{\dagger} d + t'(c_0^{\dagger} d + \text{h.c}) + U(c_0^{\dagger} c_0 - 1/2)(d^{\dagger} d - 1/2) \quad (6.112)$$

We wont go into details of the calculation of such states here, since they can be found in the appendix. The single particle states are given by:

$$\hat{H}|\Psi\rangle_1 = E_1|\Psi\rangle_1 \quad |\Psi\rangle_1 = c_0^{\dagger}|0\rangle + \zeta_d d^{\dagger}|0\rangle \quad (6.113)$$

We find for the single particle states in the lattice:

$$\begin{aligned} \phi_d &= \frac{t'\sqrt{2}}{E_1 + \varepsilon_0 + U\rho} \cos(\Delta_U/2) e^{i\Delta_U/2} \\ \phi_n &= \cos(kn + \Delta_U/2) e^{i\Delta_U/2} \\ \Delta_U &= 2 \arctan \left(-\frac{\Gamma_0}{2(E_1 + \varepsilon_0 + U\rho)} + \frac{U\pi\nu}{4} + \frac{E_1\pi\nu}{4} \right) \end{aligned} \quad (6.114)$$

where we have defined $\Gamma_0 = \pi\nu(t')^2$ and $\nu = 2(\pi t \sin(k))^{-1}$. Notice the difference between the term we previously calculated in (6.24). As a consequence of the lattice, the eigenvalue E_1 enters the argument of the single-particle phase-shift.

6.3.2 Two particle states

Having calculated the single particle states, we now look at the two-body problem. One needs to be careful here. By direct action of the hamiltonian over the two particle state:

$$\hat{H}|\Psi\rangle_2 = (E_1 + E_2)|\Psi\rangle_2 \quad (6.115)$$

we find the following equations (see appendix for details):

$$\begin{aligned} (E + \varepsilon_0 + U\rho - (U/2)\delta_{j,0})\zeta^{d,j} &= -t(\zeta^{d,j+1} + \zeta^{d,j-1}\bar{\delta}_{j,0}) + 2t'\delta_{k,0}\phi^{k,j} \\ (E + U\delta_{k,0})\phi^{k,j} &= (t'/2)\left(\delta_{k,0}\bar{\delta}_{j,0}\zeta^{d,j} - \delta_{j,0}\bar{\delta}_{k,0}\zeta^{d,k}\right) - t(\phi^{k+1,j} + \phi^{k-1,j}\bar{\delta}_{k,0}) \\ &\quad - t(\phi^{k,j+1} + \phi^{k,j-1}\bar{\delta}_{j,0}) \end{aligned}$$

where $\delta_{i,j} + \bar{\delta}_{i,j} = 1$. We look for solutions of ϕ and ζ in the form:

$$\begin{aligned} \zeta^{d,j} &= \phi_d(\varepsilon_1)\phi_j(\varepsilon_2)f(-j) - \phi_j(\varepsilon_1)\phi_d(\varepsilon_2)f(j) \\ 2\phi^{k,j} &= \phi_k(\varepsilon_1)\phi_j(\varepsilon_2)f(k-j) - \phi_k(\varepsilon_2)\phi_j(\varepsilon_1)f(j-k) \end{aligned} \quad (6.116)$$

The function $f(k-j)$ is a phase factor due to the scattering of the two particles, so:

$$f(k-j) = e^{i\Phi \text{sign}(k-j)} \quad (6.117)$$

By taking into account that the single-particle states must also satisfy the single particle equations (see appendix). If one performs the calculation, one arrives at the equation:

$$e^{i\Phi} \left(E_2 - \frac{(t')^2}{U} \right) = e^{-i\Phi} \left(E_1 - \frac{(t')^2}{U} \right) \quad (6.118)$$

which clearly requires $E_1 = E_2$, which is not allowed due to Pauli's exclusion principle. We have then to propose a different ansatz for the two particle states, in other words, modify the solutions of the form (6.116) in order to get the correspondent phase-shift between two scattering particles. This requires to take a bit of care about the *right* or *left* moving nature of our particles in the lattice. We should remember that such a lattice description does not transform left movers in $x < 0$ to be right movers in $x > 0$. We take a look at this in the next subsection.

6.3.3 The unfolded picture in the lattice

At this point, it is useful to consider all single-particle results obtained in the lattice version of the IRLM:

$$\begin{aligned}\phi_d &= \frac{\sqrt{2}t'}{E_1} \cos(\Delta_U(E_1)/2) & \Delta_U(E_1) &= -2 \arctan\left(\frac{\Gamma_0}{2E_1} - \frac{U\pi\nu}{4} - \frac{\varepsilon_1\pi\nu}{4}\right) \\ \phi_n &= \frac{1}{\sqrt{2}} \left(A e^{ikn} + B e^{-ikn} \right) & A &= e^{i\Delta_U/2} = B^{-1}\end{aligned}\quad (6.119)$$

as well as the single particle equations (6.114) and the two particle equations (6.116) (see appendix for these equations). In order to develop a valid solution of the two body problem in the lattice, scattering between right and left movers needs to be considered. Thus a new ansatz for the two-body wavefunctions is needed. The function carrying the scattering phase shift between particles will be of the form:

$$f(k - m) = e^{i\Phi \text{sign}(k-m)} \quad (6.120)$$

If we now imagine two right movers scattering from each other, then the two body wavefunction is:

$$A_1 A_2 e^{ik_1 n} e^{ik_2 m} f(n - m) \rightarrow A_1 A_2 e^{ik_1 n} e^{ik_2 m} e^{i\Phi \text{sign}(n-m)} \quad (6.121)$$

On the other hand, a left mover scattering from a right mover contains:

$$A_1 B_1 e^{ik_1 n} e^{-ik_2 m} f(n - (-m)) \rightarrow A_1 B_1 e^{ik_1 n} e^{-ik_2 m} e^{i\Phi} \quad (6.122)$$

where we have necessarily $\text{sign}(n + m) > 0$, since all coordinates on the lattice are to the right of the dot, therefore $n, m > 0$ always. Thus, the single particle states are now decomposed into right and left movers:

$$\phi_n(k) = \phi_n^R(k) + \phi_n^L(k) \quad (6.123)$$

The two-body ansatz for both the impurity filled or empty are then:

$$\begin{aligned}\zeta^{d,m} &= e^{i\Phi} \left(\phi^d(\varepsilon_1) \phi_m^L(\varepsilon_2) - \phi^d(\varepsilon_2) \phi_m^R(\varepsilon_1) \right) \\ &+ e^{-i\Phi} \left(\phi^d(\varepsilon_1) \phi_m^R(\varepsilon_2) - \phi^d(\varepsilon_2) \phi_m^L(\varepsilon_1) \right) \\ 2\phi^{n,m} &= e^{i\Phi} \left(\phi_n^R(\varepsilon_1) \phi_m^L(\varepsilon_2) - \phi_n^L(\varepsilon_2) \phi_m^R(\varepsilon_1) \right) \\ &+ e^{-i\Phi} \left(\phi_n^L(\varepsilon_1) \phi_m^R(\varepsilon_2) - \phi_n^R(\varepsilon_2) \phi_m^L(\varepsilon_1) \right) \\ &+ e^{i\Phi\epsilon} \left(\phi_n^R(\varepsilon_1) \phi_m^R(\varepsilon_2) - \phi_n^L(\varepsilon_2) \phi_m^L(\varepsilon_1) \right) \\ &+ e^{-i\Phi\epsilon} \left(\phi_n^L(\varepsilon_1) \phi_m^L(\varepsilon_2) - \phi_n^R(\varepsilon_2) \phi_m^R(\varepsilon_1) \right)\end{aligned}\quad (6.124)$$

The important quantity to calculate here is, as always, the two particle scattering phase shift Φ . We refer the reader to the appendix for a detailed calculation. By applying the above ansatz into the two body equations (6.116), we obtain:

$$\tan(\Phi) = \tan(\pi g) \frac{\varepsilon_2 - \varepsilon_1}{\varepsilon_2 + \varepsilon_1 + 2(\varepsilon_0 + U\rho)} \quad (6.125)$$

which in the rapidities representation (and making $\varepsilon_i \rightarrow \varepsilon_i + \varepsilon_0 + U\rho$) is:

$$\boxed{\Phi = -2 \arctan \left(\tan(\pi g) \tanh(\beta/2) \right)} \quad (6.126)$$

Now, by looking at equation (6.104), we see that the above method fails to reproduce the g^2 term, but reproduces the first order value of the τ parameter, the one related to both the Sine Gordon theory (β) and the Massive Thirring Model (ξ). Our attempt to recover the correct S matrix has failed once again, we believe, due to missing physics when calculating the scattering process. At the moment, this is work in progress.

6.4 Multichannel IRLM

To conclude, we look briefly at the single particle description of the multichannel IRLM. Previously, we have attempted to solve the problem of the IRLM in the single channel version by Bethe ansatz. The generalization of such a solution to an N channel IRLM has been developed by Ponomarenko [40]. However, his solution by Bethe ansatz also lacks the factor proportional to g^2 in the charge susceptibility. This is in fact a very important factor, since now the thermodynamic exponent α depends on the total number of channels N attached to the impurity:

$$\alpha = \frac{2}{1 + 2g - Ng^2} \quad (6.127)$$

To see the origin of such a term in the two-body equations, one starts to solve the generalized N channel problem.

The IRLM is written on its multichannel form in the fields components:

$$\begin{aligned} H = & -i \sum_{\alpha} \int_{-\infty}^{+\infty} dx \psi_{\alpha}^{\dagger}(x) \partial_x \psi_{\alpha}(x) - \varepsilon_0 d^{\dagger} d + t' \sum_{\alpha} \int dx \delta(x) \psi_{\alpha}^{\dagger}(x) d + \text{h.c} \\ & + U \sum_{\alpha} \int dx \delta(x) (d^{\dagger} d - 1/2) (\psi_{\alpha}^{\dagger}(x) \psi_{\alpha}(x) - \rho) \end{aligned}$$

Here α represents each channel attached to the impurity site. A rotation of the fields allows one to write the hamiltonian in terms of new fermionic operators:

$$c_i(x) (i \neq 1) \quad \chi(x) = \sum_{\alpha} \psi_{\alpha}(x) \quad (6.128)$$

Then there is only one "channel" hybridizing with the impurity site:

$$\begin{aligned}
& - i \sum_{i=2}^N \int dx c_i^\dagger(x) \partial_x c_i(x) - i \int dx \chi^\dagger(x) \partial_x \chi(x) - \varepsilon_0 d^\dagger d + t' \int dx \delta(x) \chi^\dagger(x) d + \text{h.c} \\
& + U \sum_{i=2}^N \int dx \delta(x) (d^\dagger d - 1/2) (c_i^\dagger(x) c_i(x) - \rho) \\
& + U \int dx \delta(x) (d^\dagger d - 1/2) (\chi^\dagger(x) \chi(x) - \rho)
\end{aligned} \tag{6.129}$$

We are here assuming the average values of the boundary operators to be all equal to ρ . The problem is then reduced to a single lead IRLM and $N - 1$ non-hybridizing leads interacting with the channel. We will rather choose to work with the unrotated version of the model, as opposed to Ponomarenko. The single particle state is a linear combination of all possibilities for the particle to be either in one of the leads or the dot:

$$|\Psi\rangle = \int dx \phi_\alpha(x) |x\rangle + \zeta_d |1\rangle \tag{6.130}$$

The hamiltonian acting over the state has several contributions. First, the non-interacting and dot parts:

$$(H_d + H_0) |\Psi\rangle = -\varepsilon_0 \zeta_d |1\rangle - i \sum_\alpha \int dx \partial_x \phi_\alpha(x) |x, \alpha\rangle \tag{6.131}$$

The hybridization part reads:

$$H_{t'} |\Psi\rangle = t' \sum_\alpha \int dx \delta(x) \zeta_d |x, \alpha\rangle + t' \sum_\alpha \int dx \delta(x) \phi_\alpha(x) |1\rangle \tag{6.132}$$

Finally the interacting part of the hamiltonian is:

$$H_U |\Psi\rangle = -\frac{U}{2} \sum_\alpha \int dx \delta(x) \phi_\alpha(x) |x, \alpha\rangle - \sum_\alpha U \rho \zeta_d |1\rangle \tag{6.133}$$

Therefore there are $N + 1$ single particle equations, reading:

$$\begin{aligned}
-i \partial_x \phi_\alpha(x) + t' \delta(x) \zeta_d - \frac{U}{2} \delta(x) \phi_\alpha(x) &= \varepsilon_1 \phi_\alpha(x) \\
\zeta_d (\varepsilon_1 + \varepsilon_0 + NU\rho) &= t' \delta(x) \sum_\alpha \phi_\alpha(x)
\end{aligned} \tag{6.134}$$

It is easy to see that these equations can be reduced to a set of two coupled equations in the rotated field $\chi(x)$, determining the scattering phase shift in this case. The problem is then equivalent to a single channel hybridizing with the impurity and $N - 1$ "free" channels. In other words, we use the hamiltonian above and whose states are:

$$\bar{\phi}_\alpha(x) = C e^{i\varepsilon_1 x + i\delta_\alpha \text{sign}(x)} \quad \Omega(x) = C e^{i\varepsilon_1 x + i\Delta \text{sign}(x)} \tag{6.135}$$

where the phase shifts are:

$$\delta_\alpha = \arctan\left(\frac{U}{4}\right) \quad \Delta = \arctan\left(\frac{U}{4} - \frac{Nt^2}{2E_1}\right) \quad (6.136)$$

where the equation determining Δ is:

$$-i\partial_x\Omega(x) + \left(\frac{Nt^2}{E_1} - \frac{U}{2}\right)\delta(x)\Omega(x) = \varepsilon_1\Omega(x) \quad (6.137)$$

Note the inclusion of the N factor with t' . This equation is then similar in appearance to the one obtained for the single channel version equation (6.22). In this sense, and because we work in the limit $t' \rightarrow 0$, we observe no difference between this N channel version of the model and the single channel one. The extension of the method to the two particle equations is something we are working on at the moment.

6.5 Summary of main results

In this chapter, we have presented the problems one faces with when applying the Bethe ansatz to the IRLM. Our main problem is to find the thermodynamic exponent to be equivalent to the one obtained by Bosonization and RG. It has been shown that both calculations in [56, 40] do not reproduce this exponent correctly.

One of the main points we have illustrated here is the connection of the IRLM (a quantum impurity model) with other integrable field theories: the Massive Thirring Model (MTM) and the Sine Gordon Model (SGM). In particular, relationships between parameters of the models have been established, leading us to conjecture the exact form for the two-particle scattering processes in the IRLM. We have shown the S matrix of solitons in the SGM (fermions in the MTM) to be in relation with the one in the IRLM, by means of a dressing equation of the two-particle phase shifts. It is quite remarkable that such *bulk* field theories like the MTM and the SGM find similarities with a quantum impurity model by direct relations between their microscopic parameters.

Finally, when going to a lattice description of the model, we introduce a natural regularization in the problem. By solving the two body problem in the lattice, we have reproduced the first order term that matches both the MTM and the SGM to the IRLM. The calculation of the g^2 term in such relations still remains outstanding. At the moment, we are working on these issues.

Chapter 7

Conclusions and outlook

“Real knowledge is to know the extent of one’s ignorance”

Confucius

In this work, we have studied the IRLM in thermodynamic equilibrium from a fundamental point of view, in order to get a full consistent theory of both its thermodynamic and dynamic properties at low temperatures/energies. The IRLM, being a strongly correlated impurity model, presents himself as a perfect theoretical laboratory to understand such systems. Its apparent simplicity leads, however, to an understimation of its range of applicability. In particular, its direct relation to the Kondo model, which has been established in the last years as a well understood model, can bring the idea that there are few things to say about it. This thesis has precisely illustrated that this proves not to be the case in the IRLM. Although numerous important works have been developed in the model (see the cited literature), important flaws in the theory have been fixed.

To begin with, the fact that analytical approaches to the model by perturbative RG don’t match with numerics [38] at strong values of interactions comes from a wrong interpretation of the relevant energy scale in the problem, and the lack of a prefactor that depends on interaction in a non-trivial way (the exact solution). Such a prefactor is proved here to correspond to an integrable bosonic field theory with a boundary term (the Boundary Sine Gordon Model). Secondly, in previous works [37, 38], this energy scale Γ (without the prefactor taken into account) has been associated with the impurity density of states, which is a dynamical quantity. One of the main points illustrated in this work is the sensitive distinction we must take into account when computing dynamical quantities as opposed to thermodynamic ones.

Regardless of which quantity we look at, it is the *scattering phase shift* δ of the associated central scattering problem the parameter dominating all the RG treatment, and thus all low-energy properties of the model. The RG treatment can be equally well performed by considering the IRLM as a continuous field theory with a boundary (the Boundary Sine Gordon Model (BSGM)). By making this identifica-

tion, we have proved the *exact* expression of the relevant energy scale in the BSGM to correspond to the relevant energy scale in the IRLM. Furthermore, NRG simulations have supported this idea with a very good agreement. The fact that one can reproduce field theoretic results from a lattice model with microscopic parameters is one of the central results in this thesis. One immediate consequence of this is that, at least in the single channel IRLM, both the lattice and the field theory versions of the model are equivalent to describe its low-energy properties, without taking into account any regularization scheme in the continuum. This result also connects with the exact solution of the model by Bethe ansatz, which has been believed to be dependent on different regularizations of the fields. We consider this analogy between the lattice and the field description to be an important argument in favour of our fixed cut-off theory, as opposed to regularization schemes that have been proposed in the two channel version of the model in order to match different limits [51]. To further support our arguments, a treatment in the strong coupling limit of the model has been performed in the lattice. As it has been shown, the relevant energy scale in this limit matches the analytical formula developed by integrability of the BSGM.

In general terms, thermodynamics of the multichannel IRLM have also been considered. Generalization to the multichannel case has already been discussed previously [38] presenting similar mismatches between theory and performed numerics. In analogy with the single channel version, our first approach is the calculation of the so called *thermodynamic exponent* by bosonization. This result, despite being reported in [38, 39, 50], it is not mentioned to be *exact*. The important part about this calculation shows that the N th channel generalisation introduces the total number of channels in the model N coupled to the interaction constant *in second order*. In other words, to observe differences between thermodynamics of the single channel IRLM and the multichannel version, one needs to go to second order in g . With regards to the mentioned mismatches between theory and the performed numerics [38, 52], our approach elucidates why such mismatches occur: In accordance with results from the one channel IRLM, we believe these mismatches to correspond to the lack of an exact expression for the prefactor in the relevant energy scale formula. Such prefactor has a non-trivial dependence on the interaction parameter g . This implies important changes in the computation of relevant physical properties. For instance, in the two channel version of the model, a *duality* in the thermodynamic exponent occurs. It has been said that such duality has to be preserved in the relevant energy scale of the problem [51] by introducing the appropriate cut-off regularization when going to the continuum. Performed numerics [53] have shown this not to be the case in the IRLM, suggesting the duality is broken in the strong coupling limit: Instead of recovering the non-interacting value Γ_0 for the energy scale, this one goes to a zero value, therefore implying infinite correlation length in this limit. We believe this effect, which is recovered in the strong coupling limit in the lattice, to be a real one, and not dependent on regularizations. In other words, the cut-off of the theory is fixed and does not depend on g . In this thesis, we support this idea from our treatment of the single channel version of the model, and its full capacity to reproduce results in the continuum from the lattice viewpoint. We therefore conclude that the duality is *broken* in the two lead case when going to

the strong coupling limit, and that such effect has to do with the (at the moment unknown) *exact* form of the prefactor in Γ for more than one channel. Extrapolation of exact results for the single channel IRLM to two or more leads has not been performed and would be desirable.

The separation between thermodynamic properties of the model and its dynamics (i.e. the impurity spectral function) is central in this thesis. Our results agree with previous publications [37, 38, 39, 55] in the *weak coupling* limit of the theory. Results of [38] suggested that even for small values of interaction, analytical expressions for the *dynamic* width Γ_d deviate from numerics. In this work, several important results need to be mentioned. In the weak coupling limit, the impurity spectral function is a Lorentzian, as perturbation theory shows. As soon as one goes to order g^2 , this Lorentzian shape starts to disappear. The central peak in the spectral function broadens with interaction, but at sufficiently large values of g , it develops a splitting in the central region. Such splitting has been reported for the Anisotropic Kondo Model (AKM) [95], which we know is in direct relation with the IRLM [36]. In order to define some sort of *dynamical hybridization*, one focuses in the $\omega = 0$ sector of the spectral function. It turns out that the scaling of the hybridization parameter t' with interaction g is different than the one present in the thermodynamic energy scale Γ . Despite being both exponents different, NRG simulations suggest a relation between both. The most important result on this is that the spectral function shows an *universal* curve at fixed g when scaled with this exponent. On the other hand, in such universal curves, the excitation energies of the system ω prove to scale with the thermodynamic width Γ . The origin of these two different low-energy scalings in the dynamical quantities of the model is at the moment unknown to us, and further work on this is required on the analytical side. In spite of this, we can conclude that dynamical quantities in the model behave in a different way as thermodynamic ones. Whether this is due to the appearance of a *second energy scale* in the model or not, is some that requires further investigation.

Integrability of the IRLM and its exact solution by Bethe ansatz has also been presented. In particular, it has been shown that results of [56] do not reproduce the well known thermodynamic exponent α correctly. The fact that one cannot reproduce the g^2 term in the exponent seems worrying, since it is precisely this term the one that differentiates the single channel IRLM from the multichannel case. Without it, one cannot benefit from the extension of the method to more leads [40]. One of the arguments could be that in order to reproduce such term, one needs to regularize the theory correctly. Once again, we have to disagree on this, supported by our previous arguments on the equivalence between the field and the lattice description at low-energies. We have precisely shown that, even when going to the *lattice* version, solving the two-body problem does not reproduce such term. On the other hand, a direct correspondence between the S matrix of solitons of the Sine Gordon Model and that of the IRLM has been established, by following works of [28, 35]. The search for such g^2 is of primarily importance in the model. The fact that one does not reproduce the well known result has to do with the complexity of the method as compared to the bosonization approach. Our view on this is that

either some fundamental physics are missing in the description of the problem or some technical steps have not been performed in the correct way. We will be working on these issues in the near future.

To conclude, we want to remark the importance of the IRLM in the groundbreaking study of non-equilibrium phenomena in such strongly correlated impurity systems [44]. The approach developed in [44] relies on integrability of the model, in order to extrapolate the Bethe ansatz method to the non-equilibrium case. However, the solution of the two channel version of the model in non-equilibrium (that is, allowing transport) has only been satisfactory compared to numerics at a single value of interaction [45, 48], therefore the development of a whole theory for any other value of interaction is desirable. As we have already seen in this thesis, application of Bethe ansatz even in equilibrium presents a challenging task; we give full credit to [40, 56] in this aspect, understanding that such solutions need modification in accordance with our results exposed here. We believe the study of equilibrium properties of the model to be relevant, concretely in the description of the long time (steady state) limit of such non-equilibrium situation. In this sense, the full understanding of such equilibrium properties of the model presents a problem as fundamental as its non-equilibrium variant.

Appendix A

Ground state of the Massive Thirring Model by Bethe ansatz

In the MTM, the hamiltonian is not bounded below, and therefore accounts for an infinite number of states. Such a picture is deceptive, and one then needs to fill the vacuum of the theory in the correct way. This is the approach followed by Korepin [28, 30] and we expose it here in detail.

The vacuum state of the massive Thirring model consists on filling all negative energies levels. The total energy of this state is:

$$E = -m_0 \sum_k \cosh(\alpha_k) \quad (\text{A.1})$$

where $|\alpha_k| < \Lambda$. Here, all rapidities α then have zero imaginary part, but the physical rapidities β lie along the line $i\pi$ in the complex plane. The distribution of rapidities is given by the above integral equation. For the vacuum of the theory, this equation is solved in the asymptotic limit $\Lambda \rightarrow \infty$. This procedure is also found in Bernoff and Thacker.

Now, consider adding a pseudoparticle with positive energy, which implies we add α_p with $\text{Im}(\alpha_p) = 0$. Then a new term appears in the scattering, as a scattering of one negative energyparticle with a positive energy one. The equation is then:

$$m_0 L \sinh(\alpha_i^*) = 2\pi n_i + \sum_{k \neq i} \Phi(\alpha_i^* - \alpha_k^*) + \Phi(\alpha_i^* - \alpha_p + i\pi) \quad (\text{A.2})$$

The associated wavefunction has energy:

$$E_{v+p} = -m_0 \sum_k \cosh(\alpha_k^*) + m_0 \cosh(\alpha_p) \quad (\text{A.3})$$

The following functions are conveniently introduced:

$$W_p(\alpha_i) = L(\alpha_i - \alpha_i^*) \quad F_p(\alpha_i) = W(\alpha_i)\rho(\alpha_i) = \frac{\alpha_i - \alpha_i^*}{\alpha_{i+1} - \alpha_i} = f_p(\alpha - \alpha_p) \quad (\text{A.4})$$

These are called the *shift functions*. Now, we subtract this Bethe equation from the vacuum one, and take the thermodynamic limit. Then we have:

$$m_0 L \left(\sinh(\alpha_i^*) - \sinh(\alpha_i) \right) \frac{(\alpha_i - \alpha_i^*)}{(\alpha_i - \alpha_i^*)} = \sum_k \Phi(\alpha_i - \alpha_k) - \Phi(\alpha_i^* - \alpha_k) - \Phi(\alpha_i^* - \alpha_p + i\pi) \quad (\text{A.5})$$

Taking the $L \rightarrow \infty$ limit this is:

$$m_0 \cosh(\alpha) = -(W(\alpha))^{-1} \Phi(\alpha - \alpha_p + i\pi) \quad (\text{A.6})$$

where the second term of the right hand side has been neglected in this limit, being of order $1/L$. Then using the equation for the the vacuum:

$$0 = \Phi(\alpha - \alpha_p + i\pi) + \int_{-\Lambda}^{+\Lambda} d\beta F_p(\beta) \Phi'(\alpha - \beta) + 2\pi F_p(\alpha) \quad (\text{A.7})$$

As we can see, this is a *dressing* equation for the shift function $F_p(\beta)$. Its derivative is of importance, since it allows to solve the equation by Fourier transformation:

$$0 = \Phi'(\alpha - \alpha_p + i\pi) + \int_{-\infty}^{+\infty} d\beta F_p'(\beta) \Phi'(\alpha - \beta) + 2\pi F_p'(\alpha) \quad (\text{A.8})$$

Introducing a positive energy particle in the system *pushes* some of the particles further than $\pm\Lambda$. There is then a change in the number of particles beyond the cut-off, given by the following formulas:

$$\Delta N(\Lambda) = -F_p(\Lambda) \quad \Delta N(-\Lambda) = F_p(-\Lambda) \quad (\text{A.9})$$

Then, the "true" vacuum energy due to this is:

$$E_V \rightarrow E_V - \Delta N(\Lambda)(-m_0 \cosh(\Lambda)) - \Delta N(-\Lambda)(-m_0 \cosh(\Lambda)) \quad (\text{A.10})$$

The excitation energy (of the included pseudoparticle) can then be calculated as a difference:

$$\varepsilon_p = E_{v+p} - E_v = m_0 \left(\sum_k -\cosh(\alpha_k^*) + \cosh(\alpha_k) + \cosh(\alpha_p) \right) - m_0 \cosh(\Lambda) \left(F_p(\Lambda) - F_p(-\Lambda) \right) \quad (\text{A.11})$$

This describes an excitation in the zero charge sector, where one particle has been removed from the vacuum and promoted above the highest energy level, leaving a hole behind. We can express the hyperbolic sines terms in the following way:

$$\frac{\cosh(\alpha_k) - \cosh(\alpha_k^*)}{\alpha_k - \alpha_k^*} (\alpha_k - \alpha_k^*) = \sinh(\alpha_k) (\alpha_k - \alpha_k^*) \quad (\text{A.12})$$

Then the equation is:

$$\begin{aligned}\varepsilon_p &= m_0 \cosh(\alpha_p) + m_0 \left(\int_{-\Lambda}^{+\Lambda} d\alpha \sinh(\alpha) F_p(\alpha) - \cosh(\alpha) F_p(\alpha) \Big|_{-\Lambda}^{+\Lambda} \right) \\ &= m_0 \cosh(\alpha_p) - m_0 \int_{-\Lambda}^{\Lambda} d\alpha \cosh(\alpha) F_p'(\alpha)\end{aligned}\quad (\text{A.13})$$

where the last step is the definition of integral by parts. Thing is, to know the function $F_p'(\alpha)$. This function can be calculated from eq. (4.15) by taking the derivative of the expression. Then the integral can be solved by Fourier transformation. In order for this to be finite, a renormalization of the bare mass m_0 as a function of the cut-off follows. Solved by Fourier method, the function F_p is calculated in Korepin's paper [28]:

$$\lim_{\alpha \rightarrow \infty} F_p'(\alpha) \rightarrow \frac{-1}{\pi + \xi} \sin\left(\frac{\pi\xi}{\pi + \xi}\right) \cosh\left(\frac{\pi}{(\pi + \xi)}(\alpha - \alpha_p)\right)^{-1}\quad (\text{A.14})$$

which is the asymptotic behaviour of the function. As $\Lambda \rightarrow \infty$ the integral on the right of ε_p diverge. Then, the mass is changed with a cut-off dependence of the form:

$$m_0 = a e^{-\frac{\xi\Lambda}{\pi+\xi}}\quad (\text{A.15})$$

with a being a constant. Using that choice of m_0 , the equation for the rapidities distribution $\rho(\alpha)$ is:

$$\begin{aligned}a e^{-\frac{\xi\Lambda}{\pi+\xi}} \cosh(\alpha) &= 2\pi\rho(\alpha) \\ - \int_{-\Lambda}^{+\Lambda} \rho(\beta) \frac{\sin(g)}{2 \cosh((\alpha - \beta + ig)/2) \cosh((\alpha - \beta - ig)/2)} d\beta\end{aligned}\quad (\text{A.16})$$

Lets take a closer look at the kernel of the expression:

$$K(z) = \frac{\sin(g)}{2 \cosh((z + ig)/2) \cosh((z - ig)/2)}\quad (\text{A.17})$$

Using the relations between sums of hyperbolic cosines, we get:

$$K(z) = \tan(g/2) \frac{1}{1 + (\sinh(z)/\cos(g/2))^2}\quad (\text{A.18})$$

so the equation to solve is:

$$\begin{aligned}a e^{-\frac{\xi\Lambda}{\pi+\xi}} \cosh(\alpha) &= 2\pi\rho(\alpha) \\ - \tan(g/2) \int_{-\Lambda}^{+\Lambda} \frac{\rho(\beta)}{1 + (\sinh((\alpha - \beta)/2)/\cos(g/2))^2} d\beta\end{aligned}\quad (\text{A.19})$$

The formal solution of this equation can be found in [30]. It admits a general form for every kernel and momentum distribution. For this model, it is given as:

$$\begin{aligned}\rho(\alpha) &= \frac{1}{2\pi} \int_{-\Lambda}^{\Lambda} d\beta \left(\frac{(1 + (\sinh((\alpha - \beta)/2)/\cos(g/2))^2 - (\tan(g/2)/2\pi))^{-1}}{(1 + (\sinh((\alpha - \beta)/2)/\cos(g/2))^2)} \right)^{-1} \\ &\quad \times a e^{-\frac{g\Lambda}{\pi+g}} \cosh(\beta)\end{aligned}\quad (\text{A.20})$$

The above equation is solved [30] with the following asymptotic behaviour:

$$\rho(\alpha) = \frac{ag}{2(\pi + g) \sin(g)} \cosh\left(\frac{\pi\alpha}{\pi + g}\right) \quad (\text{A.21})$$

The expression for the massless Thirring model comes from taking the limit:

$$\lim_{a \rightarrow 0, \theta_0 \rightarrow +\infty} ae^{\theta_0} = b \quad (\text{A.22})$$

being finite. Then the expression is:

$$\rho(\alpha)_{m=0} = \frac{gb}{4(\pi + g) \sin(g)} e^{-\frac{\pi}{\pi+g}\alpha} \quad (\text{A.23})$$

This is the distribution for the rapidities, where now the *physical rapidities* represent the renormalized values after filling the vacuum:

$$\theta = \frac{\alpha}{1 + g/\pi} \quad (\text{A.24})$$

Thus, the inclusion of a particle-hole excitation carries an adjustment in the physical vacuum of the theory. As a consequence, the rapidities are renormalized. Note that such a renormalization in the Massive Thirring Model has been carried for the limit of $m_0 \rightarrow 0$, i.e, the massless limit, which we know is in relation with the Interacting Resonant Level Model.

Appendix B

Bosonization in the IRLM

Consider the non-interacting term H_0 of the IRLM. We know that, once we linearize the spectrum, the hamiltonian for non-interacting fermions is a Dirac hamiltonian, just changing c by v_F :

$$H_0 = -iv_F \int_{-\infty}^0 dx (\psi^\dagger(x) \partial_x \psi(x) - \bar{\psi}^\dagger(x) \partial_x \bar{\psi}) \quad (\text{B.1})$$

Reading the expression above, the non-interacting hamiltonian for conduction electrons is divided into right and left movers. The integral just runs from $-\infty$ to 0 since the lead is semi-infinite.

In that particular model, there is a boundary condition for the conduction electrons:

$$\psi^\dagger(0) = \bar{\psi}^\dagger(0) \quad (\text{B.2})$$

wich permit us to unfold the fields. Consider a right moving fermion along the wire (negative x direction). When the fermion reaches the boundary, it scatters and moves towards left. However, we can consider instead to extend the space to $+\infty$, where the fermion would keep going as a right moving one. We can then make the following association:

$$\bar{\psi}^\dagger(x < 0) = \psi^\dagger(x > 0) \quad (\text{B.3})$$

Therefore, we can write our conduction fermions simply as right movers, thus one single fermionic operator is needed.

$$H_0 = -iv_F \int_{-\infty}^{+\infty} dx \psi^\dagger(x) \partial_x \psi(x) \quad (\text{B.4})$$

We know how to transform that into a bosonized form, by simply considering free bosons (right moving):

$$H_0 = \frac{v_F}{2} \int_{-\infty}^{+\infty} dx (\partial_x \phi(x))^2 \quad (\text{B.5})$$

so that $\phi(x)$ is a chiral bosonic field. We take a look at the hopping term of the hamiltonian:

$$H_{J'} = J'(d^\dagger \psi_0 + h.c) \quad (\text{B.6})$$

We will transform the impurity operators into spin operators as we did before, and the fields. However, we will use a more generic prefactor for the operators in order to commute, which are not relevant since they are not dynamical. They are only included to preserve the anticommutation relations.

$$\begin{aligned} d &= \eta S^- & d^\dagger &= \eta S^+ \\ (d^\dagger d - \frac{1}{2}) &= S^z & \psi(x) &= \frac{\eta}{\sqrt{2\pi}} e^{i\sqrt{4\pi}\phi(x)} \end{aligned} \quad (\text{B.7})$$

Taking that transformations into account, the IRLM hamiltonian transforms into its bosonized form:

$$H = \frac{1}{2} \int_{-\infty}^{+\infty} dx (\partial_x \phi)^2 + \frac{J'}{\sqrt{2\pi}} \left(\eta \eta S^+ e^{i\sqrt{4\pi}\phi(0)} + h.c \right) + \frac{U}{\sqrt{\pi}} S^z \partial_x \phi(0) \quad (\text{B.8})$$

Consider now the case where $J' = 0$. In that specific situation, the hamiltonian H is reduced to a scattering problem for the field ϕ (a free boson propagating freely, reaching a boundary at $x = 0$), therefore the scattering phase shift δ can be calculated, resulting to be:

$$2\delta = \arctan\left(\frac{U}{2}\right) \quad (\text{B.9})$$

We should notice that the expression above is in units of $v_F = 1$, otherwise is senseless. In the low coupling, that is, for values of U sufficiently small, the scattering phase shift can replace the interaction U , so we identify:

$$U = 2\delta \quad (\text{B.10})$$

The common trick used in impurity problems (see Gogolin et al.¹) is to make use of a unitary transformation acting on the hamiltonian. Such a unitary transformation is chosen *arbitrarily*, and dependent of a parameter α to be determined. In fact, this transformation has to depend on the operators involved in H :

$$U = e^{i\sqrt{4\pi}\alpha S^z \phi(0)} \quad (\text{B.11})$$

As we can see, U depends only on S^z and the fields $\phi(x)$. It does not depend on S^+ and S^- explicitly, but we know both are related to S^z by usual commutation relations.

We will proceed now to see how this transformation acts on every single term of H , we want:

$$H_T = U^\dagger H U \quad (\text{B.12})$$

¹Gogolin, Tsvetlik, Nersesyan. "*Bosonization and strongly correlated systems*"

We start by acting over the term with the scattering phase. Directly:

$$U^\dagger \left(\frac{2\delta}{\sqrt{\pi}} S^z \partial_x \phi(0) \right) U \quad (\text{B.13})$$

We now make use of the Baker-Hausdorff formula:

$$e^{i\lambda\hat{G}} \hat{O} e^{i\lambda\hat{G}} = \hat{O} + i\lambda[\hat{G}, \hat{O}] + \frac{(i\lambda)^2}{2!} [\hat{G}, [\hat{G}, \hat{O}]] + \dots \quad (\text{B.14})$$

We see clearly that the operator U commutes with S^z following (1.26). However, we must be careful about the commutator for bosonic operators. Since for different sites, there exists a non-locality, the following commutation relation holds:

$$[\partial_x \phi(x), \phi(y)] = -\frac{i}{2} \delta(x - y) \quad (\text{B.15})$$

Therefore, we can easily compute the terms:

$$U^\dagger \left(\frac{2\delta}{\sqrt{\pi}} S^z \partial_x \phi(0) \right) U = \frac{2\delta}{\sqrt{\pi}} S^z \partial_x \phi(0) - \lambda [\phi(0), [\phi(0), \partial_x \phi(0)]] + \dots \quad (\text{B.16})$$

We don't need to go further than the first term. We have defined λ including all terms of the unitary transformation. We see that the second term on the r.h.s is nothing but a constant (although is an infinite constant mathematically speaking!), so we can get rid of it, whereas all higher order terms are 0, since the $\delta(x)$ function commutes always with the fields. Thus, the action of the unitary transformation over the phase shift term just provides a constant, that we can forget in the following treatment, since it doesn't have any effect on the scaling of the operators.

We turn our attention now to the non-interacting part of the hamiltonian H_0 . Again, we can take out the S^z operator, which will not have any effect over H_0 , so we can insert it into the constant λ . Let's look at the first term of the BH formula:

$$U^\dagger \left(\frac{1}{2} \int dx (\partial_x \phi(x))^2 \right) U = \frac{1}{2} \int dx (\partial_x \phi(x))^2 + i\sqrt{4\pi} S^z \frac{\alpha}{2} \int dx [\phi(0), (\partial_x \phi(x))^2] + O(\alpha^2) \quad (\text{B.17})$$

We can now use the relation:

$$[\hat{A}, f(\hat{B})] = [\hat{A}, \hat{B}] f'(\hat{B}) \quad (\text{B.18})$$

and the commutation relation showing the non-locality of the fields:

$$[\partial_x \phi(x), \phi(y)] = -\frac{i}{2} \delta(x - y) \quad (\text{B.19})$$

Introducing that in (1.32), we find:

$$U^\dagger H_0 U = H_0 - \frac{\alpha}{2} \sqrt{4\pi} S^z \partial_x \phi(0) \quad (\text{B.20})$$

We see that the action of the unitary transformation over the non-interacting hamiltonian adds a shift in the derivative, that is, in the scattering phase. That is important since now, we can fix the value of α if we want to get rid of the scattering phase shift:

$$\left(\frac{2\delta}{\sqrt{\pi}} - \frac{\alpha\sqrt{4\pi}}{2}\right)S^z\partial_x\phi(0) = 0 \quad (\text{B.21})$$

Indeed, that why we used the unitary transformation U , to get rid of this interacting term. We see that this happens at the value for α :

$$\alpha = \frac{2\delta}{\pi} \quad (\text{B.22})$$

Finally, we have to treat the hopping term (the one with J'), to see how it is transformed by U . We see clearly that U commutes with the field at the impurity $\phi(0)$, however, it doesn't commute with the spin operators S^+ and S^- , since it depends on S^z . Let's see how it affects the operator S^+ . Again, using the BH formula:

$$\begin{aligned} U^\dagger S^+ U &= S^+ - i\sqrt{4\pi}\alpha\phi(0)[S^z, S^+] + \\ &\quad \frac{(-i\sqrt{4\pi}\alpha\phi(0))^2}{2!}[S^z, [S^z, S^+]] + \dots \end{aligned} \quad (\text{B.23})$$

We now use the known relations:

$$[S^z, S^+] = S^+ \quad [S^z, S^-] = -S^- \quad (\text{B.24})$$

Therefore, we obtain:

$$U^\dagger S^+ U = S^+ e^{-i\sqrt{4\pi}\alpha\phi(0)} \quad U^\dagger S^- U = S^- e^{i\sqrt{4\pi}\alpha\phi(0)} \quad (\text{B.25})$$

We turn our look back to hamiltonian (1.23). The part with U has been cancelled choosing the appropriate value of $\alpha = \frac{2\delta}{\pi}$. The H_0 part remains after the transformation, and the hopping term is expressed now in terms of *new* vertex operators:

$$U^\dagger H U = \frac{1}{2} \int_{-\infty}^{+\infty} dx (\partial_x \phi)^2 + \frac{J'}{\sqrt{2\pi}} \left(\eta \eta_l S^+ e^{i\sqrt{4\pi}\phi(0)(1-\alpha)} + h.c \right) \quad (\text{B.26})$$

We emphasize the word *new* for the operators since now we have:

$$\psi'(x) = \frac{1}{\sqrt{2\pi}} e^{i\beta\phi(x)} \quad (\text{B.27})$$

with the new scaling:

$$d = \frac{\beta^2}{8\pi} = \frac{1}{2}(1-\alpha)^2 \quad (\text{B.28})$$

We see that for $\alpha = 0$, we recover the scaling for a free fermion operator. Since the scaling is not $\frac{1}{2}$, those operators are not representing fermions anymore, but *anyons*

instead (they don't commute nor anticommute). To remember where the scaling comes from, consider the averaged vertex operators for a field $\phi(x)$:

$$\begin{aligned}\langle e^{i\beta\phi(x)} e^{-i\beta\phi(x)} \rangle &= \langle e^{i\beta(\phi(x)-\phi(y))} \rangle e^{-\frac{\beta^2}{4\pi} \log(|x-y|)} = \\ &= |x-y|^{-\frac{\beta^2}{4\pi}} = |x-y|^{-2d}\end{aligned}\quad (\text{B.29})$$

We have calculated the scaling for the new vertex operators in the one lead case. We will move now to the general case when N leads are coupled to the impurity.

The IRLM with N leads

Consider again the IRLM hamiltonian, in expression (1.23). Since having N leads just adds N different bosonic fields to it, we can write the bosonized form of the N leads IRLM just by summing up all terms:

$$H = \sum_{a=1}^N \frac{1}{2} \int_{-\infty}^{+\infty} dx (\partial_x \phi_a)^2 + \frac{J'}{\sqrt{2\pi}} \left(\eta \eta_a S^+ e^{i\sqrt{4\pi}\phi_a(0)} + h.c \right) + \frac{U}{\sqrt{\pi}} S^z \partial_x \phi_a(0)$$

The treatment of the model is exactly the same as in the one lead case. The only thing changing is the unitary transformation we will apply to the hamiltonian. Since we want to affect all fields, we can choose the easiest² transformation as:

$$U = e^{i\sqrt{4\pi}\alpha S^z \frac{1}{\sqrt{N}} (\sum_a \phi_a(0))} \quad (\text{B.30})$$

and apply it to the whole hamiltonian as we did before. The advantage we have earned with the one lead case is that now we know how such a transformation affects every term of H . But we must be careful about it.

Acting over the $U = 2\delta$ term, we know that it just produces a constat (in this case, N constants), and we can no longer consider them. We act over H_0 , and we know that, on the a lead:

$$U^\dagger H_{0,a} U = H_{0,a} - \frac{\sqrt{4\pi}}{2\sqrt{N}} \alpha S^z \partial_x \phi_a(0) \quad (\text{B.31})$$

Then to get rid of the scattering phase shift:

$$\left(\frac{2\delta}{\sqrt{\pi}} - \frac{\sqrt{4\pi}}{2\sqrt{N}} \alpha \right) S^z \partial_x \phi_a(0) = 0 \quad (\text{B.32})$$

so the condition is satisfied if:

$$\alpha = \frac{2\delta\sqrt{N}}{\pi} \quad (\text{B.33})$$

²There are infinite possibilities to choose, but for convenience we choose that one (the scaling is independent of which transformation we choose)

We are just left with the action of the unitary transformation over the S^+ and S^- part. We know from equations (1.40) how this is done. So, again for each lead, we will have:

$$U^\dagger S^+ U = S^+ e^{-i\sqrt{4\pi}\frac{\alpha}{\sqrt{N}}\sum_a \phi_a(0)} \quad (\text{B.34})$$

So, for each of the terms multiplying S^+ , the vertex operators change their scaling:

$$S^+ e^{\sqrt{4\pi}\phi_a(0)(1-\frac{\alpha}{\sqrt{N}})} e^{-i\sqrt{4\pi}\frac{\alpha}{\sqrt{N}}\sum_{j\neq a} \phi_j(0)} \quad (\text{B.35})$$

Since there are different fields in the exponentials, when we work out the correlator for the vertex operators all factorize, and the scaling is just the sum of the scalings of each vertex operator:

$$\langle e^{i\beta_1\phi_1(z)} e^{i\beta_2\phi_2(z)} \dots e^{i\beta_N\phi_N(z)} e^{-i\beta_N\phi_N(z)} \dots e^{-i\beta_1\phi_1(z)} \rangle = |z|^{-\frac{\sum_{j=1}^N \beta_j^2}{4\pi}} \quad (\text{B.36})$$

In this case, for each term there are exactly $N - 1$ equal scaling operators, and an operator with the $(1 - \frac{\alpha}{\sqrt{N}})$ factor. Therefore, one of this operators (all the exponentials multiplying S^+ for a single $\eta\eta_a$) has scaling:

$$\frac{\beta_1^2}{4\pi} + \frac{(N-1)\beta_2^2}{4\pi} \quad (\text{B.37})$$

where we define:

$$\beta_1 = \sqrt{4\pi}(1 - \frac{\alpha}{\sqrt{N}}) \quad \beta_2 = \sqrt{4\pi}\frac{\alpha}{\sqrt{N}} \quad (\text{B.38})$$

We can calculate the total scaling of this product of vertex operators:

$$2d = (1 - \frac{\alpha}{\sqrt{N}})^2 + \frac{(N-1)\alpha^2}{N} \quad (\text{B.39})$$

Now call:

$$\beta = \sqrt{N}\alpha \quad (\text{B.40})$$

We arrive at:

$$2d = (1 - \frac{2\beta}{N} + \frac{\beta^2}{N}) = \frac{1}{N}(N - 1 + (1 - \beta)^2) \quad (\text{B.41})$$

Substituting the value of β , we arrive at the result:

$$\boxed{2d = \frac{1}{N}(N - 1 + (1 - \frac{2\delta N}{\pi})^2)} \quad (\text{B.42})$$

This is the scaling of the operators associated with the hopping term. We will now proceed with a renormalization analysis to figure out the renormalized parameter when we integrate over all high energy momentum (fast oscillating modes). However, there is an important remark that has to be done here.

It turns out that, for specific values of δ , the IRLM shows a *duality*, more specifically, the scaling doesn't change. We want to replace:

$$\bar{\delta} = \delta - a \quad (\text{B.43})$$

where a has to be determined. In that case, let's work out:

$$\left(1 - \frac{2(\delta - a)N}{\pi}\right)^2 = \underbrace{\left(1 - \frac{4\delta N}{\pi} + \frac{4N^2\delta^2}{\pi^2}\right)}_{\left(1 - \frac{2N\delta}{\pi}\right)^2} + a^2 \frac{N}{\pi} - a \left(\frac{2N\delta}{\pi} - 1\right) \quad (\text{B.44})$$

The last part has to be identical to 0, so that the scaling doesn't change. Taking that into account, the non-zero solution is:

$$a = 2\delta - \frac{\pi}{N} \quad (\text{B.45})$$

So the duality occurs at:

$$\bar{\delta} = \delta - a = \frac{\pi}{N} - \delta \quad (\text{B.46})$$

At $N = 1$, there is no duality. For the case of two leads, we find out that this corresponds to an infinite interaction, and that the operators now become actual fermionic operators:

$$\delta = \frac{\pi}{2} \rightarrow d = \frac{1}{2} \quad (\text{B.47})$$

The case of $\delta = \frac{\pi}{2}$ corresponds to infinite interaction $U \rightarrow \infty$. Therefore, a new *fermionized* version of the model is recovered when this happens:

$$H = H_0 + \epsilon_0 d^\dagger d + J' (d^\dagger \psi_1^\dagger(0) + d^\dagger \psi_2^\dagger(0) + h.c) \quad (\text{B.48})$$

However, we should notice that this hamiltonian, as it is expressed, doesn't describe a hybridization between the conduction electrons and the impurity (since now, both the impurity and the conduction electron are annihilated or created at once), so it has a more difficult physical interpretation. In the case of two leads, when the interaction between the leads and the impurity is infinite, the hopping is suppressed.

Appendix C

RG treatment and the Sine Gordon model

Here we follow the treatment done in [66]. Consider a gaussian model that includes a perturbative term in the action:

$$S = S_0 + S_1 = \frac{1}{2} \int dx d\tau (\nabla\Phi)^2 + \frac{g}{a^2} \int dx d\tau \cos(\beta\Phi) \quad (\text{C.1})$$

Where a is a constant to fix the units of the expression. The S_0 part is the Euclidean action, and the perturbative part is governed by the unitless parameter g . Φ is a bosonic field.

With respect to the IRLM treated before, we can make use of this model to see how it behaves under a renormalization of the parameters. All we have to do is to consider our scaling of the operators defined by β . This field lives in the first Brillouin zone in k space, however, the model is limited in k by an ultraviolet cut-off Λ . We can now move infinitesimally from this cut-off to a lower one, lets say Λ' , and see how the parameters renormalize under this change.

The initial field limited to the cut-off Λ is then decomposed into two fields:

$$\begin{aligned} \Phi_\Lambda(x) &= \frac{1}{\sqrt{V}} \sum_{0 < k < \Lambda'} \Phi_k e^{ikx} + \frac{1}{\sqrt{V}} \sum_{\Lambda' < k < \Lambda} \Phi_k e^{ikx} \\ \Phi_\Lambda(x) &= \Phi_{\Lambda'}(x) + h(x) \end{aligned} \quad (\text{C.2})$$

We see that the field $h(x)$ includes all fast oscillating modes, those with higher k . Our purpose during the RG procedure is to integrate all these k , ending to a new cut-off Λ' . To recover the original cut-off Λ , we need to renormalize the parameters.

Consider the generating functional for the fields:

$$Z = \int D\Phi_{\Lambda'} Dh e^{-S_0[\Phi_{\Lambda'}] - S_0[h] - S_1[\Phi_{\Lambda'} + h]} \quad (\text{C.3})$$

The factorization of the fast and slow fields follows from the fact that they don't share any momentum. Let's define:

$$Z = Z_h \int D\Phi_{\Lambda'} e^{-S_0[\Phi_{\Lambda'}]} \langle e^{-S_1[\Phi_{\Lambda'+h}]} \rangle_h \quad (\text{C.4})$$

with the notation:

$$\begin{aligned} \langle e^{-S_1[\Phi_{\Lambda'+h}]} \rangle_h &= Z_h^{-1} \int Dhe^{-S_0[h]} e^{-S_1[\Phi_{\Lambda'+h}]} \\ Z_h &= \int Dhe^{-S_0[h]} \end{aligned} \quad (\text{C.5})$$

To get an effective action, we exponentiate the expression in brackets:

$$S_{\text{eff}} = S_0[\Phi_{\Lambda'}] - \log (\langle S_1[\Phi_{\Lambda'} + h] \rangle_h) \quad (\text{C.6})$$

This effective action can be expanded in powers of g , the coupling parameter in the action. We do it step by step. Clearly, the zeroth order term is $S_0[\Phi_{\Lambda'}]$. To calculate the first order term:

$$\partial_g S_{\text{eff}} = -\frac{1}{\langle S_1[\Phi_{\Lambda'} + h] \rangle_h} Z_h^{-1} \int Dhe^{-S_0[h]} \left(-\int dx^2 \cos \beta(\Phi_{\Lambda'} + h) \right) \times e^{-S_1[\Phi_{\Lambda'+h}]}$$

Evaluating this at $g = 0$ and multiplying the expression by g gives:

$$S_{\text{eff}}^{(1)} = \langle S_1[\Phi_{\Lambda'} + h] \rangle_h \quad (\text{C.7})$$

as the first order correction. When going to second order, the second derivative respect to g gives:

$$\begin{aligned} \partial_g^2 S_{\text{eff}} &= \frac{1}{\langle S_1[\Phi_{\Lambda'} + h] \rangle_h^2} \left(Z_h^{-1} \int Dhe^{-S_0[h]} \int dx^2 \cos \beta(\Phi_{\Lambda'} + h) e^{-S_1[\Phi_{\Lambda'+h}]} \right)^2 \\ &\quad - \frac{1}{\langle S_1[\Phi_{\Lambda'} + h] \rangle_h} \left(Z_h^{-1} \int Dhe^{-S_0[h]} \left(\int dx^2 \cos \beta(\Phi_{\Lambda'} + h) \right)^2 e^{-S_1[\Phi_{\Lambda'+h}]} \right)^2 \end{aligned}$$

When evaluating at $g = 0$, notice that:

$$\langle S_1[\Phi_{\Lambda'} + h] \rangle_h = 1 \quad (\text{C.8})$$

by definition. Therefore, when multiplied by $g^2/2$, the second order correction reads:

$$S_{\text{eff}}^2 = \frac{1}{2} \left(\langle S_1[\Phi_{\Lambda'} + h] \rangle_h^2 - \langle S_1^2[\Phi_{\Lambda'} + h] \rangle_h \right) \quad (\text{C.9})$$

The total effective action is, up to order g^3 :

$$S_{\text{eff}} = S_0[\Phi_{\Lambda'}] + \langle S_1[\Phi_{\Lambda'} + h] \rangle_h + \frac{1}{2} \left(\langle S_1[\Phi_{\Lambda'} + h] \rangle_h^2 - \langle S_1^2[\Phi_{\Lambda'} + h] \rangle_h \right)$$

We focus on the first term:

$$\langle S_1[\Phi_{\Lambda'} + h] \rangle_h = Z_h^{-1} \int Dhe^{-S_0[h]} \cos \beta(\Phi_{\Lambda'} + h) \quad (\text{C.10})$$

Express the cosine with its exponential form, and since $\Phi_{\Lambda'}$ doesn't play a role, it can be taken out of the integral:

$$\langle S_1[\Phi_{\Lambda'} + h] \rangle_h = \frac{Z_h^{-1}}{2} \sum_{\sigma=\pm 1} e^{i\sigma\beta\Phi_{\Lambda'}} \int Dhe^{-S_0[h]} e^{i\sigma\beta h} \quad (\text{C.11})$$

This leaves a gaussian integral in the field h , that, when passing to momentum space, will only integrate fast modes with $\Lambda' < k < \Lambda$. To see this, lets expand the exponential:

$$e^{i\sigma\beta h} \sim 1 + i\sigma\beta h - \frac{1}{2}\beta^2 h^2 + \mathcal{O}(h^3) \quad (\text{C.12})$$

Where the first momentum integral $\langle h \rangle_h = 0$ due to the asymmetry in the integral. The second momentum integral is just the propagator of the theory for S_0 . In this case, the propagator satisfies:

$$-(\partial_\tau^2 + \partial_x^2)D(\tau, x) = \delta^2(\tau, x) \quad (\text{C.13})$$

which gives:

$$D(\tau, x) = \int_{\Lambda' < k < \Lambda} \frac{d^2 k}{(2\pi)^2} \frac{e^{ik_\mu x^\mu}}{k^2 + i\epsilon} \quad (\text{C.14})$$

Since we are integrating only fast modes, the exponential above can be expanded by Taylor series. To first order of approximation, this gives:

$$D(\tau, x) = \langle h^2 \rangle_h = \int_{\Lambda' < k < \Lambda} \frac{d^2 k}{(2\pi)^2} \frac{1}{k^2} = \frac{1}{2\pi} dl \quad (\text{C.15})$$

where $dl = ((\Lambda - \Lambda')/\Lambda') = d \log \Lambda$ Therefore, the action maps into a new action:

$$S = S_0 + S_1 = \frac{1}{2} \int dx d\tau (\nabla \Phi_{\Lambda'})^2 + \frac{g(1 - ddl)}{a^2} \int dx d\tau \cos(\beta \Phi_{\Lambda'}) \quad (\text{C.16})$$

with $g' = g(1 - ddl)$ The next step is to recover the original cut-off of the theory. We have changed momentum, rescaling it by an amount Λ/Λ' , that is:

$$k' = (\Lambda/\Lambda')k \sim (1 + dl)k \quad x' = (1 - dl)x \quad (\text{C.17})$$

so that we maintain the scalar product in order dl . With that, the dx'^2 gives a term:

$$dx'^2 = (1 - dl)^2 dx d\tau \sim (1 - 2dl) dx d\tau \quad (\text{C.18})$$

We want exactly the opposite, since the terms of x and τ in the action above are the old ones, so that we can express the new action in the new space-time coordinates. Then:

$$x = \frac{\Lambda}{\Lambda'} x' \sim (1 + dl)x' \quad dx^2 \sim (1 + 2dl) dx' d\tau' \quad (\text{C.19})$$

Taking that into account that S_0 (the gaussian model) is scale invariant, we have:

$$S_{eff} = \frac{1}{2} \int dx' d\tau' (\nabla \Phi_{\Lambda'})^2 + \frac{g'}{a^2} \int dx' d\tau' \cos(\beta \Phi_{\Lambda'}) \quad (\text{C.20})$$

with $g' = g(1 + (2 - d)dl)$, a renormalized coupling constant. When the difference in $g' - g$ is small, we have the differential equation:

$$\frac{dg}{dl} = (2 - d)g \quad d = \frac{\beta^2}{4\pi} \quad (\text{C.21})$$

Here, $l = \log \Lambda$, so that this equation describes the change of the coupling constant under variations of the cut-off parameter. This provides a direct expression for the associated mass gap of the model, or the relevant energy scale:

$$\xi \sim \Lambda g^{\frac{1}{2-d}} \quad (\text{C.22})$$

This can now be applied to the IRLM. After bosonizing the hamiltonian, we can map the model to a generalised boundary sine Gordon model. The boundary comes from the fact that the fermionic fields of conduction electrons happen at $x = 0$. Thus, the only change with respect to the sine Gordon case, is that the exponent is:

$$\xi \sim \Lambda t'^{\frac{1}{1-d}} \quad (\text{C.23})$$

The exact exponent is then calculated for the IRLM in the multichannel case, giving:

$$\begin{aligned} \xi &\sim t'^{\alpha} \\ \alpha &= \frac{2}{1 + 2g - Ng^2} \\ g &= \frac{2\delta}{\pi} = \frac{2}{\pi} \arctan\left(\frac{\pi\nu U}{2}\right) \end{aligned} \quad (\text{C.24})$$

Appendix D

Strong coupling in the $N = 2$ IRLM

In this limit the impurity and the last site of the wire can be treated separately from the bath initially. However, now we have 8 states, so we work in the many-body basis with a 8×8 matrix. However, since particle number is conserved in the IRLM, this is a block matrix:

$$\begin{pmatrix} U/2 & t' & 0 & 0 & 0 & 0 & 0 & 0 \\ t' & \varepsilon_0 & t' & 0 & 0 & 0 & 0 & 0 \\ 0 & t' & U/2 & 0 & 0 & 0 & 0 & 0 \\ 0 & 0 & 0 & U/2 + \varepsilon_0 & t' & 0 & 0 & 0 \\ 0 & 0 & 0 & t' & 0 & t' & 0 & 0 \\ 0 & 0 & 0 & 0 & t' & U/2 + \varepsilon_0 & 0 & 0 \\ 0 & 0 & 0 & 0 & 0 & 0 & U & 0 \\ 0 & 0 & 0 & 0 & 0 & 0 & 0 & U + \varepsilon_0 \end{pmatrix} \quad (\text{D.1})$$

We just need to diagonalize the blocks. The first block corresponds to $N = 1$ states, just one particle in them. Note that U is a very large number, but we will take the limit at the end. In the matrix above, the states are ordered as:

$$\{|100\rangle, |010\rangle, |001\rangle, |110\rangle, |101\rangle, |011\rangle, |000\rangle, |111\rangle\} \quad (\text{D.2})$$

For the first block, we find the following eigenvalues and eigenvectors:

$$\begin{aligned} \lambda_a &= +U/2 & |a\rangle &= \frac{1}{\sqrt{2}}(|001\rangle - |100\rangle) \\ \lambda_b &= \frac{(\varepsilon_0 + U/2) - \xi}{2} & |b\rangle &= \frac{\alpha + \xi}{\zeta} |100\rangle + \frac{\alpha + \xi}{\zeta} |001\rangle - \frac{4t'}{\zeta} |010\rangle \\ \lambda_c &= \frac{(\varepsilon_0 + U/2) + \xi}{2} & |c\rangle &= \frac{\alpha - \xi}{\zeta'} |100\rangle + \frac{\alpha - \xi}{\zeta'} |001\rangle - \frac{4t'}{\zeta'} |010\rangle \end{aligned} \quad (\text{D.3})$$

where we have defined:

$$\begin{aligned}
 \xi &= \sqrt{8t'^2 + (\varepsilon_0 - U/2)^2} \\
 \alpha &= \varepsilon_0 - U/2 \\
 \zeta &= \sqrt{16t'^2 + 2(\alpha + \xi)^2} \\
 \zeta' &= \sqrt{16t'^2 + 2(\alpha - \xi)^2}
 \end{aligned} \tag{D.4}$$

We can define a new dimensionless quantity representing a very small number:

$$x = \frac{2\varepsilon_0}{U} \ll 1 \quad y = \frac{2t'}{U} \ll 1 \tag{D.5}$$

and then:

$$\lambda_b = (U/4) \left((1+x) - \sqrt{8y^2 + (1-x)^2} \right) \quad \lambda_c = (U/4) \left((1+x) + \sqrt{8y^2 + (1-x)^2} \right)$$

And the coefficients defined above become:

$$\begin{aligned}
 \frac{\alpha + \xi}{\zeta} &= \frac{x - 1 + \sqrt{8y^2 + (x-1)^2}}{\sqrt{16y^2 + 2(x-1 + \sqrt{8y^2 + (x-1)^2})^2}} \\
 \frac{-4t'}{\zeta} &= \frac{-4y}{\sqrt{16y^2 + 2(x-1 + \sqrt{8y^2 + (x-1)^2})^2}}
 \end{aligned} \tag{D.6}$$

Those are the coefficients that are relevant when we project onto the low energy subspace.

Similarly to the one particle states subspace, we find for the two particle subspace:

$$\begin{aligned}
 \lambda_d &= \varepsilon_0 + U/2 & |d\rangle &= \frac{1}{\sqrt{2}}(|011\rangle - |110\rangle) \\
 \lambda_e &= \frac{(\varepsilon_0 + U/2) - \chi}{2} & |e\rangle &= \frac{\beta - \chi}{\gamma} |110\rangle + \frac{\beta - \chi}{\gamma} |011\rangle + \frac{4t'}{\gamma} |101\rangle \\
 \lambda_f &= \frac{(\varepsilon_0 + U/2) + \chi}{2} & |f\rangle &= \frac{\beta + \chi}{\gamma'} |110\rangle + \frac{\beta + \chi}{\gamma'} |011\rangle + \frac{4t'}{\gamma'} |101\rangle
 \end{aligned} \tag{D.7}$$

where we define

$$\begin{aligned}
 \beta &= \varepsilon_0 + U/2 \\
 \chi &= \sqrt{8t'^2 + (\varepsilon_0 + U/2)^2} \\
 \gamma &= \sqrt{2(\beta - \chi)^2 + 16t'^2} \\
 \gamma' &= \sqrt{2(\beta + \chi)^2 + 16t'^2}
 \end{aligned} \tag{D.8}$$

Note now comparing the change of sign:

$$\lambda_e = (U/4) \left((1+x) - \sqrt{8\left(\frac{2t'}{U}\right)^2 + (1+x)^2} \right)$$

$$\lambda_f = (U/4) \left((1+x) + \sqrt{8\left(\frac{2t'}{U}\right)^2 + (1+x)^2} \right) \tag{D.9}$$

$$\tag{D.10}$$

Again, the coefficients we are interested in:

$$\begin{aligned}\frac{\beta - \chi}{\gamma} &= \frac{x + 1 - \sqrt{(x + 1)^2 + 8y^2}}{\sqrt{16y^2 + 2(x + 1 - \sqrt{(x + 1)^2 + 8y^2})^2}} \\ \frac{4t'}{\gamma} &= \frac{4y}{\sqrt{16y^2 + 2(x + 1 - \sqrt{(x + 1)^2 + 8y^2})^2}}\end{aligned}\tag{D.11}$$

In the large U limit, we have the following eigenvalues of the matrix:

$$\begin{aligned}\lambda_{000} &= U & \lambda_{111} &= U \\ \lambda_a &= U/2 & \lambda_d &= U/2 \\ \lambda_b &= (U/4) \left((1+x) - \sqrt{8y^2 + (1-x)^2} \right) & \lambda_e &= (U/4) \left((1+x) - \sqrt{8y^2 + (1+x)^2} \right) \\ \lambda_c &= (U/4) \left((1+x) + \sqrt{8y^2 + (1-x)^2} \right) & \lambda_f &= (U/4) \left((1+x) + \sqrt{8y^2 + (1+x)^2} \right)\end{aligned}\tag{D.12}$$

with:

$$x = \frac{2\varepsilon_0}{U} \quad y = \frac{2t'}{U}\tag{D.13}$$

We can neglect all higher powers of x and y ($x, y \ll 1$). Taking only linear terms we have:

$$\begin{aligned}\lambda_{000} &= U & \lambda_{111} &= U \\ \lambda_a &= U/2 & \lambda_d &= U/2 \\ \lambda_b &\sim \varepsilon_0 + O(x^2) & \lambda_e &\sim U.0 \sim k \\ \lambda_c &\sim U/2 & \lambda_f &= U/2(1+x)\end{aligned}\tag{D.14}$$

The next order corrections involve terms of high powers of y , and thus can be neglected. We see clearly that our ground state is λ_b for negative values of ε_0 , since λ_e remains finite but greater or equal to 0.

To summarize, there are two manifolds in the large U case: A low energy subspace, formed by two eigenvalues (λ_b and λ_e); and a high energy subspace, with degenerate eigenvalue U (for very large values of U).

As we have seen previously, the low-energy subspace is formed by two states, $|b\rangle$ and $|e\rangle$, when the value of U is high compared with the rest of parameters ε_0, t' . The diagonal part of the hamiltonian in the low energy subspace can be expressed as:

$$H_L^D = \lambda_b b^\dagger b + \lambda_e e^\dagger e + H_0^L + t\hat{P}_L (c_{1,L}^\dagger c_{0,L} + c_{1,R}^\dagger c_{0,R} + h.c.)\hat{P}_L\tag{D.15}$$

where b, e are in relation with the original fermionic operators. In fact, the ground state of the system defines the form of b :

$$|GS\rangle = b^\dagger|0\rangle = |b\rangle = (|100\rangle + |001\rangle + \beta|010\rangle) \quad (\text{D.16})$$

and therefore, we identify:

$$b = c_L + c_R + \beta d \quad (\text{D.17})$$

We are interested in getting the following operator:

$$t\hat{P}_L(c_{1,L}^\dagger c_{0,L} + c_{1,R}^\dagger c_{0,R} + h.c.)\hat{P}_L \quad (\text{D.18})$$

where t is the new hopping parameter that links the impurity + site with the bath. We are supposing that both baths, to the left and right, are equal, therefore the density of states is the same for both. \hat{P}_L is the projector of the low energy subspace, since we are only interested in how this operator acts on this manifold. The projector is:

$$\hat{P}_L = |010\rangle\langle 010| + |101\rangle\langle 101| \quad (\text{D.19})$$

Or for simplicity, we use the notation introduced before:

$$\hat{P}_L = |b\rangle\langle b| + |e\rangle\langle e| \quad (\text{D.20})$$

where the states are defined as:

$$\begin{aligned} |b\rangle &= c_1|100\rangle + c_1|001\rangle + c_2|010\rangle \\ |e\rangle &= d_1|110\rangle + d_1|011\rangle + d_2|101\rangle \end{aligned} \quad (\text{D.21})$$

where the c, d are coefficients of the change of basis. We will work out one of the terms with the projectors to see how they look like:

$$\begin{aligned} \hat{P}_L c_{1,L}^\dagger c_{0,L} \hat{P}_L &= c_{1,L}^\dagger \hat{P}_L \left(d_1|010\rangle + d_2|001\rangle \right) \langle e| = \\ &= c_{1,L}^\dagger (d_1 c_2 + d_2 c_1) |b\rangle \langle e| = (d_1 c_2 + d_2 c_1) c_{1,L}^\dagger \hat{\rho} \end{aligned} \quad (\text{D.22})$$

where we have defined ρ as the operator that changes from the state $|e\rangle$ to state $|b\rangle$.

The same treatment for all the other quantities gives us:

$$t(d_1 c_2 + d_2 c_1) (c_{1,L}^\dagger \rho + c_{1,R}^\dagger \rho + h.c.) \quad (\text{D.23})$$

The quantity $t(d_1 c_2 + d_2 c_1)$ defines the renormalized hopping parameter. According to our previous definitions (the coefficients we worked out before), this is:

$$d_1 c_2 + d_2 c_1 = \frac{4t'}{\gamma} \frac{\alpha + \xi}{\zeta} - \frac{4t'}{\zeta} \frac{\beta - \chi}{\gamma} \quad (\text{D.24})$$

So we can simplify in terms of x and y :

$$\frac{4t'}{\zeta\gamma}(-U + \xi + \chi) \quad (\text{D.25})$$

where we have used that $\alpha - \beta = -U$. Dividing everything by $U/2$ we have:

$$\frac{4y}{(2\zeta/U)(2\gamma/U)}(-2 + (2\chi/U) + (2\xi/U)) \quad (\text{D.26})$$

This expression is a complicated function of x and y , and we are interested in its behaviour at the point $(0, 0)$. If the answer is finite at this point, then the result from bosonization is recovered. We can see directly what happens at both $x = 0, y = 0$. At this point, we have $0/0$, and we need to resolve the indetermination. The series expansion for this turns out to be proportional to y and therefore, the limit is zero.

The quantity can be simplified for small values of both x and y , and it ends up being:

$$d_1c_2 + c_1d_2 = 2y = \frac{4t'}{U} \quad (\text{D.27})$$

With that, the new coupling parameter to the bath is:

$$\boxed{J' = t \frac{4t'}{U}} \quad (\text{D.28})$$

So that the new width *decreases* as $(1/U)^2$, as opposed to the one channel case.

Appendix E

The IRLM as a sequence of X-ray processes: $U \neq 0$

In this part, we attempt to generalize the method used for the $U = 0$ case, in order to calculate the impurity correlator when $U \neq 0$. At this stage, it is important to mention again that we are interested in the *local* impurity density of states, and not into the response function of conduction electrons due to a change of sign of the scatterer source.

At $U \neq 0$ but $t' = 0$, the correlators have been found in the literature [17, 54] for both the impurity and conduction electrons. The process can be understood as an X-ray edge one, where both the impurity and the conduction electrons recombine when the hole has been created in the system (see chapter 1). In that sense, one can take directly the correlators found by Nozières and De-Dominicis [17], which we write explicitly here following their notation:

$$G^d(t) = -i\text{sign}(t)(\xi_0 t)^{-g^2} \quad G^c(t) = \left(\frac{-i\nu_0}{it + \tau\text{sign}(t)} \right) (\xi_0 t)^{2g} \quad (\text{E.1})$$

where $g = 2\delta/\pi$ in the IRLM, and we have included the factor with $\tau \rightarrow 0^+$. We have also absorbed the imaginary unit in ξ_0 , as in [17] ξ_0 is said to be pure imaginary. In our notation, then ξ_0 is real. Thus, the conduction electrons propagator has two contributions:

$$G^c(t) = -i\pi\nu_0\text{sign}(t)\delta(t)(\xi_0 t)^{2g} - \xi_0\nu_0(\xi_0 t)^{2g-1} \quad (\text{E.2})$$

Now we proceed in the same way as before. All times are taken in increasing order, so $\text{sign}(t) > 0$ always. The first order correction to the impurity propagator is given by an expression similar to (5.10), by substituting the propagators for the $U \neq 0$ case:

$$G_{(1)}^d(t) \sim 2(t')^2 \int_0^t dt_2 \int_0^{t_2} dt_1 G^d(t-t_2) G^c(t_2-t_1) G^d(t_1) \quad (\text{E.3})$$

It is clear that now the imaginary part of $G^c(t)$ gives a zero contribution to this amplitude. Thus the only contribution comes from the real part. Then we find for

the first order term:

$$G_{(1)}^d(t) \sim 2(t')^2 \nu_0 \xi_0^{2g-2g^2} \int_0^t dt_2 (t-t_2)^{-g^2} \int_0^{t_2} dt_1 (t_2-t_1)^{2g-1} t_1^{-g^2} \quad (\text{E.4})$$

The total result can be written in a neater way:

$$G_{(1)}^d(t) = \frac{2\Gamma_0 \Gamma(2g) [\Gamma(1-g^2)]^2}{\pi \xi_0 \Gamma(1+\gamma)} (\xi_0 t)^\gamma \quad \gamma = 1 + 2g - 2g^2 \quad (\text{E.5})$$

where $\Gamma(x)$ represents the gamma functions, $\Gamma_0 = \pi \nu_0 (t')^2$ as usual, and we have defined the parameter γ for convenience. Note that this expression presents a divergence at the point $g = 0$. The general n th term then follows the recursion relation:

$$G_{(2n)}^d(t) = 2(t')^2 \int_0^t dt_{2n} \int_0^{t_{2n}} dt_{2n-1} G^d(t-t_{2n}) G^c(t_{2n}-t_{2n-1}) G_{(2n-1)}^d(t_{2n-1}) \quad (\text{E.6})$$

We define now the constant K :

$$K = \frac{2\Gamma_0 \Gamma(2g) [\Gamma(1-g^2)]^2}{\pi \xi_0 \Gamma(1+\gamma)} \quad (\text{E.7})$$

For the second order contribution, we find:

$$\begin{aligned} G_{(2)}^d(t) &= i \frac{2K\Gamma_0 \Gamma(2g) \Gamma(1-g^2) \Gamma(1+\gamma)}{\pi \xi_0 \Gamma(1+2\gamma+g^2)} (\xi_0 t)^{2\gamma+g^2} \\ G_{(2)}^d(t) &= i \Gamma(1-g^2) \left(\frac{2\Gamma_0 \Gamma(2g) \Gamma(1-g^2)}{\pi \xi_0} \right)^2 \frac{(\xi_0 t)^{2\gamma+g^2}}{\Gamma(1+2\gamma+g^2)} \end{aligned} \quad (\text{E.8})$$

Curiously, we find both expressions to differ by the imaginary unit and the change $\gamma \rightarrow 2\gamma + g^2$. One can then generalize this to the n th term by the appropriate substitution. The n th term of such a series is of the form:

$$G_{(2n)}^d(t) = \Gamma(1-g^2) (i)^{2n-1} \left(\frac{2\Gamma_0 \Gamma(2g) \Gamma(1-g^2)}{\pi \xi_0} \right)^{2n} \frac{(\xi_0 t)^{2n\gamma+(2n-1)g^2}}{\Gamma(1+2n\gamma+(2n-1)g^2)} \quad (\text{E.9})$$

That such a term satisfies equation (E.6) can be easily proved by induction. The total correlator then reads:

$$G^d(t) = -i \Gamma(1-g^2) \sum_{n=1}^{+\infty} \left(\frac{2i\Gamma_0 \Gamma(2g) \Gamma(1-g^2)}{\pi \xi_0} \right)^n \frac{(\xi_0 t)^{(2n/\alpha)-g^2}}{\Gamma(1+(2n/\alpha)-g^2)} \quad (\text{E.10})$$

where we have made use of the identity:

$$n\gamma + (n-1)g^2 = 2n/\alpha - g^2 \quad \alpha = \frac{2}{1+2g-g^2} \quad (\text{E.11})$$

thus referring to the thermodynamic exponent we described in previous chapters. We know in fact that such exponent appears in the relevant energy scale of the problem. Expression (E.10) can be Fourier transformed and summed over. One is

only interested in the imaginary part of such FT, so that the spectral function on the impurity site reads:

$$A(\omega) = -\frac{1}{\pi} \text{Im} \left(\int_{-\infty}^{+\infty} dt e^{i\omega t} G^d(t) \right) \quad (\text{E.12})$$

Remembering that equation (E.10) is defined for $|t|$, we can calculate the Fourier transform of each of the contributions in the series:

$$\int_{-\infty}^{+\infty} dt |t|^\gamma e^{i\omega t} = -2|\omega|^{-1-\gamma} \Gamma(1+\gamma) \sin\left(\frac{\pi\gamma}{2}\right) \quad (\text{E.13})$$

In order to get a full expression for $A(\omega)$, one needs to sum over all the contributions of the series. Whether the total sum of expression (E.10) gives the actual impurity density of states is something we are still working on. At this stage, a numerical approach results more convenient, and this is described in the next sections, where main results are presented.

Appendix F

Bethe ansatz calculations

Two body calculations

The action of the hamiltonian over the two body state $|\Psi\rangle_2$ has several contributions. We first consider the non-interacting part acting over the state. This gives the following contribution:

$$H_0|\Psi\rangle_2 = -i \int dx \psi^\dagger(x) \partial_x \psi(x) \int dx_1 dx_2 \phi(x_1, x_2) |x_2, x_1\rangle - i \int dx \psi^\dagger(x) \partial_x \psi(x) \int dx_1 \zeta(x_1) |1, x_1\rangle \quad (\text{F.1})$$

It is clear from here that there are only two non-zero possibilities: either $x = x_1$ or $x = x_2$. Thus:

$$\psi(x) |x_2, x_1\rangle = \delta(x - x_1) |x_2, 0\rangle + \delta(x - x_2) |0, x_1\rangle \quad (\text{F.2})$$

This gives the total contribution:

$$\boxed{H_0|\Psi\rangle_2 = -i \int dx_1 dx_2 (\partial_{x_1} + \partial_{x_2}) \phi(x_1, x_2) |x_2, x_1\rangle - i \int dx_1 \partial_{x_1} \zeta(x_1) |1, x_1\rangle} \quad (\text{F.3})$$

The part including the energy of the dot only couples to $|1, x_1\rangle$:

$$\boxed{H_d|\Psi\rangle_2 = -\varepsilon_0 \int dx_1 \zeta(x_1) |1, x_1\rangle} \quad (\text{F.4})$$

The hybridization term is:

$$H_V|\Psi\rangle_2 = t' \int dx \delta(x) \left(\psi^\dagger(x) d + \text{h.c.} \right) \left(\int dx_1 dx_2 \phi(x_1, x_2) |x_2, x_1\rangle + \int dx_1 \zeta(x_1) |1, x_1\rangle \right) \quad (\text{F.5})$$

Due to the minus sign arising from permuting fermionic operators, it is important to maintain a consistent order when writing the expressions. The two contributions

sum up to:

$$\begin{aligned}
 H_{t'}|\Psi\rangle_2 = t' \int dx dx_1 dx_2 \delta(x) d^\dagger \psi(x) \phi(x_1, x_2) |x_1, x_2\rangle \\
 + t' \int dx dx_1 \zeta(x_1) \delta(x) \psi^\dagger(x) d |1, x_1\rangle
 \end{aligned} \tag{F.6}$$

From the first contribution, there are two possibilities:

$$\psi(x)|x_2, x_1\rangle = \delta(x - x_1)|x_2, 0\rangle + \delta(x - x_2)|0, x_1\rangle \tag{F.7}$$

Both terms give the same contribution in the form:

$$\boxed{H_{t'}|\Psi\rangle_2 = 2t' \int dx_1 \phi(x_1, 0) |1, x_1\rangle + t' \int dx_1 dx_2 \delta(x_2) \zeta(x_1) |x_2, x_1\rangle} \tag{F.8}$$

In [56] we find the last term written as:

$$\frac{t'}{2} \left(\delta(x_2) \zeta(x_1) - \delta(x_1) \zeta(x_2) \right) \tag{F.9}$$

by using the antisymmetry property of the state $|x_2, x_1\rangle = -|x_1, x_2\rangle$.

The interacting term of hamiltonian (6.2) is:

$$\begin{aligned}
 H_U = U \int dx \delta(x) (\psi^\dagger(x) \psi(x) - \rho) (n_d - 1/2) = U \int dx \delta(x) \psi^\dagger(x) \psi(x) n_d \\
 - (U/2) \int dx \delta(x) \psi^\dagger(x) \psi(x) - U \rho \int dx \delta(x) n_d + U \rho/2
 \end{aligned} \tag{F.10}$$

where the constant part at the end is neglected. The term proportional to $\psi^\dagger(x) \psi(x)$ gives the following contribution:

$$\begin{aligned}
 + \frac{U}{2} \int dx_1 \delta(x_1) \zeta(x_1) |1, x_1\rangle - \frac{U}{2} \int dx_1 dx_2 \delta(x_1) \phi(x_1, x_2) |x_2, x_1\rangle \\
 - \frac{U}{2} \int dx_1 dx_2 \delta(x_2) \phi(x_1, x_2) |x_2, x_1\rangle
 \end{aligned} \tag{F.11}$$

The + sign for the first term comes from the fact that counting the number of electrons in x when the impurity is filled gives a permutation, by definition of the state. The part proportional to n_d gives:

$$-U \rho \int dx_1 \zeta(x_1) |1, x_1\rangle \tag{F.12}$$

And now, since there are two particles, the interacting term plays a role, giving a contribution of:

$$U \int dx_1 \zeta(x_1) \delta(x_1) |1, x_1\rangle \tag{F.13}$$

The total contribution of the interacting term is then:

$$\begin{aligned}
 H_U|\Psi\rangle_2 &= +\frac{U}{2} \int dx_1 \delta(x_1) \zeta(x_1) |1, x_1\rangle - \frac{U}{2} \int dx_1 dx_2 \delta(x_1) \phi(x_1, x_2) |x_2, x_1\rangle \\
 &- \frac{U}{2} \int dx_1 dx_2 \delta(x_2) \phi(x_1, x_2) |x_2, x_1\rangle - U\rho \int dx_1 \zeta(x_1) |1, x_1\rangle \\
 &+ U \int dx_1 \zeta(x_1) \delta(x_1) |1, x_1\rangle
 \end{aligned} \tag{F.14}$$

Putting all contributions together, we arrive at the two equations determining Φ and ζ .

The first equation with $\Phi(x_1, x_2)$ is identically 0 by substituting the form of the states. This checked carefully here by splitting all terms. Lets start by the first equation. To simplify notation, we identify $\varepsilon_1 = 1$ and $\varepsilon_2 = 2$.

The term of the derivatives can be expressed as:

$$\begin{aligned}
 -\frac{i}{2} \left(\partial_{x_1} \phi_1(x_1) \phi_2(x_2) f(\sigma) + \partial_{x_2} \phi_1(x_1) \phi_2(x_2) f(\sigma) - \partial_{x_1} \phi_1(x_2) \phi_2(x_1) f(-\sigma) \right. \\
 \left. - \partial_{x_2} \phi_1(x_2) \phi_2(x_1) f(-\sigma) \right)
 \end{aligned} \tag{F.15}$$

where we have defined $f(\sigma) = f(x_1 - x_2)$ and used the fact that:

$$\sum_i \partial_{x_i} f(\sigma) = 0 \tag{F.16}$$

The part with t' is written as:

$$\begin{aligned}
 \frac{t'}{2} \left(\delta(x_1) \zeta_1 \phi_2(x_2) f(-x_2) - \delta(x_1) \zeta_2 \phi_1(x_2) f(x_2) \right) \\
 - \frac{t'}{2} \left(\delta(x_2) \zeta_1 \phi_2(x_1) f(-x_1) - \delta(x_2) \zeta_2 \phi_1(x_1) f(x_1) \right)
 \end{aligned} \tag{F.17}$$

The part including the $-U/2$:

$$\begin{aligned}
 -\frac{U}{4} \left(\delta(x_1) \phi_1(x_1) \phi_2(x_2) f(\sigma) - \delta(x_1) \phi_1(x_2) \phi_2(x_1) f(-\sigma) \right) \\
 -\frac{U}{4} \left(\delta(x_2) \phi_1(x_1) \phi_2(x_2) f(\sigma) - \delta(x_2) \phi_1(x_2) \phi_2(x_1) f(-\sigma) \right)
 \end{aligned} \tag{F.18}$$

Finally the right hand side of the equation is:

$$\frac{(\varepsilon_1 + \varepsilon_2)}{2} \left(\phi_1(x_1) \phi_2(x_2) f(\sigma) - \phi_1(x_2) \phi_2(x_1) f(-\sigma) \right) \tag{F.19}$$

We need to check if this first equation is identically zero for this choice of the functions. They do, and to prove this, we need to separate terms with $f(\sigma)$ and $f(-\sigma)$. Thus, for the selected form of the solutions, the first equation in (6.31).

Obtaining the scattering phase-shift

We write the left-hand side first:

$$\begin{aligned}
 & -i\partial_x \left(\zeta_1 \phi_2(x) f(-x) - \zeta_2 \phi_1(x) f(x) \right) + t' \left(\phi_1(0) \phi_2(x) f(-x) - \phi_1(x) \phi_2(0) f(x) \right) \\
 & + \frac{U}{2} \delta(x) \left(\zeta_1 \phi_2(x) f(-x) - \zeta_2 \phi_1(x) f(x) \right) \\
 & = (E + \varepsilon_0 + U\rho) \left(\zeta_1 \phi_2(x) f(-x) - \zeta_2 \phi_1(x) f(x) \right) \tag{F.20}
 \end{aligned}$$

Lets spread the terms involving $f(x)$ first. We have:

$$\begin{aligned}
 & i\zeta_2 \partial_x (\phi_1(x) f(x)) - t' \phi_1(x) \phi_2(0) f(x) - \frac{U}{2} \delta(x) \zeta_2 \phi_1(x) f(x) \\
 & = -(E + \varepsilon_0 + U\rho) \zeta_2 \phi_1(x) f(x) \tag{F.21}
 \end{aligned}$$

The trick now is to realize that the one particle equation involving ζ must be satisfied, so with all terms on the left side, we have:

$$-i\zeta_2 \partial_x \phi_1(x) f(x) - i\zeta_2 \phi_1(x) \partial_x f(x) - f(x) \phi_1(x) \varepsilon_1 \zeta_2 + \frac{U}{2} \delta(x) \zeta_2 \phi_1(x) f(x) \tag{F.22}$$

Now, we add and subtract the quantity $(U/2)\delta(x)\zeta_2\phi_1(x)f(x)$ and recall that:

$$-i\partial_x \phi_k(x) - \varepsilon_k \phi_k(x) - \frac{U}{2} \delta(x) \phi_k(x) = -t' \delta(x) \zeta_k \tag{F.23}$$

so the final terms are:

$$-i\zeta_2 \phi_1(x) \partial_x f(x) - t' f(x) \zeta_1 \zeta_2 \delta(x) + U \zeta_2 \delta(x) \phi_1(x) f(x) \tag{F.24}$$

The rest of terms of the equation are calculated in the same way by just substituting $f(x) \rightarrow f(-x)$ and the index $1 \rightarrow 2$. Then the total equation to solve is:

$$\begin{aligned}
 & -i\zeta_2 \phi_1(x) \partial_x f(x) - t' f(x) \zeta_1 \zeta_2 \delta(x) + U \delta(x) \zeta_2 \phi_1(x) f(x) + \\
 & i\zeta_1 \phi_2(x) \partial_x f(-x) + t' f(-x) \zeta_2 \zeta_1 \delta(x) - U \delta(x) \zeta_1 \phi_2(x) f(-x) = 0 \tag{F.25}
 \end{aligned}$$

where there is a term:

$$t' \zeta_1 \zeta_2 \delta(x) (f(-x) - f(x)) \tag{F.26}$$

that is zero exactly at $x = 0$. We now recall that:

$$\phi_k(x = 0) = \alpha_k \zeta_k \tag{F.27}$$

where $\alpha_k = \frac{\varepsilon_0 + \varepsilon_k + U\rho}{t'}$. Using this, the above equation can be simplified:

$$-i \frac{\phi_1(x)}{\zeta_1} \partial_x f(x) + i \frac{\phi_2(x)}{\zeta_2} \partial_x f(-x) = E_2 \delta(x) f(-x) - E_1 \delta(x) f(x) \tag{F.28}$$

where we have defined:

$$E_i = \frac{U(\varepsilon_0 + \varepsilon_i + U\rho)}{t'} \quad (\text{F.29})$$

The equation above is the equation for $f(x)$ at $x = 0$. Since both $f(-x) = f(x = 0)$, then we define:

$$f(0) = \frac{1}{2}(e^\Phi + e^{-i\Phi}) = \cos \Phi \quad (\text{F.30})$$

and we integrate both sides between an infinitesimal interval $[-\epsilon, \epsilon]$. The functions ϕ can well be approximated by their values at $x = 0$, therefore the equation looks like:

$$\begin{aligned} -i \int_{-\epsilon}^{\epsilon} dx \left((E_1/U) \partial_x f(x) - (E_2/U) \partial_x f(-x) \right) &= (E_2 - E_1) \cos \Phi = \\ -i \left((E_1/U)(f(\epsilon) - f(-\epsilon)) - (E_2/U)(f(-\epsilon) - f(\epsilon)) \right) &= (E_2 - E_1) \cos \Phi \end{aligned} \quad (\text{F.31})$$

Now making the substitutions $f(\epsilon) \rightarrow e^{i\Phi}$ and $f(-\epsilon) \rightarrow e^{-i\Phi}$, we find:

$$-i \left(((E_1 + E_2)/U)(e^{i\Phi} - e^{-i\Phi}) \right) = 2((E_1 + E_2)/U) \sin \Phi = (E_2 - E_1) \cos \Phi \quad (\text{F.32})$$

So the final equation for the phase shift is:

$$\boxed{\Phi(\varepsilon_2, \varepsilon_1) = \arctan \left(\frac{U}{2} \frac{\varepsilon_2 - \varepsilon_1}{\varepsilon_1 + \varepsilon_2 + 2(\varepsilon_0 + U\rho)} \right)} \quad (\text{F.33})$$

and so the final form of $f(x)$ is:

$$\boxed{f(x_1 - x_2) = f(0)e^{-i\Phi(\varepsilon_1, \varepsilon_2)\text{sign}(x_1 - x_2)}} \quad (\text{F.34})$$

Wiener-Hopf method in the IRLM

We want to apply the Wiener Hopf method in order to find the rapidities distribution for the IRLM. The rapidities distribution equation is given in Filyov-Wiegmann's paper [56]:

$$\Lambda e^{-\alpha} = 2\pi\rho(\alpha) + \int_0^{+\infty} \frac{\partial\Phi(\alpha - \beta)}{\partial\alpha} \rho(\beta) d\beta \quad (\text{F.35})$$

where we have:

$$\Phi(\alpha - \beta) = -2 \arctan \left(\frac{U}{2} \tanh \left(\frac{\alpha - \beta}{2} \right) \right) \quad (\text{F.36})$$

This can be written as:

$$\begin{aligned}\rho(\alpha) &= (\Lambda/2\pi)e^{-\alpha} - \frac{1}{2\pi} \int_0^{+\infty} \frac{\partial\Phi(\alpha - \beta)}{\partial\alpha} \rho(\beta) d\beta \\ \rho(\alpha) &= \rho^0(\alpha) + \int_0^{+\infty} K(\alpha - \beta) \rho(\beta) d\beta\end{aligned}\quad (\text{F.37})$$

It is convenient to make it look similar to the kernel for the massive Thirring model, since results derived by Korepin can be used. The massive Thirring model has the following scattering phase shift:

$$\Phi_{\text{MTM}}(\beta) = i \log \left(\frac{\sinh(i\omega - \beta/2)}{\sinh(i\omega + \beta/2)} \right) = -2 \arctan \left(\cot(\omega) \tanh(\beta/2) \right) \quad (\text{F.38})$$

where $\omega = (\pi - \xi)/2$, being ξ the coupling in the Thirring model. For the IRLM, we have $\tau = U/2$ and:

$$\Phi_{\text{IRLM}}(\beta) = -i \log \left(\frac{1 - i\tau \tanh(\beta/2)}{1 + i\tau \tanh(\beta/2)} \right) \quad (\text{F.39})$$

defining a new parameter $\tau = \cot \mu$, we can express it as:

$$\Phi_{\text{IRLM}}(\beta) = i \log \left(\frac{\sinh(i\mu - \beta/2)}{\sinh(i\mu + \beta/2)} \right) \quad (\text{F.40})$$

It is clear that both kernels are equivalent if we identify:

$$\mu = \omega = \frac{\pi}{2} - \frac{\xi}{2} \rightarrow \xi = 2 \arctan(U/2) \rightarrow (2\mu/\pi) = 1 - g \quad (\text{F.41})$$

In order to apply the Wiener-Hopf method, we calculate the Fourier transforms of each of the terms. For the r.h.s of the integral equation, a trick is to extend the values of α also to be negative. In this case, we have:

$$\boxed{\rho^0(p) = \int_{-\infty}^{+\infty} \frac{\Lambda}{2\pi} d\alpha e^{ip\alpha} e^{-\alpha} \theta(\alpha) = \frac{\Lambda}{2\pi} \frac{i}{p+i}} \quad (\text{F.42})$$

which has a pole at $-i$. This Fourier transform is only valid if the variable p satisfies $\text{Im}(p) > -1$, otherwise, the integral diverges. The Fourier transform of the kernel is the same for both the massive Thirring model and the IRLM. The kernel is:

$$\begin{aligned}(1/2\pi)\partial\Phi/\partial\alpha &= -K(\alpha - \beta) = \frac{1}{2(2\pi)} \frac{\sin(2\mu)}{\sinh((\alpha - \beta + i2\mu)/2) \sinh((\alpha - \beta - i2\mu)/2)} \\ &= \frac{1}{2\pi} \frac{\sin(2\mu)}{\cos(2\mu) - \cosh(\alpha - \beta)}\end{aligned}\quad (\text{F.43})$$

This is the result of the following inverse Fourier transform:

$$K(\alpha) = \int_{-\infty}^{+\infty} \frac{dp}{2\pi} e^{-ip\alpha} \underbrace{\left(\frac{\sinh(p(\pi - 2\mu))}{\sinh(p\pi)} \right)}_{K(p)} = -(1/2\pi)\partial\Phi/\partial\alpha \quad (\text{F.44})$$

Then the Fourier transform of the kernel is:

$$\boxed{K(p) = \frac{\sinh(p(\pi - 2\mu))}{\sinh(p\pi)} = \frac{\sinh(\pi p g)}{\sinh(p\pi)}} \quad (\text{F.45})$$

The Wiener Hopf equation above can be written as:

$$\begin{aligned} \rho(\alpha) &= (\Lambda/2\pi)e^{-\alpha} - \frac{1}{2\pi} \int_0^{+\infty} \frac{\partial\Phi(\alpha - \beta)}{\partial\alpha} \rho(\beta) d\beta \\ \rho(\alpha) &= \rho^0(\alpha) + \int_0^{+\infty} K(\alpha - \beta) \rho(\beta) d\beta \end{aligned} \quad (\text{F.46})$$

Our treatment follows Tselvick and Wiegmann [60], and Hewson [61]. The first step of the Wiener Hopf method is to separate the distribution $\rho(\alpha) = \rho^+(\alpha) + \rho^-(\alpha)$ as a sum of an analytic part in the upper/lower half planes of α . We have:

$$\begin{aligned} \rho^+(\alpha) &= \rho^0(\alpha) + \int_0^{+\infty} d\beta K(\alpha - \beta) \rho(\beta)^+ \quad \alpha > 0 \\ \rho^-(\alpha) &= \int_0^{+\infty} d\beta K(\alpha - \beta) \rho(\beta)^+ \quad \alpha < 0 \end{aligned} \quad (\text{F.47})$$

Then we can take all Fourier transforms, and the equation is:

$$\rho^-(p) + (1 - K(p))\rho^+(p) = \rho^0(p) \quad (\text{F.48})$$

Here, the Fourier transforms of ρ are defined as:

$$\rho^\pm(p) = \pm \int_0^{\pm\infty} d\alpha \rho^\pm(\alpha) e^{i\alpha p} \quad \rho^0(p) = \int_0^{+\infty} d\alpha e^{i\alpha p} \rho^0(\alpha) \quad (\text{F.49})$$

The next step is to factorize the kernel into a part analytic in the upper half plane and another in the lower part. Then we find:

$$1 - K(p) = \gamma^+(p)\gamma^-(p) \quad (\text{F.50})$$

The following identities for the gamma functions are useful here:

$$\begin{aligned} \sinh(\pi y) &= \frac{\pi y}{\Gamma(1 + iy)\Gamma(1 - iy)} \\ \cosh(\pi y) &= \frac{\pi}{\Gamma(1/2 + iy)\Gamma(1/2 - iy)} \end{aligned} \quad (\text{F.51})$$

Then we can rewrite:

$$1 - K(p) = 1 + \frac{\sinh(-\pi p g)}{\sinh(\pi p)} \rightarrow \frac{\sinh(x) + \sinh(y)}{\sinh(x)} \quad (\text{F.52})$$

Now we make use of the identity:

$$\sinh(x) + \sinh(y) = 2 \sinh\left(\frac{x+y}{2}\right) \cosh\left(\frac{x-y}{2}\right) \quad (\text{F.53})$$

So the function to factorize is:

$$1 - K(p) = \frac{2 \sinh\left(\frac{\pi p(1-g)}{2}\right) \cosh\left(\frac{\pi p(1+g)}{2}\right)}{\sinh(\pi p)} \quad (\text{F.54})$$

Making use of the identities with the Gamma functions, we can rewrite this as:

$$1 - K(p) = \frac{\pi(1-g) \prod_{\pm} \Gamma(1 \pm ip)}{\prod_{\pm} \Gamma(1 \pm ip(1-g)/2) \Gamma(1/2 \pm ip(1+g)/2)} \quad (\text{F.55})$$

To get analytic results at $i\infty$, we include a phase $e^{ip\Delta}$ in each solution. Then we identify now:

$$\begin{aligned} \gamma^+(p) &= \frac{\sqrt{\pi(1-g)} \Gamma(1-ip)}{\Gamma(1-ip(1-g)/2) \Gamma(1/2-ip(1+g)/2)} e^{-ip\Delta} \\ \gamma^-(p) &= \frac{\sqrt{\pi(1-g)} \Gamma(1+ip)}{\Gamma(1+ip(1-g)/2) \Gamma(1/2+ip(1+g)/2)} e^{ip\Delta} \end{aligned} \quad (\text{F.56})$$

where the phase Δ is defined [35] as:

$$\begin{aligned} \Delta &= \frac{1}{2} \log\left(\frac{1+g}{1-g}\right) - \frac{1}{1+g} \log\left(\frac{2}{1-g}\right) \\ &= \log\left(\frac{(1+g)^{1/2}(1-g)^{(1-g)/2(1+g)}}{2^{1/1+g}}\right) \end{aligned} \quad (\text{F.57})$$

which is always < 0 . The following relation for the gamma functions is useful here:

$$\Gamma(z+1/2) = 2^{1-2z} \pi^{1/2} \frac{\Gamma(2z)}{\Gamma(z)} \quad \Gamma(z+1) = z\Gamma(z) \quad (\text{F.58})$$

The function $\rho^0(p)/\gamma^-(p)$ can be separated into a sum of an analytic part in the upper half-plane and another analytic in the lower-half plane. For this, the function is analytic within some strip of the complex p plane, that is, within a region $a < \text{Im}(p) < b$.

$$\rho^0(p)/\gamma^-(p) = u^+(p) - u^-(p) \quad u^{\pm}(p) = \frac{1}{2\pi i} \int_{-\infty}^{+\infty} dz \frac{\rho^0(z)/\gamma^-(z)}{z-p} \quad (\text{F.59})$$

Note that the minus sign arises when we integrate in the complex plane in opposite direction, that is, the lower half-plane. In this case, the region of analyticity of the function is the strip $-1 < \text{Im}(k) \leq 1/(1+g)$. Coming back to the Fourier transform equation we have:

$$\rho^-(p)/\gamma^-(p) + u^-(p) = u^+(p) - \gamma^+(p)\rho^+(p) = F(p) \quad (\text{F.60})$$

being $F(p)$ an entire function whose value is necessarily 0 for all p . Therefore, we have the solutions:

$$\rho^+ = \frac{1}{2\pi i} \frac{1}{\gamma^+(p)} \int_{-\infty}^{+\infty} dk \frac{(\rho^0(k)/\gamma^-(k))}{k-p-is} \quad \rho^- = -\frac{\gamma^-(p)}{2\pi i} \int_{-\infty}^{+\infty} dk \frac{(\rho^0(k)/\gamma^-(k))}{k-p+is}$$

with $s > 0$. Now, by proper choice of the contour of integration, we can calculate this distribution functions. The integrand has an isolated pole in the lower half-plane at $p = -i$, and all other poles are in the upper half-plane. The solution for $\rho^+(p)$ can be written as:

$$\rho^+(p) = \frac{i\Lambda}{i+p} \frac{\Gamma((1-g)/2)\Gamma(1/2+(1+g)/2)}{2\pi} \frac{\Gamma(1-ip(1-g)/2)\Gamma(1/2-ip(1+g)/2)}{\Gamma(1-ip)} \times e^{(1-ip)\Delta}$$

Then the distribution of positive rapidities can be calculated as:

$$\begin{aligned} \rho^+(\alpha) &= \int_{-\infty}^{+\infty} \frac{dp}{2\pi} \rho^+(p) e^{-ip\alpha} \\ \rho^+(\alpha) &= \Lambda \underbrace{\frac{\Gamma((1-g)/2)\Gamma(1/2+(1+g)/2)}{(2\pi)^2}}_{f(g)} e^{\Delta} \\ &\times \int_{-\infty}^{+\infty} dp e^{-ip\alpha} \frac{\Gamma(1-ip(1-g)/2)\Gamma(1/2-ip(1+g)/2)}{\Gamma(2-ip)} e^{-ip\Delta} \end{aligned} \quad (\text{F.61})$$

Now, for the integral to converge, we have to close the contour in the lower-half plane of p , where there is a whole set of poles. The poles are located at the points:

$$p_{(1)} = -i2(n+1)/(1-g) \quad p_{(2)} = -i2(n+1/2)/(1+g) \quad (\text{F.62})$$

Also, for the gamma function the residues at the pole $z = -n$ are:

$$\text{Res}\Gamma(z = -in) = i \frac{(-1)^n}{n!} \quad (\text{F.63})$$

Let us call $a = (1-g)/2$ and $b = (1+g)/2$. Then the integral has two contributions:

$$\begin{aligned} (1) \quad & 2\pi \sum_{n=1}^{+\infty} \frac{(-1)^n}{n!} e^{-\alpha(n/a)} \frac{\Gamma(1/2-n(b/a))}{\Gamma(2-n/a)} e^{-\Delta(n/a)} \\ (2) \quad & 2\pi \sum_{n=1}^{+\infty} \frac{(-1)^n}{n!} e^{-\alpha((2n-1)/2b)} \frac{\Gamma(1-(2n-1)(a/2b))}{\Gamma(2-(2n-1)/2b)} e^{-\Delta((2n-1)/2b)} \end{aligned} \quad (\text{F.64})$$

Now one can take the limit $\Delta \rightarrow 0$, and obtain the rapidities distribution, which is related to the energy eigenvalues distribution as:

$$\rho^+(\alpha) = \Lambda e^{-\alpha} \rho(\varepsilon) \quad (\text{F.65})$$

Calculation of the susceptibility at zero field ($\varepsilon_0 = 0$)

Knowing the rapidities distribution, we can calculate the impurity energy by the following integral:

$$E_I = \int_{-\Lambda}^0 d\varepsilon \arctan\left(\frac{t'^2}{2(\varepsilon + \varepsilon_0)}\right) \rho(\varepsilon) \quad (\text{F.66})$$

Then the occupation on the dot can be obtained as:

$$n_d = \frac{\partial E_I}{\partial \varepsilon_0} \quad (\text{F.67})$$

The second derivative of the integrand is the one providing the susceptibility:

$$\chi \sim \left. \frac{\partial n_d}{\partial \varepsilon_0} \right|_{\varepsilon_0=0} \quad (\text{F.68})$$

The integrand is differentiated twice:

$$\partial_{\varepsilon_0}^2 \arctan \left(\frac{\Gamma_0}{(\varepsilon + \varepsilon_0)} \right) = \frac{\Gamma_0 \varepsilon}{(\Gamma_0^2 + \varepsilon^2)^2} = \frac{1}{\varepsilon^2} \frac{(\Gamma_0/\varepsilon)}{(1 + (\Gamma_0/\varepsilon)^2)^2} \quad (\text{F.69})$$

with $\Gamma_0 = (t^2/2)$. This is the solution at $\varepsilon_0 = 0$. The true distribution function in energies is then obtained by replacing the decaying exponentials ($\Delta = 0$):

$$\begin{aligned} \rho(\varepsilon) &= \sum_{n=1}^{+\infty} A_n (-\varepsilon/\Lambda)^{-1+(n/a)} + B_n (-\varepsilon/\Lambda)^{-1+(2n-1)/2b} \\ A_n &= \frac{\Gamma((1-g)/2)\Gamma(1/2 + (1+g)/2)}{2\pi} \frac{(-1)^n \Gamma(1/2 - (n/a))}{n! \Gamma(2 - (n/a))} \\ B_n &= \frac{\Gamma((1-g)/2)\Gamma(1/2 + (1+g)/2)}{2\pi} \frac{(-1)^n \Gamma(1 - ((2n-1)/2b))}{n! \Gamma(2 - ((2n-1)/2b))} \end{aligned} \quad (\text{F.70})$$

Now the integrand consists on this function and the derivative of the arctan. Since the integral is a sum of different contributions, we only focus on the dominant term of the expansion. That is the one with the smallest exponent:

$$\rho(\varepsilon) \sim A_{n=1}(g) (-\varepsilon/\Lambda)^{-1+(1/1+g)} = A_{n=1}(g) (-\varepsilon/\Lambda)^{-g/(1+g)} \quad (\text{F.71})$$

where $T(g)$ is the prefactor for $n = 1$. Then the first contribution to the integral reads:

$$\chi \sim A_{n=1}(g) \int_{-\Lambda}^0 d\varepsilon \frac{1}{\varepsilon^2} \frac{(\Gamma_0/\varepsilon)}{(1 + (\Gamma_0/\varepsilon)^2)^2} (-\varepsilon/\Lambda)^{-g/1+g} \quad (\text{F.72})$$

Now we change variables as $z = -\Gamma_0/\varepsilon$. Then we have:

$$dz = \frac{d\varepsilon}{\varepsilon^2} \Gamma_0 \quad (\text{F.73})$$

and the integral is now:

$$\chi \sim A_{n=1}(g) \int_{\Gamma_0/\Lambda}^{+\infty} dz \Gamma_0^{-1} \frac{z}{(1+z^2)^2} (\Gamma_0/\Lambda)^{-g/1+g} z^{g/1+g} \quad (\text{F.74})$$

Lattice treatment

One particle states

We move now to the lattice version of the model, in order to understand the origin of interactions in the scattering phase-shift. We look at a chain of N sites in total. In this case, the hamiltonian is:

$$H = -t \sum_{i=0}^{N-2} c_{i+1}^\dagger c_i - t \sum_{i=0}^{N-2} c_i^\dagger c_{i+1} - \varepsilon_0 d^\dagger d + t'(c_0^\dagger d + \text{h.c.}) + U(c_0^\dagger c_0 - 1/2)(d^\dagger d - 1/2) \quad (\text{F.75})$$

The dot is occupying the site $i = 0$ of the lattice. We will start with the single-particle problem. In this case, the state is just a linear combination of all possible one-particle states:

$$|\Psi\rangle = \sum_{i=0}^{N-2} \phi_i c_i^\dagger |\Omega\rangle + \phi_d |\uparrow\rangle \quad (\text{F.76})$$

where the normalization condition reads:

$$\sum_{i=0}^{N-2} |\phi_i|^2 + |\phi_d|^2 = 1 \quad (\text{F.77})$$

and $|\Omega\rangle$ is the empty state. The hamiltonian has four terms acting over this state:

$$H = H_0 + H_{\varepsilon_0} + H_{t'} + H_U \quad (\text{F.78})$$

The non interacting part acting on the state is:

$$H_0 |\Psi\rangle = -t \sum_{j \geq 0} (\phi_{j-1} (1 - \delta_{j,0}) + \phi_{j+1}) |j\rangle \quad (\text{F.79})$$

The dot site part is:

$$H_d |\Psi\rangle = -\varepsilon_0 \phi_d |\uparrow\rangle \quad (\text{F.80})$$

The interacting term is only counting the number of particles in the last two sites:

$$H_U |\Psi\rangle = (-U/2) \phi_0 |0\rangle + (-U\rho) \phi_d |\uparrow\rangle \quad (\text{F.81})$$

The mixing part is:

$$H_{t'} |\Psi\rangle = t' \phi_d |0\rangle + t' \phi_0 |\uparrow\rangle \quad (\text{F.82})$$

The eigenvalue equation leads to:

$$\begin{aligned} E_1 \phi_j &= -t(\phi_{j+1} + \phi_{j-1}(1 - \delta_{j,0})) - (U/2)\delta_{0,j}\phi_j + t'\delta_{0,j}\phi_d \\ (E_1 + \varepsilon_0 + U\rho)\phi_d &= t'\delta_{0,j}\phi_j \end{aligned} \quad (\text{F.83})$$

The states inside the wire can be regarded as a set of right and left moving plane waves:

$$\phi_n = Ae^{ikn} + Be^{-ikn} \quad (\text{F.84})$$

Then the equations transform to a single one:

$$(E_1 + \varepsilon_0 + U\rho)\phi_d = t'(A + B) \quad (\text{F.85})$$

$$(E_1 + U/2)(A + B) = t'\phi_d - tAe^{ik} - tBe^{-ik} \quad (\text{F.86})$$

which is expressed in a single equation:

$$\frac{t'^2}{(E_1 + \varepsilon_0 + U\rho)}(A + B) = (E_1 + U/2)(A + B) + tAe^{ik} + tBe^{-ik} \quad (\text{F.87})$$

. The relation between A, B is given by a scattering phase shift:

$$A = Be^{i\Delta} = -e^{i2\alpha}B = e^{i(\pi+2\alpha)}B \quad (\text{F.88})$$

The phase α is calculated from the complex number above:

$$z = \frac{t'^2}{(E_1 + \varepsilon_0 + U\rho)} - \frac{U}{2} - E_1 - t \cos(k) + it \sin(k) \quad (\text{F.89})$$

The term with the cosine disappears close to the Fermi level, since then we have:

$$E_1 + t \cos(k) = E_1/2 \quad (\text{F.90})$$

And the term with the sine is just the Fermi velocity, related to the density of states:

$$E_1 = -2t \cos(k) \rightarrow \nu/2 = \frac{1}{\Delta_k t \sin(k)} \rightarrow t \sin(k) = \frac{2}{\pi\nu} \quad (\text{F.91})$$

Then the phase shift α is:

$$\alpha = \frac{\pi}{2} - \arctan \left(\frac{\Gamma_0}{2(E_1 + \varepsilon_0 + U\rho)} - \frac{U\pi\nu}{4} - \frac{E_1\pi\nu}{4} \right) \quad (\text{F.92})$$

Therefore, the single particle states for the dot site are:

$$\phi_d = \frac{t'}{E_1 + \varepsilon_0 + U\rho} B(1 + e^{i\Delta}) \quad (\text{F.93})$$

with $e^{i\Delta} = e^{i\pi+2\alpha}$. Then we identify:

$$\Delta_U = 2 \arctan \left(-\frac{\Gamma_0}{2(E_1 + \varepsilon_0 + U\rho)} + \frac{U\pi\nu}{4} + \frac{E_1\pi\nu}{4} \right) \quad (\text{F.94})$$

Then the state on the dot, or quantum probability amplitude of occupation there, is:

$$\phi_d = \frac{t'\sqrt{2}}{E_1 + \varepsilon_0 + U\rho} \cos(\Delta_U/2) e^{i\Delta_U/2} \quad (\text{F.95})$$

By the normalization condition, we have $B = 1/\sqrt{2}$. Therefore, a factor $\sqrt{2}$ multiplies the whole expression. We will compare the obtained expression with the one obtained by the field theory, were we had:

$$\phi_d^F = \frac{t'}{E_1 + \varepsilon_0 + U\rho} \cos(\Delta_U^F) \quad \Delta_U^F = \arctan\left(\frac{t'^2}{2(E_1 + \varepsilon_0 + U\rho)} - \frac{U}{4}\right) \quad (\text{F.96})$$

We see that the field theory treatment includes a different phase, moreover, is a real number, whereas the lattice version of this number is complex. The origin of these differences between both versions can be related with the way how the Dirac delta is regularized in the field theory treatment. Therefore, for the lattice version of the model, we have the following single-particle states:

$$\begin{aligned} \phi_d &= \frac{t'\sqrt{2}}{E_1 + \varepsilon_0 + U\rho} \cos(\Delta_U/2) e^{i\Delta_U/2} \\ \phi_n &= \sqrt{2} \cos(kn + \Delta_U/2) e^{i\Delta_U/2} \end{aligned} \quad (\text{F.97})$$

and Δ_U is defined above. We will see later the case of the two body problem in the lattice. However, the phase factor appearing here has no effect on the system, and can be removed by $B \rightarrow B e^{-i\Delta_U/2}$. Then the solutions in the lattice version can be written as:

$$\begin{aligned} \phi_d &= \frac{t'\sqrt{2}}{E_1 + \varepsilon_0 + U\rho} \cos(\Delta_U/2) \\ \phi_n &= \sqrt{2} \cos(kn + \Delta_U/2) = (1/\sqrt{2})(e^{ikn+i\Delta_U/2} + e^{-ikn-i\Delta_U/2}) \end{aligned} \quad (\text{F.98})$$

If instead of taking the last site of the chain to be at $n = 0$ we would have taken it to be at $n = 1$, then the scattering phase shift changes and it is given by:

$$\alpha = \arctan\left(\tan(k) \frac{t'^2/(\varepsilon_1 + \varepsilon_0 + U\rho) - U/2}{t'^2/(\varepsilon_1 + \varepsilon_0 + U\rho) + t - U/2}\right) \quad (\text{F.99})$$

Two body calculation

For the two body calculation, we seek for states in the form:

$$|\Psi\rangle_2 = \sum_{i,j=0}^{N-2} \phi_{i,j} c_i^\dagger c_j^\dagger |0\rangle + \sum_{i=0}^{N-2} \zeta_{i,d} d^\dagger c_i^\dagger |0\rangle \quad (\text{F.100})$$

We might find easier to use tensor notation for the indices, so that:

$$|\Psi\rangle_2 = \phi^{k,j} c_k^\dagger c_j^\dagger |0\rangle + \zeta^{d,j} d^\dagger c_j^\dagger |0\rangle \quad (\text{F.101})$$

We start with the non-interacting part of the hamiltonian:

$$\begin{aligned} H_0 |\Psi\rangle_2 &= -t\phi^{k,j} |k+1, j\rangle - t\phi^{k,j} |k, j+1\rangle - t\phi^{k,j} |k, j-1\rangle \\ &\quad - t\phi^{k,j} |k-1, j\rangle - t\zeta^{d,j} |\uparrow, j+1\rangle - t\zeta^{d,j} |\uparrow, j-1\rangle \end{aligned} \quad (\text{F.102})$$

The non-interacting part of the hamiltonian acting over the state is:

$$H_0|\Psi\rangle_2 = -t(\phi^{k+1,j} + \phi^{k-1,j}(1 - \delta_{k,0}) + \phi^{k,j+1} + \phi^{k,j-1}(1 - \delta_{j,0}))|k, j\rangle - t(\zeta^{d,j-1}(1 - \delta_{j,0}) + \zeta^{d,j+1})|\uparrow, j\rangle \quad (\text{F.103})$$

The part on the dot reads:

$$H_d|\Psi\rangle_2 = -\varepsilon_0\zeta^{d,j}|\uparrow, j\rangle \quad (\text{F.104})$$

The hybridization part gives:

$$H_V|\Psi\rangle_2 = t'\zeta^{d,j}|0, j\rangle + t'\phi^{k,j}\delta_{k,0}|\uparrow, j\rangle + t'\phi^{k,0}|k, \uparrow\rangle \quad (\text{F.105})$$

We can now use the fact that $\phi^{k,j} = -\phi^{j,k}$, so that the total contribution is:

$$H_V|\Psi\rangle_2 = t'\zeta^{d,j}\delta_{k,0}(1 - \delta_{j,0})|k, j\rangle + 2t'\phi^{k,j}\delta_{k,0}|\uparrow, j\rangle \quad (\text{F.106})$$

Finally, the interacting term:

$$H_U|\Psi\rangle_2 = U(c_0^\dagger c_0 - 1/2)(d^\dagger d - 1/2)|\Psi\rangle_2 \quad (\text{F.107})$$

There are three terms coming out from the interacting part:

$$\begin{aligned} H_{n_d}|\Psi\rangle_2 &= -(U\rho)n_d|\Psi\rangle_2 \rightarrow -(U\rho)\zeta^{d,j}|\uparrow, j\rangle \\ H_{n_0}|\Psi\rangle_2 &= -(U/2)\zeta^{d,0}|\uparrow, 0\rangle - (U/2)\phi^{k,j}\delta_{k,0}|k, j\rangle - (U/2)\phi^{k,j}\delta_{j,0}|k, j\rangle \\ H_U &= U c_0^\dagger c_0 d^\dagger d|\uparrow, j\rangle = U\zeta^{d,0}|\uparrow, 0\rangle = U\zeta^{d,j}\delta_{0,j}|\uparrow, j\rangle \end{aligned} \quad (\text{F.108})$$

So the total interacting part is then:

$$\begin{aligned} H_{UT}|\Psi\rangle_2 &= -(U\rho)\zeta^{d,j}|\uparrow, j\rangle + (U/2)\delta_{j,0}\zeta^{d,j}|\uparrow, j\rangle \\ &\quad - (U/2)(\delta_{k,0} + \delta_{j,0})\phi^{k,j}|k, j\rangle \end{aligned} \quad (\text{F.109})$$

Due to the property $\phi^{k,j} = -\phi^{j,k}$, the last term has a total contribution of $-U$. The eigenvalue equation to solve is then:

$$H|\Psi\rangle_2 = (\varepsilon_1 + \varepsilon_2)|\Psi\rangle_2 = E|\Psi\rangle_2 \quad (\text{F.110})$$

The equations for the state $|\uparrow, j\rangle$ and $|k, j\rangle$ are:

$$\begin{aligned} (E + \varepsilon_0 + U\rho - (U/2)\delta_{j,0})\zeta^{d,j} &= -t(\zeta^{d,j+1} + \zeta^{d,j-1}\bar{\delta}_{j,0}) + 2t'\delta_{k,0}\phi^{k,j} \\ (E + U\delta_{k,0})\phi^{k,j} &= (t'/2)\left(\delta_{k,0}\bar{\delta}_{j,0}\zeta^{d,j} - \delta_{j,0}\bar{\delta}_{k,0}\zeta^{d,k}\right) - t(\phi^{k+1,j} + \phi^{k-1,j}\bar{\delta}_{k,0}) \\ &\quad - t(\phi^{k,j+1} + \phi^{k,j-1}\bar{\delta}_{j,0}) \end{aligned} \quad (\text{F.111})$$

where we have defined:

$$\bar{\delta}_{ij} = 1 - \delta_{i,j} \quad (\text{F.112})$$

to use short hand notation.

The relevant states to cover the boundary effect are $|\uparrow, 0\rangle, |0, j\rangle = -|j, 0\rangle$. We look for solutions in the form:

$$\begin{aligned}\zeta^{d,j} &= \phi_d(\varepsilon_1)\phi_j(\varepsilon_2)f(-j) - \phi_j(\varepsilon_1)\phi_d(\varepsilon_2)f(j) \\ 2\phi^{k,j} &= \phi_k(\varepsilon_1)\phi_j(\varepsilon_2)f(k-j) - \phi_k(\varepsilon_2)\phi_j(\varepsilon_1)f(j-k)\end{aligned}\quad (\text{F.113})$$

At the same time, the single-particle equations must be satisfied. Due to Pauli exclusion principle, the values of $k \neq j$ always. The form of the function is chosen to be:

$$f(k-j) = e^{i\Phi \text{sign}(k-j)} \quad (\text{F.114})$$

Then, the ansatz used for the two body wavefunctions is:

$$\begin{aligned}\zeta^{d,j} &= \phi_d(\varepsilon_1)\phi_j(\varepsilon_2)e^{i\Phi} - \phi_j(\varepsilon_1)\phi_d(\varepsilon_2)e^{-i\Phi} \\ 2\phi^{k,j} &= \phi_k(\varepsilon_1)\phi_j(\varepsilon_2)e^{i\Phi} - \phi_k(\varepsilon_2)\phi_j(\varepsilon_1)e^{-i\Phi}\end{aligned}\quad (\text{F.115})$$

The single particle equations need to be satisfied at the same time:

$$\begin{aligned}(\varepsilon_1 + \varepsilon_0 + U/2)\phi_d &= t'\delta_{0,j}\phi_j \\ (\varepsilon_1 + (U/2)\delta_{0,j})\phi_j &= t'\delta_{0,j}\phi_d - t(\phi_{j+1} + \phi_{j-1}\bar{\delta}_{j,0})\end{aligned}\quad (\text{F.116})$$

With this form of the solutions, the second of the eigenvalue equations is automatically satisfied. Therefore, it is the first equation the one defining Φ . From the single particle equations, we can derive the following identity:

$$\begin{aligned}-te^{i\Phi}\phi^d(\varepsilon_1)(\phi^{j+1}(\varepsilon_2) + \phi^{j-1}(\varepsilon_2)) &= e^{i\Phi}\phi^d(\varepsilon_1)\left((\varepsilon_2 + (U/2)\delta_{0,j})\phi^j(\varepsilon_2) \right. \\ &\quad \left. -t'\phi^d(\varepsilon_2)\delta_{0,j}\right) \\ te^{-i\Phi}\phi^d(\varepsilon_2)(\phi^{j+1}(\varepsilon_1) + \phi^{j-1}(\varepsilon_1)) &= -e^{-i\Phi}\phi^d(\varepsilon_2)\left((\varepsilon_1 + (U/2)\delta_{0,j})\phi^j(\varepsilon_1) \right. \\ &\quad \left. -t'\phi^d(\varepsilon_1)\delta_{0,j}\right)\end{aligned}\quad (\text{F.117})$$

The first equation is transformed taking this into consideration:

$$\begin{aligned}\phi^d(\varepsilon_1)\phi^j(\varepsilon_2)e^{i\Phi}\left(\varepsilon_1 + \varepsilon_0 + U/2 - U\delta_{j,0}\right) - \phi^d(\varepsilon_2)\phi^j(\varepsilon_1)e^{-i\Phi}\left(\varepsilon_2 + \varepsilon_0 + U/2 \right. \\ \left. -U\delta_{j,0}\right) = \\ -i2t'\sin(\Phi)\phi^d(\varepsilon_1)\phi^d(\varepsilon_2) + t'\delta_{k,0}\left(\phi^k(\varepsilon_1)\phi^j(\varepsilon_2)e^{i\Phi} - \right. \\ \left. \phi^k(\varepsilon_2)\phi^j(\varepsilon_1)e^{-i\Phi}\right)\end{aligned}\quad (\text{F.118})$$

Notice that the $2t'$ has changed to t' , since $\Phi^{k,j}$ carries a factor $1/2!$ in front of the expression. We now take into account that:

$$\delta_{k,0}\phi^k(\varepsilon_1) = \frac{\phi^d(\varepsilon_1)}{t'}(\varepsilon_1 + \varepsilon_0 + U/2) \quad \chi_i = \frac{\phi^j(\varepsilon_i)}{\phi^d(\varepsilon_i)} \quad (\text{F.119})$$

Therefore the equation transforms to:

$$U\chi^1 e^{i\Phi} - U\chi^2 e^{-i\Phi} = t'^2 e^{i\Phi} - t'^2 e^{-i\Phi} \quad (\text{F.120})$$

Let us now calculate the χ functions from the single particle solutions. They are of the form (at position n of the lattice):

$$\chi_i(n) = \frac{\varepsilon_i + \varepsilon_0 + U/2}{t'} \cos(k_i n) \left(1 - \tan(\Delta_U(\varepsilon_i)) \tan(k_i n) \right) \quad (\text{F.121})$$

For the above identity to hold, we just took $n = 0$, for otherwise the t' term doesn't exist. Then the total equation is:

$$e^{i\Phi} \left(E_2 - \frac{t'^2}{U} \right) = e^{-i\Phi} \left(E_1 - \frac{t'^2}{U} \right) \quad (\text{F.122})$$

which implies $E_1 = E_2$, therefore the treatment is not correct. A different ansatz for the two particle solutions needs to be done.

The unfolded picture in the lattice

We present here a detailed calculation of the two particle scattering phase shift in the lattice version of the IRLM. For single particle states, we have the following solutions:

$$\begin{aligned}\phi_d &= \frac{\sqrt{2}t'}{E_1} \cos(\Delta_U(E_1)/2) & \Delta_U(E_1) &= -2 \arctan\left(\frac{\Gamma_0}{2E_1} - \frac{U\pi\nu}{4} - \frac{\varepsilon_1\pi\nu}{4}\right) \\ \phi_n &= \frac{1}{\sqrt{2}} \left(A e^{ikn} + B e^{-ikn} \right) & A &= e^{i\Delta_U/2} = B^{-1}\end{aligned}\quad (\text{F.123})$$

Also, it will be useful to have the single particle equations:

$$\begin{aligned}(\varepsilon_1 + \varepsilon_0 + U\rho)\phi_d &= t'\delta_{0,n}\phi_n \\ (\varepsilon_1 + (U/2)\delta_{0,n})\phi_n &= t'\delta_{0,n}\phi_d - t(\phi_{n+1} + \phi_{n-1}\bar{\delta}_{n,0})\end{aligned}\quad (\text{F.124})$$

The two particle equations coming from the hamiltonian acting over the state $|\Psi\rangle_2$ are:

$$\begin{aligned}(E + \varepsilon_0 + (U\rho) - (U/2)\delta_{m,0})\zeta^{d,m} &= -t(\zeta^{d,m+1} + \zeta^{d,m-1}\bar{\delta}_{m,0}) + 2t'\delta_{n,0}\phi^{n,m} \\ (E + U\delta_{n,0})\phi^{n,m} &= (t'/2)\left(\delta_{n,0}\bar{\delta}_{m,0}\zeta^{d,m} - \delta_{m,0}\bar{\delta}_{n,0}\zeta^{d,n}\right) \\ &\quad -t(\phi^{n+1,m} + \phi^{n-1,m}\bar{\delta}_{n,0}) - t(\phi^{n,m+1} + \phi^{n,m-1}\bar{\delta}_{m,0})\end{aligned}$$

We will try a new ansatz for the two particle processes. We know that when two particles scatter from each other, there is a phase shift Φ . The function inserted would be of the form:

$$f(k-m) = e^{i\Phi \text{sign}(k-m)} \quad (\text{F.125})$$

Thus, imagine two particles, one right moving wave scattering with a right moving one. Then the product is:

$$A_1 A_2 e^{ik_1 n} e^{ik_2 m} f(n-m) \rightarrow A_1 A_2 e^{ik_1 n} e^{ik_2 m} e^{i\Phi \text{sign}(n-m)} \quad (\text{F.126})$$

However, if we have a right mover scattering off a left mover:

$$\begin{aligned}A_1 B_1 e^{ik_1 n} e^{-ik_2 m} f(n - (-m)) &\rightarrow A_1 B_1 e^{ik_1 n} e^{-ik_2 m} e^{i\Phi \text{sign}(n+m)} \\ &= A_1 B_1 e^{ik_1 n} e^{-ik_2 m} e^{i\Phi}\end{aligned}\quad (\text{F.127})$$

since the $\text{sign}(n+m) > 0$ always, since all coordinates on the lattice are to the right of the dot, therefore $n, m > 0$ always. In order to avoid confusion in the notation, we will substitute $k \rightarrow n$ and $j \rightarrow m$. The two solutions need to satisfy the antisymmetry:

$$\zeta^{d,m} = -\zeta^{m,d} \quad \phi^{n,m} = -\phi^{m,n} \quad (\text{F.128})$$

To make identifications easier, the single particle solutions can be written as:

$$\phi_n = \phi_n^R + \phi_n^L \quad (\text{F.129})$$

where R/L represent right and left moving waves. The following ansatz for the two particle solutions will be tried for the occupied dot:

$$\begin{aligned}
 \zeta^{d,m} &= \phi^d(\varepsilon_1) \left(\phi_m^R(\varepsilon_2) e^{i\Phi \text{sign}(d-m)} + \phi_m^L(\varepsilon_2) e^{-i\Phi \text{sign}(d-m)} \right) \\
 &\quad - \phi^d(\varepsilon_2) \left(\phi_m^R(\varepsilon_1) e^{i\Phi \text{sign}(m-d)} + \phi_m^L(\varepsilon_1) e^{-i\Phi \text{sign}(m-d)} \right) \\
 \zeta^{d,m} &= \left(\phi^d(\varepsilon_1) \phi_m^R(\varepsilon_2) e^{-i\Phi} - \phi^d(\varepsilon_2) \phi_m^R(\varepsilon_1) e^{i\Phi} \right) \\
 &\quad + \left(\phi^d(\varepsilon_1) \phi_m^L(\varepsilon_2) e^{i\Phi} - \phi^d(\varepsilon_2) \phi_m^L(\varepsilon_1) e^{-i\Phi} \right)
 \end{aligned} \tag{F.130}$$

Here we have used the fact that $\text{sign}(m-d) > 0$ always, since the dot position is always to the left of all lattice sites. For the states with two fermions on the wire, the ansatz will have more terms. Let us define $\epsilon = \text{sign}(n-m)$. Then in terms of right and left moving scatterers we have:

$$\begin{aligned}
 2\phi^{n,m} &= \phi_n^R(\varepsilon_1) \phi_m^L(\varepsilon_2) e^{i\Phi} + \phi_n^L(\varepsilon_1) \phi_m^R(\varepsilon_2) e^{-i\Phi} + \phi_n^R(\varepsilon_1) \phi_m^R(\varepsilon_2) e^{i\Phi\epsilon} \\
 &\quad + \phi_n^L(\varepsilon_1) \phi_m^L(\varepsilon_2) e^{-i\Phi\epsilon} \\
 &\quad - \left(\phi_n^R(\varepsilon_2) \phi_m^L(\varepsilon_1) e^{-i\Phi} + \phi_n^L(\varepsilon_2) \phi_m^R(\varepsilon_1) e^{i\Phi} + \phi_n^R(\varepsilon_2) \phi_m^R(\varepsilon_1) e^{-i\Phi\epsilon} + \phi_n^L(\varepsilon_2) \phi_m^L(\varepsilon_1) e^{i\Phi\epsilon} \right) \\
 2\phi^{n,m} &= e^{i\Phi} \left(\phi_n^R(\varepsilon_1) \phi_m^L(\varepsilon_2) - \phi_n^L(\varepsilon_2) \phi_m^R(\varepsilon_1) \right) \\
 + e^{-i\Phi} &\left(\phi_n^L(\varepsilon_1) \phi_m^R(\varepsilon_2) - \phi_n^R(\varepsilon_2) \phi_m^L(\varepsilon_1) \right) + \left(\phi_n^R(\varepsilon_1) \phi_m^R(\varepsilon_2) e^{i\Phi\epsilon} - \phi_n^R(\varepsilon_2) \phi_m^R(\varepsilon_1) e^{-i\Phi\epsilon} \right) \\
 &\quad + \left(\phi_n^L(\varepsilon_1) \phi_m^L(\varepsilon_2) e^{-i\Phi\epsilon} - \phi_n^L(\varepsilon_2) \phi_m^L(\varepsilon_1) e^{i\Phi\epsilon} \right)
 \end{aligned}$$

It is better to separate each of the terms by the phases involved, therefore the two particle functions are:

$$\begin{aligned}
 \zeta^{d,m} &= e^{i\Phi} \left(\phi^d(\varepsilon_1) \phi_m^L(\varepsilon_2) - \phi^d(\varepsilon_2) \phi_m^R(\varepsilon_1) \right) + e^{-i\Phi} \left(\phi^d(\varepsilon_1) \phi_m^R(\varepsilon_2) - \phi^d(\varepsilon_2) \phi_m^L(\varepsilon_1) \right) \\
 2\phi^{n,m} &= e^{i\Phi} \left(\phi_n^R(\varepsilon_1) \phi_m^L(\varepsilon_2) - \phi_n^L(\varepsilon_2) \phi_m^R(\varepsilon_1) \right) + e^{-i\Phi} \left(\phi_n^L(\varepsilon_1) \phi_m^R(\varepsilon_2) - \phi_n^R(\varepsilon_2) \phi_m^L(\varepsilon_1) \right) \\
 &\quad + e^{i\Phi\epsilon} \left(\phi_n^R(\varepsilon_1) \phi_m^R(\varepsilon_2) - \phi_n^L(\varepsilon_2) \phi_m^L(\varepsilon_1) \right) + e^{-i\Phi\epsilon} \left(\phi_n^L(\varepsilon_1) \phi_m^L(\varepsilon_2) - \phi_n^R(\varepsilon_2) \phi_m^R(\varepsilon_1) \right)
 \end{aligned}$$

Now it is convenient to express the single particle equations in terms of these right and left moving waves:

$$\begin{aligned}
 (\varepsilon_1 + \varepsilon_0 + U\rho)\phi_d &= t'\delta_{0,n}(\phi_n^R + \phi_n^L) \\
 (\varepsilon_1 + (U/2)\delta_{0,n})(\phi_n^R + \phi_n^L) &= t'\delta_{0,n}\phi_d - t(\phi_{n+1}^R + \phi_{n-1}^R\bar{\delta}_{n,0}) - t(\phi_{n+1}^L + \phi_{n-1}^L\bar{\delta}_{n,0})
 \end{aligned} \tag{F.131}$$

The second equation should be satisfied with this ansatz. For the first equation, we need $\phi^{0,m}$, which is:

$$2\phi^{0,m} = e^{i\Phi} \left(\phi^0(\varepsilon_1)\phi_m^L(\varepsilon_2) - \phi^0(\varepsilon_2)\phi_m^R(\varepsilon_1) \right) + e^{-i\Phi} \left(\phi^0(\varepsilon_1)\phi_m^R(\varepsilon_2) - \phi^0(\varepsilon_2)\phi_m^L(\varepsilon_1) \right)$$

Now we can substitute:

$$\phi^0(\varepsilon_1) = \frac{E_1}{t'}\phi^d(\varepsilon_1) \quad (\text{F.132})$$

from the single particle equations. Therefore the two particle function with $n = 0$ is:

$$\begin{aligned} 2\phi^{0,m} &= \frac{e^{i\Phi}}{t'} \left(E_1\phi^d(\varepsilon_1)\phi_m^L(\varepsilon_2) - E_2\phi^d(\varepsilon_2)\phi_m^R(\varepsilon_1) \right) \\ &+ \frac{e^{-i\Phi}}{t'} \left(E_1\phi^d(\varepsilon_1)\phi_m^R(\varepsilon_2) - E_2\phi^d(\varepsilon_2)\phi_m^L(\varepsilon_1) \right) \\ \phi^{0,m} &= \frac{E_1\phi^d(\varepsilon_1)}{2t'} \left(e^{i\Phi}\phi_m^L(\varepsilon_2) + e^{-i\Phi}\phi_m^R(\varepsilon_2) \right) \\ &- \frac{E_2\phi^d(\varepsilon_2)}{2t'} \left(e^{i\Phi}\phi_m^R(\varepsilon_1) + e^{-i\Phi}\phi_m^L(\varepsilon_1) \right) \end{aligned} \quad (\text{F.133})$$

Substituting this into the equation, we get the following:

$$\begin{aligned} &\left(E_1/2 + E_2/2 + E/2 \right) \left(e^{i\Phi}(\phi^d(\varepsilon_1)\phi_m^L(\varepsilon_2) - \phi^d(\varepsilon_2)\phi_m^R(\varepsilon_1)) + e^{-i\Phi}(\phi^d(\varepsilon_1)\phi_m^R(\varepsilon_2) \right. \\ &- \left. \phi^d(\varepsilon_2)\phi_m^L(\varepsilon_1)) \right) = -t \left(e^{i\Phi}(\phi^d(\varepsilon_1)\phi_{m+1}^L(\varepsilon_2) - \phi^d(\varepsilon_2)\phi_{m+1}^R(\varepsilon_1)) \right. \\ &+ \left. e^{-i\Phi}(\phi^d(\varepsilon_1)\phi_{m+1}^R(\varepsilon_2) - \phi^d(\varepsilon_2)\phi_{m+1}^L(\varepsilon_1)) \right) - t \left(e^{i\Phi}(\phi^d(\varepsilon_1)\phi_{m-1}^L(\varepsilon_2) \right. \\ &- \left. \phi^d(\varepsilon_2)\phi_{m-1}^R(\varepsilon_1)) + e^{-i\Phi}(\phi^d(\varepsilon_1)\phi_{m-1}^R(\varepsilon_2) - \phi^d(\varepsilon_2)\phi_{m-1}^L(\varepsilon_1)) \right) \\ &+ E_1\phi^d(\varepsilon_1) \left(e^{i\Phi}\phi_m^L(\varepsilon_2) + e^{-i\Phi}\phi_m^R(\varepsilon_2) \right) \\ &- E_2\phi^d(\varepsilon_2) \left(e^{i\Phi}\phi_m^R(\varepsilon_1) + e^{-i\Phi}\phi_m^L(\varepsilon_1) \right) \end{aligned} \quad (\text{F.134})$$

with $E = \varepsilon_1 + \varepsilon_2$, and $E_{1/2} = \varepsilon_{1/2} + \varepsilon_0 + U/2$. We can write that in a neater way:

$$\begin{aligned} &e^{i\Phi}\phi^d(\varepsilon_1) \left(\left(\frac{E_2 - E_1}{2} + \frac{E}{2} \right) \phi_m^L(\varepsilon_2) + t(\phi_{m+1}^L(\varepsilon_2) + \phi_{m-1}^L(\varepsilon_2)) \right) \\ &+ e^{-i\Phi}\phi^d(\varepsilon_1) \left(\left(\frac{E_2 - E_1}{2} + \frac{E}{2} \right) \phi_m^R(\varepsilon_2) + t(\phi_{m+1}^R(\varepsilon_2) + \phi_{m-1}^R(\varepsilon_2)) \right) \\ &= e^{i\Phi}\phi^d(\varepsilon_2) \left(\left(\frac{E_1 - E_2}{2} + \frac{E}{2} \right) \phi_m^R(\varepsilon_1) + t(\phi_{m+1}^R(\varepsilon_1) + \phi_{m-1}^R(\varepsilon_1)) \right) \\ &+ e^{-i\Phi}\phi^d(\varepsilon_2) \left(\left(\frac{E_1 - E_2}{2} + \frac{E}{2} \right) \phi_m^L(\varepsilon_1) + t(\phi_{m+1}^L(\varepsilon_1) + \phi_{m-1}^L(\varepsilon_1)) \right) \end{aligned} \quad (\text{F.135})$$

Now we use the definition of single particle states, where we have:

$$\begin{aligned} e^{i\Phi} \phi_m^R(\varepsilon_1) &= \frac{1}{\sqrt{2}} e^{i\Phi} e^{ik_1 m} e^{i\Delta_U(\varepsilon_1)/2} = \frac{1}{\sqrt{2}} e^{i\gamma_1} \\ e^{-i\Phi} \phi_m^L(\varepsilon_1) &= \frac{1}{\sqrt{2}} e^{-i\Phi} e^{-ik_1 m} e^{-i\Delta_U(\varepsilon_1)/2} = \frac{1}{\sqrt{2}} e^{-i\gamma_1} \end{aligned} \quad (\text{F.136})$$

Both sides of the identity are identically equal to 0. This happens when $n = 0 \neq m$. We will see now how this changes when $n = m = 0$. In that case, the two particle equation reduces to:

$$(E_1 + E_2 + E - U)\zeta^{d,0} = -2t\zeta^{d,1} \quad (\text{F.137})$$

We also need to impose the condition that the single particle equations need to be satisfied. Therefore, we can write:

$$\begin{aligned} \zeta^{d,0} &= 2 \left(\frac{\phi^d(\varepsilon_1)\phi^d(\varepsilon_2)}{t'} (E_2 - E_1) \cos(\Phi) + \frac{1}{\sqrt{2}} \left(\phi^d(\varepsilon_2) \cos(\Phi - \Delta_1) \right. \right. \\ &\quad \left. \left. - \phi^d(\varepsilon_1) \cos(\Phi + \Delta_2) \right) \right) \end{aligned} \quad (\text{F.138})$$

The right and left movers for the $m = 1$ site are:

$$\phi_1^R(\varepsilon_1) = e^{ik_1} \phi_0^R = e^{ik_1} \left(\frac{E_1}{t'} \phi^d(\varepsilon_1) - \frac{1}{\sqrt{2}} e^{-i\Delta_1} \right) \quad (\text{F.139})$$

The only difference with the $m = 0$ case is that now the Φ is shifted by the single particle momentums. Then we have:

$$\begin{aligned} \zeta^{d,1} &= 2 \left(\frac{\phi^d(\varepsilon_1)\phi^d(\varepsilon_2)}{t'} \left(E_2 \cos(\Phi - k_2) - E_1 \cos(\Phi + k_1) \right) \right. \\ &\quad \left. + \frac{1}{\sqrt{2}} \left(\phi^d(\varepsilon_2) \cos(\Phi - \Delta_1 + k_1) - \phi^d(\varepsilon_1) \cos(\Phi + \Delta_2 - k_2) \right) \right) \end{aligned}$$

Then the two particle equation is:

$$\begin{aligned} &\left(E_1 + E_2 + E - U \right) \left(\frac{\phi^d(\varepsilon_1)\phi^d(\varepsilon_2)}{t'} (E_2 - E_1) \cos(\Phi) \right. \\ &\quad \left. + \frac{1}{\sqrt{2}} \left(\phi^d(\varepsilon_2) \cos(\Phi - \Delta_1) - \phi^d(\varepsilon_1) \cos(\Phi + \Delta_2) \right) \right) = \\ &\quad -2t \left(\frac{\phi^d(\varepsilon_1)\phi^d(\varepsilon_2)}{t'} \left(E_2 \cos(\Phi - k_2) - E_1 \cos(\Phi + k_1) \right) \right. \\ &\quad \left. + \frac{1}{\sqrt{2}} \left(\phi^d(\varepsilon_2) \cos(\Phi - \Delta_1 + k_1) - \phi^d(\varepsilon_1) \cos(\Phi + \Delta_2 - k_2) \right) \right) \end{aligned} \quad (\text{F.140})$$

Multiplying everything by $t'/\phi^d(1)\phi^d(2)$ we get:

$$\begin{aligned} &\left(E_1 + E_2 + E - U \right) \left((E_2 - E_1) \cos(\Phi) + \frac{t'}{\sqrt{2}} \left((1/\phi^d(\varepsilon_1)) \cos(\Phi - \Delta_1) \right. \right. \\ &\quad \left. \left. - (1/\phi^d(\varepsilon_2)) \cos(\Phi + \Delta_2) \right) \right) = -2t \left(\left(E_2 \cos(\Phi - k_2) - E_1 \cos(\Phi + k_1) \right) \right. \\ &\quad \left. + \frac{t'}{\sqrt{2}} \left((1/\phi^d(\varepsilon_1)) \cos(\Phi - \Delta_1 + k_1) - (1/\phi^d(\varepsilon_2)) \cos(\Phi + \Delta_2 - k_2) \right) \right) \end{aligned} \quad (\text{F.141})$$

Taking into account that:

$$(1/\phi^d(1)) = \frac{E_1}{\cos(\Delta_1)t'\sqrt{2}} \quad (\text{F.142})$$

We can write:

$$\begin{aligned} & \left(E_1 + E_2 + E - U \right) \left[(E_2 - E_1) \cos(\Phi) + \frac{1}{2} \left(E_1 \frac{\cos(\Phi - \Delta_1)}{\cos(\Delta_1)} \right. \right. \\ & \quad \left. \left. - E_2 \frac{\cos(\Phi + \Delta_2)}{\cos(\Delta_2)} \right) \right] = -2t \left[\left(E_2 \cos(\Phi - k_2) \right. \right. \\ & \left. \left. - E_1 \cos(\Phi + k_1) \right) + \frac{1}{2} \left(E_1 \frac{\cos(\Phi - \Delta_1 + k_1)}{\cos(\Delta_1)} - E_2 \frac{\cos(\Phi + \Delta_2 - k_2)}{\cos(\Delta_2)} \right) \right] \quad (\text{F.143}) \end{aligned}$$

The equation above is the one determining Φ , the two particle scattering phase-shift. Using the formula for the cosine of a sum we have:

$$\begin{aligned} & \left(E_1 + E_2 + E - U \right) \left[(E_2 - E_1) \cos(\Phi) + \frac{1}{2} \left(E_1 \cos(\Phi) + E_1 \tan(\Delta_1) \sin(\Phi) \right. \right. \\ & \left. \left. - E_2 \cos(\Phi) + E_2 \tan(\Delta_2) \sin(\Phi) \right) \right] = -2t \left(\left(E_2 \cos(\Phi - k_2) - E_1 \cos(\Phi + k_1) \right) + \right. \\ & \quad \left. \frac{1}{2} \left(E_1 \cos(\Phi + k_1) + E_1 \tan(\Delta_1) \sin(\Phi + k_1) \right. \right. \\ & \quad \left. \left. - E_2 \cos(\Phi - k_2) + E_2 \tan(\Delta_2) \sin(\Phi - k_2) \right) \right) \\ & \left(E_1 + E_2 + E - U \right) \left((E_2 - E_1) \cos(\Phi) + \left(E_1 \tan(\Delta_1) + E_2 \tan(\Delta_2) \right) \sin(\Phi) \right) \\ & = -2t \left(\left(E_2 \cos(\Phi - k_2) - E_1 \cos(\Phi + k_1) \right) + \left(E_1 \tan(\Delta_1) \sin(\Phi + k_1) \right. \right. \\ & \quad \left. \left. + E_2 \tan(\Delta_2) \sin(\Phi - k_2) \right) \right) \end{aligned}$$

The right hand side is splitted in terms of sines and cosines:

$$\begin{aligned} & -2t \left(\cos(\Phi) \left(E_2 \cos(k_2) - E_1 \cos(k_1) \right) + \sin(\Phi) \left(E_2 \sin(k_2) + E_1 \sin(k_1) \right) + \right. \\ & \quad \left. \sin(\Phi) \left(E_1 \tan(\Delta_1) \cos(k_1) + E_2 \tan(\Delta_2) \cos(k_2) \right) \right. \\ & \quad \left. + \cos(\Phi) \left(E_1 \tan(\Delta_1) \sin(k_1) - E_2 \tan(\Delta_2) \sin(k_2) \right) \right) \end{aligned}$$

Separating terms we arrive at the following expression:

$$\begin{aligned}
 \tan \Phi &= -\frac{N}{D} \\
 N &= (E_1 + E_2 + E - U)(E_2 - E_1) + 2t \left(E_2 \left(\cos(k_2) - \sin(k_2) \tan(\Delta_2) \right) \right. \\
 &\quad \left. - E_1 \left(\cos(k_1) - \sin(k_1) \tan(\Delta_1) \right) \right) \\
 D &= (E_1 + E_2 + E - U)(E_2 \tan(\Delta_2) + E_1 \tan(\Delta_1)) \\
 &\quad + 2t \left(E_2 \left(\sin(k_2) + \cos(k_2) \tan(\Delta_2) \right) + E_1 \left(\sin(k_1) + \cos(k_1) \tan(\Delta_1) \right) \right)
 \end{aligned}$$

When constructing the single particle states, the phase shift Δ was defined as:

$$\Delta_{1/2} = \arctan \left(-\frac{t^2}{E_{1/2} t \sin(k_{1/2})} + \frac{U}{2t \sin(k_{1/2})} + \frac{\varepsilon_{1/2}}{2t \sin(k_{1/2})} \right) \quad (\text{F.144})$$

Taking that into account, the part inside brackets with E_2 reads:

$$\begin{aligned}
 2t \cos(k_2) - 2t \sin(k_2) \tan(\Delta_2) &= \frac{2t^2}{E_2} - U - 2\varepsilon_2 \\
 2t \cos(k_1) - 2t \sin(k_1) \tan(\Delta_1) &= \frac{2t^2}{E_1} - U - 2\varepsilon_1
 \end{aligned} \quad (\text{F.145})$$

where we have used that $E = \varepsilon_1 + \varepsilon_2$. In total, the numerator of the above expression is simplified:

$$N = 2U(E_1 - E_2) \quad (\text{F.146})$$

Now we go with the denominator, which includes the following:

$$\begin{aligned}
 &E_2 \left(\tan(\Delta_2)(E_1 + E_2 + E - U - \varepsilon_2) + 2t \sin(k_2) \right) \\
 &+ E_1 \left(\tan(\Delta_1)(E_1 + E_2 + E - U - \varepsilon_1) + 2t \sin(k_1) \right)
 \end{aligned} \quad (\text{F.147})$$

Let us identify $2t \sin(k_{1/2}) = v_{1/2}$, which is the Fermi velocity by definition, and then we have:

$$\tan(\Delta_{1/2}) = \frac{1}{v_{1/2}} \left(-\frac{2t^2}{E_{1/2}} + U + \varepsilon_{1/2} \right) \quad (\text{F.148})$$

With this transformation, the denominator is:

$$\begin{aligned}
 &E_2 \left(v_2 + \frac{1}{v_2} \left(-\frac{2t^2}{E_2} + (U + \varepsilon_2) \right) (\alpha - (U + \varepsilon_2)) \right) \\
 &+ E_1 \left(v_1 + \frac{1}{v_1} \left(-\frac{2t^2}{E_1} + (U + \varepsilon_1) \right) (\alpha - (U + \varepsilon_1)) \right) = \\
 &\hspace{15em} \tau(E_1 + E_2)
 \end{aligned} \quad (\text{F.149})$$

with $\alpha = E_1 + E_2 + E$. Lets see the two terms separately. For E_2 we have:

$$\frac{E_2}{v_2} \left(v_2^2 + \left(-\frac{2t'^2}{E_2} (\alpha - (U + \varepsilon_2)) + \alpha(U + \varepsilon_2) - U^2 - \varepsilon_2^2 - 2U\varepsilon_2 \right) \right) \quad (\text{F.150})$$

Now we calculate:

$$\begin{aligned} v_2^2 + \alpha(U + \varepsilon_2) - U^2 - \varepsilon_2^2 - 2U\varepsilon_2 &= \underbrace{4t^2 - \varepsilon_2^2}_{v_2^2} + \underbrace{2U\varepsilon_1 + 2U\varepsilon_2 + 2U\varepsilon_0 + 2U^2\rho}_{U\alpha} \\ &+ \underbrace{2\varepsilon_2^2 + 2\varepsilon_2\varepsilon_1 + 2\varepsilon_2\varepsilon_0 + 2\varepsilon_2U\rho}_{\varepsilon_2\alpha} - U^2 - \varepsilon_2^2 - 2U\varepsilon_2 = 4t^2 - U^2 + 2E_1(U + \varepsilon_2) \end{aligned}$$

The same applies to the part of E_1 , so the denominator D reads:

$$\begin{aligned} &\frac{E_2}{v_2} \left(\left(-\frac{2t'^2}{E_2} (\alpha - (U + \varepsilon_2)) + 4t^2 - U^2 + 2E_1(U + \varepsilon_2) \right) \right) \\ &+ \frac{E_1}{v_1} \left(\left(-\frac{2t'^2}{E_1} (\alpha - (U + \varepsilon_1)) + 4t^2 - U^2 + 2E_2(U + \varepsilon_1) \right) \right) \end{aligned}$$

Now lets work out the following limit, when $t', \varepsilon_i \rightarrow 0$ but the *renormalized* eigenvalues of the problem E_i remain finite, that is:

$$\lim_{t', \varepsilon_{1/2} \rightarrow 0} \frac{2t'^2}{\varepsilon_{1/2}} = E_{1/2} \quad (\text{F.151})$$

In this limit, wich is the *field theory* limit, the Fermi velocity is equal to $v_{1/2} = 2t$, and we are left with:

$$\left(\frac{E_2}{2t} + \frac{E_1}{2t} \right) (4t^2 - U^2) + \frac{4U}{2t} E_1 E_2 \quad (\text{F.152})$$

We will call now $U = U/2t$. We arrive at the equation describing the scattering phase shift between particles in the lattice model:

$$\tan(\Phi) = 2U \frac{(E_2 - E_1)}{(E_2 + E_1)(1 - U^2) + (4U/2t)E_1 E_2} \quad (\text{F.153})$$

The second order term can be neglected respect to the other one being second order in the eigenvalues in the limit we are working. We identify now $U = \tan(\delta) = \tan(\pi g/2)$. Therefore, we have:

$$\boxed{\tan(\Phi) = \tan(\pi g) \left(\frac{E_2 - E_1}{E_2 + E_1} \right)} \quad (\text{F.154})$$

where g is defined as usual for the IRLM:

$$g = \frac{2}{\pi} \arctan \left(\frac{U\pi\nu}{2} \right) = \frac{2}{\pi} \arctan \left(\frac{U}{2t} \right) \quad \nu = \frac{1}{\pi t} \quad (\text{F.155})$$

Notice that, although we are working in the limit $\varepsilon_{1/2} \rightarrow 0$, the difference $\varepsilon_2 - \varepsilon_1 \neq 0$, since of course the eigenvalues need to be different. We have then

recovered Filyov and Wiegmann's result but in a slightly different way, starting from the lattice version of the model.

Let us now see how this changes under the assumption that all Fermi velocities are equal to $2t$, but without neglecting any other terms. The equation to look at is:

$$\frac{E_2}{v_2} \left(1 - U^2 + 2E_1(U + \varepsilon_2) \right) + \frac{E_1}{v_1} \left(1 - U^2 + 2E_2(U + \varepsilon_1) \right)$$

where all energies are expressed in units of $2t$. We know from bosonization and the field theory correspondence, that the result of the parameter has to be:

$$\tau = \cot \left(\frac{\pi}{2} (1 - g)^2 \right) \quad (\text{F.156})$$

It is curious to see that the expression:

$$\frac{2U}{1 - U^2} \quad (\text{F.157})$$

translates to that to first order in $g = 2\delta/\pi$. If we identify:

$$U = \tan(\delta) \quad 1/U = \tan(\beta) \quad (\text{F.158})$$

Then we have:

$$\begin{aligned} \frac{2U}{1 - U^2} &= \frac{1}{\frac{1}{2}(\tan(\beta) - \tan(\delta))} = \frac{1}{\frac{1}{2}(1 + \tan(\delta) \tan(\beta))(\tan(\beta - \delta))} = \cot(\beta - \delta) \\ &= \cot((\beta + \delta) - 2\delta) \end{aligned} \quad (\text{F.159})$$

and since $\beta + \delta = \pi/2$, we have:

$$\tau = \cot \left(\frac{\pi}{2} (1 - 2g) \right) \quad (\text{F.160})$$

where $g = 2\delta/\pi$. Looking at the equation above, the assumption that both Fermi velocities are equal implies to neglect terms of order $\varepsilon_{1/2}^2$, therefore only terms linear in the eigenvalues are kept. The product $2E_1E_2$ is then:

$$2E_1E_2 \sim 2E\alpha + 2\alpha^2 \quad (\text{F.161})$$

where we have called $U\rho = \alpha$ and $E = \varepsilon_1 + \varepsilon_2$. Then the denominator in total is:

$$\begin{aligned} &E(1 - U^2) + 2\alpha(1 - U^2) + 2E_1E_2(2U + E) = \\ &E \left(1 - U^2 + 4U\alpha + 2\alpha^2 \right) + \left(4U\alpha^2 + 2\alpha(1 - U^2) \right) \end{aligned} \quad (\text{F.162})$$

With this, the two particle scattering phase shift is:

$$\Phi = \arctan \left(\tau \frac{\varepsilon_2 - \varepsilon_1}{\varepsilon_2 + \varepsilon_1 + \gamma} \right) \quad (\text{F.163})$$

where τ and γ are defined as:

$$\tau = \frac{2U}{1 - U^2 + 4U\alpha + 2\alpha^2} \quad \gamma = \frac{4U\alpha^2 + 2\alpha(1 - U^2)}{1 - U^2 + 4U\alpha + 2\alpha^2} \quad (\text{F.164})$$

Bibliography

- [1] G.Ben-Shach, A.Haim, I.Appelbaum, Y.Oreg, A.Yacobi, and B.I.Halperin. Detecting majorana modes in one-dimensional wires by charge sensing. *Physical Review B*, 91, 2015.
- [2] S.M.Albrecht, E.B.Hansen, A.P.Higginbotham, F.Kuemmeth, T.S.Jespersen, J.Nygaard, P.K.Jeppesen, J.Danon, K.Flensberg, and C.M.Marcus. Transport signatures of quasiparticle poisoning in a majorana island. *Physical Review Letters*, 118(13), 2017.
- [3] M.Heiblum. Fractional Charge Determination via Quantum Shot Noise Measurements. *Perspectives of Mesoscopic Physics: World Scientific*, 115, 2010.
- [4] E. Levy, I. Sternfeld, M. Eshkol, M. Karpovski, B. Dwir, A. Rudra, E. Kapon, Y. Oreg, and A. Palevski. Experimental evidence for Luttinger liquid behavior in sufficiently long GaAs V-groove quantum wires. *Physical Review B*, 85, 2012.
- [5] W.J. de Hass, J.De Boer, and G.J. van den Berg. The electrical resistance of gold, copper and lead at low temperatures. *Physica*, 1:1115–1124, 1934.
- [6] W.J. de Hass and J.De Boer. The electrical resistance of platinum at low temperatures. *Physica*, 1:609–616, 1934.
- [7] P.W. Anderson. Localised magnetic states in metals. *Physical Review*, 124(1), 1961.
- [8] U.Fano. Effect of configuration interactions on intensities and phase-shifts. *Physical Review*, 124(6), 1964.
- [9] J. Kondo. Resistance minimum in dilute magnetic alloys. *Progress of Theoretical Physics*, 32(1), 1964.
- [10] J.R. Schrieffer and P.A.Wolff. Relation between the Anderson and Kondo hamiltonians. *Physical Review*, 149(2), 1966.
- [11] P.W. Anderson. A poor man’s derivation of scaling laws for the Kondo problem. *J.Physics C: Solid St. Physics*, 3, 1970.
- [12] K.G. Wilson. Renormalization group and critical phenomena. i. Renormalization group and the Kadanoff scaling picture. *Physical Review B*, 4, 1971.
- [13] L.P. Kadanoff. Scaling laws for Ising models near T_c . *Physics*, 2:263–272, 1966.

-
- [14] G.D. Mahan. Excitons in metals: infinite hole mass. *Physical Review*, 163:612, 1967.
- [15] B. Roulet, J.Gavoret, and P.Nozières. Singularities in the x-ray absorption and emission of metals. I. First order parquet calculation. *Physical Review*, 178(3), 1969.
- [16] P. Nozières, B. Roulet, and J.Gavoret. Singularities in the x-ray absorption of metals. II. Self consistent treatment of divergences. *Physical Review*, 178(3), 1969.
- [17] P. Nozières and C.T. De Dominicis. Singularities in the x-ray absorption and emission of metals. III. One body theory exact solution. *Physical Review*, 178(3), 1969.
- [18] K.D. Schotte and U. Schotte. Threshold behaviour of the x-ray spectra of light metals. *Physical Review*, 2(185), 1969.
- [19] K.D. Schotte and U. Schotte. Tomonaga's model and the threshold singularity of the x-ray spectra of metals. *Physical Review*, 2(182), 1969.
- [20] S. Tomonaga. Remarks on bloch method of sound waves applied to many fermion problems. *Progress of Theoretical Physics*, 5(4), 1950.
- [21] J.M. Luttinger. An exactly soluble model of a many fermion system. *Journal of Mathematical Physics*, 4(1154), 1963.
- [22] P.W. Anderson and G. Yuval. Exact results in the kondo problem: equivalence to a one dimensional coulomb gas. *Physical Review Letters*, 23(2), 1969.
- [23] P.W. Anderson and G. Yuval. Exact results for the Kondo problem: One body theory and extension to finite temperatures. *Physical Review B*, 1(4), 1970.
- [24] P.W. Anderson, G. Yuval, and D.R. Hamman. Exact results in the Kondo problem II. Scaling theory, qualitatively correct solution and some new results on one dimensional classical statistical models. *Physical Review B*, 1, 1970.
- [25] K.G. Wilson. The Renormalization Group: critical phenomena and the Kondo problem. *Rev.Mod. Physics*, 47(733), 1975.
- [26] H. Bethe. Zur theorie der metalle. *Zeitschrift für physik*, 1931.
- [27] W.E. Thirring. A soluble relativistic field theory. *Annals of Physics*, 3(1), 1958.
- [28] V.E. Korepin. Direct calculation of the S matrix in the massive Thirring model. *Theo.Math.Phys.*, 41:953–967, 1979.
- [29] H. Bergknoff and H.B. Thacker. Method for solving the massive Thirring model. *Phys. Review Letters*, 42(3), 1979.
- [30] V.E. Korepin, N.M. Bogoliubov, and A.G. Izergin. *Quantum Inverse Scattering Method and Correlation Functions*. Cambridge University Press, 1993.
-

-
- [31] A.B. Zamolodchikov. Exact two particle S matrix of quantum sine-Gordon solitons. *Communications in Mathematical Physics*, 5:183–186, 1977.
- [32] S. Coleman. Quantum Sine Gordon equation as the massive Thirring model. *Physical Review D*, 11(8), 1975.
- [33] S. Goshal and A. Zamolodchikov. Boundary S matrix and boundary state in a two dimensional quantum integrable field theory. *Int.J.Mod.Phys.A*, 09(3841), 1994.
- [34] H. Saleur, S.Skorik, and N.P. Warner. The boundary sine Gordon theory: classical and semiclassical analysis. *Nuclear Physics B*, 441(3), 1995.
- [35] P. Fendley, A.W.W. Ludwig, and H. Saleur. Exact non-equilibrium transport through point contacts in quantum wires and fractional quantum Hall devices. *Physical Review B*, 52(12), 1995.
- [36] P.B. Wiegmann and A.M.Finkel'shtein. Resonant Level Model in the Kondo problem. *Zh.Eksp.Teor.Fiz.*, 75:204–216, 1978.
- [37] P. Schlottman. The Kondo problem. i. Transformation of the model and its renormalization. *Physical Review B*, 25(7), 1982.
- [38] L. Borda, K. Vl̇adar, and A. Zawadowski. Theory of a resonant level coupled to several conduction electron channels in equilibrium and out of equilibrium. *Physical Review B*, 75, 2007.
- [39] L. Borda, A. Schiller, and A. Zawadowski. Applicability of bosonization and the Anderson-Yuval methods at the strong coupling limit of quantum impurity problems. *Physical Review B*, 78, 2008.
- [40] V.V. Ponomarenko. Resonant tunneling and low-energy impurity behaviour in a resonant level model. *Physical Review B*, 48(8), 1993.
- [41] I.V.Lerner, V.I.Yudson, and V.Yurkevich. Quantum Wire Hybridized with a Single Level Impurity. *Physical Review Letters*, 100, 2008.
- [42] M. Goldstein, Y. Weiss, and R. Berkovits. Interacting Resonant Level Model coupled to a Luttinger liquid: population vs density of states. *Physica E*, 42:610–613, 2010.
- [43] M. Goldstein, Y. Weiss, and R. Berkovits. Interacting Resonant Level Model coupled to a Luttinger liquid: Universality of thermodynamic properties. *EPL*, 86(67012), 2009.
- [44] P. Mehta and N. Andrei. Non equilibrium transport in quantum impurity models: The bethe ansatz for open systems. *Physical Review Letters*, 96, 2006.
- [45] E.Boulat, H.Saleur, and P.Schmitteckert. Twofold Advance in the Theoretical Understanding of Far-From-Equilibrium Properties of Interacting Nanostructures. *Physical Review Letters*, 101, 2008.
-

-
- [46] E. Boulat and H. Saleur. Exact low temperature results for transport properties of the Interacting Resonant Level Model. *Physical Review B*, 77, 2008.
- [47] A. Branschädel, E. Boulat, H. Saleur, and P. Schmitteckert. Shot noise in the self-dual Interacting Resonant Level Model. *Physical Review Letters*, 105, 2010.
- [48] S.T. Carr, D.A. Bagrets, and P. Schmitteckert. Full counting statistics in the self-dual Interacting Resonant Level Model. *Physical Review Letters*, 107, 2011.
- [49] Y. Vinkler Aviv, A. Schiller, and F.B. Anders. From thermal equilibrium to non equilibrium quench dynamics: A conserving approximation for the Interacting Resonant Level Model. *Physical Review B*, 90, 2014.
- [50] A. Kiss, J. Otsuki, and Y. Kuramoto. Scaling theory vs exact numerical results for the spinless resonant level model. *J.Phys.Soc.Jpn*, 82(124713), 2014.
- [51] A. Schiller and N. Andrei. Strong to weak coupling duality in the non-equilibrium Interacting Resonant Level Model. *arxiv 0710.0249*, 2007.
- [52] A. Braun and P. Schmitteckert. Numerical evaluation of green's functions based on the chebyshev expansion. *Physical Review B*, 90, 2014.
- [53] D. Bohr and P. Schmitteckert. Strong enhancement of transport by interaction on contact links. *Physical Review B*, 75(24), 2007.
- [54] T. Giamarchi, C.M. Varma, A.E. Ruckenstein, and P. Nozières. Singular low energy of an impurity model with finite range interactions. *Physical Review Letters*, 70(25), 1993.
- [55] A. Kiss, Y. Kuramoto, and J. Otsuki. Exact dynamics of charge fluctuations in the multichannel Interacting Resonant Level Model. *J.Phys.Soc.Jpn*, 84(104602), 2015.
- [56] V.M. Filyov and P.B. Wiegmann. A method for solving the kondo problem. *Physics Letters*, 76A(3), 1980.
- [57] P.B. Wiegmann. Exact solution of the s-d exchange model at $T=0$. *Pis'ma.Zh.Eksp.Teor.Fiz.*, 31(7), 1980.
- [58] P.B. Wiegmann. Exact solution of the s-d exchange model (kondo problem). *J.Phys. C:Solid State Physics*, 14:1463–1478, 1981.
- [59] N. Andrei. Diagonalization of the Kondo hamiltonian. *Physical Review Letters*, 45(379), 1980.
- [60] A.M. Tsvelick and P.B. Wiegmann. Exact results in the theory of magnetic alloys. *Advances in Physics*, 32(4):453–713, 1983.
- [61] A.C. Hewson. *The Kondo problem to heavy fermions*. Cambridge University press, 1993.
-

-
- [62] P. Coleman. *Introduction to many-body physics*. Cambridge University press, 2015.
- [63] T. Giamarchi. *Quantum Physics in one dimension*. Clarendon Press, Oxford, 2003.
- [64] D. Langreth. Friedel sum rule for the anderson model of localised impurity states. *Physical Review*, 150(2), 1966.
- [65] G.D. Mahan. *Many particle physics*. Kluwer academic/Plenum publishers, 2000.
- [66] A.O. Gogolin, A.A. Nersesyan, and A.M. Tsvelick. *Bosonization and strongly correlated systems*. Cambridge University press, 1998.
- [67] P.W.Anderson. Infrared catastrophe with Fermi gases in local scattering potentials. *Physical Review Letters*, 18(24), 1967.
- [68] H.Suhl. Dispersion theory of the Kondo effect. *Phys.Review*, 138, 1965.
- [69] A.A.Abrikosov. Magnetic impurities in non-magnetic metals. *Physics*, 2, 1965.
- [70] P.W. Anderson. *A career in Theoretical Physics*. World Scientific Series in 20th Century Physics, 1994.
- [71] D.E. Logan, M.P. Eastwood, and M.A. Tusch. A local moment approach to the anderson model. *J. Phys. Condens. Matter*, 10:2673–2700, 1998.
- [72] D. Senechal. An introduction to bosonization. *cond-mat/9908262*, 1999.
- [73] E. Miranda. Introduction to bosonization. *Brazilian Journal of Physics*, 33(1), 2003.
- [74] J.V. Delft and H. Schoeller. Bosonization for beginners - refermionization for experts. *Annalen der Physik*, 7, 1998.
- [75] R.Bulla, T.A.Costi, and T.Pruschke. Numerical renormalization group method for quantum impurity systems. *Reviews of Modern Physics*, 80, 2008.
- [76] R.Bulla, A.C.Hewson, and T.Pruschke. Numerical renormalization group calculations for the self-energy of the impurity Anderson model. *J. Phys: Condens. Matter*, 10, 1998.
- [77] A.Weischelbaum and J.von Delft. Sum-rule conserving spectral functions from the numerical renormalization group. *Physical Review Letters*, 99, 2007.
- [78] W.Hofstetter. Generalized Numerical Renormalization Group for Dynamical Quantities. *Physical Review Letters*, 85(7), 2000.
- [79] R.Zitko and T.Pruschke. Energy resolution and discretization artefacts in the numerical renormalization group. *Physical Review B*, 79, 2009.
-

-
- [80] V.L.Campo and J.N.L.Oliveira. Alternative discretization in the numerical renormalization-group method. *Physical Review B*, 72, 2005.
- [81] R.Bulla, T.A.Costi, and D.Vollhardt. Finite-temperature numerical renormalization group study of the Mott transition. *Physical Review B*, 64, 2001.
- [82] R.Peters, T.Pruschke, and F.B.Anders. Numerical renormalization group approach to Green's functions for quantum impurity models. *Physical Review B*, 74, 2006.
- [83] A.Rosch, T.A.Costi, J.Paaske, and P.Wolfe. Spectral function of the kondo model in high magnetic fields. *Physical Review B*, 68, 2003.
- [84] Alexander Altland and Ben Simons. *Condensed Matter Field Theory*. Cambridge University Press, 2010.
- [85] B. Sutherland. *Beautiful models: 70 years of exactly solved quantum many body problems*. World Scientific Publishing Co.Pte.Ltd, 2004.
- [86] A.M. Tsvelick. *Quantum Field Theory in Condensed Matter Physics*. Cambridge University press, 2010.
- [87] A.B.Zamolodchikov and Al.B.Zamolodchikov. Factorised S- matrices in two dimensions as the exact solutions of certain relativistic Quantum Field Theory models. *Annals of Physics*, 120:253–291, 1979.
- [88] A.D.Polyanin and A.V.Manzhairov. *Handbook of integral equations*. Chapman & Hall/CRC, 2008.
- [89] P.Fendley, H.Saleur, and N.P.Warner. Exact solution of a massless scalar field with a relevant boundary interaction. *Nuclear Physics B*, 430, 1994.
- [90] M.Fabrizio, A.O.Gogolin, and P.Nozières. Anderson-Yuval approach to the Multichannel Kondo model. *Physical Review B*, 51(22), 1995.
- [91] A. Branschädel, E. Boulat, H. Saleur, and P. Schmitteckert. Shot noise in the self-dual Interacting Resonant Level Model. *Physical Review Letters*, 2010.
- [92] P. Coleman. New approach to the mixed valence problem. *Physical Review B*, 29(6), 1984.
- [93] V.J.Emery and S.Kivelson. Mapping of the two channel Kondo problem to a Resonant Level Model. *Physical Review B*, 46(17), 1992.
- [94] R.Zitko, R.Peters, and Th.Pruschke. Splitting of the Kondo resonance in anisotropic magnetic impurities on surfaces. *New Journal of Physics*, 11, 2009.
- [95] T.Costi. Scaling and Universality in the Anisotropic Kondo Model and the Dissipative Two-State System. *Physical Review Letters*, 80(5), 1998.
- [96] Colin Rylands and Natan Andrei. Quantum dot at a Luttinger liquid edge. *Physical Review B*, (115424), 2017.
-